TESE DE DOUTORAMENTO

COMPUTATIONAL METHODS FOR THE DESIGN AND APPLICATIONS OF SELF-ASSEMBLED CYCLIC PEPTIDE NANOTUBES

Martín Calvelo Souto

ESCOLA DE DOUTORAMENTO INTERNACIONAL DA UNIVERSIDADE DE SANTIAGO DE COMPOSTELA

PROGRAMA DE DOUTORAMENTO EN CIENCIA E TECNOLOXÍA QUÍMICA

SANTIAGO DE COMPOSTELA

2021

USC
UNIVERSIDADE
DE SANTIAGO
DE COMPOSTELA

DECLARACIÓN DEL AUTOR/A DE LA TESIS

D./Dña. **Martín Calvelo souto**

Título da tese: **Computational methods for the design and applications of self-assembled cyclic peptide nanotubes**

Presento mi tesis, siguiendo el procedimiento adecuado al Reglamento y declaro que:

1) La tesis abarca los resultados de la elaboración de mi trabajo.
2) De ser el caso, en la tesis se hace referencia a las colaboraciones que tuvo este trabajo.
3) Confirmo que la tesis no incurre en ningún tipo de plagio de otros autores ni de trabajos presentados por mí para la obtención de otros títulos.

Y me comprometo a presentar el Compromiso Documental de Supervisión en el caso que el original no esté depositado en la Escuela.

En **Santiago de Compostela**, **01 de febrero de 2021**.

Firma electrónica

AUTORIZACIÓN DEL TUTOR DE LA TESIS

[Computational methods for the design and applications of self-assembled cyclic peptide nanotubes]

D. Juan Ramón Granja Guillán

INFORMA:

Que la presente tesis, se corresponde con el trabajo realizado por D. Martín Calvelo Souto, bajo mi dirección, y autorizo su presentación, considerando que reúne los requisitos exigidos en el Reglamento de Estudios de Doctorado de la USC, y que como director de esta no incurre en las causas de abstención establecidas en la Ley 40/2015.

De acuerdo con lo indicado en el Reglamento de Estudios de Doctorado, declara también que la presente tesis doctoral es idónea para ser defendida en base a la modalidad de Monográfica con reproducción de publicaciones, en los que la participación del doctorando/a fue decisiva para su elaboración y las publicaciones se ajustan al Plan de Investigación.

En Santiago de Compostela, 12 de Febrero de 2021

AUTORIZACIÓN DEL DIRECTOR DE LA TESIS

[Computational methods for the design and applications of self-assembled cyclic peptide nanotubes]

D. Juan Ramón Granja Guillán
Dª. Rebeca García Fandiño

INFORMAN:

Que la presente tesis, se corresponde con el trabajo realizado por D. Martín Calvelo Souto, bajo mi dirección, y autorizo su presentación, considerando que reúne los requisitos exigidos en el Reglamento de Estudios de Doctorado de la USC, y que como director de esta no incurre en las causas de abstención establecidas en la Ley 40/2015.

De acuerdo con lo indicado en el Reglamento de Estudios de Doctorado, declara también que la presente tesis doctoral es idónea para ser defendida en base a la modalidad de Monográfica con reproducción de publicaciones, en los que la participación del doctorando/a fue decisiva para su elaboración y las publicaciones se ajustan al Plan de Investigación.

En Santiago de Compostela, 12 de Febrero de 2021

USC
UNIVERSIDADE
DE SANTIAGO
DE COMPOSTELA

Agradecementos

En primeiro lugar, gustaríame comezar agradecéndolle ós meus titores o seu esforzo, supervisión, trato persoal e confianza depositada en min para que este proxecto saíse adiante. A Juan, por darme a oportunidade de pertencer ó seu grupo e propoñerme ideas e retos que me fixeron avanzar e mellorar. Aínda que non son un químico experimental, sen a súa axuda e supervisión esta tese sería imposible. A Rebeca, "simplemente", por todo. Porque se non chega ser por ela, non me dedicaría a isto. Todo o que aprendín nestes anos foi gracias a ti. Aínda recordo a nosa primeira reunión para pedirche información sobre un posible TFG. Xa nese momento convencíchesme de que sería unha boa idea enrolarme neste campo (tiña pensado escoller outro proxecto!), e non me arrepinto, foi unha das mellores decisións da miña vida. Lévome desta experiencia os coñecementos e valores que me inculcaches, as ganas por seguir investigando, un sombreiro pirata e, sobre todo, a túa amizade. Son case oito anos baixo a túa supervisión, e aínda que agora veña un parón, estou seguro que seguirá perdurando.

Ós demais profesor que me axudaron nestes anos. Especialmente a Ángel Piñeiro, por actuar como o meu titor non oficial e resolverme máis de mil dúbidas (conteinas!).

A Javier Montenegro e Manuel Amorín, polos seus consellos e discusións nos seminarios.

Ós profesores do grupo de Química Teórica, especialmente a Saulo pola súa titorización no meu TFG e TFM, e Toño, polos seus consellos e incontables cafés.

Ó profesor José Luis Mascareñas e Fernando López, pola súa colaboración durante estes anos.

Gustaríame agradecer ás entidades financiadoras desta tese. En especial á Xunta de Galicia pola bolsa predoutoral (ED481A-2017/068). Tamén ós meus directores, por buscar liñas de finaciación

debaixo das pedras antes de conseguir a bolsa, e de novo ó grupo do profesor Mascareñas.

Ó profesor Mark S. P. Sansom e todo o seu grupo da Universidade de Oxford, en especial a Charlotte, por darme a oportunidade de realizar a miña estancia predoutoral alí e pola súa supervisión e colaboración.

A todas os colaboradores doutros grupos que axudaron en maior ou menor medida a que os proxectos nos que participei durante estes anos saíran adiante.

A toda a xente do grupo de Juan, Manuel e Javier, por facerme sentir sempre como un máis.

Ós meus compañeiros de despacho, tanto ós integrados no grupo de Química Teórica como ós do grupo de Rebeca. En especial a David e Iván, por tantos anos de convivencias. Deixo o despacho sendo, sen ningunha dúbida, o campión absoluto da escoba. Prometo deixarvos gañar algún día.

A Pablo, Andrea, Adrián, Hugo e Isaac pola vosa amizade dende sempre. Tamén a Alex, Xabi e Darío, polo tempo que compartimos en Santiago.

A toda a xente da que me puiden esquecer mentres escribo estas liñas. Non mo teñades en conta, a miña memoria é limitada. Compensareivos!

Á miña familia. En especial, por suposto, ós meus pais. Por todo o voso traballo e esforzo para permitirme estudar sen que me tivese que preocupar por absolutamente de nada. Por todo o que fixestes para darme esta oportunidade que vos non tivestes. Por educarme e converterme en quen son. Por todo o voso amor e apoio incondicional. Por ser os meus referentes. Tamén á miña avoa, por todo o seu cariño. E ós avós que xa non están aquí, pero que sempre están presentes.

E, por último, a Andrea. Polo día a día. Polo teu apoio sempre, de mar en mar. Por animarme sempre a mirar cara diante, non dar ningún paso atrás. Por ser ti, gracias por todo.

USC
UNIVERSIDADE
DE SANTIAGO
DE COMPOSTELA

USC
UNIVERSIDADE
DE SANTIAGO
DE COMPOSTELA

Index

USC
UNIVERSIDADE
DE SANTIAGO
DE COMPOSTELA

Abstract

During last decades, and enhanced by the development of the power of computers, Computational Chemistry has emerged as a powerful tool not only for complementing the work that experimental chemists carry out, but also for going beyond the limits of the laboratory. This PhD thesis presents an *in silico* study of the nanotubes composed by the self-assembly of disk-shaped cyclic peptides developed by the group of Prof. Juan R. Granja. These tubular-shape structures incorporate non-natural residues (γ- and δ-amino acids), which increases the versatility of these structures. *Via* Molecular Dynamic simulations and Quantum approaches, these systems have been evaluated, taking advantage of the atomic resolution that these techniques provide us. Using these computational methods, the most stable conformation of the nanotubes, as well as their possible application as transmembrane channels, antibiotic agents or molecule containers, have been systematically analysed. Altogether, this work is expected to provide light in the mechanism of formation and activity of these nanotubes in order to contribute to a more rational design following a *bottom-up* approach.

USC
UNIVERSIDADE
DE SANTIAGO
DE COMPOSTELA

List of publications

The results showed in this thesis are included in the following publications:

- Calvelo, M.; Lamas, A.; Guerra, A.; Amorin, M.; Garcia-Fandiño, R.; Granja, J. R. *Chem. – A Eur. J.* **2020**, *26*, 5846-5858. *Impact Factor (IF): 4.857*
- Pizzi, A.; Ozores, H. L.; Calvelo, M.; García-Fandiño, R.; Amorín, M.; Demitri, N.; Terraneo, G.; Bracco, S.; Comotti, A.; Sozzani, P.; Bezuidenhout, C. X.; Metrangolo, P.; Granja, J. R. *Angew. Chemie - Int. Ed.* **2019**, *58* (41), 14472–14476. *IF: 12.959*
- Calvelo, M.; Granja, J. R.; Garcia-Fandiño, R. *Phys. Chem. Chem. Phys.* **2019**, *21* (37), 20750–20756. *IF: 3.430*
- Calvelo, M.; Lynch, C.; Granja, J. R.; Sansom, M. S. P.; Garcia-Fandiño, R. *ACS Nano, accepted*. *IF: 14.588*
- Claro, B.; González-Freire, E.; Calvelo, M.; Bessa, L. J.; Goormaghtigh, E.; Amorín, M.; Granja, J. R.; Gracia-Fandiño, R.; Bastos, M. *Colloids and Surfaces B: Biointerfaces* **2020**, *196*, 111349. *IF: 4.389*
- Otero-Mato, J. M.; Montes-Campos, H.; Calvelo, M.; García-Fandiño, R.; Gallego, L. J.; Pineiro, Á.; Varela, L. M. *J. Chem. Theory Comput.* **2018**, *14* (2), 466-478. *IF: 5.313*

Note: **The work carried out by the author of this thesis (Martín Calvelo Souto) in those publications is the one described in this dissertation**. The affiliations of the other of authors are presented in the publications. The authorizations from the journals for the use the material of the publications in this thesis can be found in the following links:
https://www.wiley.com/network/researchers/latest-content/how-to-clear-permissions-for-a-thesis-or-dissertation
https://www.elsevier.com/about/policies/copyright/permissions
https://pubs.acs.org/pb-assets/acspubs/Migrated/dissertation.pdf
https://www.rsc.org/journals-books-databases/journal-authors-reviewers/licences-copyright-permissions/

In parallel to the studies presented in this dissertation, computational tools have also been applied to other chemical problems proposed through different collaborations. Thus, the study of organometallic reaction mechanisms using *DFT* methods, in collaboration with Prof. J. L. Mascareñas and F. López [Centro Singular de Investigación en Química Biolóxica e Materiais Moleculares (CiQUS), University of Santiago de Compostela], was carried out, leading to the following publications:

- Fernández, D. F.; Rodrigues, C. A. B. B.; Calvelo, M.; Gulías, M.; Mascareñas, J. L.; López, F. *ACS Catal.* **2018**, *8* (8), 7397–7402. *Impact Factor (IF): 12.221*
- Verdugo, F.; da Concepción, E.; Rodiño, R.; Calvelo, M.; Mascareñas, J. L.; López, F. *ACS Catal.* **2020**, *10* (14), 7710-7718. *Impact Factor (IF): 12.350*
- Nelson, R.; Calvelo, M.; García-Fandiño, R.; Lledós, A.; Ujaque, G.; Mascareñas, J. L.; López, F. *Chem. Sci.* **2020**, *11* (16), 4209–4220. *Impact Factor (IF): 9.346*

Additionally, using *Coarse-Grained* and *All-Atom* Molecular Dynamics and in collaboration with Prof. M. de la Fuente [Nano-Oncology and Translational Therapeutics Unit, Health Research Institute of Santiago de Compostela (IDIS), SERGAS, Santiago de Compostela], we pursued a computational approach to gain an improved understanding of the assembling, structure, dynamics, and drug-loading capacity of vitamin E–sphingomyelin nanosystems, using both small molecules and biomolecules (resveratrol, curcumin, gemcitabine, and two peptides), leading to the following publication:

- Bouzo, B. L.; Calvelo, M.; Martin-Pastor, M.; Garcia-Fandiño, R.; de la Fuente, M. *J. Phys. Chem. B* **2020**, *124* (28), 5788-5800. *Impact Factor (IF): 2.857*

Moreover, in collaboration with Prof. Á. Piñeiro (Departamento de Física de Aplicada, Facultade de Física, University of Santiago de Compostela) the behaviour of supramolecular complexes formed by cyclodextrins was studied, being tested eight different parameterizations of the GROMOS and AMBER force fields, including

several methods aimed to increase the conformational sampling in computational Molecular Dynamics simulation trajectories. This led to the following publication:

- F. Garrido, P.; Calvelo, M.; Garcia-Fandiño, R.; Piñeiro, Á. Rings, *Biomolecules* **2020**, *10* (3), 431. *Impact Factor (IF): 4.082*

Furthermore, and motivated by the health situation we are living nowadays, caused by the SARS-CoV-2 pandemic, two paper revisions focused on the use of cyclodextrins for COVID-19 treatments and the power of virtual reality to better understand the structure of the virus were carried out:

- Garrido, P. F.; Calvelo, M.; Blanco-González, A.; Veleiro, U.; Suárez, F.; Conde, D.; Cabezón, A.; Piñeiro, Á.; Garcia-Fandiño, R. *Int. J. Pharm.* **2020**, *588*, 119689. *Impact Factor (IF): 4.845*
- Calvelo, M.; Piñeiro, Á.; Garcia-Fandiño, R. *Comput. Struct. Biotechnol. J.* **2020**, *18*, 2621–2628. *Impact Factor (IF): 6.018*

Finally, we also contributed to the development of a number of apps for the visualization of different molecules using augmented or virtual reality:

- **Dimerdice:**
  For Android:
  https://play.google.com/store/apps/details?id=com.mduse.DimerDice&hl=en
  For iOS:
  https://apps.apple.com/app/dimer-dice/id1481408050#?platform=ipad
- **GADDLE Maps:**
  For Android:
  https://play.google.com/store/apps/details?id=com.mduse.GADDLEMAPS&hl=en
  For iOS:
  https://apps.apple.com/app/gaddle-maps-ar/id1311726695
- **Corona VRus coaster:** http://mduse.com/coronavruscoaster/

USC
UNIVERSIDADE
DE SANTIAGO
DE COMPOSTELA

Resumo

As enfermidades infecciosas son unha das principais causas de morte no mundo, afectando especialmente a nenos en países en desenvolvemento. Estas doenzas son provocadas por microorganismos que son capaces de transmitirse dende unha persoa a outra, tales como bacterias, virus ou outros parasitos. O seu control é crítico para o correcto funcionamento do mundo tal e como o coñecemos, sendo a pandemia provocada pola expansión do Covid-19 un exemplo actual da súa potencial mortalidade. Para levalo a cabo, é necesario o desenvolvemento de fármacos capaces de neutralizar ós axentes infecciosos externos de forma selectiva, deixando sen destruír o microbioma propio.

O descubrimento no ano 1928 da penicilina supuxo un fito na loita contra infeccións provocadas por bacterias, converténdose no primeiro antibiótico empregado na medicina moderna. Este feito provocou un auxe neste campo nos seguintes anos, permitindo o descubrimento de máis axentes eficaces. Non obstante, esta loita non está nin moito menos gañada, xa que as bacterias foron capaces de desenvolver por si mesmas estratexias para defenderse dos fármacos. Esta resistencia adquirida confírelles ás bacterias a capacidade de resistir os efectos dos antibióticos e facerse inmunes a eles. Aínda que se trata dun proceso natural coñecido, o mal uso e consumo abusivo de antibióticos tanto en persoas como en animais durante as últimas décadas está a acelerar este fenómeno ata velocidades máis que preocupantes. Se non somos capaces de reverter esta tendencia, estaremos condenados a un futuro sen ningún axente antibacteriano efectivo, un mundo no que operacións cirúrxicas que hoxe son rutineiras traerán consigo perigos imposibles de combater. Este futuro case distópico está máis próximo do que poderíamos imaxinar, xa que segundo a OMS (Organización Mundial da Saúde) no ano 2050 a maioría dos antibióticos presentes na actualidade non serán útiles, tan só 120 anos despois do descubrimento da penicilina. Deste xeito, o descubrimento de novos axentes

antibacterianos que suplan este baleiro preséntase como algo fundamental nas vindeiras décadas.

Coñecendo estes antecedentes, cómpre investigar antibióticos cuxo mecanismo de acción sexa distinto ós dos convencionais, agardando así superar os problemas relacionados coa resistencia antibacteriana. Unha alternativa interesante podería ser a utilización das membranas lipídicas como diana terapéutica, dado que a maioría de antibióticos actuais céntranse en dianas proteicas o nucleotídicas. Neste sentido, os péptidos antimicrobianos (AMPs, das súas siglas en inglés *Antimicrobial peptides*) emerxeron como potenciais candidatos para esta labor. É importante destacar que estes sistemas están presentes en multitude de organismos, actuando como unha das primeiras barreiras naturais en caso de infeccións. Non obstante, a vasta versatilidade inherente a estes AMPs, con infinidade de secuencias e tamaños, fai imposible o seu completo estudo e entendemento debido ó enorme custo tanto económico como de esforzo. Deste xeito, técnicas que permitan a redución de sistemas a probar, seleccionando unicamente aqueles que *a priori* terían unha mellor actividade, preséntanse como fundamentais.

Motivado polo desenvolvemento da ciencia da computación, o que permitiu o aumento da capacidade de cálculo de maneira exponencial, xunto co desenvolvemento de novos e mellores algoritmos, a química computacional emerxeu como unha poderosa ferramenta neste ámbito. Esta rama da química, en lugar de basearse nos clásicos experimentos de laboratorio, intenta entender e predicir o comportamento dos sistemas estudiados a través dun conxunto de ecuacións. Tradicionalmente, a química computacional dividiuse en dous bloques principais: un deles utilizando métodos cuánticos, baseados na ecuación de Schrödinger; e outro utilizando métodos clásicos, seguindo as leis de Newton do movemento. Os métodos cuánticos mostráronse como máis exactos, pero o seu alto coste computacional limitou o seu uso a sistemas relativamente pequenos, na escala dos centos de átomos. Por outra parte, os métodos clásicos, aínda que non tan precisos, amosáronse útiles para o estudo de sistemas máis grandes, na escala dos miles de átomos.

Os métodos anteriormente expostos poderían ser beneficiosos para o descubrimento de novos axentes antibacterianos. Dentro das múltiples posibilidades, esta tese centrouse no estudo de ciclopéptidos (CPs) formadores de nanotubos. Estes sistemas, teorizados por De Santis en 1974 e sintetizados por primeira vez polo grupo do Prof. Ghadiri no ano 1993, están formados por aminoácidos nos que se alternan os de quiralidad *D*- e *L*-, deixando unha cavidade interior baleira e orientando as cadeas laterais dos aminoácidos cara o exterior. Entre as posibles vantaxes que presentan estes sistemas con respecto ós naturais destaca a súa maior resistencia a proteólise, dado que son cíclicos e conteñen aminoácidos non naturais. Ademais, nos seguintes anos demostrouse que a versatilidade de estes CPs pode ser aumentada inserindo nas secuencias aminoácidos con unidades cíclicas de *cis-3-aminocycloalkanecarboxylic acid*, dando lugar ós α,γ-CPs; ou de *trans-4-aminocyclohexanecarboxylic acid*, resultando nos α,δ-CPs. Estes sistemas presentan por cada unidade cíclica un (α,γ-CPs) ou dous (α,δ-CPs) grupos metileno orientados cara o interior da cavidade, o que incrementa a súa hidrofobicidade alén de posibilitar a súa funcionalización interna. Do mesmo xeito, demostrouse que os CPs son capaces de ensamblarse por si mesmos a través de interaccións supramoleculares, dando lugar á formación de nanotubos (SCPNs, das súas siglas en inglés *Self-assembled Cyclic Peptides*), aproveitando que os osíxenos dos grupos carbonilo e os hidróxenos do grupo amida quedan orientados de maneira perpendicular ó plano dos CPs, o que facilita a formación de enlaces de hidróxeno entre distintas unidades e resultando nunha lámina β. Estas estruturas mostráronse útiles para tarefas de almacenaxe de moléculas e mais de catálise, alén de ser capaces de interactuar con membranas lipídicas. Esta interacción está dirixida polo carácter hidrofílico das cadeas laterais dos aminoácidos. Propúxose e demostrouse que os CPs formados completamente por cadeas hidrofóbicas deberían ensamblarse nas bicapas de forma perpendicular ó plano destas, dando lugar á formación de canais transmembrana. Pola contra, CPs con carácter anfipático, cunha cara hidrofóbica e outra hidrofílica, poden adoptar dúas orientacións: unha paralela e outra perpendicular á membrana. A adopción da orientación perpendicular prodúcese trala formación de macroporos compostos de

varios nanotubos, dependendo a súa aparición da existencia de interaccións estabilizantes que favorezan a formación destes agregados. Todas estas estruturas poderían mostrar actividade antibacteriana, a través da alteración do potencial eléctrico ou do transporte específico de determinadas moléculas, ou seguindo un mecanismos tipo alfombra (*carpet-like*) nos anfipáticos. É importante sinalar que o grupo no que se realizou a tese, dirixido polo Profesor Juan R. Granja, é pioneiro e referencia no uso e síntese destes sistemas, o que proporcionou un ambiente perfecto para o seu estudo en profundidade.

Nesta tese aplicáronse métodos da química computacional, tanto cuánticos como clásicos, para levar a cabo un exhaustivo estudo de estruturas supramoleculares formadas polo autoensamblaxe de CPs, as cales poderían ter potencial actividade antibacteriana. Ó longo dos capítulos que compoñen este traballo, distintos aspectos relacionados con estes sistemas foron avaliados, utilizando diferentes aproximacións computacionais cando fose necesario. Para unha maior claridade e seguimento máis sinxelo, esta tese estruturouse en tres seccións, utilizando en cada unha delas unha técnica computacional determinada.

Sección I: Nesta primeira parte da tese utilizáronse métodos cuánticos para o cálculo enerxético de diferentes estruturas, o que permitiría a obtención dos sistemas máis estables. No primeiro capítulo desta sección comparáronse distintos dímeros (estrutura formada polo autoensamblaxe de dous CPs), tratando de atopar que lámina β, a paralela ou a antiparalela, é a máis estable. Aínda que é coñecido que os CPs de Ghadiri, formados unicamente por aminoácidos α, dan lugar a nanotubos amosando preferentemente unha lámina β antiparalela, debido á novidade dos α,γ- e, sobre todo, dos α,δ-CPs, a orientación máis favorable destes non é tan clara. Deste xeito, este capítulo amósase como fundamental para ter un maior coñecemento das bases estruturais destes péptidos. A través da aplicación de cálculos DFT (das súas siglas en inglés *Density Functional Theory*), comezouse optimizando a xeometría de dímeros compostos por α,δ-CPs, cuxa interacción nun caso é unha lámina β paralela e noutro unha antiparalela. Para este primeiro estudo seleccionáronse dodecámeros como CPs, estando formados por seis α- e por seis δ-aminoácidos. Para impedir o crecemento do nanotubo, metilouse a cara que non participa na rede de

enlaces de hidróxeno. Esta aproximación permite a comparación con resultados obtidos na parte experimental do grupo, creando unha colaboración na que se aproveita a sinerxía entre técnicas *in silico* e *in vitro*. A maiores, utilizáronse alaninas como cadeas laterais dos aminoácidos α, o que permite excluír a súa interacción, considerando unicamente as interaccións pertencentes ó esqueleto dos péptidos.

Unha vez optimizadas as estruturas, obtivéronse as enerxías correspondentes a cada un dos dímeros, podendo observar que a orientación paralela é a máis estable. Esta observación foi corroborada experimentalmente, obtendo *in vitro* as mesmas conclusións. Non obstante, cómpre recordar que estes resultados foron obtidos sen considerar a influencia das cadeas laterais. Coa intención de avaliar o seu posible efecto, realizáronse cálculos cunha secuencia composta por unha leucina, dúas histidinas, un ácido glutámico (cargado negativamente), unha arxinina (cargada positivamente) e unha lisina (cargada positivamente). Neste caso, ó romperse a simetría do CP, aparecen posibles rotámeros (dímeros que se diferencian na rotación relativa dun dos CPs frente ó segundo, que se mantén fixo) que complican o estudo dos dímeros. Así, poderíanse formar tres dímeros paralelos e outros tres antiparalelos. Non obstante, unicamente se consideraron aqueles nos que *a priori* as repulsión entre cargas estiveran minimizadas, limitando o escenario a un dímero antiparalelo e dous paralelos. Ademais, o maior número de átomos deste CP obrigou ó cambio de nivel de cálculo usado na optimización das xeometrías, tendo que utilizar un método semiempírico, menos preciso pero menos esixente computacionalmente. O cálculo das enerxías correspondentes a cada dímero revela que o apilamento antiparalelo é o máis favorecida para estes sistemas, ó contrario do observado anteriormente. Este resultado suxire que aínda que as interaccións do esqueleto peptídico favorezan unha determinada lámina, é posible reverter esta tendencia a través da modulación da secuencia do CP.

Tralas anteriores observacións, decidiuse estender o estudo a dímeros compostos por α,γ-CPs. Dende a súa síntese no grupo do Profesor Juan R. Granja, asumiuse a formación dunha lámina antiparalela como a máis favorable, pero non existía un cálculo equivalente ó descrito para os α,δ-CPs. Deste xeito, realizáronse

cálculos análogos ós descritos anteriormente con hexámeros compostos por tres α- e por tres γ-aminoácidos. De novo, metiláronse os grupos amida das caras que non participan nos enlaces de hidróxeno, alén de utilizar alaninas como cadeas laterais. Porén, este tipo de CPs presentan un esquema máis complexo que os α,δ-, xa que os grupos carboxilo e amida de tódolos aminoácidos α están orientados cara a mesma dirección, mentres que os análogos das unidades γ apuntan cara a contraria. Este feito provoca a formación de dous dímeros antiparalelos distintos: un deles a través dunha interacción α-α, entre os aminoácidos deste tipo; e outra γ-γ. Así mesmo, tamén se considerou a formación dun dímero paralelo, cunha interacción α-γ. Trala optimización e cálculo enerxético vía DFT dos tres dímeros considerados, o paralelo amosouse como o máis favorable, de maneira contraria ó esperado. Estas observacións foron ratificadas pola parte experimental do grupo, o que supón un cambio de paradigma no futuro deseño destes CPs. É importante sinalar que estas conclusións obtivéronse considerando un só enantiómero do α,γ-CP, pero se se consideran os dous posibles ó mesmo tempo aparecen novas estruturas. Cálculos DFT suxiren que estas novas formas heterodiméricas tamén son posibles, aínda que non son tan favorables como o dímero paralelo formado por un só enantiómero. Así e todo, neste traballo é a primeira vez que se propoñen estes sistemas, o que incrementa ó número de posibles dímeros que se poden formar cando se deseñan nanotubos peptídicos con estes α,γ-CPs. Ademais, para unha visualización distinta dos resultados, desenvolveuse unha aplicación que mostra as estruturas anteriormente utilizadas en realidade aumentada, denominada *DimerDice* e dispoñible gratis no *Play Store* para dispositivos Android.

A continuación, analizouse o posible uso de estruturas formadas por estes CPs como contedores moleculares: estruturas capaces de atrapar outras moléculas máis pequenas no seu interior. Dependendo do tipo de CP, distintas moléculas hóspede foron consideradas, aproveitando o distinto diámetro interno e hidrofobicidade das cavidades. Deste xeito, utilizáronse dímeros formados por α,γ-CPs para encapsular gases nobres (Kr, Xe e Rn), alén de cloroformo. Este estudo xustifícase polo feito de que experimentalmente demostrouse que dímeros compostos por hexámeros de α,γ-CPs podían almacenar no seu

interior tanto Xe como cloroformo. Cálculos DFT mostraron que a encapsulación de tódolas especies consideradas é favorable, aínda que parece existir unha dependencia co tamaño, sendo a entrada de cloroformo á máis favorecida. Do mesmo xeito, mostrouse que os dímeros son capaces de distorsionarse para adaptar as súas xeometrías para facilitar a encapsulación.

No caso dos α,δ-CPs, avaliouse a entrada de fullerenos C_{60} e C_{70}. É importante sinalar que xa no primeiro traballo de síntese destes α,δ-nanotubos demostrouse que podían encapsular moléculas de C_{60} no seu interior. A través de optimizacións semiempíricas e cálculos enerxéticos utilizando DFT obtívose que a encapsulación de ambas moléculas é favorable. Como pasaba cos α,γ-CPs, os nanotubos foron capaces de deformarse para maximizar as interaccións coas moléculas hóspede. Posteriores cálculos demostraron que estes péptidos tamén son capaces de encapsular nanotubos de carbonos, dependendo esta interacción do seu tamaño. Para o CP utilizado, composto seis α- e por seis δ-aminoácidos, a encapsulación de nanotubos de carbono con diámetro 6,6 e 7,7 resultou a máis favorable.

Sección II: Na segunda sección da tese utilizáronse simulacións de Dinámica Molecular (MD) *All-Atom* (considerando tódolos átomos) para o estudo de SCPNs que posúen cadeas hidrofóbicas inseridos en membranas lipídicas. Anteriormente, demostrouse tanto experimental como computacionalmente que SCPNs formados por octámeros de α,γ-CPs son capaces de transportar catións ó seu través. Máis alá de bloquear a entrada de anións, non se demostrou selectividade significativa entre os distintos catións estudados (Li^+, Na^+, K^+, Cs^+ e Ca^{2+}). O seguinte paso foi introducir grupos funcionais no interior dos SCPNs, aproveitando a posibilidade de funcionalizar os γ-aminoácidos. Con esta idea, simuláronse vía MD α,γ-SCPNs funcionalizados con grupos hidroxilo, esperando que o aumento da polaridade mellorase a selectividade destes sistemas. Non obstante, este estudo revelou resultados moi similares ós nanotubos sen funcionalizar, o que abre a porta á utilización de grupos cargados. Deste xeito, no primeiro capítulo desta sección avaliouse a actividade de SCPNs formados por α,γ-CPs internamente funcionalizados con grupos carboxilo, tanto protonados como deprotonados, introducindo carga negativa neste segundo caso.

As simulacións realizadas demostraron que os péptidos cargados negativamente perdían a conformación tubular, aínda que o agregado amorfo resultante é capaz de atraer catións cara rexión hidrofóbica da membrana. No nanotubo protonado, polo contrario, aínda que mantivo a súa estrutura ó longo das simulacións, non se observou entrada de ningún catión, indicando que a introdución destes grupos funcionais reduce demasiado o diámetro do poro. Así e todo, estes resultados permiten suxerir a utilización destes α,γ-SCPNs funcionalizados como sistemas sensibles a un segundo estímulo externo (además da presencia ou ausencia da membrana): o pH. Deste xeito, en ambientes ácidos, nos que o SCPN estaría protonado, o nanotubo manteríase formado, pero sen transportar ningún ión, mentres que en ambientes básicos, a desprotonación do SCPN leva consigo a deformación do nanotubo e a entrada de catións na membrana.

O segundo capítulo desta sección centrouse no estudo de nanotubos compostos por α,δ-CPs, sendo o primeiro traballo con estes sistemas levado a cabo. A través de simulacións de MD, tratouse de elucidar se estes nanotubos serían estables inseridos nunha membrana lipídica. Como sistema de control, simulouse tamén un α,γ-SCPN seguindo o mesmo protocolo, xa que a súa estabilidade neste ambiente é coñecida. Do mesmo xeito, avaliouse a posible influencia que distintos modelos de auga poderían ter, realizándose cálculos con 4 parametrizacións distintas: os coñecidos e amplamente utilizados TIP3P e TIP4P, xunto con dúas aproximacións máis modernas: TIP4P/2005 e OPC. Os resultados obtidos salientan que os α,δ-SCPNs son estables na membrana, sen observarse diferencias estruturais entre os modelos de auga utilizados. Análogas conclusións foron obtidas tralo análise dos cálculos co α,γ-SCPN. Porén, si que se observan diferencias no comportamento das augas dentro dos nanotubos, xa que as augas TIP3P e TIP4P móvense máis e máis rápido cós outros dous modelos. Así mesmo, este maior movemento produce que o transporte de ións sexa maior con estes modelos de auga. Ademais, merece a pena salientar que nos α,δ-SCPNs, a diferencia dos sistemas α,γ-, observouse a entrada de anións cloruro no interior dos nanotubos, aínda que nunha escala menor que os catións.

Sección III: Na última sección da tese estudouse o auto ensamblaxe dos nanotubos en membranas lipídicas de diferente composición a través simulacións de MD utilizando resolución *Coarse-Grained*. Esta aproximación permite simular sistemas máis grandes durante escalas de tempo maiores, o que a converte nunha ferramenta moi útil para observar este tipo de procesos biolóxicos. Non obstante, hai que ter en conta que estas modificacións reducen a precisión dos cálculos. Para este estudo utilizáronse dous SCPNs compostos por CPs de Ghadiri distintos cunha secuencia de aminoácidos con carácter anfipático (**SCPN15** e **SCPN16**), as cales amosaron actividade antibacteriana anteriormente. En ambos casos a carga neta por CP é de +3. Nestas simulacións usáronse 4 modelos distintos de membrana, nas que se intentou imitar a composición de células mamíferas e bacterianas: DMPC, DMPC:DMPG (3:1), DMPE:DMPG (3:1) e DMPE:DMPG (1:9). Nunha primeira aproximación, dadas as limitacións deste método no que os enlaces de hidróxeno non están explicitamente descritos, engadíronse restricións nas distancias entre os átomos do esqueleto dos CPs, conxelando o SCPN para asegurarse que a forma tubular preservábase durante toda a simulación. Os resultados obtidos nesta primeira etapa mostraron a inserción espontánea de ambos nanotubos en tódalas membranas consideradas. Nestas simulacións, a parte hidrofóbica do SCPN queda orientada cara a membrana mentres que a cargada queda cara a fase acuosa, agás no caso de **SCPN15** na membrana DMPE:DMPG (1:9). Neste caso, o nanotubo muda a súa conformación, orientando os residuos hidrofóbicos á auga forzado pola interacción da cara catiónica do nanotubo coas cabezas polares dos fosfolípidos, seguramente provocado pola gran cantidade de cargas negativas presentes nesta membrana. Nunha segunda etapa, e partindo da última estrutura dos cálculos anteriores, estendéronse as simulacións eliminando as restricións, có obxectivo de avaliar a estabilidade do nanotubo na membrana. Os resultados obtidos mostran que a presenza de lípidos DMPE provocan a perda da estrutura tubular do **SCPN15**.

Por último, avaliouse a utilidade dunha ferramenta que permite a transformación de estruturas entre diferentes resolucións (*All-atom* e *Coarse-Grained*) chamada *Gaddle Maps*. Utilizando esta ferramenta,

realizouse unha simulación multiescala cun SCPN anfipático en presenza dunha membrana lipídica, comezando cun cálculo *Coarse-Grained*, co cal se observou a inserción na membrana, para posteriormente transformase en *All-atom* para aproveitar a súa maior precisión, obtendo resultados prometedores.

En xeral, este traballo foi realizado coa intención de axudar no entendemento dun posible candidato para ser usado como ferramenta antibacteriana: os SCPNs. Nesta tese estudáronse diferentes parámetros estruturais e dinámicos destes sistemas, alén do seu comportamento en posibles aplicacións. O coñecemento xerado pode ser utilizado para axudar a futuros deseños máis eficientes e racionais destes sistemas.

1. Introduction

1.1. NANOTECHNOLOGY AND SUPRAMOLECULAR CHEMISTRY.

"There's Plenty of Room at the Bottom." Richard Feynman.

The 29th of December of 1959 meant a milestone in the word of the Science. In his lecture entitled "There's Plenty of Room at the Bottom: An Invitation to Enter a New Field of Physics" during the annual meeting of the American Physical Society at the California Institute of Technology (Caltech) in Pasadena, Richard Feynman inspired the birth of a new field in science: *Nanotechnology*.[1] Although the word "Nanotechnology" was not mentioned until 1974 by the Prof. Taniguchi, Feynman spoked about miniaturization, electric motors of the size of a nail and writing the whole entire Encyclopaedia Britannica on the head of a pin, being remarkable that he claimed that all these revolutionary ideas could be done starting from previously known physical phenomena.[2] His ideas about computers composed by wires with a diameter of 10 or 100 atoms at a time when a single computer could fill a whole room, as well as the direct manipulation of individual atoms, encouraged the development of nanotechnology. Feynman took as reference the cells: they are very tiny but, at the same time, very active, being able to manufacture other molecules, move by themselves or store information. Other authors, like K. Eric Drexler, also pointed in the same direction with his vision about *molecular self-replicators*.[3]

1. Feynman, R. In *Engineering and Science*; 1959; Vol. 23 (5), pp 22–36.
2. Taniguchi, N. In *Proceedings of the International Conference on Production Engineering, Tokyo, Part II, Japan Society of Precision Engineering*; 1974; pp 18–23.
3. Drexler, K. E. *Proc. Natl. Acad. Sci. U. S. A.* **1981**, *78* (9 I), 5275–5278.

Later on, during the 80's, this field took off thanks to the invention of the Scanning Tunnelling Microscope (STM) and the Atomic Force Microscope (AFM), as well as the breakthrough of materials in the nanometer scale, like carbon nanotubes.[4–6]

Nanotechnology is often defined as the science which studies matter at scales in between 1 to 100 nm (nanostructures). This field has become very popular during last decades, producing a high impact on several industrial and research areas, and being nowadays present in a wide variety of commonly used items. Actually, it is still nowadays one of the hottest topics in science, as it has been shown with the Nobel Prize in Chemistry award to Bernard Feringa, Sir Fraser Stoddart and Jean-Pierre Sauvage in 2016 for "the design and synthesis of molecular machines". Current research in nanotechnology is focused on nanostructured materials and nanodevices, as well as techniques and methods for their synthesis. Regarding the design of nanostructures, we can distinguish between top-down and *bottom-up* approaches:

Top-down approach is the physical process most used in the industry nowadays due to its relatively simple concept. It is based on going from big structures towards nanocompounds, reducing systematically their size until the obtainment of the desired dimensionality. The most common techniques employed for the fabrication of nanostructures in this approach are photon or electron beam lithography.[7] One example of the use of a top-down approach is the preparation of metal-oxide-semiconductor Field-effect transistors (MOSFETs) through the previous mentioned lithography processes.

4. Binnig, G. et al. *Surf. Sci.* **1983**, *126*, 236–244.
5. Binnig, G. et al. *Phys. Rev. Lett.* **1986**, *56* (9), 930–933.
6. Kroto, H. W. et al. *Nature* **1985**.
7. Hashemi, P. *Gate-All-Around Silicon Nanowire MOSFETs: Top-down Fabrication and Transport Enhancement Techniques*; Massachusetts Institute of Technology, 2010.

The strategy adopted in *bottom-up* approaches, however, is the opposite: starting from small molecules or atoms, the idea is to enhance their assembly and organization through chemical methods in order to obtain the desired nanostructures. This approach is present in Nature, being known that a huge number of biological structures are formed by the self-assembly of smaller molecules. This process has been widely studied by scientists, trying to reproduce and mimic this self-organization, enhancing the development of a number of fields like chemical vapor deposition, electroplating or *supramolecular chemistry*.[8]

In its modern sense, we can broadly define supramolecular chemistry as "the chemistry beyond the molecule" or "nonmolecular chemistry". Jean-Marie Lehn, Nobel Prize laureated in Chemistry together with Donald Cram and Charles Pedersen in 1987 for "their development and use of molecules with structure-specific interactions of high selectivity", defined supramolecular chemistry as "the chemistry of molecular assemblies and of the intermolecular bond".

Supramolecular compounds are formed through a series of noncovalent interactions, being the most common the following ones:

- *Hydrogen bonds (H-bonds)*: This kind of interaction, firstly proposed by Linus Pauling in 1931, is defined by IUPAC as "a form of association between an electronegative atom and a hydrogen atom attached to a second, relatively electronegative atom. It is best considered as an electrostatic interaction, heightened by the small size of hydrogen, which permits proximity of the interacting dipoles or charges".[9,10] We could represent it schematically as a hydrogen linked to an atom A interacting with an atom B: A---H···B. It is highly directional, depending its strength on the geometry of the donor (A---H) and the acceptor (B), resulting into preferred orientations. Angles from 90º until 180º can be adopted, as well as a wide range of lengths (approx. 1 to 3 Å).

8. Kanani, N. *Electroplating: Basic Principles, Processes and Practice*; Elsevier Ltd, 2005.
9. Pauling, L. *J. Am. Chem. Soc.* **1931**, *53* (4), 1367–1400.
10. Muller, P. *Pure Appl. Chem.* **1994**, *66* (5), 1077–1184.

Regarding energies, for breaking the weakest H-bonds around 10 kJ mol^{-1} are required, and between 60 and 120 kJ mol^{-1} for the strongest. The differences in energies are coming from the partially covalent character of the strong H-bonds, whereas the weak ones present an electrostatic nature. In between them, we can speak about "moderate" H-bonds, which are also mainly electrostatic, but not completely.

- *Electrostatic interactions*: Formed by the interaction of two ions, these are the strongest non-covalent interactions, with energies required for its dissociation from 100 to 350 kJ mol^{-1}. They result from the attraction between ions with opposite charge, being, in this case, a nondirectional interaction.
- *π-π stacking*: It is coming from the interaction between aromatic surfaces. It plays a crucial role in biological systems, as it is shown in the DNA structure, with the piling among nucleobases (although it is worth to mention that the recognition between pairs is coming from H-bonds). Since it is mandatory that the aromatic rings adopt an optima conformation (one ring placed parallel over other), π-π stacking is considered a directional interaction. The range of energies comes from 2 up to 50 kJ mol^{-1} when a T-shape interaction is considered.
- *Van der Waals forces*: It is formed by the interaction between one nucleus and an induced dipole produced by the polarization of its electron cloud due to the proximity of the nucleus. It is also worth to mention the London dispersion forces, produced by the attraction of two non-polar molecules due to the formation of induced dipoles. Since the nature of this interaction is electrostatic, it does not present directionality. This type of intermolecular force is considered the weakest, being usually the energies smaller than 5 kJ mol^{-1}. However, it is worth to mention that this force is additive, resulting in quite interesting effects as the adhesive capability of geckos.[11,12]

11. Autumn, K. et al. *Nature* **2000**, *405* (6787), 681–685.
12. Autumn, K. et al. *Proc. Natl. Acad. Sci. U. S. A.* **2002**, *99* (19), 12252–12256.

- *Cation-π and anion-π interactions*: This interaction involves an ion (cation or anion) with aromatic compounds. Cations are able to interact with the π-electron density, leading to its binding. A bit more counterintuitive is the analogous interaction with anions, but it has been shown that they could interact with aromatic rings bearing electron withdrawing groups.[13] This interaction can be considered as electrostatic and nondirectional, including a range of energies from 5 to 80 kJ mol^{-1}.
- *Ion/Dipole-dipole interactions*: Formed by the attraction between an ion and a polar molecule thanks to the dipole moment of the second one, this electrostatic interaction covers a wide range of energies, from 5 to 200 kJ mol^{-1}. It is also possible to find this interaction between two polar molecules, without the presence of an ion, due to the interaction between both dipoles. Furthermore, we can observe a certain degree of directionality due to the presences of the dipoles.
- *Halogen bonds*: Proposed by Metrangolo and Resnati in the 90s, this interaction is defined by IUPAC as the attraction between an electrophilic moiety of a halogen bond and a nucleophilic entity.[14,15] Although it is possible to find examples up to 200 kJ mol^{-1}, the most common range is in between 10 and 50 kJ mol^{-1} and presents directionality. In the last years, halogen bonds have also found interestingly application in supramolecular chemistry.[16]
- *Metal-ligand interactions*: Although it is a covalent bond, their versatility and the possible interaction with the non covalent ones has made them well used in supramolecular chemistry. It can be found in the coordination bonds between transition metals complexes with different ligands, being especially important in inorganic chemistry as well as for catalysis purposes. It is very directional and the geometry that the complex adopts is defined by the available geometries allowed by the metal.

13. Mascal, M. et al. *J. Am. Chem. Soc.* **2002**, *124* (22), 6274–6276.
14. Metrangolo, P. et al. *Science.* **2008**, *321* (5891), 918–919.
15. Gilday, L. C. et al. *Chem. Rev.* **2015**, *115* (15), 7118–7195.
16. Benz, S. et al. *Chem. Sci.* **2017**, *8* (12), 8164–8169.

Its typical range of energies goes from 100 kJ mol^{-1} up to 300. It is also worth to mention that closed-shell metals are also able to interact between them, as we can find in gold or silver nanoparticles.[17]

- *Dynamic covalent bonds*: Although in supramolecular chemistry non covalent interactions are the most common, it is also possible to find a kind of covalent bonds that can be reversed, allowing their use in the building of supramolecular assemblies with kinetic stability. Whereas in classical synthesis the reactions are performed under kinetic control, being the selectivity among different species determined by thermodynamics, in this case the control of the reactions is done through thermodynamic factors, as in the typical non covalent synthesis. Its interest comes from the possibility of linking covalently two molecules and, under certain conditions, reverse the process and divide them. As it is a covalent interaction, the energy needed for breaking these bonds is higher than in all of the previous intermolecular interactions. Transaminations or hydrazone and oxime exchanges are typical reversible reactions in this chemistry, as well as the use of boronic acid or disulfide bonds.[18,19]

The origin of supramolecular chemistry is widely related with host-guest interactions, being the discovery of the clathrate hydrates in 1778 probably the first example.[20] These molecules are crystalline structures based on water, similar to ice, but with hydrophobic cavities where gas molecules can be trapped. Also, the breakthrough made by Emil Fisher, suggesting that the binding between molecules should be selective, introducing the *lock and key* concept, as well as the discovery in 1891 of the cyclodextrins (CDs), cyclic oligosaccharides with an internal cavity, are another milestone in this field.[21–23]

17. Pyykkö, P. *Chem. Rev.* **1997**, *97* (3), 597–636.
18. Yoon, J. et al. *J. Am. Chem. Soc.* **1992**, *114* (14), 5874–5875.
19. Louzao, I. et al. *J. Mater. Chem. B* **2017**, *5* (23), 4426–4434.
20. Partington, J. R. *Nature* **1933**, *131* (3306), 348–350.
21. Fischer, E. *Berichte der Dtsch. Chem. Gesellschaft* **1894**, *27* (3), 3479–3483.
22. Crini, G. *Chem. Rev.* **2014**, *114* (21), 10940–10975.
23. Villiers, A. *Compt. Rend. Acad. Sci* **1891**, *112*, 536–538.

However, supramolecular chemistry is nowadays understood not just as an interaction between a host and a guest molecule, but also including self-assembly processes.[24] In this sense, it is worth to mention that this phenomenon was described firstly in 1774, when Benjamin Franklin recognized the self-organization of monolayers after spreading oil in water.[25,26]

Since then, at the same time that our knowledge about supramolecular chemistry rules was increasing, our understanding of biological nanostructures was also improving.[27] Nature provides many examples of self-assembled and self-organized structures, although at first sight it could seem counterintuitive due to its inherent entropic cost. A wide range of proteins, virus or DNA and RNA complexes are made up of the spontaneous grouping of smaller subunits through supramolecular interactions. Among others, peptides result particularly interesting.[28–31] The combination of the 20 natural amino acids could provide us different structures with a wide range of possible applications. In addition, the vast number of existing works studying this kind of molecules allow a very helpful background in current research. One example could be the study of amphiphilic peptides, composed by a balanced ratio between hydrophobic and charged residues, which have shown a good antimicrobial activity, especially when they adopt a helical conformation.[32,33] These structures are usually called *Antimicrobial Peptides* (AMPs), becoming one of the hottest topics nowadays.[34,35]

24. Whitesides, G. M. et al. *Science.* **2002**, *295* (5564), 2418–2421.
25. Franklin, B. et al. *Philos. Trans. R. Soc. London* **1774**, *64*, 445–460.
26. Whitesides, G. M. et al. *Science.* **1991**, *254* (5036), 1312–1319.
27. Mann, S. *Angew. Chemie - Int. Ed.* **2008**, *47* (29), 5306–5320.
28. Kent, S. B. H. *Chem. Soc. Rev.* **2009**, *38* (2), 338–351.
29. Hughes, A. B. *Amino Acids, Peptides and Proteins in Organic Chemistry*; Hughes, A. B., Ed.; Wiley-VCH: Weinheim, Germany, 2011; Vol. 5.
30. Kuan, S. L. et al. *Chem. Soc. Rev.* **2018**, *47* (24), 9069–9105.
31. Yuan, C. et al. *Nat. Rev. Chem.* **2019**, *3* (10), 567–588.
32. Sitaram, N. et al. *Curr. Pharm. Des.* **2002**, *8* (9), 727–742.
33. Papagianni, M. *Biotechnol. Adv.* **2003**, *21* (6), 465–499.
34. Chen, C. H. et al. *Antibiotics* **2020**, *9* (1).
35. Kang, X. et al. *Sci. data* **2019**, *6* (1), 148.

More detailed information about supramolecular chemistry, reporting more examples and explaining more carefully its basis, can be found in the literature.[36]

1.2. NANOSTRUCTURES BASED ON THE SELF-ASSEMBLY OF CYCLIC PEPTIDES.

"If we knew what it was we were doing, it would not be called research, would it?" Albert Einstein.

Among other examples, tubular assemblies are known to develop an important number of biological functions. One of the most remarkable is their role in the transport of ions and molecules, taking advantage of the presence of a hollow in its inner part.[37,38] In addition, tubular structures are also interesting due to their application in other fields, as catalysis, separation, optics, electronics, drug delivery and antimicrobial and anticancer treatments.[39–46] Some proteins are able to adopt a tubular shape and develop similar functions.[47,48] A number of them are present in Nature, as the potassium and chloride channels, β-barrels pores, hemolysin or aquaporins.[49–54] Supramolecular chemists

36. Chierotti, M. R. et al. *Supramolecular Chemistry: From Molecules to Nanomaterials*; 2012.
37. Choi, W. et al. *Nat. Commun.* **2013**, *4* (1), 1–8.
38. Farshad, M. et al. *J. Phys. Chem. B* **2020**, *124* (6), 937–943.
39. Kang, S. et al. *Langmuir* **2008**, *24* (13), 6409–6413.
40. Madani, S. Y. et al. *Int. J. Nanomedicine* **2011**, *6*, 2963–2979.
41. Ye, Y. et al. *Crit. Rev. Solid State Mater. Sci.* **2012**, *37* (2), 75–93.
42. Lamanna, G. et al. *Nanoscale* **2013**, *5* (10), 4412–4421.
43. Yan, Y. et al. *Chem. Soc. Rev.* **2015**, *44* (10), 3295–3346.
44. Karatas, A. et al. *Curr. Top. Med. Chem.* **2017**, *17* (13), 1555–1563.
45. Jiao, Y. et al. *Adv. Energy Mater.* **2018**, *8* (15), 1702779.
46. Jawed, A. et al. *J. Water Process Eng.* **2020**, *33*, 101009.
47. Kashiwagi, D. et al. *J. Am. Chem. Soc.* **2018**, *140* (1), 26–29.
48. Thomas, F. et al. *ACS Synth. Biol.* **2018**, *7* (7), 1808–1816.
49. Song, L. et al. *Science.* **1996**, *274* (5294), 1859–1866.
50. Szewczyk, A. *Mol. Membr. Biol.* **1998**, *15* (2), 49–58.
51. Fairman, J. W. et al. *Curr. Opin. Struct. Biol.* **2011**.
52. Noinaj, N. et al. *Nature* **2013**, *501* (7467), 385-390.
53. Day, R. E. et al. *Biochim. Biophys. Acta - Gen. Subj.* **2014**.
54. Verkman, A. S. et al. *Nat. Rev. Drug Discov.* **2014**, *13* (4), 259–277.

have been trying to propose new synthetic structures which could mimic the behaviour of the natural ones, as well as developing functions not observed in Nature.[55–59]

Tubular structures can be made up of different building blocks.[60] Nanotubes formed by the self-assembly of helical molecules, as DNA, or adopting a rod-like conformation have been reported.[61] One interesting category comprises those formed by the stacking of planar cyclic units, similar to disks, which allow to control the size of the inner diameter of the nanotube. Examples of these subunits are the macrocycles composed of urea proposed by Shimizu, the arylene ethynylene macrocycles of Moore or the rings containing Pt_4 designed by MacLachlan.[62–64] Nanotubes composed by the assembly of cyclodextrins can be also included in this field due to the cyclic shape of these molecules, although in this case they are not flat.[65] However, it is known that peptide motifs could be good candidates for the production of nanotubular structures because of their presumably biocompability and dynamic behaviour.[66–68] Following this strategy, the use of cyclic peptides as building blocks for the formation of nanotubes has been proposed as highly promising.[69,70]

55. Matile, S. *Chem. Soc. Rev.* **2001**, *30* (3), 158–167.
56. Fyles, T. M. *Chem. Soc. Rev.* **2007**, *36* (2), 335–347.
57. García-Fandiño, R. et al. *Proc. Natl. Acad. Sci. U. S. A.* **2012**, *109* (18), 6939–6944.
58. Alfonso, I. et al. *Chem. Sci.* **2013**, *4* (8), 3009–3019.
59. Chen, J. Y. et al. *Org. Chem. Front.* **2018**, *5* (10), 1728–1736.
60. Bong, D. T. et al. *Angew. Chemie Int. Ed.* **2001**, *40* (6), 988–1011.
61. García-Fandiño, R. et al. In *Supramolecular Chemistry*; John Wiley & Sons, Ltd: Chichester, UK, 2012.
62. Shimizu, L. S. et al. *J. Am. Chem. Soc.* **2003**, *125* (49), 14972–14973.
63. Balakrishnan, K. et al. *J. Am. Chem. Soc.* **2006**, *128* (20), 6576–6577.
64. Frischmann, P. D. et al. *J. Am. Chem. Soc.* **2010**, *132* (22), 7668–7675.
65. Yun, M. et al. *J. Polym. Sci. Part A Polym. Chem.* **2010**, *48* (3), 730–734.
66. Hamley, I. W. *Angew. Chemie - Int. Ed.* **2014**, *53* (27), 6866–6881.
67. Rodríguez-Vázquez, N. et al. *Org. Biomol. Chem.* **2017**, *15* (21), 4490–4505.
68. Brea, R. J. et al. *Chem. Soc. Rev.* **2010**, *39* (5), 1448–1456.
69. Chapman, R. et al. *Chem. Soc. Rev.* **2012**, *41* (18), 6023–6041.
70. Hsieh, W. H. et al. *J. Food Drug Anal.* **2019**, *27* (1), 32–47.

The first self-assembled cyclic peptide nanotubes (SCPNs) were synthetized by Ghadiri in 1993, almost 20 years after being firstly proposed by De Santis in 1974.[71,72] These cyclic peptides (CPs) were formed by a combination of alternating *D*- and *L*-amino acid residues, which are able to stack through H-bonds. The diameter is controlled by the number of amino acids that composes the cyclic structure. CPs adopt a flat conformation, leaving the oxygens of the carbonyl groups (C=O) and the hydrogens of the amide groups (NH) perpendicular to the CP plane, allowing the formation of H-bonds between these groups of two different units, acquiring a β-sheet disposition (**Figure 1**). The C=O and the NH groups from the residues with same chirality are pointing to the same direction, making the two faces of the CP not identical. In addition, the lateral chains of the amino acids are oriented outwards, allowing the modulation of the external character of the nanotube.

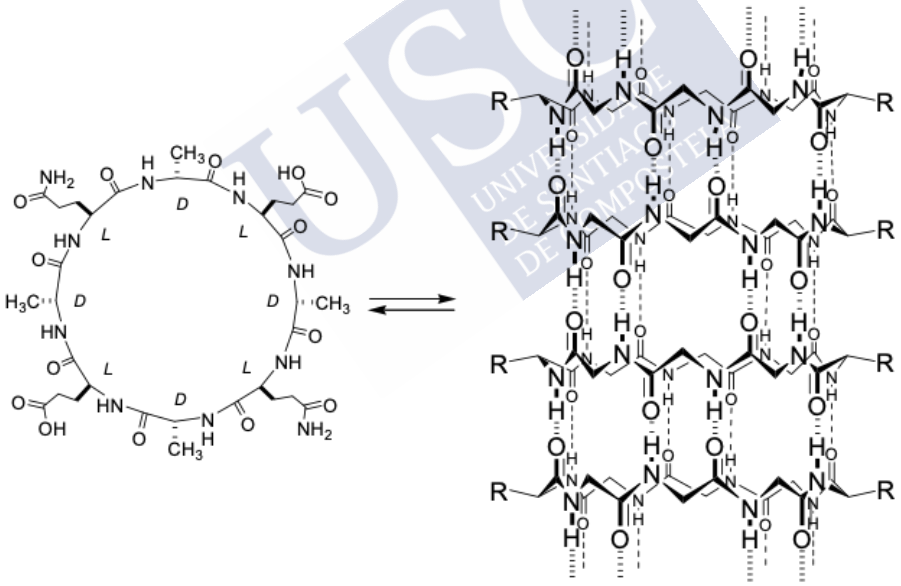

***Figure 1.** Schematic representation of a D,L-α-CP and their corresponding assembling into a SCPN.*

71. De Santis, P. et al. *Macromolecules* **1974**, *7* (1), 52–58.
72. Ghadiri, M. R. et al. *Nature* **1993**, *366* (6453), 324–327.

In 1994, Ghadiri's group showed the first SCPN which could self-assembly in a lipid bilayer acting as a transmembrane channel selecting CPs composed by hydrophobic side-chains, as Leu or Trp.[73] This fact opens the door to the modulation of the interaction of SCPNs with membranes depending on the sequences of the CPs. In other words, varying the hydrophobic/hydrophilic character of the CPs sequences, SCPNs could adopt different orientations in a lipid bilayer (**Figure 2**). It has been suggested that when CPs are formed by hydrophobic sequences they are able to self-assembly in a lipid membrane forming a tubular structure, acquiring a perpendicular position and acting as transmembrane proteins, as Ghadiri proposed (**Figure 2***A*). This fact could make possible to use them as ion or molecule channels.[74–77]

The introduction of charged amino acids changes the orientation of the SCPNs in the membrane. Whereas fully hydrophobic sequences form single channels, substituting amino acids of the same chirality by charged side-chains, resulting in an alternation between hydrophobic and hydrophilic residues, leads to the aggregation of the SCPNs, forming larger pores following a barrel stave model (**Figure 2***B*).[78]

Another proposed conformation comes from the use of amphipathic CPs, which have one hydrophilic face and another hydrophobic. In this case, the CPs self-assemble in a parallel orientation to the membrane, showing good antimicrobial activity, presumably following a carpet-like mechanism (**Figure 2***C*).[79–83]

73. Ghadiri, M. R. et al. *Nature* **1994**, *369* (6478), 301–304.
74. Kim, H. S. et al. *J. Am. Chem. Soc.* **1998**, *120* (18), 4417–4424.
75. Sánchez-Quesada, J. et al. *J. Am. Chem. Soc.* **2002**, *124* (34), 10004–10005.
76. Montenegro, J. et al. *Acc. Chem. Res.* **2013**, *46* (12), 2955–2965.
77. Granja, J. R. et al. *J. Am. Chem. Soc.* **1994**, *116* (23), 10785–10786.
78. Danial, M. et al. *Org. Biomol. Chem.* **2015**, *13* (8), 2464–2473.
79. Fernandez-Lopez, S. et al. *Nature* **2001**, *412* (6845), 452–455.
80. Dartois, V. et al. *Antimicrob. Agents Chemother.* **2005**, *49* (8), 3302–3310.
81. Motiei, L. et al. *Chem. Commun.* **2009**, No. 25, 3693–3695.
82. Huang, M. L. et al. *European J. Org. Chem.* **2013**, *2013* (17), 3560–3566.
83. Richman, M. et al. *J. Am. Chem. Soc.* **2013**, *135* (9), 3474–3484.

During last decades, these SCPNs have been deeply studied, showing promising results in different fields as drug delivery, anticancer treatments or material science.[84–89]

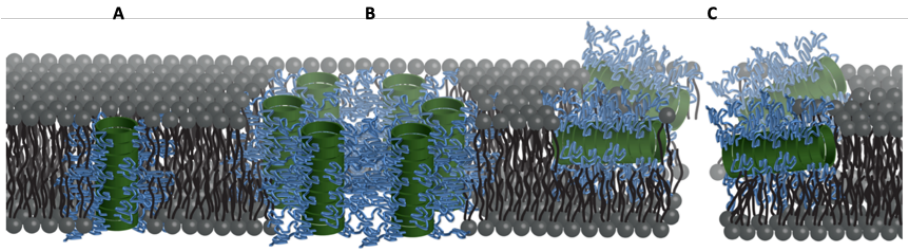

***Figure 2.** Different modes of lipid bilayer disruption shown by SCPNs: A) Unimeric channel, B) Barrel stave and C) Carpet-like. Image was taken from J. Am. Chem. Soc. **2014**, 136, 22, 8018-8026*

Since their discovery up to now, different designs using different combinations and types of amino acids have been considered.[68,69,90] Particularly engaging is the use of non-natural amino acids, since it opens the door to new SCPNs with other behaviours apart from those made up of just standard residues.[91] In 2014, based on this strategy, Perrier's group designed a series of thermosensitive CP-polymer conjugates whose transport activity could be controlled changing the temperature.[92] In this approach, a series of polymeric substituents was used as side-chains, allowing the preparation of different structures whose properties depend on the polymer employed. This group was also able to develop a SCPN having two faces with different properties.[93] Another contribution to this area was made by the group

68. Brea, R. J. et al. *Chem. Soc. Rev.* **2010**, *39* (5), 1448–1456.
69. Chapman, R. et al. *Chem. Soc. Rev.* **2012**, *41* (18), 6023–6041.
84. Hartgerink, J. D. et al. *J. Am. Chem. Soc.* **1996**, *118* (1), 43–50.
85. Xu, T. et al. *ACS Nano* **2011**, *5* (2), 1376–1384.
86. De La Rica, R. et al. *Adv. Funct. Mater.* **2011**, *21* (6), 1018–1026.
87. Chen, J. et al. *Nanoscale* **2016**, *8* (13), 7127–7136.
88. Larnaudie, S. C. et al. *Biomacromolecules* **2017**, *19* (1), 239–247.
89. Zhao, Y. et al. *ACS Cent. Sci.* **2017**, *3* (6), 639–646.
90. Fuertes, A. et al. *Chem. Commun.* **2017**, *53* (56), 7861–7871.
91. Drienovská, I. et al. *Nat. Catal.* **2020**, *3* (3), 193–202.
92. Danial, M. et al. *J. Am. Chem. Soc.* **2014**, *136* (22), 8018–8026.
93. Danial, M. et al. *Nat. Commun.* **2013**, *4* (1), 1–13.

of Schmuck, showing that incorporating a non-natural arginine analogue into a CP was able to form a positively charged nanofiber capable of transfecting genes.[94]

An especially attractive strategy was proposed by Prof. Juan Granja, from Santiago de Compostela University. It is based on the substitution of α-amino acids by a cycloalkyl-like amino acid residues (cis-3-aminocycloalkanecarboxylic acid, γ-Acas) of equivalent chirality, resulting in the formation of α,γ-CPs (**Figure 3**).[95] In the original design the γ-units were alternated with α-residues. The chirality of these residues has to be precisely controlled to ensure the planarity of the CP. Therefore, the 1*R*,3*S*-Acas has to be alternated with *D*-α-residues. One interesting feature of this approach is that one methylene moiety of the γ-residues is oriented inwards, increasing the hydrophobicity of the lumen of the SCPN. In addition, this inner cavity can be modulated by chemical modification of these methylene groups.[96–99] During last years, several studies on these systems have been carried out, exploring different possible applications.[68,100–104] Other analogous systems have been suggested so far, as the proline-derivative α,γ-CPs proposed by Kubik and Goddard or the ones made up of fluorinated sugar amino acids developed by the group of Dhavale, which were able to form SCPNs with properties to transport anions.[105,106]

68. Brea, R. J. et al. *Chem. Soc. Rev.* **2010**, *39* (5), 1448–1456.
94. Li, M. et al. *Angew. Chemie Int. Ed.* **2016**, *55* (2), 598–601.
95. Amorín, M. et al. *J. Am. Chem. Soc.* **2003**, *125* (10), 2844–2845.
96. Reiriz, C. et al. *Org. Biomol. Chem.* **2009**, *7* (21), 4358–4361.
97. Rodríguez-Vázquez, N. et al. *Chem. Sci.* **2016**, *7* (1), 183–187.
98. Rodríguez-Vázquez, N. et al. *Angew. Chemie Int. Ed.* **2016**, *55* (14), 4504–4508.
99. Guerra, A. et al. *Org. Biomol. Chem.* **2012**, *10* (44), 8762–8766.
100. Rodriguez-Vazquez, N. et al. *Curr. Top. Med. Chem.* **2015**, *14* (23), 2647–2661.
101. Reiriz, C. et al. *J. Am. Chem. Soc.* **2009**, *131* (32), 11335–11337.
102. Montenegro, J. et al. *J. Am. Chem. Soc.* **2014**, *136* (6), 2484–2491.
103. Cuerva, M. et al. *ACS Nano* **2015**, *9* (11), 10834–10843.
104. Fuertes, A. et al. *Nanoscale* **2017**, *9* (2), 748–753.
105. Kubik, S. et al. *Angew. Chem. Int. Ed. Engl.* **2001**, *40* (14), 2648–2651.
106. Burade, S. S. et al. *Org. Lett.* **2017**, *19* (21), 5948–5951.

Later on, the group of Prof. Granja proposed another class of cyclic structure: α,δ-CPs (**Figure 3**).[107] In this case, a trans-4-aminocyclohexanecarboxylic acid (δ-Ach) is inserted between each residue of *D*,*L*-α-CPs. These α,δ-CPs form SCPNs with larger internal diameters where each δ-amino acid projects two methylene groups towards the lumen of the nanotube, increasing the hydrophobicity and, potentially, the number of positions that can be functionalized.

The ambitious challenge of understanding the mechanisms of action of these and other nanostructures would require atomic resolution, which is still unattainable by most experimental techniques known today. Furthermore, it is important to remember that the majority of functional biochemical systems are not static. Only by visualizing molecules in action it is possible to anticipate and understand how structure and function are related. To fully understand these processes at the molecular level it is required the ability to watch molecules as they react, interact or transform in real time by structurally characterizing the, often short-lived, transient species and intermediates that occur. Without the capability to understand dynamic structural changes, the design and creation of new supramolecular compounds with desired properties must rely on empirical rule-based approaches as well as a fair degree of serendipity. In this way, it is clear that for a full understanding of functional dynamics the combination of structural and spectroscopic techniques is required, as well as their combination with computational simulation approaches that permit the generation of dynamic structural models consistent with all available experimental data.[108] Although a vast range of experimental studies about CPs have been carried out so far in the case of SCPNs, very little has been done using theoretical methods.[109–114] This number decreases even more if

107. Lamas, A. et al. *Chem. Sci.* **2018**, *9* (43), 8228–8233.
108. Fraser, J. S. et al. *J. Chem. Inf. Model.* **2020**, *60* (5), 2410–2412.
109. Chen, G. et al. *J. Phys. Chem. B* **2002**, *106* (7), 1570–1575.
110. Tarek, M. et al. *Biophys. J.* **2003**, *85* (4), 2287–2298.
111. Hwang, H. et al. *J. Phys. Chem. A* **2009**, *113* (16), 4780–4787.
112. Khalfa, A. et al. *Chem. Phys.* **2009**, *358* (1–2), 161–170.
113. Khalfa, A. et al. *J. Phys. Chem. B* **2010**, *114* (8), 2676–2684.
114. Song, X. et al. *J. Mol. Model.* **2013**, *19* (10), 4271–4282.

we focus only in the α,γ- and α,δ-CPs developed by Prof. Juan Granja in our group.[115,116] Nonetheless, having a proper knowledge about the different possible hydrogen patterns in the self-assembly or the more stable conformations that these systems could form seems crucial in order to make a rational design of SCPNs or to understand their mechanism at the molecular level.

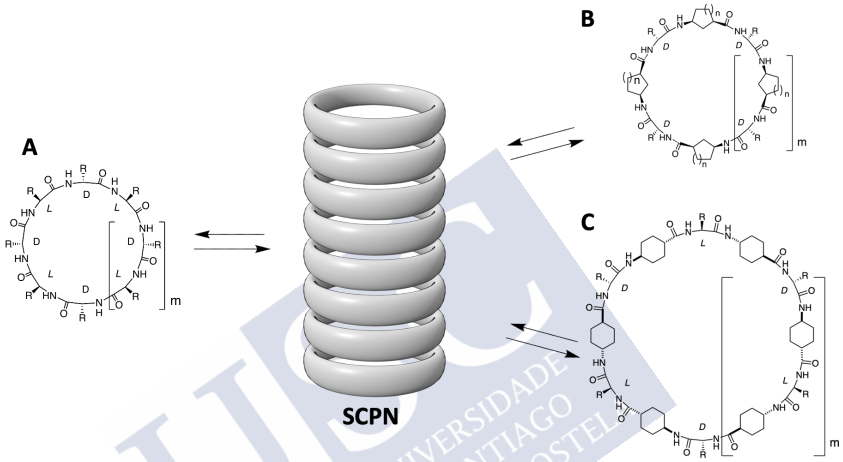

***Figure 3. A)** D,L-α-CP, **B)** α,γ-CP and **C)** D,L-α,δ-CP, as well as their assembly in a SCPN, proposed by the group of Prof. Ghadiri (D,L-α-CP) and Prof. Juan Granja (α,γ-CP and D,L-α,δ-CP).*

115. García-Fandiño, R. et al. *J. Am. Chem. Soc.* **2009**, *131* (43), 15678–15686.
116. García-Fandiño, R. et al. *J. Phys. Chem. B* **2010**, *114* (15), 4973–4983.

USC
UNIVERSIDADE
DE SANTIAGO
DE COMPOSTELA

2. Theory and methods

2.1. SYNERGY BETWEEN IN VITRO AND IN SILICO EXPERIMENTS.

"And so these men of Indostan
Disputed loud and long,
Each in his own opinion
Exceeding stiff and strong,
Though each was partly in the right,
And all were in the wrong!"
The blind men and the elephant, from *The Poems of John Godfre Saxe* (1881).

The parable of *The blind men and the elephant*, originally from India but introduced to the Western by John Godfre Saxe, it is an ancient story used even today as warning for theories which promise an absolute truth (**Figure 4**).[117] Basically, this story is about six men, all of them blind, who try to explain how an elephant is just touching it. One of them touched its trunk, so he claimed that an elephant was like a snake; other touched its tusks, saying that it was like a spear; another touched one side of the elephant, suggesting that it was as a wall; another touches a leg, so he said that it was like a tree; another touched one of the elephant's ear, claiming that it was similar to a fan and the last one of the blind men, touching the tail of the animal, said that it was like a rope. All of them were partially right, but none of them was capable to provide a real description about how an elephant really is. Actually, the parable continues with the men arguing among them, with every of them suspecting that the others were not telling the true.

117. The poems of John Godfrey Saxe/The Blind Men and the Elephant - Wikisource, the free online library https://en.wikisource.org/wiki/The_poems_of_John_Godfrey_Saxe/The_Blind_Men_and_the_Elephant (accessed Jun 15, 2020).

Although this parable has been usually used in order to show how our personal experiences and beliefs could lead us to the misinterpretation, being difficult to be able of claiming big facts when only a limited access of the whole is available, this can help us to illustrate how important could be the cooperation in Science. If instead of disputing and claiming that they were right, the six blind men collaborated between them, putting their observations together and trying to look for the whole solution of the problem, it could be possible (at least easier) to obtain a correct representation of the elephant.

Sciences like Chemistry had been usually seen as pure experimental. However, a new trend has emerged since the 20th century: *Computational chemistry*. This discipline, instead of performing an *in vitro/in vivo* research, tries to understand and predict the behaviour of a studied system through a set of equations, using both quantum or classical approaches.

Fortunately, in the field of chemistry, a synergy between *in silico* and *in vitro* experiments is widely accepted, being usual to find many publications using both techniques.[118,119] One of the most common examples of this cooperation is the mixing of synthetic experiments and quantum calculations, usually DFT (*Density Functional Theory*), in order to enquire the possible mechanisms of any chemical transformation. In this kind of studies, the different reactants, transition states, intermediates and products, as well as the quantification of their energies, are evaluated through computational techniques. Not only quantum calculations have been carried out, but also classical mechanics have been applied to study biological systems. In general, classical methods are used to study large molecules (thousands of atoms), since its lower computational requirements allow to increase the size of the systems.

118. Nasica-Labouze, J. et al. *Chem. Rev.* **2015**, *115* (9), 3518–3563.
119. Sperger, T. et al. *Acc. Chem. Res.* **2016**, *49* (6), 1311–1319.

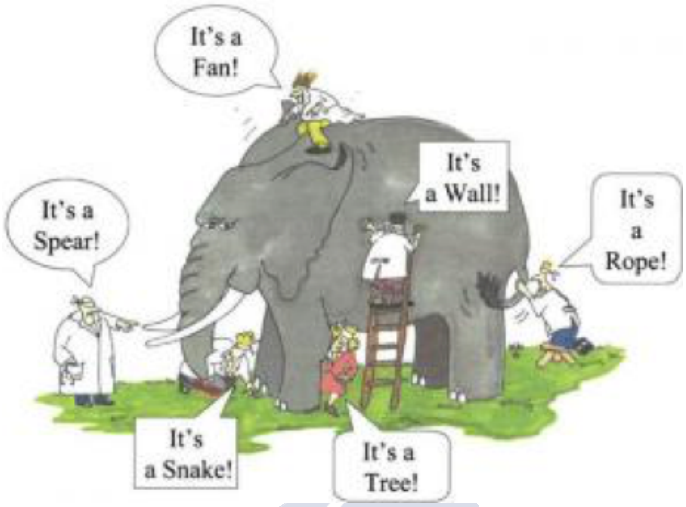

***Figure 4.** Representation of the parable "The blind men and the elephant". The figure was taken from https://www.patheos.com/blogs/driventoabstraction/2018/07/blind-men-elephant-folklore-knowledge/.*

However, the main point of this is that we can speak about consolidated collaborations between experimental chemistry and computational calculations, which could allow to overcome some of the limitations of both approximations thanks to the combination of their results. Nowadays it is not easy to obtain experimentally an atomic resolution of any chemical structure. Some techniques, like AFM (*Atomic Force Microscopy*) or STM (*Scanning Tunnelling Microscopy*), could give us the opportunity to do it, but only under certain requirements.[120–123] Furthermore, the biggest part of biological processes and chemical reactions take place under conditions not suitable for obtaining that level of resolution. Actually, other techniques can be used to overcome that, as X-ray or NMR (*Nuclear Magnetic Resonance*), but the data obtained are not always easy to

120. Sugimoto, Y. et al. *Nature* **2007**, *446* (7131), 64–67.
121. Gross, L. et al. *Science.* **2009**, *325* (5944), 1110–1114.
122. Gross, L. et al. *Science.* **2012**, *337* (6100), 1326–1329.
123. Hanssen, K. Ø. et al. *Angew. Chemie Int. Ed.* **2012**, *51* (49), 12238–12241.

process and understand. Additionally, the use of X-ray is limited to solid crystallin materials. Needless to say the difficulties in the obtainment of the double-helix structure of DNA by Watson and Crick, with the priceless help of Rosalin Franklin, in the 50s.[124] Under this panorama, computational chemistry could emerge as a pretty good alternative, since it allows us to follow processes atom by atom. Both quantum chemistry, which give us accurate geometries and energies, and classical methods, which allow us to follow bigger phenomena, as drug delivery or the folding of a protein, would provide us atomic information which could complement or anticipate experimental observations.

In conclusion, the combination of computational models (*in silico*) and experimental measures (wet-lab) could give a whole picture of a problem, being crucial to take advantage of both techniques. The work carried out during this thesis has been done in a research group where part of the people were working in wet-labs, doing *in vitro*/*in vivo* experiments, while other performed computational *in silico* experimentation without using flasks, safety glasses or gloves, having always present the profits of this synergy.

Computational methods not only complement the work that experimental chemists carry out, but also allow researchers to go beyond the limits of the laboratory.

2.2. COMPUTATIONAL SIMULATIONS.

"I do not fear computers. I fear the lack of them." Isaac Asimov.

It is impossible to imagine how the world would be nowadays without computers. Since the Turing machine was invented in 1936, almost every day a new technological advance appears, pushing the borders of this field until unsuspected limits.[125] In all smartphones, tablets or smart TVs there are processors with more power than the ones used by the NASA for the Moon landing in 1969. The reduction in the size of the

124. Watson, J. D. et al. *Nature* **1953**, *171* (4356), 737–738.
125. Turing, A. M. *Proc. London Math. Soc.* **1937**, *s2-42* (1), 230–265.

processors brought along the increase capacity of the computers. In 1965, Moore proposed that the number of transistors in a processor doubles about every 18 months, although years later this rate was revised and downgraded.[126] This trend could be widely surpassed with the use of quantum computers. This possibility was firstly suggested in the 80's by Benioff, when he proposed a quantum mechanical model of Turing machines.[127] Very recently, a new quantum computer developed by Google has been able to perform in 200 seconds a task than in a conventional computer would take around 10.000 years, opening the door to dream about a future where things that today we only can see in sci-fi become real.[128] In this scenario, it seems pretty obvious that science should take advantage of this power. Fortunately, several steps have been done in this direction.

The power of modern computation allows us to decipher the mysteries of how molecules behave. In this context, computational chemistry has emerged as a powerful tool.[129,130] This new branch of chemistry uses computer simulation in order to assist in solving chemical problems, using mathematical and physical models incorporated into efficient computer programs. The pillars of computational chemistry are molecular quantum methods and classical statistical mechanics.[131] The biggest restriction of the quantum chemistry is that it is constrained to relatively small systems due to the significant (and proportional to the size of the system) computational effort that it needs. Although the existence of approximations like semiempirical or embedding methods allows to partially overcome this limitation, it is quite hard to study supramolecular events with these techniques, particularly if the size of the system is big.[132,133] Maybe in

126. Moore, G. E. *IEEE Solid-State Circuits Soc. Newsl.* **2006**, *11* (3), 33–35.
127. Benioff, P. *J. Stat. Phys.* **1980**, *22* (5), 563–591.
128. Arute, F. et al. *Nature* **2019**, *574* (7779), 505–510.
129. Barberousse, A. et al. *Synthese* **2009**, *169*, 557–574.
130. Schlick, T. *Molecular Modeling and Simulation*; Interdisciplinary Applied Mathematics; Springer New York: New York, NY, 2002; Vol. 21.
131. Fernández, I. et al. *Chem. Soc. Rev.* **2014**, *43* (14), 4906–4908.
132. Christensen, A. S. et al. *Chem. Rev.* **2016**, *116* (9), 5301–5337.
133. Jones, L. O. et al. *J. Am. Chem. Soc.* **2020**, *142* (7), 3281–3295.

the next years, and thanks to the power of quantum computers, this challenge could be affordable, but not today. Molecular Dynamics (MD) simulations appear as a good alternative to quantum calculations.[134,135] This method describes the movement of the atoms integrating the classical equations of the Newton's Second Law. The forces acting over each particle are calculated using *Force Fields*, a set of expressions with parameters for describing different kinds of *inter* and *intra* interactions. As the classical mechanics equations of the movement are mathematically simpler than the analogous Schrodinger's expressions, using this technique we can simulate bigger systems.

The first MD simulation was introduced in the late 50s, when Alder and Wainwright used it for calculating the behaviour of several hundred of hard spheres towards classical interactions.[136] As curiosity, the computer used for these calculations was an IBM 704, the first computer which was able to synthesize speech, fact which inspired the *HAL 900* of the Stanley Kubrick's film *2001: A Space Odyssey*. Previously, Monte Carlo methods were the most used technique for the calculation of molecular motions, but this technique only allows to obtain equilibrium properties.[137,138] However, with MD, the dynamical performance can be evaluated. The next step was done in 1964, when Rahman simulated 864 particles of argon using and Lennard-Jones potential.[139] Later on, in 1974, Stillinger and Rahman presented the first simulation of a box of liquid water.[140] The evolution of this methodology has gone hand in hand with the evolution in supercomputer power. The size of the simulated systems and the simulation times have grown exponentially, converting MD in a widely used technique for the study of biological systems, being common to

134. Entel, P. et al. In *Computational Materials Science*; Springer, Berlin, Heidelberg, 2004; pp 177–206.
135. Grimaldo, M. et al. *Q. Rev. Biophys.* **2019**, *52*, E7.
136. Alder, B. J. et al. *J. Chem. Phys.* **1959**, *31* (2), 459–466.
137. Harrison, R. L. *AIP Conf. Proc.* **2009**, *1204*, 17–21.
138. Chen, J. *IOP Conf. Ser. Earth Environ. Sci* **2018**, *128*, 12110.
139. Rahman, A. *Phys. Rev.* **1964**, *136* (2A), 405–411.
140. Stillinger, F. H. et al. *J. Chem. Phys.* **1974**, *60* (4), 1545–1557.

find in the literature studies of proteins, DNA/RNA complexes or lipid systems using MD simulations.[141–146] Furthermore, MD has been used for describing self-organization processes, as the formation of vesicles and micelles, and even viruses.[147] The expectations for this technique in the next years are very promising. For example, the possibility of attending the simulation of a complete cell for 1000 seconds it is envisioned for the next decades.[148] The importance of this technique was manifested with the award of the Nobel Prize of Chemistry in 2013 to Martin Karplus, Michael Levitt and Arieh Warshel for "the development of multiscale models for complex chemical systems".[149] In addition, a vast literature focused on the theoretical development has been also reported during last decades.[130,150,151]

In MD the atoms are described as simple particles in which electrons are not explicitly considered, precluding the study of reactions where bonds are formed/broken. Some Force Fields were parametrized in order to include this reactivity, although their use is no so widely implemented.[152,153] Between quantum and classical methods we can found the hybrid method QM/MM (Quantum Mechanic / Molecular Mechanic). These techniques split the system of study in different *layers* and treat each one of them with a different level of theory. One

130. Schlick, T. *Molecular Modeling and Simulation*; Interdisciplinary Applied Mathematics; Springer New York: New York, NY, 2002; Vol. 21.
141. Karplus, M. et al. *Nat. Struct. Biol.* **2002**, *9* (9), 646–652.
142. Karplus, M. et al. *Proc. Natl. Acad. Sci. U. S. A.* **2005**, *102* (19), 6679–6685.
143. Childers, M. C. et al. *Mol. Syst. Des. Eng.* **2017**, *2* (1), 9–33.
144. Sponer, J. et al. *Chem. Rev.* **2018**, *118* (8), 4177–4338.
145. Marrink, S. J. et al. *Chem. Rev.* **2019**, *119* (9), 6184–6226.
146. Bissaro, M. et al. *Front. Chem.* **2020**, *8*, 107.
147. Rapaport, D. C. *J. Biol. Phys.* **2018**, *44* (2), 147–162.
148. Schlick, T. In *Molecular Modeling and Simulation: An Interdisciplinary Guide*; 2010; pp 1–40.
149. The Royal Swedish Academy of Sciences. *Press. Press release* **2013**.
150. Stone, A. *The Theory of Intermolecular Forces*; Oxford University Press, 2013.
151. Frenkel, D. et al. *Understanding molecular simulation. From Algorithms to Applications*; Elsevier: San Diego, 2002.
152. Senftle, T. P. et al. *npj Comput. Mater.* **2016**, *2* (1), 1–14.
153. Meuwly, M. *Wiley Interdiscip. Rev. Comput. Mol. Sci.* **2019**, *9* (1), e1386.

typical case of the use of this technique is the study of enzymatic reactions.[154] In this case, the main part of the protein is treated using classical expressions, restricting the use of quantum calculations to the small part of the system where the chemical reaction is taking place.

The selection of one or other technique is not a trivial decision that depends on the size of the system and the available computational resources (**Figure 5**).

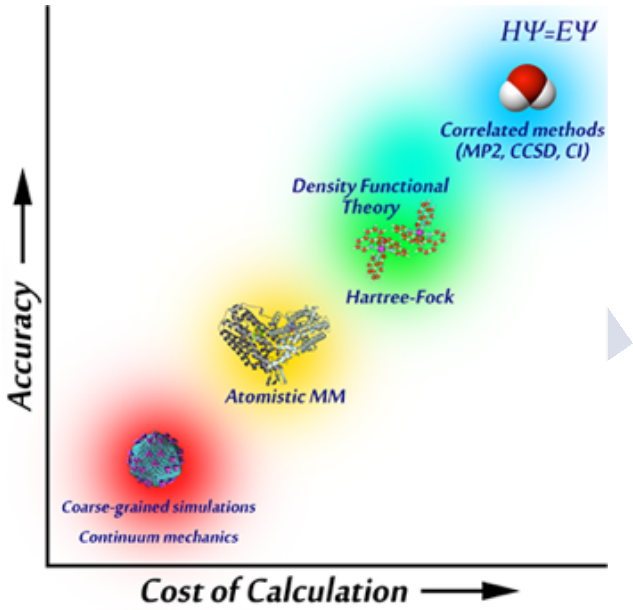

***Figure 5.** Relation between computational cost and accuracy of different computational methods. The figure was taken from https://leeping.github.io/forcebalance/doc/html/index.html*

154. Van Der Kamp, M. W. et al. *Biochemistry* **2013**, *52* (16), 2708–2728.

2.2.1. Quantum Calculations.

"The general theory of quantum mechanics is now almost complete...The underlying physical laws necessary for the mathematical theory of...the whole of chemistry are thus completely known, and the difficulty is only that the exact application of these laws leads to equations much too complicated to be soluble." Paul Dirac.

Quantum mechanics is a field of physics dedicated to the study of particles at the microscopic scale, including the atomic and subatomic ones. In contrast to classical mechanics, in this theory energy is not a continuous, but it is restricted to just a number of discrete values; in other words: energy is quantized. This theory was mainly developed in the 20th century, after that classical approximations did not match with solutions provided for the black-body radiation problem by Max Planck, where the emission of radiation was quantized, or the explanation of the photoelectric effect by Albert Einstein, where the radiation was made up of photons. Further contributions to this field were made by de Broglie, with the duality wave-particle, and Heisenberg, with the uncertainty principle. However, the milestone in this field was the proposal of the Schrödinger equation, published by Erwin Schrödinger in 1926. If in classical mechanics the position and the momentum of a system as a function of an external force can be obtained at each time from the Netwon's second law, the analogous in quantum mechanics is the Schrödinger equation. For a stationary system, the Schrödinger equation can be expressed independently of the time as follows:

$$\hat{H}|\Psi\rangle = E|\Psi\rangle$$

Where $\hat{H}$ corresponds with the *Hamiltonian operator*, E with the *energy of the system* and Ψ with the *wave function*. The state of a system is given by Ψ, whose square modulus gives the probability density for finding particles at given locations in space, and will be only *acceptable* (univocal, continuous and square integrable) for just certain values of E. In this way, only a number of energy levels are allowed.

The previous Hamiltonian can be written depending on the coordinates (r) of the system in the following manner:

$$\widehat{H}(r) = \frac{-\hbar}{2m}\nabla^2 + V(r)$$

Where:

$$\hbar = \frac{h}{2\pi}$$

and ∇^2 is the Laplacian operator. In order to express the Hamiltonian as above, the Born Oppenheimer approximation must be done, which allows the separation of the movement of the electrons and the nucleus of the atom, since the movement of the nucleus will be much slower than the analogous of the electron due to its much bigger mass. One macroscopic analogy could be the interaction between the Sun and the Earth, being the Sun the nucleus and the Earth the electron. Owe to the big difference in mass between them (the Sun is more than 300000 times heavier than the Earth), it is possible to neglect the movement of the Sun and consider it static when it is compared with the Earth. In this way, the first term of the Hamiltonian corresponds to the kinetic energy, which comes from the momentum of electrons (and the m which appears in this term is the electron mass), and the second term corresponds to the potential, which comes from the special coordinates of the electrons and nucleus. It is worth to mention that the Schrödinger equation only has analytical solution for monoelectronic atoms (H, He^+,…). Consequently, for systems with more than one electron the computationally effort needed for solving the electronic interactions is inaccessible. Instead, numerical methods are applied for obtaining the approximate wavefunctions. Even though, they are still more complex than the classical expressions, being Hartree-Fock one of the most used.[155] This fact results in the restriction that for quantum calculations a bigger computational effort and systems made up of a small number of particles are mandatory, compared with classical mechanic calculations.

155. Hartree, D. R. et al. *Proc. R. Soc. London. Ser. A Math. Phys. Sci.* **1935**, *150* (869), 9–33.

In order to overcome the above mentioned limitations, a number of approaches have been proposed during last decades, being the use of semiempirical methods one of them.[156] Following this procedure, the computational cost is shortened by reducing the multi-electrons integrals approximating its result to experimental data. However, although this method reduces considerably the time of calculations, they pay the lost in accuracy.[157]

Another interesting alternative is the use of *Density Functional Theory* (DFT). In this method, the ground state electronic energy is determined by the electron density, since it is considered that there is a correspondence between the electronic density of a system and its energy. Owing this approach, it is possible to obtain the energy through a functional. This is a function that takes other functions as arguments. The basis of this method was proposed by Hohenberg, Khon and Sham in 1960's, although it was not until the 1990's when the use of DFT calculations showed a meteoric rise, probably linked to the improvement of the computer power.[158–161]

For the calculation of the energy in DFT, different functionals have been developed during last decades, being the hybrid functionals developed by Becke, as for example B3LYP, and the highly parametrized Minnesota Functionals, like M06, the most used worldwide.[162–164] The vast increase in the use of DFT brought with it the development of programs, as Gaussian, which allows this kind of calculations in an easy way.[165]

156. Stewart, J. J. P. *J. Comput. Chem.* **1989**, *10* (2), 209–220.
157. Thiel, W. *Wiley Interdiscip. Rev. Comput. Mol. Sci.* **2014**, *4* (2), 145–157.
158. Hohenberg, P. et al. *Phys. Rev.* **1964**, *136* (3B), B864.
159. Kohn, W. et al. *Phys. Rev.* **1965**, *140* (4A), A1133.
160. Raghavachari, K. *Theor. Chem. Acc.* **2000**, *103* (3–4), 361–363.
161. Cohen, A. J. et al. *Chem. Rev.* **2012**, *112* (1), 289–320.
162. Mardirossian, N. et al. *Mol. Phys.* **2017**, *115* (19), 2315–2372.
163. Becke, A. D. *J. Chem. Phys.* **1993**, *98* (7), 5648–5652.
164. Zhao, Y. et al. *Theor. Chem. Acc.* **2008**, *120* (1–3), 215–241.
165. Frisch, M. J. et al. *Gaussian, Inc., Wallingford CT,* 2016.

Thanks to the huge increment in the use of DFT, a wide range of fields have applied this method.[166] It is worth to mention that the accuracy obtained has been relatively good, with errors smaller than 2 kcal mol^{-1}.[167]

Although it is well known the use of DFT in catalysis research, it has been also widely used for the study of supramolecular interactions.[168–171] Particularly common are works about protein-ligand interactions.[172,173] This method could be also used for studying self-assembly processes, dividing them into a series of steps, taking into account the limitation in the size of the system.[174–176] However, it is known that DFT fails to describe dispersions effects.[177–179] In order to overcome this problem, some corrections have been proposed, being the method developed by Grimme and Becke and Johnson the most used.[180–182] These methods include a series of parameters that allow the reproduction of van der Waals as well as others dispersion interactions in a better way.

The importance of DFT has been clearly demonstrated with the Nobel Prize of Chemistry to Pople and Kohn in 1998 for "his development of computational methods in quantum chemistry". In addition, it has been claimed that this method is, nowadays, the most used in quantum chemical and solid state calculations.[183] Additional

166. Jones, R. O. *Rev. Mod. Phys.* **2015**, *87* (3), 897–923.
167. In *A Chemist's Guide to Density Functional Theory*; Wiley, 2001; pp 117–118.
168. Sperger, T. et al. *Chem. Rev.* **2015**, *115* (17), 9532–9586.
169. Weijing, D. et al. *Energy Procedia* **2018**, *152*, 997–1002.
170. Cortese, R. et al. *Theor. Chem. Acc.* **2018**, *137* (4).
171. Riley, K. E. et al. *Chem. Rev.* **2010**, *110* (9), 5023–5063.
172. Antony, J. et al. *J. Phys. Chem. A* **2011**, *115* (41), 11210–11220.
173. Yilmazer, N. D. et al. *J. Phys. Chem. B* **2013**, *117* (27), 8075–8084.
174. González, J. et al. *J. Chem. Theory Comput.* **2016**, *12* (2), 523–534.
175. Petelski, A. N. et al. *J. Mol. Model.* **2017**, *23* (9).
176. González-Díaz, N. E. et al. *J. Phys. Chem. C* **2019**, *123* (4), 2526–2532.
177. Tsuzuki, S. et al. *J. Chem. Phys.* **2001**, *114* (9), 3949–3957.
178. Allen, M. J. et al. *J. Chem. Phys.* **2002**, *117* (24), 11113–11120.
179. Zimmerli, U. et al. *J. Chem. Phys.* **2004**, *120* (6), 2693–2699.
180. Grimme, S. et al. *J. Chem. Phys.* **2010**, *132* (15), 154104.
181. Grimme, S. et al. *J. Comput. Chem.* **2011**, *32* (7), 1456–1465.
182. Becke, A. D. et al. *J. Chem. Phys.* **2007**, *127* (15), 154108.
183. Becke, A. D. *J. Chem. Phys.* **2014**, *140* (18), 18–301.

information about the development and theory of DFT, as well as other quantum methods, can be found in the extensive literature about this topic.[184–187]

2.2.2. Molecular Dynamics.

"Trying to understand molecules from a static vision is as useless as trying to understand a machine when it is off."
Modesto Orozco.

Molecular Dynamics simulations provide a different point of view in the study of macromolecular systems, since with this technique relatively big compounds, like proteins, can be considered as dynamic structures instead of rigid models. This change is allowed due to the moderately simplicity of the mathematical expression of the algorithm, at least compared with the analogous quantum models. The reduction in the difficulty solving the equations decreases the computational requests, allowing the study of systems with more particles. In addition, MD simulations provide temporal information, allowing to observe the evolution of a system with the time. Thus, MD is occasionally compared with a "virtual microscope".

Modelling the motion of a complex molecule by solving the wave functions of the various subatomic particles would be more accurate, but it would also be very hard to program and take more computing power than anyone has! In MD simulations it is assumed that the dynamic behaviour of the particles is governed by the classical mechanical equations expressed in the second Newton's laws of motion. It shows that the force can be expressed as:

$$F = m \cdot a = m\frac{d^2x}{dt^2}$$

184. Piela, L. *Ideas of Quantum Chemistry*; Elsevier, 2007.
185. Szabo, A. et al. *Modern quantum chemistry : introduction to advanced electronic structure theory / Attila Szabo, Neil S. Ostlund*; 2018.
186. Jensen, F. *Introduction to Computational Chemistry*; John Wiley & Sons, 2013.
187. Levine, I. N. *Quantum Chemistry*; Pearson, Ed.; 2014.

This is a simplification of what is actually going on, and is therefore less accurate. To alleviate this problem, MD include the use of parameters derived from QM for the constants in classical equations (*vide infra*).

If the force acting over the particles of a system depends only on their position (conservative force), the expression can be rewritten relating it to the potential energy:

$$F = -\vec{\nabla}V$$

Being $\vec{\nabla}$ the gradient. V is the potential energy and is represented by a function called *Force Field*, which contains a set of expressions and parameters for describing the forces and interactions among the particles that composed the studied system. Thus, a Force Field can be defined as an equation that links the potential energy of a system with its internal coordinates, such as bond distances, bond angles, torsions…Usually, the Force Fields divide the energy into bonded and non-bonded terms:

$$V = V_{bonded} + V_{non-bonded}$$

In general, the first of them is related with the interaction between pairs of atoms separated by no more than 3 covalent bonds, whereas the second one includes the electrostatic and van der Waals parameters. In addition, most of the Force Fields make use of Born-Oppenheimer approximation, since it is considered that the electrons move so fast that they reorganize immediately after the movement of the atomic nucleus, allowing to work only with nuclear coordinates. The electrons are not described explicitly, being the electronic potential included inside other terms.

We can split both V_{bonded} and $V_{non-bonded}$ in the different interactions that they describe. Regarding the bonded terms, we could consider three elements:

$$V_{bonded} = \sum_{i=1}^{N_{bond}} V_{bond} + \sum_{i=1}^{N_{angle}} V_{angle} + \sum_{i=1}^{N_{dih}} V_{dih}$$

The first term (V_{bond}) describes the bond stretching between an atom pair, the second one (V_{angle}) describes the angle bending between three atoms and the last one (V_{dih}) describes the potential related with

the torsions between four atoms. Most of the Force Fields describe the first two terms using a harmonic potential:

$$V_{bond} = \frac{1}{2} k_b (r - r_0)^2$$

$$V_{angle} = \frac{1}{2} k_a (\theta - \theta_0)^2$$

Being k_b a force constant for describing the bond strength, r the actual bond distance, r_0 the equilibrium bond distance. It is worth to mention that the harmonic potentials only provide reliable descriptions for geometries close to the equilibrium. This provokes that harmonic potentials are not suitable for studying the formation or breaking of bonds, since the description obtained for longer distances than the ones in the equilibrium fails. The definition of the parameters of the angle potential is analogous: k_a is a force constant for describing the strength of the bending of the angle and θ and θ_0 are the actual angle and the equilibrium angle, respectively.

Concerning the torsions (also called 1-4 interactions), V_{dih} describes two different types: *Proper torsions*, which are the dihedral angle formed by four atoms; and *Improper torsions*, used for forcing an atom to be in the plane formed by other three. This term, unlike the previous ones, presents periodicity. This fact becomes its definition slightly more difficult, being necessary the addition of more terms. The more complex the real energetic profile of the torsion, the bigger number of terms needed. Most of the Force Fields describe this interaction using Fourier potentials:

$$V_{dih} = k_t (1 + \cos(n\omega - \gamma))$$

Being k_t a force constant for describing the strength of the torsion, n the periodicity of the of the term, ω the angle formed by the planes defined by the atoms 1-2-3 and 2-3-4 and γ the phase angle. The number of terms of this potential can be different depending on the Force Field employed and the complexity of the torsion.

$V_{non-bonded}$ can be also split in the terms used by its description:

$$V_{non-bonded} = V_{ele} + V_{vdw}$$

The first term refers to the electrostatic interactions between all pairs of atoms. The most common way to describe this phenomenon is using a Coulomb potential:

$$\sum_i \sum_{j>i} \frac{q_i q_j}{4\pi\varepsilon_0 r_{ij}}$$

Where q_i and q_j are the punctual charges of each particle, ε_0 is the dielectric constant of the media and r_{ij} is de distance between a pair of atoms.

Inside the second term (V_{vdw}), we can find a term for the repulsion of two very close particles due to the overlapping of the electron orbitals (Pauli repulsion) and another one for the attractive van der Waals interaction at long distances (dispersion force). Usually, this interplay is described using a Lennard-Jones potential:

$$V_{vdw} = \sum_i \sum_{j>i} 4\varepsilon_{ij} \left[\left(\frac{\sigma_{ij}}{r_{ij}} \right)^{12} - \left(\frac{\sigma_{ij}}{r_{ij}} \right)^{6} \right]$$

Where the term $\left(\frac{\sigma_{ij}}{r_{ij}}\right)^{12}$ represents the repulsion and $\left(\frac{\sigma_{ij}}{r_{ij}}\right)^{6}$ attraction. ε represents how strong is the interaction, whereas σ gives the distance at which the interaction between particles become zero. These two parameters (ε and σ) are different for each atom type. It is worth to mention that, in general, one atom can be labelled as different types depending on its environment. For example, one carbon atom will be tagged unequal depending on if it is in an aliphatic tail or if it is in a carbonyl group. Furthermore, other approximations, like the Buckingham potential, are also used for treating these interactions, but the Lennard-Jones expression is the most used.

In addition, it is possible to find an extra parameter called *crossing terms*. This term covers couplings between two (or more) of the previous parameters, allowing a more real description of the studied system.

The main objective of MD simulations is the integration of the equations of motion of Newton in order to obtain how the position of the particles of a system changes with time. Some algorithms exist for this numerical integration, being the Verlet and Leap-Frog the most used. In all of them, the positions and velocities of the atoms are recalculated at a time $t+dt$ using the forces acting over them at a time t, which depends on the positions and velocities of the atoms at this time. Usually, the velocities at the initial time (t=0) are obtained from a

Maxwell-Boltzmann distribution at the temperature of simulation, whereas the initial coordinates are taken from experiments (like X-ray), on-line repositories (like the Protein Data Bank), other theoretical models or they are directly drawn using some specific software (like GaussView, ChemOffice or Avogadro, for example).[188–192] The selection of the time step (*dt*) is also an important issue. This value depends on the fastest movement in the studied molecules, which typically corresponds to the vibration of bonds containing hydrogens atoms, such as C-H, O-H or N-H bonds, which usually takes around 1fs. Due to the high velocity of such movement, some corrections have to be applied in order to preserve properly the internal energy, being the LINCS and SHAKE algorithms some of most used.[193–195] In a typical MD simulation, the time step is often 1 or 2 fs, although it could be increased by doing certain approximations.[196]

The parameters that have been shown up to now, like the force constants or the equilibrium distances and angles, are the elements that allow to distinguish among Force Fields and they are different for each one of them. This fact could lead to different results depending on which Force Field has been selected.[197–201] These parameters are fitted for reproducing experimental measurements or quantum calculations. Usually each particle of a Force Field matches with an atom (as in the

188. Dennington, R. et al. *Semichem Inc. , Shawnee Mission, KS*. 2019.
189. Cousins, K. R. *J. Am. Chem. Soc.* **2011**, *133* (21), 8388.
190. Hanwell, M. D. et al. *J. Cheminform.* **2012**, *4* (8), 17.
191. Protein Data Bank. RCSB PDB: Homepage https://www.rcsb.org/ (accessed Jun 15, 2020).
192. Berman, H. et al. *Nat. Struct. Biol.* **2003**, *10* (12), 980.
193. Use of constraints in molecular dynamics - Robin Corey's Posts - Quora https://www.quora.com/q/gnvbdldrivyzzipw/Use-of-constraints-in-molecular-dynamics (accessed May 22, 2020).
194. Hess, B. et al. *J. Comput. Chem.* **1997**, *18* (12), 1463–1472.
195. Ryckaert, J. P. et al. *J. Comput. Phys.* **1977**, *23* (3), 327–341.
196. Feenstra, K. A. et al. *J. Comput. Chem.* **1999**, *20* (8), 786–798.
197. Martín-García, F. et al. *PLoS One* **2015**, *10* (3), e0121114.
198. Cino, E. A. et al. *J. Chem. Theory Comput.* **2012**, *8* (8), 2725–2740.
199. Shirts, M. R. et al. *J. Chem. Phys.* **2003**, *119* (11), 5740–5761.
200. Beauchamp, K. A. et al. *J. Chem. Theory Comput.* **2012**, *8* (4), 1409–1414.
201. Piggot, T. J. et al. *J. Chem. Theory Comput.* **2012**, *8* (11), 4593–4609.

Amber or CHARMM Force Fields, for example), but this is not always true. It is also possible to represent only the heavy atoms and the polar hydrogens, grouping the heavy atoms and the non-polar hydrogens in one single particle, as for example it is done in the GROMOS Force Field.[202] The type of approximation used is called *resolution*. For example, when all the atoms are represented explicitly, it is called *All-atom (AA) resolution*, whereas when only the polar H atoms are present it is called *United-atom (UA) resolution*.

One step forward is the *Coarse-Grained (CG) resolution*. In this approximation the number of particles that composes a system is significantly reduced grouping a number of heavy atoms in only one "bead". Different Force Fields for this representation exist, being the *Martini Force Field* one of the most used.[203–205] In this model, four heavy atoms and their corresponding hydrogens are coupled in a single particle (**Figure 6**). In addition, there are only 4 types of main interactions between particles: polar, intermediate, apolar and charged. This simplicity represents an advantage, since it allows to use this Force Field for a wide range of systems. It is also important to note that the Non-bonded interactions are parametrized based on the reproduction of experimental partitioning free energies between polar and apolar phases, whereas the bonded interactions are obtained from All-Atom Molecular Dynamics (AA-MD) simulations.

202. Schmid, N. et al. *Eur. Biophys. J.* **2011**, *40* (7), 843–856.
203. Chebaro, Y. et al. *J. Phys. Chem. B* **2012**, *116* (30), 8741–8752.
204. Periole, X. et al. *Methods Mol. Biol.* **2013**, *924*, 533–565.
205. Singh, N. et al. *Int. J. Mol. Sci.* **2019**, *20* (15), 3774.

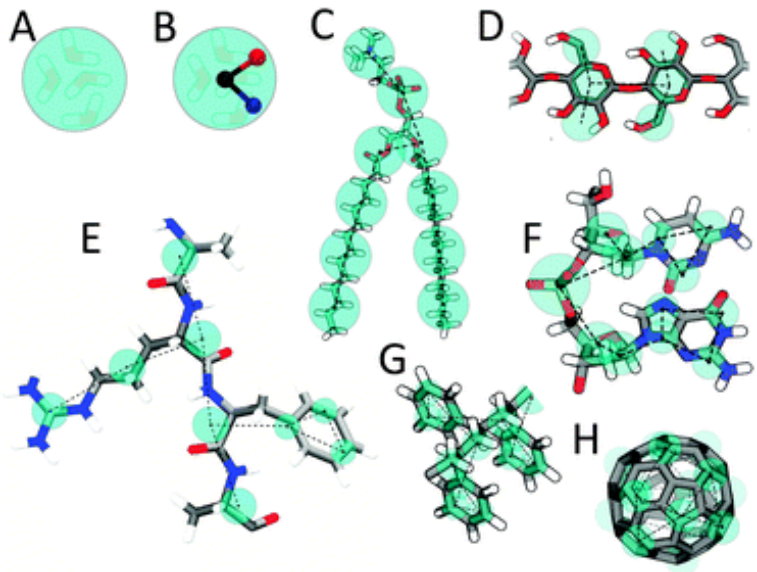

***Figure 6.** Mapping from AA to CG examples using Martini Force Field of **A)** Martini water particle, **B)** Polarizable water particle, **C)** DMPC, **D)** Polysaccharide fragment, **E)** Peptide, **F)** DNA, **G)** Polystyrene and **H)** Fullerene. The image was taken from the Martini website (http://cgmartini.nl/index.php/about).*

The use of CG resolution involves some considerations. Thanks to the reduction in the total number of particles of the system (since the atoms are grouped), it is possible to simulate bigger systems than in traditional AA-MD simulations. In this way, the study of proteins with several domains or big lipid membranes can be reached. Other advantage of the use of CG is that the time step can be increased. In CG, the vibration of the bonds containing hydrogens is not described, since there are not explicit hydrogens. Consequently, the fastest movement is much slower than in an analogous AA/UA, allowing the increment of the time step up to 20 or 30 fs, one order of magnitude bigger. In this way, the use of CG resolution allows also to reach longer time scales, since doing the same number of steps than in an AA-MD simulation the total time is going to be longer, thanks to the bigger time-step. Nevertheless, there are also some limitations in the use of CG. The clearest one is the loss of accuracy, due to big approximation that is

done grouping four heavy atoms in just one particle. The reduction in the number of explicit atoms provokes that some interaction, such as the formation of H-bonds, cannot be reproduced directly. This causes that some effects, like the formation/keeping of the secondary structure of proteins, are not well described. This problem can be overcome adding additional restraints. The use of Coarse-Grained Molecular Dynamics (CG-MD) for the study of lipid membranes or proteins have been widely implemented.[206–209]

Despite the big increment in the power of the computers, like the introduction of GPU's (*Graphics Processing Unit*), and the use of techniques like CG-MD, we are still far from being able to simulate "real" systems, since the number of atoms is too big for being affordable. This generates some limitations. One of them is that without any correction, a number of particles of the simulation box will interact directly with the vacuum/air/surface, being a huge difference with real systems, since in this case only the atoms of the edges interact in this way. In order to overcome this problem, Periodic Boundary Conditions (PBC) emerge as a good alternative.

206. Bond, P. J. et al. *J. Am. Chem. Soc.* **2006**, *128* (8), 2697–2704.
207. Bond, P. J. et al. *J. Struct. Biol.* **2007**, *157* (3), 593–605.
208. Scott, K. A. et al. *Structure* **2008**, *16* (4), 621–630.
209. Marrink, S. J. et al. *Chem. Soc. Rev.* **2013**, *42* (16), 6801–6822.

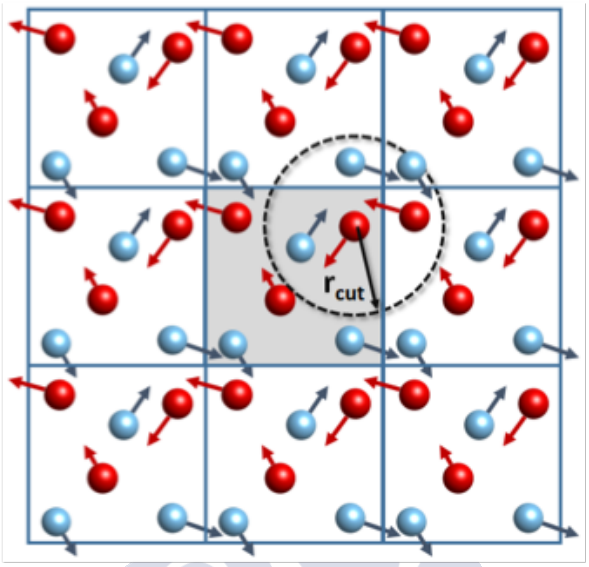

***Figure 7.** PBC example, with the principal box (grey shadow) and the corresponding replica. Only 2D replicas are shown. The cut-off (r_{cut}) is also shown. Figure was taken from J. Chapman's thesis.*[210]

With this correction the simulation box is replicated a number of times in all directions, occurring the same simulation of the principal box in every replica. In this way, if one atom leaves the simulation box through one border, one identical atom will enter in the box towards the opposite border, since the same movement is happening in all replicas (**Figure 7**). In addition, it is important to note that the atoms of the principal box will interact with the nearest particle, and it could be in a replicated box. Furthermore, in order to reduce the computational cost and calculate the same interaction no more than once, it is very usual the definition of a *cut-off* distance. In this way, only interactions with a distance between particles shorter than the cut-off are calculated, being the rest depreciated (**Figure 7**). This procedure is made for calculating both van der Waals as well as electrostatic interactions. For the latest

210. Chapman, J. B. J. Improving the Functional Control of Ferroelectrics using Insights from Atomistic Modelling, UCL (University College London), 2018.

one, an especial technique was proposed, called Particle mesh Ewald (PME) method.[211] In this method the short-range and long-range interactions are treated in different ways, since the short-range ones are calculated in real space and long-range using a Fourier transform.

Another important issue in MD simulations is the control of the temperature and the pressure. For that purpose, thermostats are defined. The most famous are the V-rescale, Berendsen, Nose-Hoover and Andersen thermostat.[212–214] In these cases, the temperature is set adjusting the kinetic energy of the atoms of the system modifying their velocities. For controlling the pressure, barostats are defined, being the most used Berendsen and Parrinello-Rahman, which fix the pressure adapting the volume of the simulation box.[213,215]

Several software packages have been developed so far for performing MD simulations. Programs like GROMACS, Amber, Charmm or NAMD are widely used.[216–219] Obviously, the development of more powerful computers, with the introduction in the field of calculation of GPU's as well as the refining of the parallelization of the codes, allow to reduce the simulation time and reach longer time scales for bigger systems.

211. Essmann, U. et al. *J. Chem. Phys.* **1995**, *103* (19), 8577–8593.
212. Woodcock, L. V. *Chem. Phys. Lett.* **1971**, *10* (3), 257–261.
213. Berendsen, H. J. C. et al. *J. Chem. Phys.* **1984**, *81* (8), 3684–3690.
214. Andersen, H. C. *J. Chem. Phys.* **1980**, *72* (4), 2384–2393.
215. Parrinello, M. et al. *J. Appl. Phys.* **1981**, *52* (12), 7182–7190.
216. Brooks, B. R. et al. *J. Comput. Chem.* **2009**, *30* (10), 1545–1614.
217. Phillips, J. C. et al. *J. Comput. Chem.* **2005**, *26* (16), 1781–1802.
218. Case, D. A. et al. *J. Comput. Chem.* **2005**, *26* (16), 1668–1688.
219. Van Der Spoel, D. et al. *J. Comput. Chem.* **2005**, *26* (16), 1701–1718.

2.3. VISUALIZATION TECHNIQUES: WHEN SCIENCE MEETS ARTS.

"The greatest scientists are artists as well." Albert Einstein.

Although at first glance Science and Arts may seem unrelated, they have more in common that one could expect. Galileo, Newton, Faraday, van't Hoff…the list of successful scientists who were also poets, artists or writers is highly surprising. Indeed, it has been shown that Nobel laurates are more likely to participate in artistical activities.[220] Other study has suggested that scientists who show artistic trends tend to publish in higher impact journals.[221] That is not a trivial issue, since one of our most important duties as scientists is to transmit our work. If we focus only in our closest scientific environment, this task results affordable. However, when we try to inform general public or policymakers, it becomes much trickier. We should never forget that people, with their taxes, pay for our researching. They are entitled to know what we are doing…and, of course, we need money for funding our work. In this regard, a marriage between art and science could help us to disseminate our results to a bigger part of society, allowing to increase the impact and real effect of our research.

The relationship between art and science has existed for a long time and now, with the digital revolution, it is speeding up. New forms of expression are appearing almost every day, leveraging the combined power of the rigorous scientific approach with the subjectivity and experimentalism of creative arts. These advances have allowed to introduce science easier to more people, facilitating also the teaching process.[222–224] In this context, one study carried out by Daniel Gurnon revealed the benefits of integrating art and science in undergraduate students.[225] In this work, Gurnon and collaborators showed how students learn about the secondary structure of proteins by sculping, pointing out the improvements in understanding the 3D shape of these

220. Root-Bernstein, R. et al. *J. Psychol. Sci. Technol.* **2009**, *1* (2), 51–63.
221. Root-Bernstein, R. S. et al. *Creat. Res. J.* **1995**, *8* (2), 115–137.
222. Bennie, S. J. et al. *J. Chem. Educ.* **2019**, *96* (11), 2488–2496.
223. Lohning, A. E. et al. *J. Chem. Educ.* **2019**, *96* (11), 2497–2502.
224. Li, L. et al. *Am. J. Transl. Res.* **2017**, *9* (9), 3867–3880.
225. Gurnon, D. et al. *PLoS Biol.* **2013**, *11* (2), e1001491.

molecules when a visual representation is provided.

Since the first obtainment of a 3D structure of a protein (myoglobin), proposed by Kendrew et al. using X-ray, different models for a simpler and more intuitive representation of molecules have been developed.[226] These representations of science are mainly symbolic, similar to the conventions of art, but they have to preserve the relevant scientific information. The first of them was the *ball-and-stick* model, introduced in 1960's, in which the lines that link atoms provide a rough idea of the distances between atoms, but the atom labels are just a convention. Later on, in the 1970's, the introduction of the *Byron's Bender* by the crystallographer Byron Rubin was a milestone in the 3D representation of proteins (**Figure 8**).[227] This device was designed for bending a wire in order to reproduce the backbone of a peptide, producing structures rather similar to artistic sculptures.

In the 1980's, another very important step in this direction was done by Jane Richardson, who proposed the *Ribbon diagram*, a schematic model in which the different motifs of secondary structure are represented in a dissimilar way, allowing a fast discrimination between them.[228,229]

226. Kendrew, J. C. et al. *Nature* **1958**, *181* (4610), 662–666.
227. Rubin, B. et al. *Biopolymers* **1972**, *11* (11), 2381–2385.
228. Richardson, J. S. *Methods Enzymol.* **1985**, *115* (C), 359–380.
229. Richardson, J. S. *Nat. Struct. Biol.* **2000**, *7* (8), 624–625.

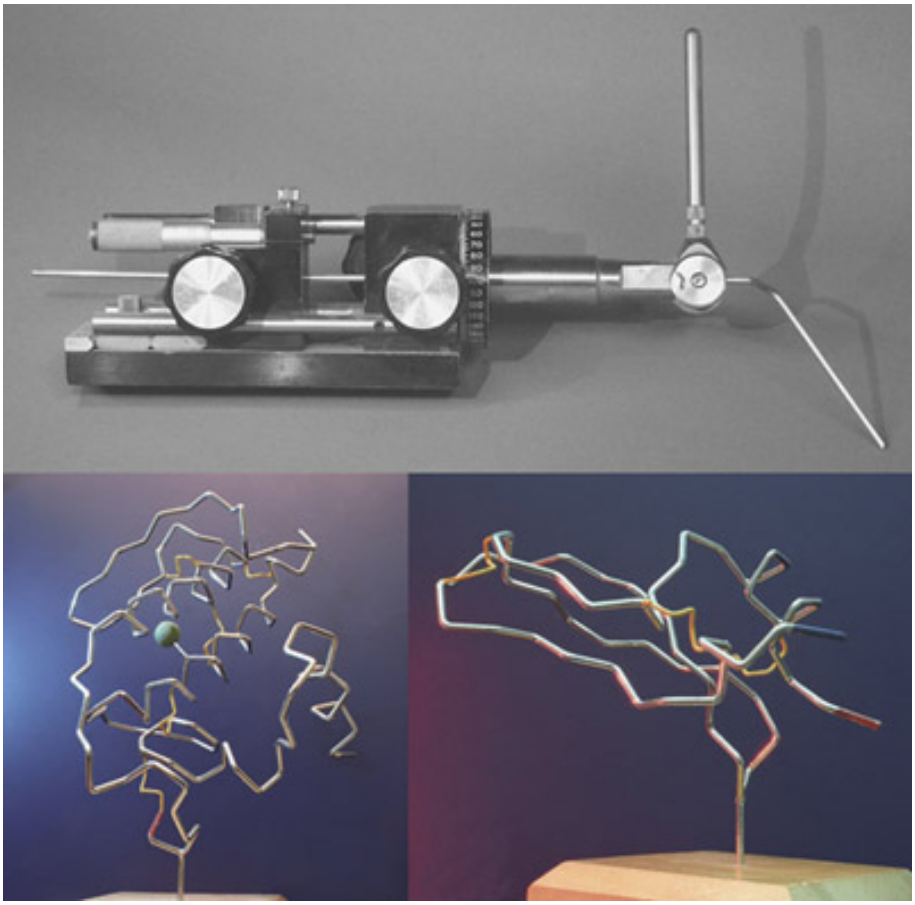

***Figure 8.** Byron's Bender (top) and two examples of obtained protein backbones (bottom). The picture has been taken from http://dataphys.org/list/byrons-bender//*

The growth of computers carried out the development of artistic-scientific representation of molecules.[230] Nowadays, a broad variety of software for the visualization of 3D molecular structures have been implemented, being VMD, PyMol or UCSF Chimera some of the most

230. Lesk, A. M. et al. *Science.* **1982**, *216* (4545), 539–540.

famous.[231–233] These programs allow the display of a simulation in a computer, facilitating the analysis of the results. The inclusion of GPU's as well as the development of new algorithms for visualization significantly improve the quality of the representations that we can obtain.[234–236]

During last decades, the massive implementation of augmented reality (AR), virtual reality (VR) and mixed reality (MR) in a large variety of fields, together with the increasingly easy access of these technologies with high quality, is gradually transforming media and entertainment and has already impacted, as it could not be otherwise, the world of Chemistry and Biology, changing the way we visualized MD simulations.[237] Although these technologies have existed since years ago, it has not been until very recently when they start to be successfully exploited enhanced by the continuous performance increases and the reduction of costs.[238,239] This fact allows to complement traditional pictures by adding new dimensions and information, as movement, 3D representations and even sound.[240,241]

Several steps have been done in this direction, being developed a number of software for the visualization of molecules in both VR and AR.[241–244] One of the most salient has been done by the group of Marc Baaden with the development of UnityMol, and interactive tool which allows the manipulation of RNA and other biomolecules taking

231. Humphrey, W. et al. *J. Mol. Graph.* **1996**, *14* (1), 27-28,33-38.
232. DeLano, W. L. *CCP4 Newsletter On Protein Crystallography*. 2002.
233. Pettersen, E. F. et al. *Journal of Computational Chemistry*. 2004.
234. Chavent, M. et al. *Brief. Bioinform.* **2011**, *12* (6), 689–701.
235. Chavent, M. et al. *J. Comput. Chem.* **2011**, *32* (13), 2924–2935.
236. Kozlíková, B. et al. *Comput. Graph. Forum* **2017**, *36* (8), 178–204.
237. Liu, X. H. et al. *Expert Opin. Drug Discov.* **2018**, *13* (12), 1103–1114.
238. Kenngott, H. G. et al. *Surg. Endosc.* **2018**, *32* (6), 2958–2967.
239. Cipresso, P. et al. *Front. Psychol.* **2018**, *9*, 2086.
240. Lv, Z. et al. *PLoS One* **2013**, *8* (3), e57990.
241. Yu, C. H. et al. *ACS Nano* **2019**, *7*, 7471–7482.
242. Zheng, M. et al. *J. Mol. Graph. Model.* **2017**, *73*, 18–23.
243. Borrel, A. et al. *Bioinformatics* **2017**, *33* (23), 3816–3818.
244. Kingsley, L. J. et al. *J. Mol. Graph. Model.* **2019**, *89*, 234–241.

advantage of the facilities of VR.[245–247] A steep forward using VR have been done by the group of David Glowacki. They developed a tool that can be used for performing on-the-fly interactive MD simulations, which enables users to manipulate molecules and observe their dynamics.[248,249] Although the application of these techniques has been widely focused to teaching proposed, its power can be clearly applied to research goals. One of the most engaging examples have been carried out by Glowacki, who has used its previous mentioned tool for training neural nets to predict potential energy surfaces.[250]

In our group, we have also tried to contribute to demolishing the wall between science and art, creating tools for real dissemination of scientific results using state-of-the-art visualization technologies, such as AR and VR. Some examples are *Ollomol for Captisol AR* and *Ollomol for Captisol VR*, which allows the representation of MD simulations of Captisol, a particular cyclodextrin, with different ligands, using AR or VR immersion, respectively. In this line, we have also developed some tools to visualize, in a different way, some of the results that will be presented in this memory.

Furthermore, considering that the explosion of immersive technologies has bumped head-on with the coronavirus disease 2019 (COVID-19) global pandemic caused by the severe acute respiratory syndrome–coronavirus 2 (SARS-CoV-2), we have proposed that they may be used to better understand the three-dimensional structures that compose the virus, as well as of those involved in the infection process and in possible treatments. Recently, we have reviewed the software implementations currently available for VR visualization of SARS-CoV-2 molecular structures, trying to impulse and facilitate the use of

245. Pérez, S. et al. *Glycobiology* **2015**, *25* (5), 483–491.
246. Doutreligne, S. et al. In *IEEE Symposium on Large Data Analysis and Visualization 2014, LDAV 2014 - Proceedings*; Institute of Electrical and Electronics Engineers Inc., 2014; pp 109–110.
247. Doutreligne, S. et al. In *2015 IEEE 1st International Workshop on Virtual and Augmented Reality for Molecular Science, VARMS@IEEEVR 2015*; Institute of Electrical and Electronics Engineers Inc., 2015; pp 1–6.
248. O'Connor, M. et al. *Sci. Adv.* **2018**, *4* (6), eaat2731.
249. O'Connor, M. et al. *J. Chem. Phys.* **2019**, *150* (22), 220901.
250. Amabilino, S. et al. *J. Phys. Chem. A* **2019**, *123* (20), 4486–4499.

these emerging technologies in research against COVID-19.[251] Additionally, we have also designed an application for smartphones and headsets (*Corona VRus Coaster*) which allows sliding down on the backbone of the protein structures from SARS-CoV-2, as if they were a roller coaster, providing unique perspectives. The application will be freely available at http://mduse.com/coronavruscoaster/.

251. Calvelo, M. et al. *Comput. Struct. Biotechnol. J.* **2020**, *18*, 2621–2628.

3. Objectives

Given the versality of SCPNs, this thesis has been designed to study these systems via a computational approach. It will be focused in four different points:

- **Study of the most stable β-sheet: parallel or antiparallel**: Due to the limited number of works using α,γ- or α,δ-CPs, the type of β-sheet that is formed when these systems form nanotubes remains unclear. In this way, the investigation of a possible preferred orientation will be evaluated.
- **SCPNs as molecular capsules**. Thanks to the inner cavity presented by these nanotubes, their use as containers for noble gases or carbon nanostructures (fullerenes and carbon nanotubes) will be considered.
- **SCPNs as transmembrane channels**. The stability and activity of different nanotubes formed by hydrophobic sequences and embedded in lipid membranes will be investigated, focusing on the transport properties of the internal cavity of these systems.
- **SCPNs as antimicrobial agents**. The self-assembly of amphipathic CPs, which ideally could show antibacterial activity, will be evaluated via the study of the interaction of these systems with membranes of different compositions, trying to elucidate the effect of the presence of certain lipids.

It is important to note that the time scales as well as the measured properties for the evaluation of the previous points will be different. Hence, different computational approaches have been used depending on the task of interest. In this way, this thesis will be split in three different sections, each one applying a certain computational method:

1. **Section I: Quantum methods.** The accuracy of these techniques will be applied to the study of the most stable β-sheet and the use of SCPNs as molecular capsules. Using

quantum methods, the obtainment of an optimized geometry together with an estimation of the energy is possible, which would allow a rigorous comparison between the possible candidates. These techniques will be restricted only to these two tasks due to the relatively small number of particles that compose these systems (less than 600 atoms), which allows to overcome the exigent computational effort.

2. **Section II: All-Atom Molecular Dynamics.** By using classical methods, the study of systems with a higher number of atoms is possible. Taking advantage of this fact, AA-MD simulations will be used for the study of SCPNs acting as transmembrane channels. The analysis of these simulations will allow the evaluation of the stability of nanotubes in this environment, as well as the analysis of the water and ion transport through their inner cavities.
3. **Section III: Coarse-Grained Molecular Dynamics.** Although the use of AA-MD allows the study of systems bigger than those using quantum methods, sometimes the time scales that can be reached are too short to observe some phenomena of interest. In this sense, CG-MD simulations appear as a promising alternative for the investigation of systems with a considerably high number of atoms, as well as for the easily reaching of time scales of the order of microseconds. This technique will allow to study the interaction between amphipathic CPs with membranes, being useful for observing the self-assembly and the stability of potential antimicrobial SCPNs in a lipid environment.

The designed tasks are expected to provide a whole overview of the SCPNs, including a structural, energetic and dynamical study, which will help to understand some of the main basis that govern their function in some of the most common applications of these novel systems. Furthermore, in order to present some of the results of the work in a different way, we have developed tools based on state-of-the art technologies (AR and VR), for the molecular visualization of particular structures.

I. Quantum methods applied to the study of cyclic peptide structures

Enhanced by the development of the power of computers, *in silico* approaches for the study of chemical and biological systems have emerged as suitable and versatile tools. Thanks to these approximations, the study of such systems even at atomistic level becomes affordable, to go deep into the frontiers of knowledge not reachable by wet-lab techniques. These properties have transformed computational chemistry into a basic tool to better understand the properties of biomaterials and putting at hand new abilities for the efficient design of new biomolecules. With these in mind, quantum mechanics studies have been carried out in order to elucidate the most stable stacking of α,γ- and α,δ-CPs, as well as their possible application as molecular containers. This level of theory allows to consider quantum effects, such as the presence of electrons and the polarization of bonds, at the cost of losing the explicit treatment of the solvent and the limitation of the size of the system. This research is expected to bring structural and energetic information, enhancing a more rational *bottom-up* design.

In the first of the following chapters, a deep analysis of the self-assembling properties of a new type of cyclic peptides based on the alternation of α-residues and cyclic δ-amino acids (α,δ-CPs) has been carried out. In order to examine the preferred stacking properties adopted by cyclic peptides bearing this type of amino acids, we carried out DFT and semi empirical calculations using simple dimeric models, being then extended to nanotubes. Although these new α,δ-CPs can interact either in a parallel or antiparallel fashion, our results confirm that the parallel β-sheet is the preferred, although it can be switched to the antiparallel stacking by modulating the lateral chains of the α-residues that can establish favourable cross-strand interactions. Moreover, the analogous comparison using the same methodology but

applied to α,γ-CPs models –up to the moment assumed as antiparallel like *D*,*L*-α-CPs– led to unforeseen conclusions, later confirmed by experimental studies, that the most stable conformation is the parallel β-sheet directed by the skeleton interactions through the interaction of α- and γ-faces. The results obtained in this chapter have been published in Calvelo, M.; Lamas, A.; Guerra, A.; Amorín, M.; Garcia-Fandiño, R.; Granja, J. R. *Chem. – A Eur. J.* **2020**, *26*, 5846-5858.

In the second chapter, the trapping capabilities of different noble gases by α,γ-CPs dimers have been evaluated *via* DFT calculations. The obtained results suggest that the encapsulation of Kr, Xe and Rn is favoured, although the entrance of chloroform emerges as the most stable. Additionally, it has been found that these receptors are able to adapt their geometry in order to adopt a more suitable conformation for the guest. This study is included in Pizzi, A.; Ozores, H. L.; Calvelo, M.; García-Fandiño, R.; Amorín, M.; Demitri, N.; Terraneo, G.; Bracco, S.; Comotti, A.; Sozzani, P.; Bezuidenhout, C. X.; Metrangolo, P.; Granja, J. R. *Angew. Chemie - Int. Ed.* **2019**, *58* (41), 14472–14476. Moreover, and taking advantage of the larger diameter of α,δ-CPs dimers, the encapsulation of carbon structures, as fullerenes or nanotubes, has been also tested by these new peptide assemblies. Using both semiempirical and DFT approximations, our results show favourable energies for such processes, opening the door to the use of α,δ-CPs nanotubes as containers of these kind of molecules.

Author affiliations:
-Calvelo, M.; Lamas, A.; Guerra, A.; Amorín, M; García-Fandiño, R.; Granja, J. R. and Ozores, H. L.: Centro Singular de Investigación en Química Biolóxica e Materiais Moleculares (CiQUS), Departamento de Química Orgánica, Universidade de Santiago de Compostela, 15782 Santiago de Compostela, Spain
-Pizzi, A.; Terraneo, G. and Metrangolo, P.: Laboratory of Supramolecular and Bio-Nanomaterials (SupraBioNanoLab) Department of Chemistry, Materials, and Chemical Engineering "Giulio Natta" Politecnico di Milano 20131 Milano (Italy)
-Dimitri, N.: Elettra—Sincrotrone Trieste S.S. 14 Km 163.5 in Area Science Park 34149 Basovizza—Trieste (Italy)
-Bracco, S.; Comotti, A.; Sozzani, P. and Bezuidenhout, C. X.: Department of Materials Science University of Milano Bicocca Via R. Cozzi 55, 20125 Milan (Italy)

4. Dimeric systems based on CPs

4.1. PRECEDENTS AND MOTIVATION.

Ghadiri's CPs are disk shaped structures able to stack forming nanotubes through the formation of β-sheet-like interactions between discs.[252] They consist on macrocycles made of an even number of α-residues in which *D*- and *L*-amino acids are alternated (*D*,*L*-α-CPs). This design predisposes the proton of the amide (NH) and carbonyl (C=O) groups of peptide bond to orient perpendicular to the plane of the backbone of the CPs. This orientation allows the interaction with a second unit in the same conformation through the formation of hydrogen bonds (H-bonds). Furthermore, the NH and C=O groups of the amino acids of the same chirality are pointing towards the same direction, whereas the analogous of the other chirality are oriented towards the opposite side. As natural protein sheets,[253–255] this cyclic peptide pairing can be stablished throughout two different types of interactions: the *parallel* (**Figure 9***A*) and the *antiparallel β-sheet* (**Figure 9***B*).[256] Regarding the parallel orientation, the H-bond network is formed by interactions between amino acids of opposite chirality (*D*-*L* interaction). Conversely, in the antiparallel arrangement the amino acids of the same chirality are the ones which are forming the H-bonds, resulting in the arisen of a *D*-*D* and a *L*-*L* interaction. It is important to note that whereas in the parallel orientation one amino acid is interacting with two residues of the facing CP, in the antiparallel the interaction each amino acid is forming H-bonds with only one residue of the facing CP. In any case, as it can be visualized in **Figure 9**, all the residues of the same chirality lye aligned along the nanotube structure.

252. Bong, D. T. et al. *Angew. Chem. Int. Ed. Engl.* **2001**, *40* (6), 988–1011.
253. Richardson, J. S. et al. *Proc. Natl. Acad. Sci. U. S. A.* **2002**, *99* (5), 2754–2759.
254. Fraser, R. D. B. et al. *Biophys. Rev.* **2009**, *1* (1), 27–35.
255. Chothia, C. et al. *Proc. Natl. Acad. Sci.* **1981**, *78* (7), 4146–4150.
256. Silk, M. R. et al. *Chem. Commun.* **2017**, *53* (49), 6613–6616.

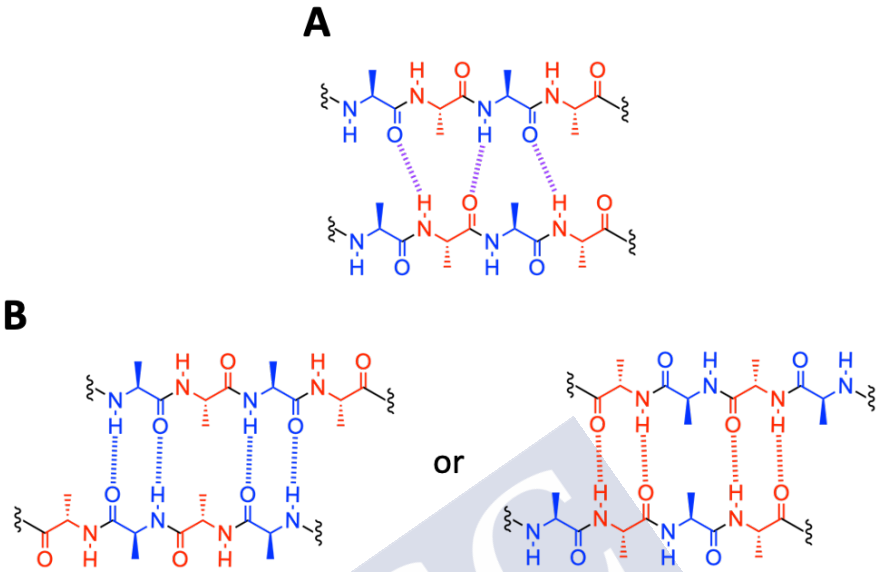

Figure 9. *Hydrogen pattern **A)** parallel and **B)** antiparallel in a β-sheet. The colors of the amino acids represent different chirality (D- in red and L- in blue). The H-bonds types are also coloured: red for those between D-residues, blue between L-residues and purple corresponds to H-bond between D- and L-amino acids.*

In order to determine the preferred orientation (if one would exist), a number of studies have been carried out so far. When Prof. Ghadiri's group synthetized these CPs for the first time, the antiparallel β-sheet was suggested as the most likely considering the observed electron diffraction pattern and FTIR (*Fourier-transform infrared spectroscopy*) studies.[72,84] Later on, in 1997, Gailer and Feigel performed the first computational study of two CPs composed by eight amino acids using semiempirical methods.[257] Their results showed almost identical energies for both interactions, finding a slightly preference for the antiparallel arrangement of only 0.13 kJ/mol, as well as a good concordance with the structure obtained by X-ray. On the other hand, NMR studies with CPs composed by Ala and Phe (cyclo-*D*,*L*-$(Ala)_4(Phe)_4$) in deuterated chloroform showed a preference

72. Ghadiri, M. R. et al. *Nature* **1993**, *366* (6453), 324–327.
84. Hartgerink, J. D. et al. *J. Am. Chem. Soc.* **1996**, *118* (1), 43–50.
257. Gailer, C. et al. *J. Comput. Aided. Mol. Des.* **1997**, *11* (3), 273–277.

for the antiparallel conformation.[258] Further studies with a higher calculation level also suggest some bias towards the antiparallel arrangement.[259,260] A more detailed explanation for the formation of the antiparallel orientation rather than the parallel was proposed by Liu and coworkers, who attributed the preference for this kind of β-sheet to the steric interactions between cross-strand side-chains which appear in the parallel structure.[261] Nevertheless, parallel nanotubes have been also reported, as the ones proposed by Silk et al.[256] In their work, they claimed that the formation of one or another β-sheet is directed by both intra- and inter-interactions and not only by the H-bonding pattern of the backbone, highlighting the importance of the side-chains interactions and crystal lattice. Another engaging model has been reported by the group of Undén, in which they were able to form nanotubes that could be made only from enantiomeric pairs of α-CPs.[262] This fact is due to the steric impediment of bulky side-chains, which prevents the formation of dimers of CPs with the same chirality and enhances the interaction between enantiomers (**Figure 10**).

256. Silk, M. R. et al. *Chem. Commun.* **2017**, *53* (49), 6613–6616.
258. Kobayashi, K. et al. *Angew. Chemie Int. Ed. English* **1995**, *34* (1), 95–98.
259. Scheiner, S. *J. Phys. Chem. B* **2006**, *110* (37), 18670–18679.
260. Kuzuya, A. et al. *Nano Lett.* **2007**, *7* (6), 1757–1763.
261. Qu, W. et al. *Int. J. Quantum Chem.* **2010**, *110* (9), 1648–1659.
262. Rosenthal-Aizman, K. et al. *J. Am. Chem. Soc.* **2004**, *126* (11), 3372–3373.

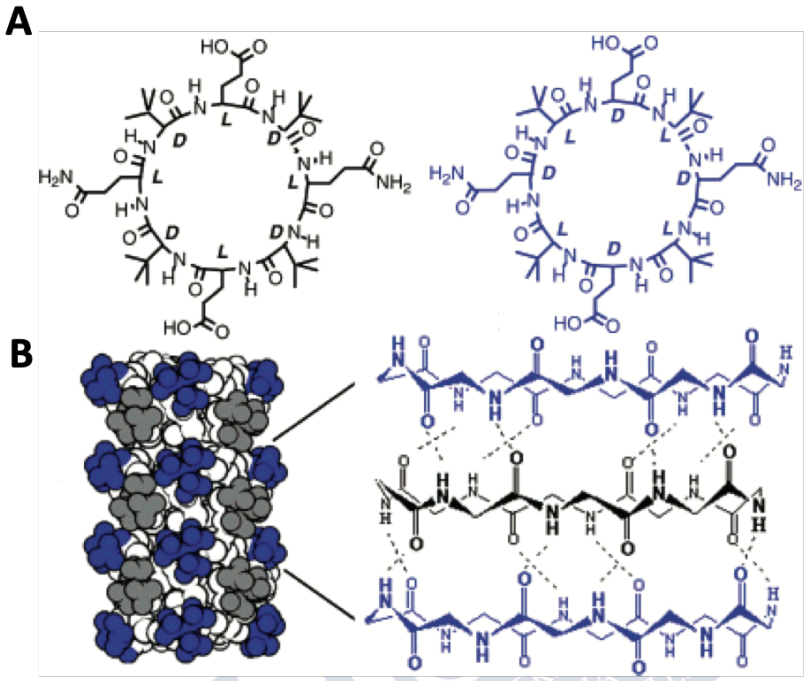

Figure 10. A) *α-CPs sequences and* ***B)*** *nanotube structure proposed by Undén, in which the steric impediment of the tert-leucine groups favours the stacking of alternating enantiomeric units. Image taken from* [262].

Apart from the SCPN model proposed by Prof. Ghadiri, based on α-amino acids, other alternatives using new CP motifs have been proposed so far.[67–69] One interesting example could be the α,γ-CPs developed by Prof. Juan Granja, from the University of Santiago de Compostela, which include a non-natural residue: cis-3-aminocycloalkanecarboxylic acid (γ-Acas).[95] α,γ-CPs can be derived from *D*,*L*-α-CPs by replacing any (or all) α-amino acid by a γ-residue of equivalent chirality, or in other words, replacing *L*-α-amino acids by a (1*R*,3*S*)-γ-Acas (or the analogous amino acids for the ones with

67. Rodríguez-Vázquez, N. et al. *Org. Biomol. Chem.* **2017**, *15* (21), 4490–4505.
68. Brea, R. J. et al. *Chem. Soc. Rev.* **2010**, *39* (5), 1448–1456.
69. Chapman, R. et al. *Chem. Soc. Rev.* **2012**, *41* (18), 6023–6041.
95. Amorín, M. et al. *J. Am. Chem. Soc.* **2003**, *125* (10), 2844–2845.

opposite chirality).[101–104,263] During last years, different motifs haven been proposed, changing the type as well as the number of α- and γ-residues.[99,106,264] In this chapter, we were focused in the CPs composed by the alternation of α-amino acids and cis-3-aminocyclohexanecarboxylic acid (γ-Ach), considering both enantiomers (**Figure 11**).

99. Guerra, A. et al. *Org. Biomol. Chem.* **2012**, *10* (44), 8762–8766.
101. Reiriz, C. et al. *J. Am. Chem. Soc.* **2009**, *131* (32), 11335–11337.
102. Montenegro, J. et al. *J. Am. Chem. Soc.* **2014**, *136* (6), 2484–2491.
103. Cuerva, M. et al. *ACS Nano* **2015**, *9* (11), 10834–10843.
104. Fuertes, A. et al. *Nanoscale* **2017**, *9* (2), 748–753.
106. Burade, S. S. et al. *Org. Lett.* **2017**, *19* (21), 5948–5951.
263. Brea, R. J. et al. *Angew. Chemie - Int. Ed.* **2005**, *44* (35), 5710–5713.
264. Amorín, M. et al. *Chem. - A Eur. J.* **2008**, *14* (7), 2100–2111.

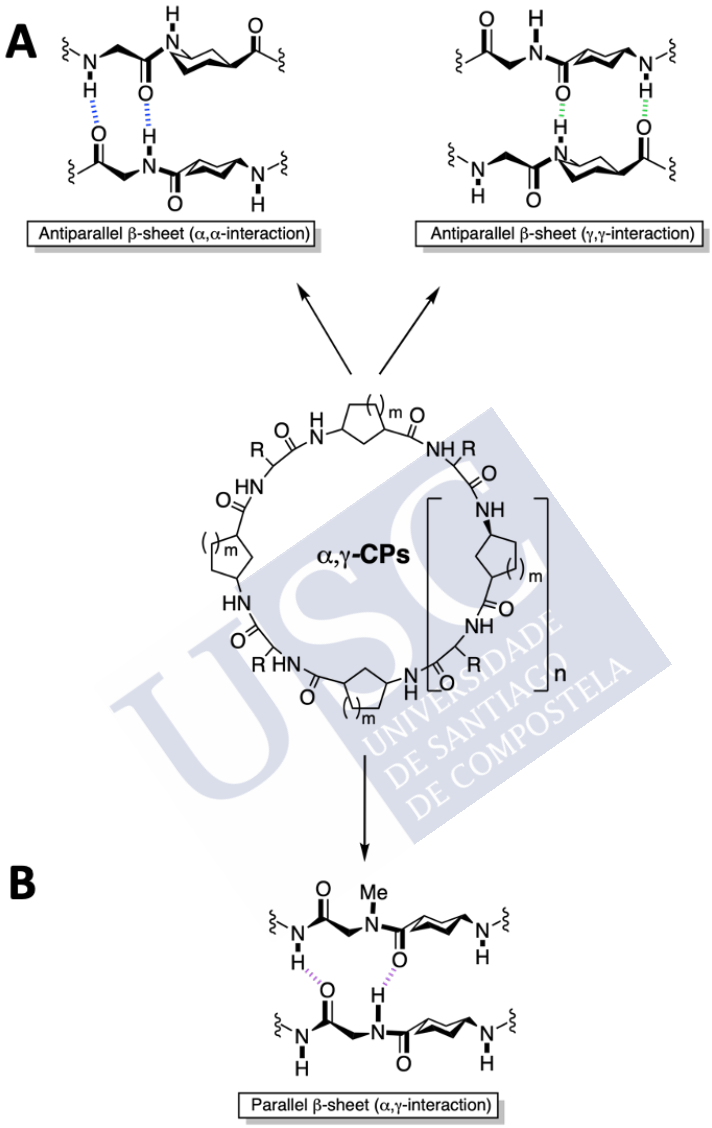

Figure 11*. Schematic representation of the H-bond pattern for the* ***A)*** *parallel and* ***B)*** *antiparallel* β*-sheets made of* α,γ*-CPs. The H-bonds between* α*-residues are coloured in blue, between* γ*-residues in green and purple was selected for H-bonds between* α*- and* γ*-amino acids.*

In the model proposed by Prof. Granja, every C=O and NH groups of the α-amino acids are pointing towards the same direction, whereas the analogous of the γ-Acas point towards the opposite side, analogously to the Ghadiri's CPs. First approximations, considering the different distance between the NH and C=O groups, suggest the adoption of an antiparallel β-sheet as the most favorable, leading to two different kind of interactions: α-α, between the α-amino acids, and γ-γ, between the γ-residues **Figure 11***A).* Theoretical studies carried out in the group suggest that the strength of both interactions is rather similar.[116] However, the dimerization energy shows a clear preference for the α-α, agreeing with previous experimental observations.[95] This effect could be due to the formation of intramolecular H-bonds between γ-amino acids when these groups are not participating in the H-bond network, stabilizing the monomeric form. Regarding the parallel orientation, the H-bond pattern changes, appearing a new kind of cross interaction between both faces: α-γ. In this case, each α-amino acid is interacting with the two γ-residues that are flanking the α-unit of the facing CP (**Figure 11***B*).

Furthermore, it is worth to mention that when a CP is composed by only four γ-amino acids, the aggregation and formation of nanotubes is also observed.[265] However, in this case both theoretical and experimental studies (NMR and FTIR) suggest that the formation of the parallel β-sheet is the most favored, although this was not confirmed for larger macrocycles, like octamers.[99]

More recently, the group of the Prof. Juan Granja has also proposed a new class of CPs, containing in this case trans-4-aminocyclohexanecarboxylic acids (δ-Ach).[107] Given that in this amino acid the 180º angle formed by the bond of the carboxylic and the Cα with the bond of N and the Cδ, a cyclic structure composed only by δ-Ach cannot be achieved. In this way, for the formation of SCPNs its combination with α-amino acids is mandatory. The group has shown

95. Amorín, M. et al. *J. Am. Chem. Soc.* **2003**, *125* (10), 2844–2845.
99. Guerra, A. et al. *Org. Biomol. Chem.* **2012**, *10* (44), 8762–8766.
116. García-Fandiño, R. et al. *J. Phys. Chem. B* **2010**, *114* (15), 4973–4983.
265. Li, L. et al. *Adv. Funct. Mater.* **2012**, *22* (14), 3051–3056.

that δ-Ach can be intercalated in between each pair of α-residues in Ghadiri's CPs, leading to the formation of *D*,*L*-α,δ-CPs (**Figure 11**).[107] These systems form nanotubes in which the δ-Ach residues adopt the role of rigid extenders, allowing to obtain assemblers with larger diameters than in the previous α,γ- and *D*,*L*-α-SCPNs.

It has been reported that CPs composed exclusively by residues with an even number of carbon atoms between the NH and C=O groups, as is the case of δ- and β-amino acids, can only form nanotubes following a parallel β-sheet.[266–273] However, thanks to the intercalation of α-amino acids, this limitation can be overcome, allowing the assembly of α,δ-CPs through both parallel and antiparallel arrangements. In the parallel sheet the NH and C=O groups of each α-residue are interacting with the complementary groups of the two δ-units which are flanking the α-amino acid of the same chirality in the neighbour CP (**Figure 12***A*). On the other hand, in the antiparallel orientation the α-amino acids of the same chirality are H-bonded. In both sheets the δ-Ach units are only forming one H-bond by residue either through the carbonyl or the amide proton (**Figure 12***B*). The main difference is that in the antiparallel organization these residues are mutually H-bonded. Due to the novelty of this *D*,*L*-α,δ-CPs, no theoretical (and very little experimental) studies have been carried out so far.

107. Lamas, A. et al. *Chem. Sci.* **2018**, *9* (43), 8228–8233.
266. Gauthier, D. et al. *Angew. Chemie Int. Ed.* **2001**, *40* (24), 4635–4638.
267. Baillargeon, P. et al. *Chem. - A Eur. J.* **2007**, *13* (33), 9223–9235.
268. Marmin, T. et al. *Chem. - A Eur. J.* **2019**, *25* (27), 6707–6711.
269. Seebach, D. et al. *Helv. Chim. Acta* **1997**, *80* (1), 173–182.
270. Clark, T. D. et al. *J. Am. Chem. Soc.* **1998**, *120* (4), 651–656.
271. Jagannadh, B. et al. *Chem. Commun.* **2006**, No. 46, 4847–4849.
272. Ishihara, Y. et al. *J. Pept. Sci.* **2010**, *16* (2), 110–114.
273. Fujimura, F. et al. *Biomacromolecules* **2006**, *7* (8), 2394–2400.

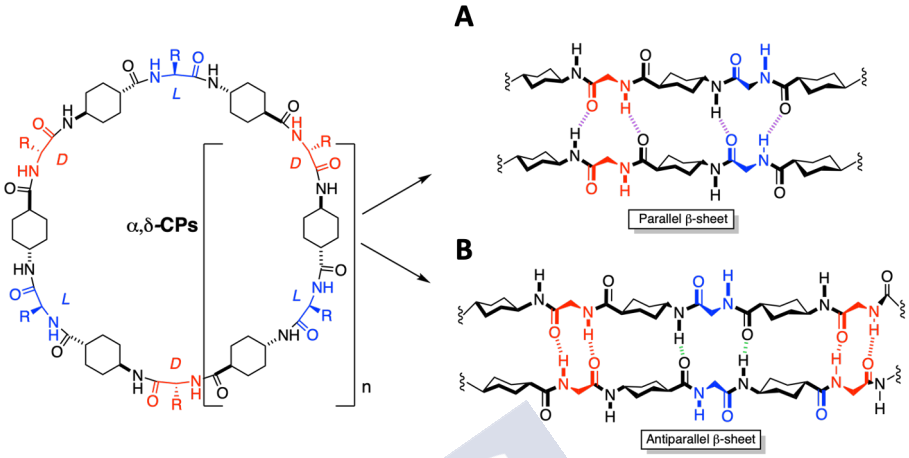

***Figure 12.** Schematic representation of the H-bond pattern for the **A)** parallel and **B)** antiparallel β-sheets made of D,L-α,δ-CPs. The colors of the α-amino acids represent different chirality (D- in red and L- in blue). The hydrogen bond types are also coloured: red for those between D-residues, green for those between δ-residues and purple correspond to H-bond between α- and δ-amino acids.*

4.2. AIM.

Knowing the most stable packing of dimers and nanotubes composed by the stacking of CPs could help to a better understanding of self-assembly processes, allowing a more rational design, improving their development following a *bottom-up* approach. With this in mind, a systematic computational study has been carried out, evaluating the different interactions in the dimers composed by α,γ-CPs and *D,L*-α,δ-CPs, trying to elucidate which β-sheet is the most stable: parallel or antiparallel.

Since this knowledge could be extrapolated to the formation of SCPNs, it would help to make a smarter and more efficient design of these structures. Although a number of works have been developed

focusing in Ghadiri's CPs,[256–262] very little have been done with α,γ-CPs and *D*,*L*-α,δ-CPs, proving the novelty of this goal.

4.3.METHODS.

The evaluation of which interaction is obtained from *in vitro* experiments is not so direct as using a computational approach. In order to facilitate this task, partially methylated CPs can be used. Using this strategy, the amide protons of one the two faces of the CPs are substituted by methyl groups, blocking the possibility of formation of H-bonds through this face, restricting the equilibria to the formation of dimers.[258] In this way, using this simple dimeric model of N-methylated peptides, competitive experiments can be carried out more easily. Considering this, the computational evaluation of the possible interactions between monomers in dimers made of α,γ-CPs and *D*,*L*-α,δ-CPs was done using these methylated models, with the idea of comparing the trends obtained from wet-lab experiments. Nevertheless, analogous studies using unmethylated peptides were also carried out, in order to try to extrapolate these results to SCPNs.

DFT calculations were performed using the Gaussian package.[165] Geometries of the systems were obtained from previous studies of the group as well as using chemical drawing software, as Avogadro and ChemOffice.[189,190] The structures were optimized using the B3LYP functional together with the standard 6-31G(d) basis set.[274–276] Due to convergence problems, the optimization of the geometries of more complex α,δ-dimers, such as those charged, was carried out using a

165. Frisch, M. J. et al. *Gaussian, Inc., Wallingford CT,* 2016.
189. Cousins, K. R. *J. Am. Chem. Soc.* **2011**, *133* (21), 8388.
190. Hanwell, M. D. et al. *J. Cheminform.* **2012**, *4* (8), 17.
256. Silk, M. R. et al. *Chem. Commun.* **2017**, *53* (49), 6613–6616.
257. Gailer, C. et al. *J. Comput. Aided. Mol. Des.* **1997**, *11* (3), 273–277.
258. Kobayashi, K. et al. *Angew. Chemie Int. Ed. English* **1995**, *34* (1), 95–98.
259. Scheiner, S. *J. Phys. Chem. B* **2006**, *110* (37), 18670–18679.
260. Kuzuya, A. et al. *Nano Lett.* **2007**, *7* (6), 1757–1763.
261. Qu, W. et al. *Int. J. Quantum Chem.* **2010**, *110* (9), 1648–1659.
262. Rosenthal-Aizman, K. et al. *J. Am. Chem. Soc.* **2004**, *126* (11), 3372–3373.
274. Becke, A. D. *J. Chem. Phys.* **1993**, *98* (7), 5648–5652.
275. Rassolov, V. A. et al. *J. Chem. Phys.* **1998**, *109* (4), 1223–1229.
276. Rassolov, V. A. et al. *J. Comput. Chem.* **2001**, *22* (9), 976–984.

semiempirical method: PM7.[156]

The interaction and dimerization energies were calculated using the same functional but with a higher-level basis set: 6-31+G(d,p), except for the charged α,δ-CPs, in which 6-31G(d) was used due to the previous mentioned issues. The energies were corrected for basis set superposition error (BSSE) using the Counterpoise approach.[277] In addition, terms for the treatment of empirical dispersion were included using the Becke-Johnson (D3BJ) correction.[180,181] Some recent studies have demonstrated that this functional does quite well among traditional DFT functionals, especially in the case of systems containing amino acids, as in this case.[278]

The interaction energy is defined as follows:[279]

$$\boldsymbol{Interaction\ Energy} = Energy_{dimer} - (Energy_{CP-A} + Energy_{CP-B})$$

This magnitude provides the contribution to the total energy coming from the interaction between both CPs. In this case, the geometry considered for calculating the energy of the CPs ($Energy_{CP-A}$ and $Energy_{CP-B}$) is the one that each CP has when they are forming a dimer.

Dimerization energy was also calculated, and it can be written as:

$$\boldsymbol{Dimerization\ Energy} = Interaction\ Energy - (Energy_{CP-A\ isol.} + Energy_{CP-B\ isol.})$$

Where $Energy_{CP-A\ isol.}$ and $Energy_{CP-B\ isol.}$ correspond to the energy of the isolated CPs. So, the difference between Interaction and Dimerization energy is that in the second one the deformation energy is considered. In this way, the penalty for changing the geometry that each CP has in its monomeric form until acquiring the conformation that they have in a dimer is taking into consideration.

156. Stewart, J. J. P. *J. Comput. Chem.* **1989**, *10* (2), 209–220.
180. Grimme, S. et al. *J. Chem. Phys.* **2010**, *132* (15), 154104.
181. Grimme, S. et al. *J. Comput. Chem.* **2011**, *32* (7), 1456–1465.
277. Simon, S. et al. *J. Chem. Phys.* **1996**, *105* (24), 11024–11031.
278. Kesharwani, M. K. et al. *J. Chem. Theory Comput.* **2016**, *12* (1), 444–454.
279. Boys, S. F. et al. *Mol. Phys.* **1970**, *19* (4), 553–566.

Moreover, QTAIM (Quantum Theory of Atoms in Molecules) calculations have been carried out for the α,γ-dimers using the same level of theory that the Counterpoise calculation. With that, the electron density of the BCPs (Bond Critical Points) corresponding to the H-bonds and the interaction between the oxygens of the carbonyl groups oriented towards the face of the H-bond network with near hydrogens were calculated. These calculations have been carried out using the program *Multiwfn*.[280]

Furthermore, and in order to provide a new and fancy visualization of the dimers composed by α,γ-CPs, a tool for displaying these systems using AR has been developed: *Dimerdice*, which is available for Android in the Play Store (https://play.google.com/store/apps/details?id=com.mduse.DimerDice&hl=es).[281] The images of different CPs are used as trackers for the different faces of a dice. Pointing with a smartphone or tablet device to each tracker separately, an AR image of the corresponding monomer is viewed. When the tracker images of two monomers are placed close to each other, the structure of the dimer formed by that combination of cyclic peptides is shown.

4.4. RESULTS.

4.4.1. α,*δ*-CPs.

Recently, it has been shown that *D*,*L*-α,δ-CPs can be obtained from Ghadiri's *D*,*L*-α-CPs.[107] Depending on the number of amino acids that form the CPs, octamers (8 amino acids, 4 α and 4 δ), dodecamers (12 amino acids, 6 α and 6 δ) and hexadecamers (16 amino acids, 8 α and 8 δ) were designed. Following the recommendations obtained from the experimental studies, these studies started considering dodecamers (**Figure 13**) due to their larger association constant. For the exclusive evaluation of the interaction between the backbone, alanines (Ala) were selected to avoid possible side-chain related conformational diversity

107. Lamas, A. et al. *Chem. Sci.* **2018**, *9* (43), 8228–8233.
280. Lu, T. et al. *J. Comput. Chem.* **2012**, *33* (5), 580–592.
281. Dimer dice - Apps on Google Play https://play.google.com/store/apps/details?id=com.mduse.DimerDice&hl=en (accessed Jun 18, 2020).

and also attractions/repulsions between side-chains. N-methylated models, blocking one of the faces of the CPs, were used in order to allow the comparison with *in vitro* experiments. It is important to note that the selective methylation of peptide bonds led to the formation of two new species of CPs, depending on which face were incorporated methyl groups. In one of the CPs (**CP1**) each *L*-α-amino acid and the previous δ-Ach (whose amide protons are pointing towards the same direction) are methylated, whereas in the other CP (**CP2**) the NH of the *D*-α-amino acids and the groups of the δ-Ach pointing to the same direction are substituted by the methyl groups. In this way, **CP1** and **CP2** are enantiomers.

In **Figure 13** the three possible dimers which could be constructed doing combinations of **CP1** and **CP2** are shown. **CP1** can interact with itself (another **CP1**), leading to a dimer with an antiparallel β-sheet (**D1a**). For the enantiomer **CP2**, the process is analogous, resulting in the antiparallel dimer **D2a**. Both dimers (**D1a** and **D2a**) are also enantiomers. Moreover, **CP1** and **CP2** can also interact, leading to the formation of a heterodimeric structure: **D1-2p**. In this case, the complex exhibits a parallel β-sheet like structure.

Since these α,δ-CPs are able to form nanotubes, analogous unmethylated dimers were also computationally evaluated. However, it should be noted that these unmethylated models are deformed as result of the formation of intramolecular H-bonds between the C=O and NH groups of different residues of the face that is not involved in the formation of the dimer. Therefore, the extrapolation of these dimers to the nanotube structure should be taken with care, since such a situation would only take place at the edges of the nanotube. Furthermore, in the unmethylated model only one CP is required because **CP1**$_{\textbf{unmeth.}}$ and **CP2**$_{\textbf{unmeth.}}$ are identical, leading in this case to just one parallel (**D1p**$_{\textbf{unmeth.}}$) and one antiparallel (**D1a**$_{\textbf{unmeth.}}$) dimers.

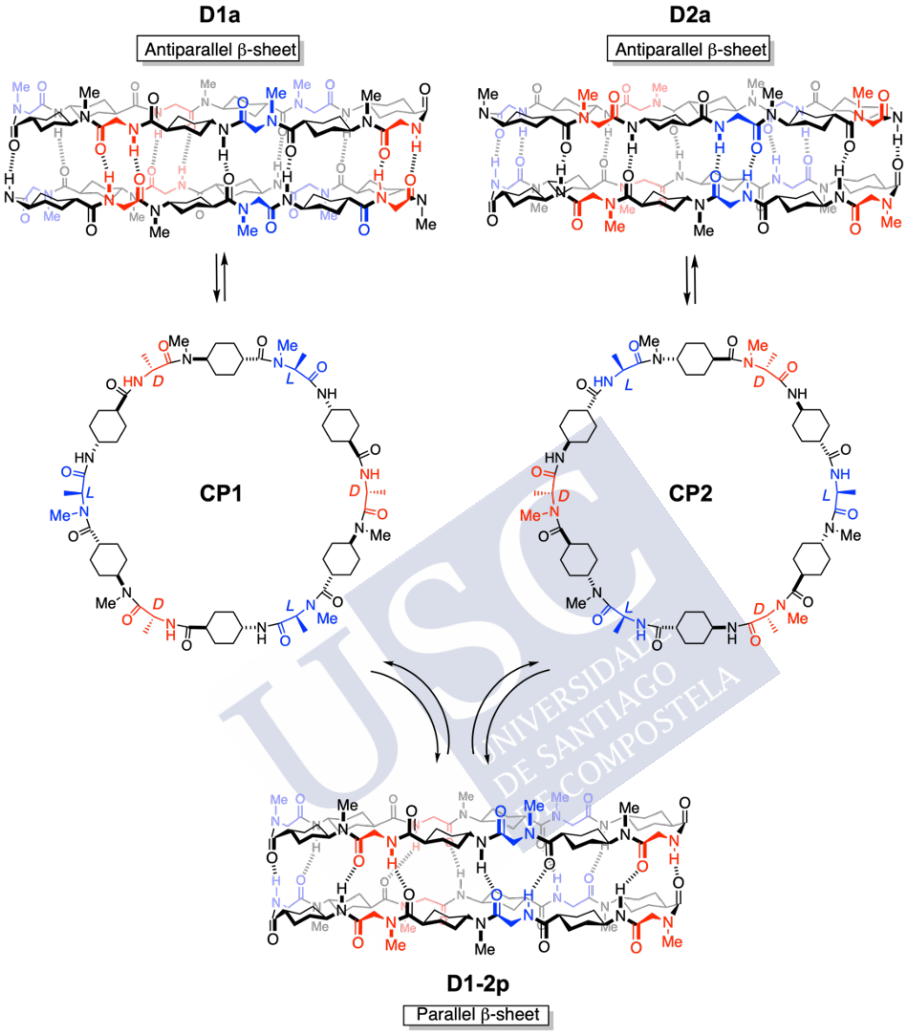

Figure 13. *Methylated α,δ-CPs studied (**CP1** and **CP2**) and their corresponding homo- and heterodimers: **D1a** and **D2a** (antiparallel β-sheet) or **D1-2p** (parallel β-sheet).*

DFT calculations were carried out with the model systems **D1-2p**, **D1a** and **D2a**, as well as with the isolated **CP1** and **CP2** monomers. The optimized structures are shown in **Figure 14***A*. It is important to note that only **D1a** and **CP1** are printed, since the structure and energy of the corresponding enantiomer (**D2a** and **CP2**) were considered

identical, by definition. The visual analysis of the structures reveals the hexagonal-like shapes of both dimers, showing an approximate C6 symmetry. The side views representations allowed to note that the parallel dimer presents a slight deviation from planarity that, in principle, could be attributed to steric interactions between N-methyl and carbonyl groups of the α-amino acid. However, analogous calculations with non-methylated CPs also showed this deviation, leading to the rejection of this hypothesis (**Figure 14***B*). Additionally, a chair conformation of the cyclohexane rings is found. In any case, the C=O and NH groups in both arrangements remain oriented roughly perpendicular to the ring planes for both methylated and non-methylated CPs, allowing the formation of tight H-bonds.

The optimization of the monomer **CP1** led to a structure with symmetry C3, changing its conformation with respect to that exhibited in the dimer due to the emergence of intramolecular H-bonds between the C=O of N-methylated δ-Ach and the NH of the nearest non-methylated δ-Ach (distances around 2.11 Å). (**Figure 14***A*). It may be anticipated that this stabilization of the monomeric form will have a significant influence on the dimerization energies, since it will provoke and increase in the energy needed for the deformation of the CP in order to reach the conformation that it has in the dimer.

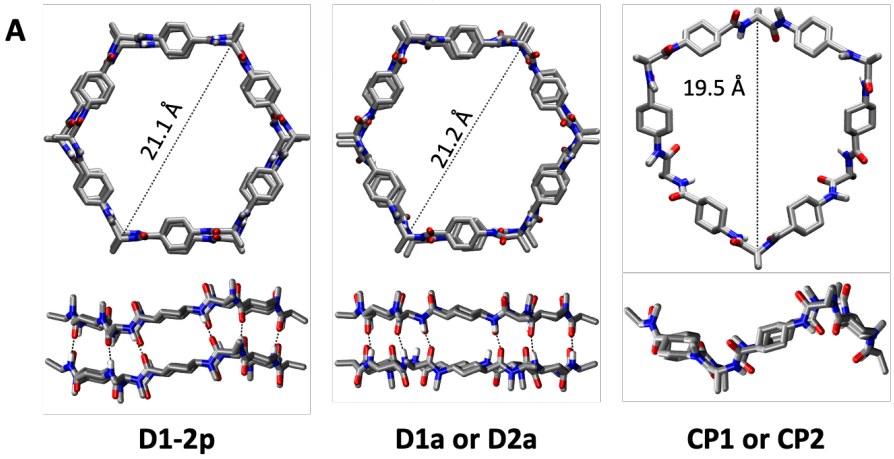

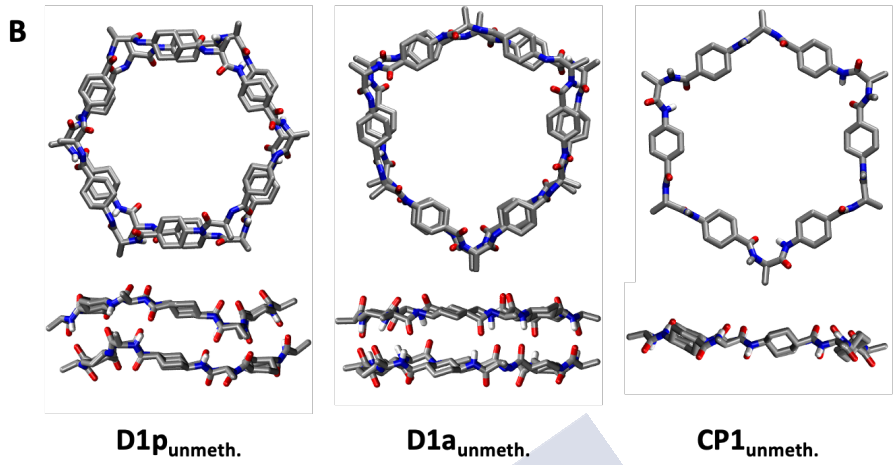

Figure 14. *A) Top and side view of the optimized geometries of the parallel* ***D1-2p*** *and antiparallel* ***D1a*** *dimers and monomer* ***CP1*** *(or* ***CP2****). For simplicity, only the polar hydrogens are displayed. B) Top and side view of the more stable conformations of the non-methylated parallel* ***D1-2p*** *and antiparallel* ***D1a*** *dimers and monomer* ***CP1*** *(or* ***CP2****). All structures were optimized at the B3LYP/6-31G(d) level.*

It can be also noted that the largest distances between Cα atoms of non-consecutive amino acids of opposite chirality of the same monomer are very similar in both orientations, being around 21.1 Å in the parallel and 21.2 Å in the antiparallel arrangement. This distance is shorter for the monomeric form, with a value of 19.5 Å. The inter-peptide distances, considering the centre of mass of both CPs, are about 5.1-5.2 Å, slightly longer than those corresponding to α,γ-dimers.[116]

Interaction and dimerization energies calculated using the Counterpoise approach are displayed in **Table 1A**. These results show that the interaction energy for the methylated parallel dimer **D1-2p** is 3.7 kcal/mol more favourable than the antiparallel (**D1a** and **D2a**). The same trend can be observed for the dimerization energy, although in this case the difference is slightly smaller (2.6 kcal/mol). However, in a competitive experiment, it has to be noted that both **CP1** and **CP2** are present in equilibrium conditions. Additionally, given the fact that **D1a** and **D2a** are enantiomers, its energy is the same. Thus, the formation of

116. García-Fandiño, R. et al. *J. Phys. Chem. B* **2010**, *114* (15), 4973–4983.

two methylated parallel dimers **D1-2p** would be favoured over the formation of two antiparallel arrangements (**D1a** and **D2a**) in 8.4 kcal/mol (considering the interaction energy) or 5.2 kcal/mmol (considering the dimerization energy).

Same tendency is observed considering the unmethylated model (**Table 1B**). It is worth to mention that same conclusions were obtained experimentally, being the formation of the parallel heterodimer **D1-2p** the most favoured.[282]

***Table 1A.** Interaction and dimerization energies (in kcal/mol) for the methylated α,δ-dimers.*

Parallel D1-2p		**Antiparallel (D1a** or **D2a)**	
Interaction Energy	Dimerization Energy	Interaction Energy	Dimerization Energy
-124.4	-95.0	-120.7	-92.4

***Table 1B.** Interaction and dimerization energies (in kcal/mol) for the non-methylated α,δ-dimers.*

Parallel D1p$_{unmeth.}$		**Antiparallel D1a$_{unmeth.}$**	
Interaction Energy	Dimerization Energy	Interaction Energy	Dimerization Energy
-143.7	-128.7	-138.4	-120.8

In order to understand better these results, the most relevant geometrical descriptors of the H-bonds (O···N and O···H distances as well as O···H-N and C=O···H angles) for both arrangements were calculated and presented in **Table 2**. Due to the similar energy trend, only the methylated model was considered.

282. Calvelo, M. et al. *Chem. – A Eur. J.* **2020**, *26* (26), 5846–5858.

Table 2. *Relevant geometrical parameters for the optimized geometries of methylated α,δ-dimers. Blue and red colours are used to identify the different H-bond types, corresponding to those involving α-amino acids or and δ-Ach, respectively. Distances are presented in Å and angles in degrees.*

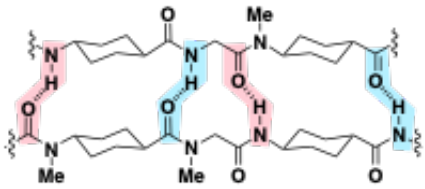

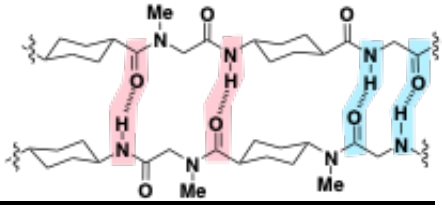

D1-2p				D1a or D2a			
O···N	**O···H**	**O···H–N**	**C=O···H**	**O···N**	**O···H**	**O···H–N**	**C=O···H**
2.95	1.93	174.85	168.68	3.00	1.99	168.69	146.31
2.97	1.96	170.80	174.25	3.00	1.99	168.74	146.34
2.95	1.93	174.68	168.57	3.01	2.02	164.52	159.07
2.97	1.96	170.59	174.19	3.01	2.02	164.32	159.13
2.95	1.93	174.82	168.60	3.00	2.00	168.58	146.23
2.97	1.96	170.64	174.19	3.00	2.00	168.61	146.25
2.95	1.93	174.94	168.75	3.01	2.02	164.17	159.09
2.97	1.96	170.76	174.12	3.01	2.02	164.24	159.14
2.95	1.93	174.70	168.50	3.00	2.00	168.67	146.27
2.97	1.96	170.86	174.50	3.00	2.00	168.51	146.13
2.95	1.93	174.78	168.67	3.01	2.02	164.26	158.97
2.97	1.96	170.71	174.25	3.01	2.02	164.31	159.06

For the parallel dimer (**D1-2p**), both O···N and O···H distances are lightly shorter when the H is coming from the α-unit (2.95 and 1.93 Å vs 2.97 and 1.96 Å), which probably is caused by a smaller rigidity of these amino acids. This alternation is also observed for the antiparallel disposition (3.00 and ~2.00 Å vs 3.01 and 2.02 Å), corresponding the shortest values to the H-bonds between α-amino acids. Furthermore, the H-bond distances are slightly larger compared to the parallel dimers.

The alignment of the atoms intervening in H-bonds is also an issue. In principle, due to its directionality, it is known that the larger the O···H-N angle, the stronger the interaction. In the case of C=O···H angles, the strongest interaction is expected to be found at angles of 120º due to the directionality of the lone pair of the oxygen atom of the carboxylic group.[283,284] In all the dimers the alternation found for the distances is also observed for the angles. Regarding the parallel dimer **D1-2p**, the most favourable O···H-N (~174º) and C=O···H (~169º) angles are in agreement with the shorter H-bonds distances (~1.93 Å) corresponding to the H-bonds involving the NH of the α-units. In the antiparallel dimers (**D1a** or **D2a**), the shortest H-bond distances (~1.99 Å) and most favourable angles (O···HN~169º and C=O···H~146º) are found in the bonds between α-amino acids. It is worth to mention that although H-bond distances as well as O···H-N angles are more favourable in the case of the parallel disposition, suggesting a better H-bonding alignment for this stacking, the antiparallel conformation displays lower C=O···H angles, contrary to which one could expect.

The differences in the stability of these systems could also be related to the relative disposition of the axial protons that were not directly participating in the H-bond network: the cyclohexyl moieties, which are parallelly oriented with respect to the D3 axis of the dimers; the α-hydrogens (H-α) and one of the protons of the side chain of the Ala residues (H_{SC}) of each CP (**Figure 15**). Average distances, together with minimum inter-hydrogen distances histograms for **D1-2p** and **D5a** or **D6a**, are presented in **Table 3**.

283. Taylor, R. et al. *Acc. Chem. Res.* **1984**, *17* (9), 320–326.
284. Desiraju, G. R. *Acc. Chem. Res.* **1996**, *29* (9), 441–449.

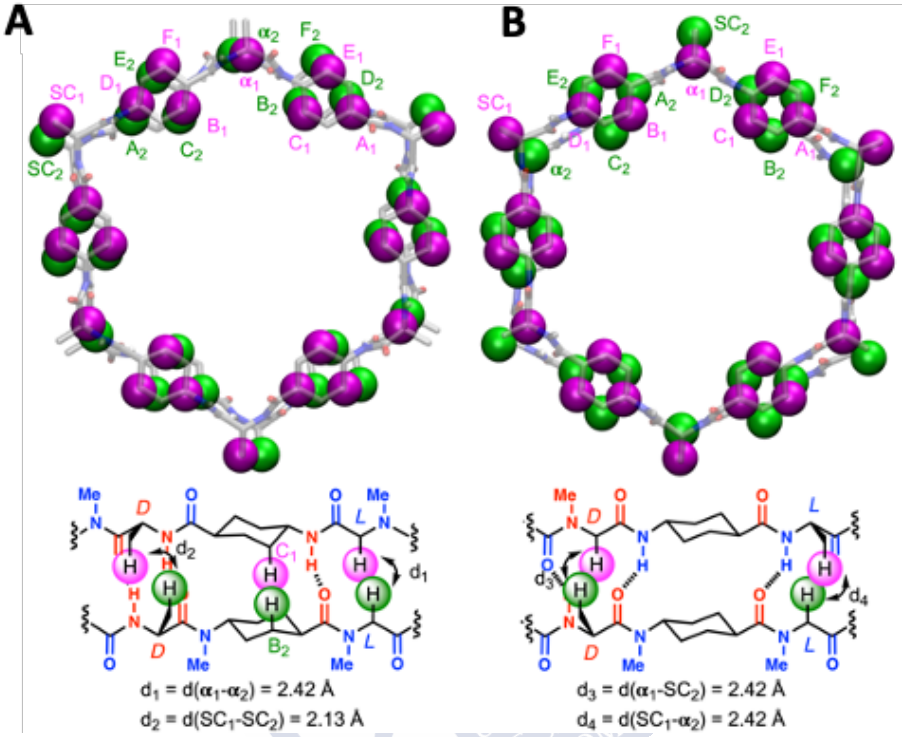

Figure 15. *Top (up) and side (bottom) view of the cyclic dodecapeptide dimers in which the axial protons of the cyclohexyl moieties are represented as CPK models and highlighted in colours (pink for the hydrogens of the top CP and green for those corresponding to the bottom CP);* ***A)*** *antiparallel* ***D1a*** *or* ***D2a*** *and* ***B)*** *parallel* ***D1-2p*** *representation. Hydrogen labels A, B, C, D, E and F correspond to the cyclohexyl moieties of each Ach residue, α to the H-α and SC to the side chain (SC) hydrogens Subscript (1 and 2) denotes the two different types of dipeptides that constitute the CP sequence.*

***Table 3.** Up: Minimum inter-hydrogen distances histograms in the parallel **D1-2p** and the antiparallel **D1a** or **D2a** dimers. Down: Average distances (in Å) and standard deviation in the optimized geometries, in which hydrogen labels A, B, C, D, E and F correspond to the cyclohexyl moieties of each Ach residue. Standard deviations smaller than 0.01 are omitted.*

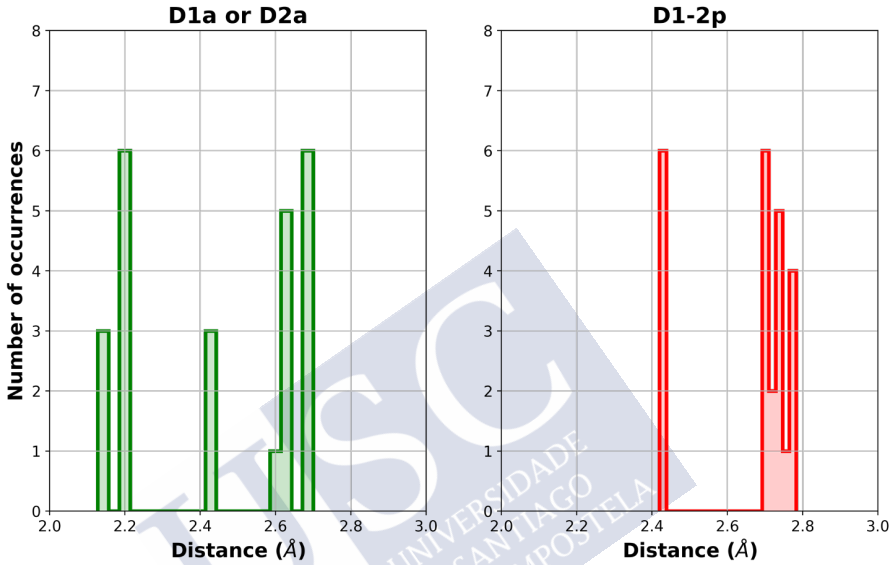

	Antiparallel (D1a or **D2a)**			**Parallel D1-2p**		
	B	D	F	B	D	F
A	–	2.70	–	2.76±0.01	–	2.81±0.01
C	**2.21**	–	–	2.70±0.01	2.92±0.02	–
E	–	–	2.62	–	2.73±0.01	3.14±0.01

As it is possible to observe in **Figure 15**, in the antiparallel structure the axial hydrogen atoms of the cyclohexyl moieties lie almost aligned on top of each other. In addition, H-α of the methylated α-residues and H of the Ala side chain (H_{SC}) are also close to each other (d_1 and d_2, respectively). Although most of the inter-hydrogen distances are longer than the sum of the van der Waals radii (~2.4 Å), there are a couple of contacts below that range, as it could be seen in the histogram

of **Table 3**. These distances were observed before in some X-ray crystal structure reported by the group.[263] The three values shorter than 2.2 Å (d_2) correspond to the distances between the side chain hydrogens (H_{SC}), and also to the 6 values corresponding to the distance between hydrogens B and C of each facing cyclohexyl moieties (the ones corresponding to the methylene group projected towards inner cavity of the dimer). This fact could be produced due to the twisting of the cyclohexyl ring in order to minimize those interactions. The values longer than the van der Waals radii correspond to the distances between the H-α (α_1- α_2, the three values at ~2.4 Å) and between the remaining axial hydrogens of each facing cyclohexyl moieties (A-D and E-F, twelve distances at ~2.6-2.7 Å).

On the other hand, in the parallel β-sheet all the axial hydrogen of both peptides are interdigitated and the inter-hydrogen distances are always longer than the sum of the van der Waals radii, as illustrated in the corresponding histogram of the **Table 3**. This could be the reason for the shorter H-bonds found for the parallel β-sheet. In this conformation, each axial H-atoms of the cyclohexyl moieties of each CP are flanked by two protons of the paired CP, *i.e.* H_A by H_B and H_F. In the histogram two values are reported for each hydrogen with distances ranging between 2.7-2.8 Å. In this β-sheet, each H-α is packed together with the side chain proton of Ala residue of the paired CP (distances d_3 and d_4 in **Figure 15**, depending on the chirality of the residues) at a distance around ~2.4 Å (in the histogram, the three distances at that value).

After the study of dodecameric CPs, the next step was the evaluation of dimers made up of octameric α,δ-CPs. For that purpose, DFT studies with **CP3** and **CP4** have been carried out (**Figure 16**).

263. Brea, R. J. et al. *Angew. Chemie - Int. Ed.* **2005**, *44* (35), 5710–5713.

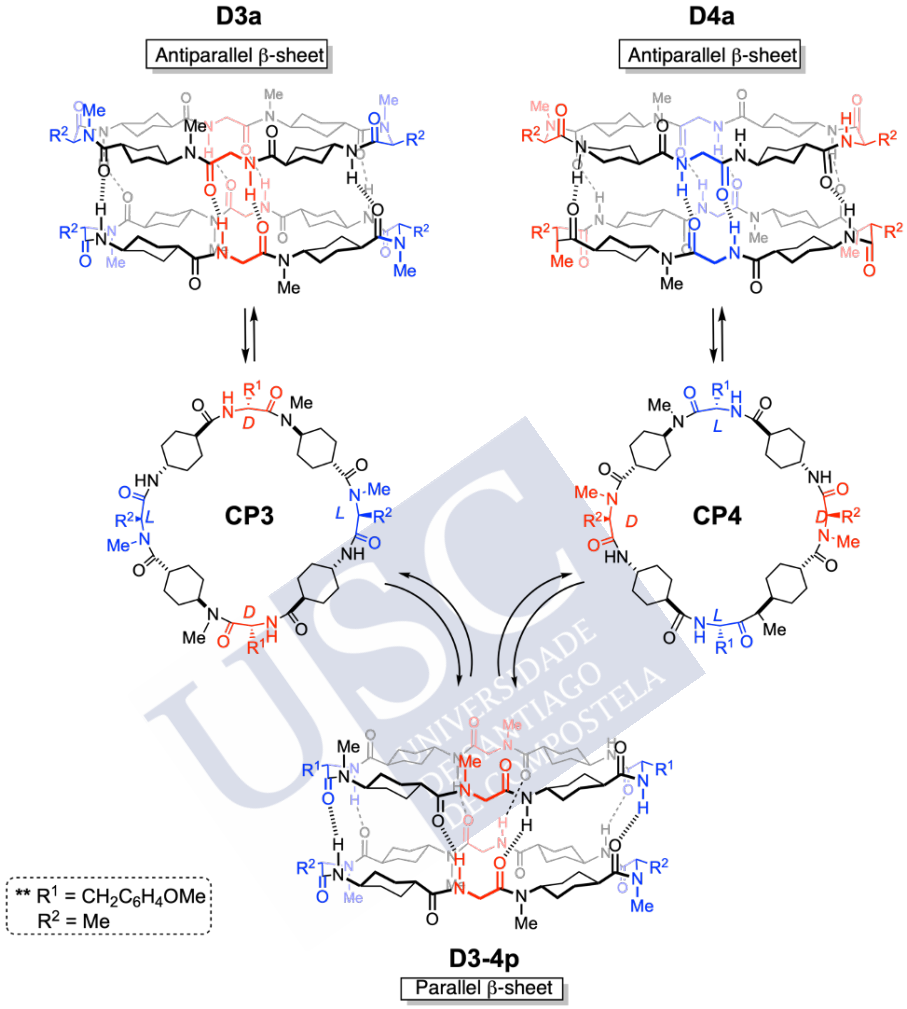

Figure 16. *Partially methylated octameric α,δ-CPs studied (**CP3** and **CP4**) and the corresponding dimers obtained by combinations between them: **D3a** and **D4a** (antiparallel β-sheet) or **D3-4p** (parallel β-sheet).*

Experimentally, it has been found that analogous CPs do not form antiparallel β-sheets (analogous to **D3a** and **D4a**), remaining as monomers in solution, whereas the mixture of both peptides provided the formation of a new specie that was assigned as the parallel dimer (analogous to **D3-4p**). In this way, in order to mimic more carefully the experimental sequence, tyrosines (Tyr) protected as methyl or benzyl

ethers were selected as side chains for *L*- or *D*- residues in **CP3** and **CP4**, respectively.

The interaction and dimerization energies are presented in **Table 4**, together with the optimized structures at B3LYP/6-31G(d). Despite the experimental conclusions, the computationally results suggest that formation of both dimers (parallel and antiparallel) is possible with a very similar stability, being impossible to discriminate between them. This fact opens de door to other possible experimental factors that could be acting in the prevention of the antiparallel arrangements.

Table 4. *Top: Optimized geometries of* ***A)*** *the parallel* ***D3-4p*** *and* ***B)*** *antiparallel* ***D3a*** *(or* ***D4a****) dimers and* ***C)*** *the monomer* ***CP3*** *or (****CP4****) (top and side views). For simplicity, only the polar hydrogens are displayed. Down: Interaction and Dimerization Energies (in kcal/mol) for the octameric α,δ-Dimers.*

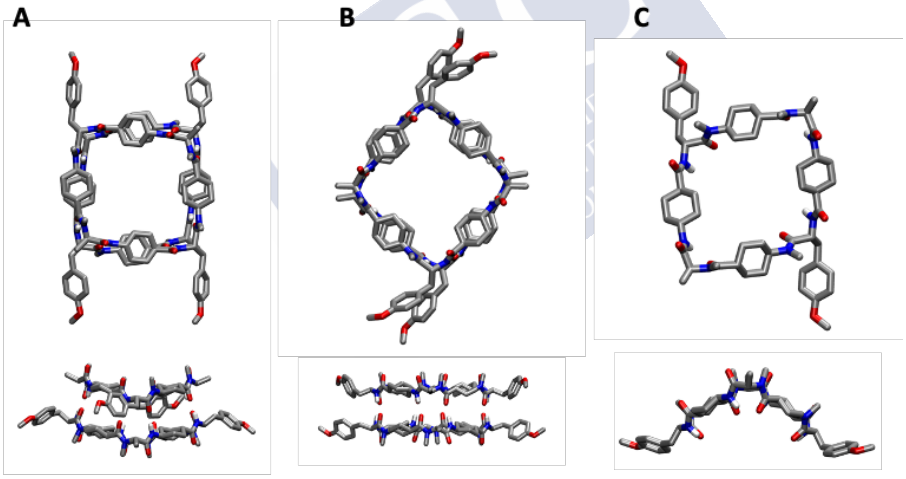

Parallel D3-4p		**Antiparallel (D3a** or **D4a)**	
Interaction Energy	Dimerization Energy	Interaction Energy	Dimerization Energy
-82.6	-55.5	-83.8	-54.3

After evaluating the interaction properties of the CPs with dimeric models, the next step was the study of these systems in nanotubes. For that, computational calculations of the dimeric models presented in **Figure 17**, which correspond to the first attempt to obtain α,δ-SCPN with hydrophobic cavity, were carried out.[107] **CP5** was designed to form single nanotubes that could be characterized by AFM on mica surface, assuming that the antiparallel sheet was the main interactions that dove the formation of the tubular aggregate (**SCPN5**). In this design, cationic *D*-Arginines (*D*-Arg) were introduced to interact with mica, facilitating nanotube deposition on this surface. In addition, glutamic acid (Glu) and lysine (Lys) with the same chirality were incorporated with the aim to control the β-sheet register in the nanotube through the formation of salt bridge interactions. In this way, stacking in which Glu and Lys are close should maximize the attractive interactions.

Different rotamers can be proposed following this design: three antiparallel (**D5a$_A$**, **D5a$_B$** and **D5a$_C$**) and three parallel (**D5p$_D$**, **D5p$_E$** and **D5p$_F$**) (**Figure 17**). Each of these three dimers derive by rotating one of the CPs along the C3 axis perpendicular to the plane of the disc-shaped structure. Regarding the antiparallel possibilities, it seems that **D5$_C$** should be the most stable, since in this form the electrostatic interactions (Glu-Lys) are maximized. In addition, in **D5a$_A$** and **D5a$_B$** Lys-Lys and Glu-Glu pairing were found, which would destabilize the dimers. On the other hand, in the parallel β-sheets, **D5p$_D$** should be the least favoured due to the pairing between Arg and Arg, Lys and Lys and Glu and Glu. Considering that, the study was focused in the **D5a$_C$**, **D5p$_E$** and **D5p$_F$** structures.

107. Lamas, A. et al. *Chem. Sci.* **2018**, *9* (43), 8228–8233.

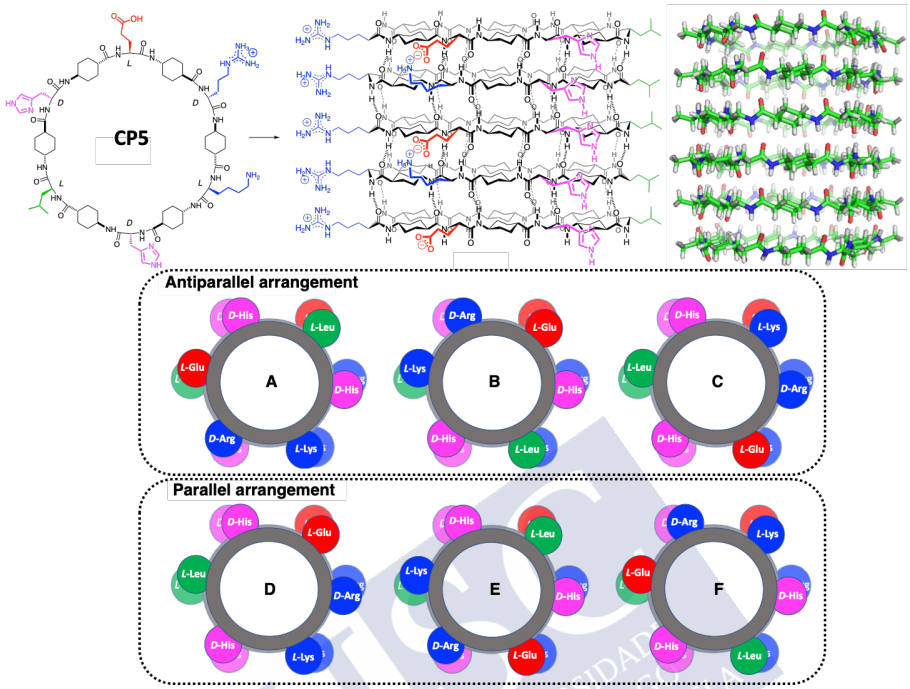

Figure 17. *Model of nanotube (**SCPN5**) obtained by the assembling of six units of **CP5** and, on the right, the computer-generated model in which all the amino acids side chains were changed by methyl groups. At the bottom, top-view model of the three different dimeric forms derived from this CP for each type of interactions (parallel and antiparallel) to evaluate the side chain cross-strand interactions between two CPs. Only in the antiparallel form C can form two salt-bridged interactions between Glu and Lys side chains. His-Arg pairs are also observed in other stacking models (E, A or F) but in these cases, the alignment of Arg residues to facilitate the interaction with the mica surface or Leu to maximize hydrophobic contacts are not observed.*

As in the previous systems, dimers were selected as model of study, using in this case no methylated amide bonds that would not allow the formation of nanotubes. Given the higher number of atoms of these systems as well as the presence of charged residues, convergence problems were found. In order to overcome this issue, an optimization using a lower level of theory was selected: the semiempirical PM7 method. Same strategy was followed for the Counterpoise calculations,

using in this case B3LYP-D3BJ together with the 6-31G(d) basis set. The results, together with the optimized geometries at PM7 level, are shown in **Figure 18**. Since in this case all dimers were composed by the same CP, only the interaction energy was evaluated.

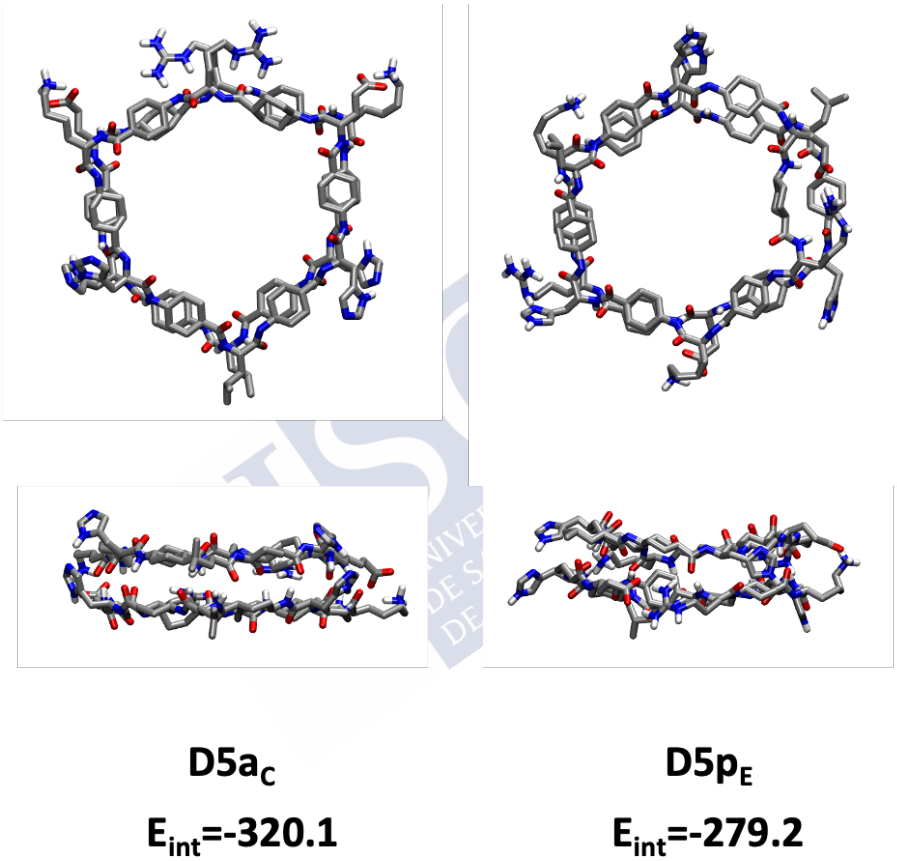

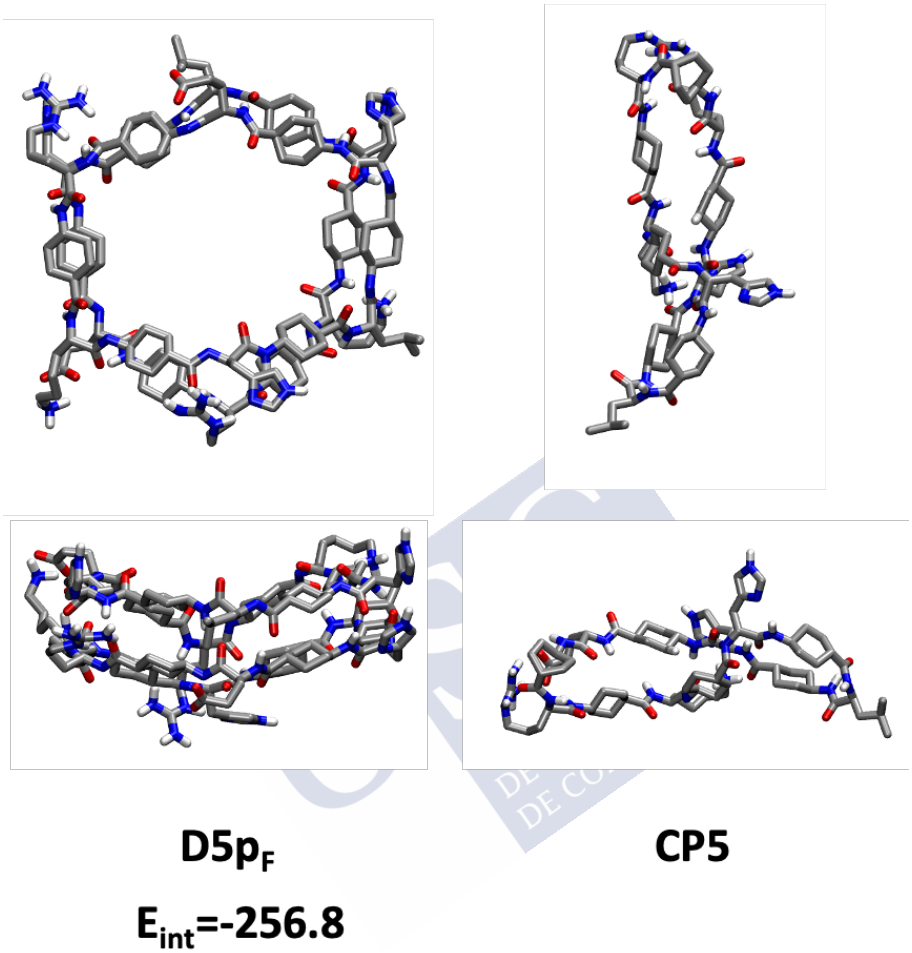

Figure 18. *Computer generated structures of the antiparallel **D5a**$_C$ and parallel **D5p**$_E$ and **D5p**$_F$ dimers, together with the monomer **CP5** optimized at the PM7 level (top and side views). For simplicity, only the polar hydrogens are displayed. Interaction energies (in kcal/mol) calculated at B3LYP-D3BJ/6-31G(d) level of theory are shown in each case.*

The calculated interaction energies suggest that, in this case, and accordingly to the designed experiment, the antiparallel dimer **D5a**$_C$ is the most favourable structure, being its interaction energy 40.9 and 63.3 kcal/mol more stable than the parallel dimers **D5p**$_E$ and **D9p**$_F$, respectively. These huge energy differences suggest that the

experimental nanotubes must be formed by the antiparallel packing of cyclic peptides. In addition, these results intimate that the parallel and antiparallel arrangements in *D*,*L*-α,δ-CPs can be controlled by the modulation of the peptide sequence by placing the mutually favourable cross-strand interactions between the residues along the nanotube.

Up to this point, a new class of dimers and nanotubes composed by CPs based on the alternation of α-residues and δ-Ach residues has been analysed using quantum methods (DFT and semiempirical). Our results suggest that when the side chains of the CPs are not involved in the interaction (interaction governed by the backbone), the preferred pattern of arrangement for these systems is the parallel β-sheet. However, this pattern could be reverted modulating the contribution of the side chain interactions through specific combinations among them.

4.4.2. α,γ-CPs.

In view of the above results, we decided to extend our study to classical α,γ-dimers, which were supposed to adopt an antiparallel arrangement. For that purpose, the N-methylated models represented in **Figure 19** were selected. As it was mentioned, in these kinds of CPs, because of the alternation between α- and γ-amino acids, two different hydrogen bond patterns are observed, since C=O and NH groups of each type of residue (α or γ) pointed towards opposite directions, the α- and the γ-faces. Therefore, the alkylation of one face forces the CP to interact through the other face. If the N-methyl groups are on the α-amino acids (**CP6**), this CP would dimerize through the γ-face, whereas the CP having methylated the γ-residues (**CP7**) it would self-assemble through its α-face. These CPs lead to the formation of dimers: **D6a**, which shows an antiparallel β-sheet through a γ-γ interaction; **D7a**, which presents another antiparallel β-sheet formed through an α-α interaction. Additionally, heterodimer **D6-7p** would be formed by mixing both peptides. This dimer forms a parallel sheet through the interaction of α-γ faces. In this first step, only one enantiomer was considered (all α-amino acids were *D-,* being all the *L*-residues substituted by γ-Ach units), but it is worth to mention that the number of possible sheets increases if the other enantiomer is present. This issue will be discussed further.

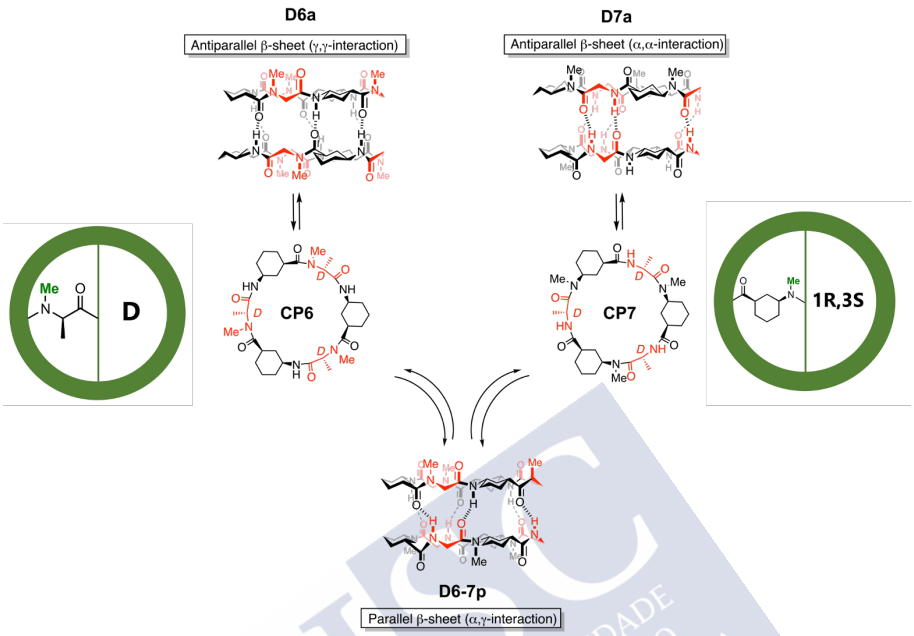

Figure 19. *Structure of the α,γ-CPs studied (**CP6** and **CP7**) and their corresponding dimers. **CP6** was prepared as a model of antiparallel interaction through the γ,γ-interaction (homodimer **D6a**), **CP7** as a model of antiparallel α,α-interaction (homodimer **D7a**). Combination of **CP6** and **CP7** provides a model of the parallel β-sheet (dimer **D6-7p**), in which all the residues of the same type and chirality (α- or γ-amino acids) are aligned and thus the interaction takes place between the γ-face of one CP (**CP6**) with the α-face of the other peptide (**CP7**). The molecular viewer Dimerdice AR®, developed by us, can be used for displaying **CP6** and **CP7** in AR using the trackers on the sides of the figure.*

In **Figure 20** and **Figure 21** the optimized dimers at B3LYP/6-31G(d) level together with some geometrical parameters are illustrated. The geometries of the antiparallel dimers (**D6a** and **D7a**) match well with those previously described in the literature, as well as the H···O and the N···O distances.[95,116,263] Whereas in the antiparallel

95. Amorín, M. et al. *J. Am. Chem. Soc.* **2003**, *125* (10), 2844–2845.
116. García-Fandiño, R. et al. *J. Phys. Chem. B* **2010**, *114* (15), 4973–4983.
263. Brea, R. J. et al. *Angew. Chemie - Int. Ed.* **2005**, *44* (35), 5710–5713.

arrangements all those distances are similar, in the parallel **D6-7p** dimer there is an alternation between shorter and longer distances, which corresponds to the two kind of H-bonds that the dimeric structure holds: the H-bonds between the C=O groups of the α-residues and the NH groups of the γ-amino acids and the interaction between the C=O of the γ-residues and the NH of the α-amino acids. It is important to note that in this case the shortest O···H distances correspond to H-bonds that involve amide proton of the non-natural amino acid (γ-amino acid), contrary to the observed for the *D*,*L*-α,δ-dimers. Additionally, the H-bond distances (~1.92 Å) and the O···H-N angles of the shortest H-bonds (~174º) of **D6-7p** are more favourable than those in the antiparallel dimers [**D6a** (~166º) or **D7a** (~167º)], which might correspond to stronger H-bonding interactions. The C=O···H angles, contrary, are larger in **D6-7p** dimer (~165º versus ~156º for **D6a** and ~144º for **D7a**), and thus less favourable.

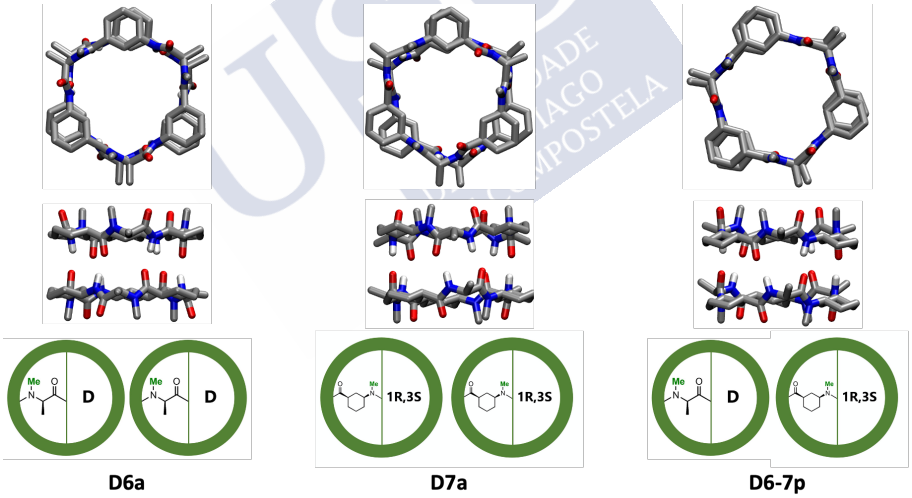

D6a **D7a** **D6-7p**

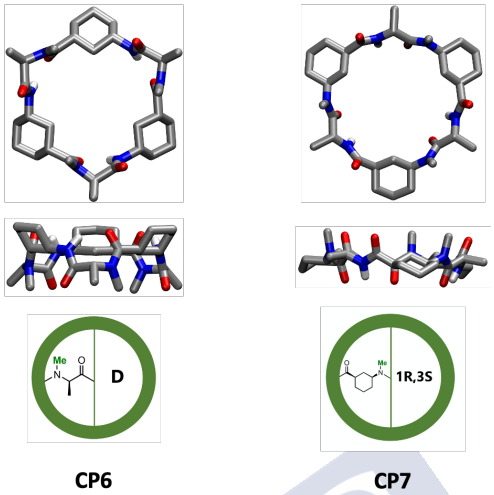

Figure 20. *DFT optimized geometries of the parallel* ***D6-7p*** *and antiparallel* ***D6a*** *and* ***D7a*** *α,γ-dimers (top and side views), together with the monomers* ***CP6*** *and* ***CP7****. For simplicity, only the polar hydrogens are displayed. The molecular viewer Dimerdice AR®, developed by us, can be used for displaying the dimers in AR using the trackers above the side views.*

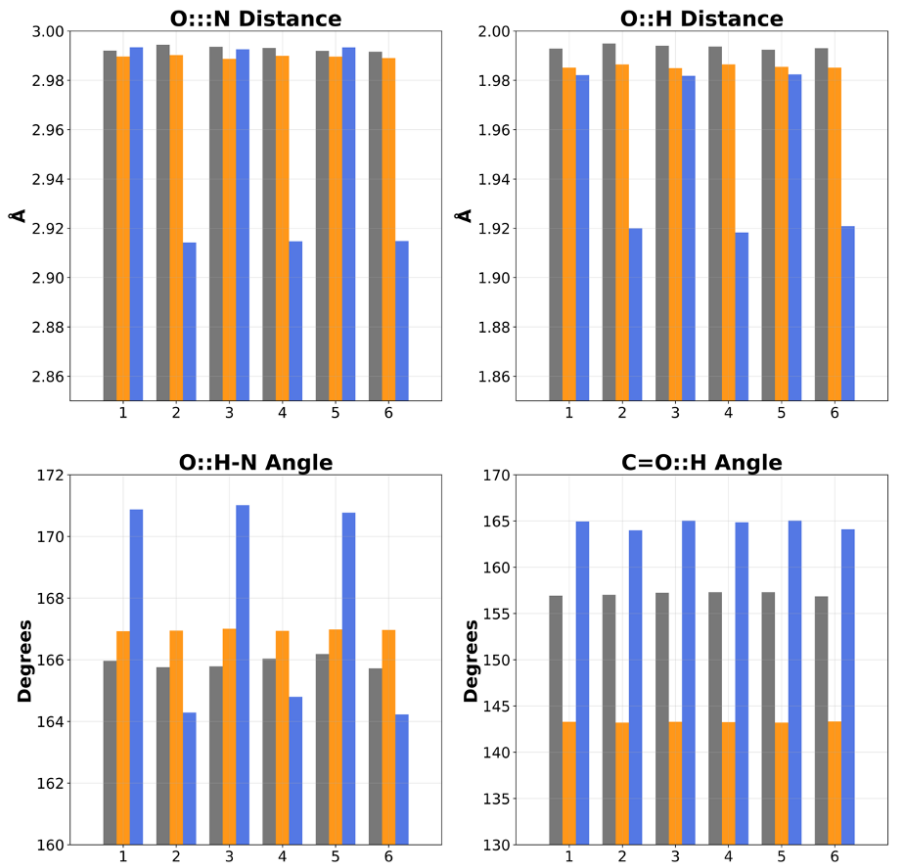

Figure 21. *H-bond distances and angles of the dimeric structures* ***D6a***, ***D7a*** *and* ***D6-7p***. *The colour code is grey for* ***D6a***, *orange for* ***D7a*** *and blue for* ***D6-7p***. *Each value of the x axis corresponds to a bond or angle between each pair of residues of the hexameric dimer*.

Table 5 depicts the interaction and dimerization energies calculated at B3LYP/6-31+G(d,p) level using the Counterpoise method. The combination of two parallel **D6-7p** dimers is 4.3 kcal/mol more favourable than the sum of two antiparallel **D6a** and **D7a** dimers. In terms of the dimerization energy, this preference for the parallel arrangement is even greater, since the difference is 6.4 kcal/mol. This result is highly remarkable since, as far as we know, this parallel stack had never been previously contemplated for these CPs.

Table 5*. Interaction and Dimerization Energies (in kcal/mol) for α,γ-dimers in the parallel* ***D6-7p*** *and antiparallel* ***D6a*** *and* ***D7a*** *arrangements.*

	D6a	**D7a**	**D6-7p**
	γ-γ	α-α	α-γ
Interaction Energy	-61.1	-59.6	-62.5
Dimerization Energy	-38.6	-51.8	-48.4

The results also suggests that the interaction energy is pretty similar for both α-α and γ-γ interactions, as it was previously reported.[116] The slight differences which favour the γ-γ interaction could come from a better alignment of the H-bonds formed in **D6a** (lower O···N and O···H distances, larger O···H-N angles and lower C=O···H angles, **Figure 21**). However, **CP6** could present H-bonds between the non-methylated NH and C=O groups of the γ-residues which do not appear in **CP7** (since these residues are methylated), leading to the stabilization of the monomeric form. This fact inverts the trend of the dimerization energy, enhancing the formation of **D7a** over **D6a** and **D6-7p**.

As it was mentioned before for the α,δ-CPs, the different pattern in the disposition of the axial hydrogens could explain the stability differences of the β-sheet structures α,γ-systems (**Figure 22** and **Table 6**). In the antiparallel **D6a** and **D7a** dimers, there is a certain superposition of those hydrogens, leading to distances smaller than the van der Waals radii, especially in the case of the γ-γ interaction (**D6a**). In this dimer, there are three distances with a value shorter than 2.2 Å, which correspond to the interaction of the axial hydrogens of the methylene moieties projected towards the cavity of the dimer. The remaining six axial hydrogens of the cyclohexyl moiety stand at a distance of around 2.4 Å with respect the facing ones. In addition, the three distances between H-α have a value of around 2.5 Å. Regarding the other antiparallel dimer (**D7a**), there are three distances around 2.2 Å corresponding to the H_{SC} (dSC1-SC2), as well as another nine nearly 2.8 Å, which correspond to the distances between the resting axial

hydrogens of the cyclohexyl moiety. In the parallel dimer (**D6-7p**), none distance with values clearly shorter than the van der Waals radii are found. In this case, three distances at 2.4 Å corresponding to the interaction between H-α and H_{SC} emerge, together with another nine distances at around 2.6 Å that can be linked with the interactions between the three axial hydrogens of the cyclohexyl residues.

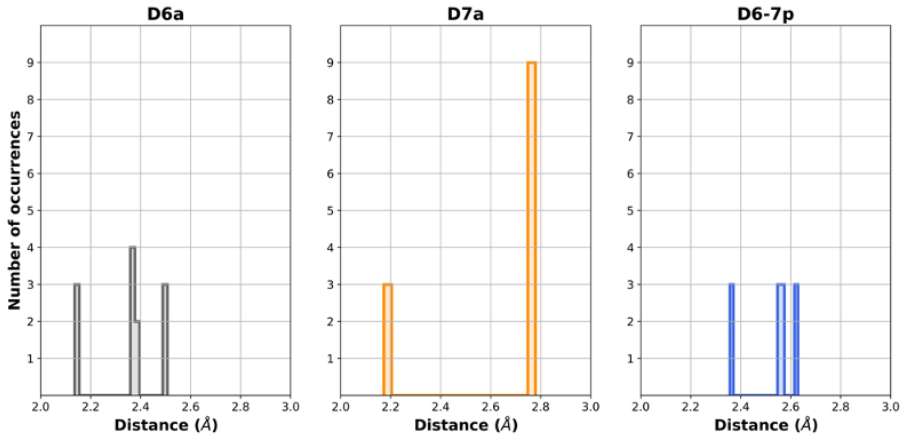

***Figure 22.** Minimum inter-hydrogen distances histograms between the cyclohexyl axial-hydrogens, H-α and H_{SC} of both CPs in the parallel **D6-7p**, the antiparallel **D6a** and the antiparallel **D7a** dimers.*

Table 6*. Average distances (in Å) and standard deviation in the optimized geometries of the antiparallel* ***D6a*** *and* ***D7a*** *and the parallel* ***D6-7p*** *dimers, in which hydrogen labels A, B, C, D, E and F correspond to the cyclohexyl moieties of each Ach residue and the subindex (1 or 2) corresponds to the top or bottom CP, respectively. In the antiparallel β-sheets, in brackets the hydrogen to which the distance was determined. When no standard deviation is indicated means that it is smaller than 0.01 Å.*

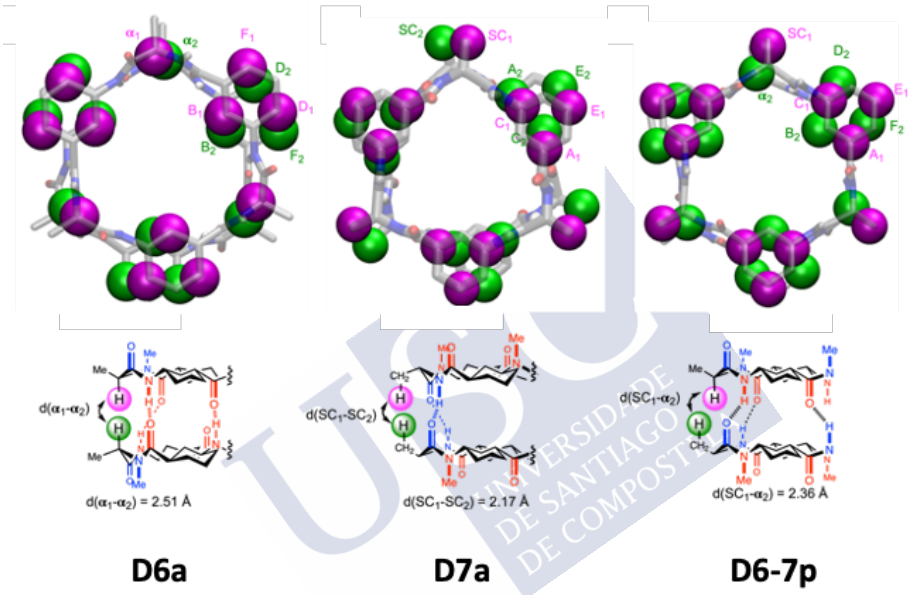

Antiparallel				Parallel (D6-7p)		
D6a		D7a		B_2	D_2	F_2
B_1	2.14 (B_2)	A_1	2.77±0.01 (C_2)	3.08±0.01	-	2.55
D_1	2.37 (F_2)	C_1	2.77±0.01 (A_2)	2.94	2.57	-
F_1	2.37±0.01 (D_2)	E_1	3.00±0.01 (E_2)	-	3.34±0.01	2.63±0.01

Finally, we also evaluated the combinations between the enantiomers of **CP6** and **CP7**: **CP8** and **CP9**, respectively. These peptides can be combined among themselves (in a similar manner to the described before but also with the corresponding enantiomers, increasing the number of possible combinations for the formation of dimers (**Figure 23**). In both cases, the enantiomers **CP8** and **CP9** are composed by *L*-α-amino acids. These CPs can form dimers similarly to those formed by **CP6** and **CP7** and, assuming that the energy of enantiomers is the same, **D6a** = **D8a**, **D7a** = **D9a** and **D6-7p** = **D8-9p**. However, when both enantiomers are mixed, two new parallel (**D6-8p** and **D7-9p**) and one new antiparallel (**D7-8a** and **D6-9a**) β-sheets could be proposed. In all these structures the α-residues are aligned with the γ-amino acids, in contrast with previous dimers in which γ- and α-residues are paired with themselves. The parallel arrangements are formed between CPs with the same methylation pattern: **D6-8p**, which presents a γ-γ interaction, in which both CPs have all the α-amino acids N-methylated; and **D7-9p**, whose CPs have the N-methylated γ-residues and consequently they are forming the β-sheet packing through their α-α faces. The antiparallel motif comes from the formation of an α-γ interaction between one CP with N-methylated α-residues and another CP with N-methylated γ-amino acids: **D6-9a** or **D7-8a**. These two dimers are enantioforms and, thus, equivalent from an energetic point of view. It is worth to mention that whereas the interactions coming from dimers composed by one enantiomer (**D6a**, **D7a**, **D8a**, **D9a**, **D6-7p** and **D8-9p**) as well as the arrangement of the dimer made of two enantiomers (**D6-9a** and **D7-8a**) had been previously reported,[285] this is the first time that the α-α and the γ-γ interactions of the dimers composed by two enantiomers (**D6-8p** and **D7-9p**) are proposed.

285. Brea Fernández, R. J. Diseño, síntesis y aplicaciones de sistemas supramoleculares homo- y heterodiméricos selectivos y eficientes basados en α, γ ciclopéptidos, Universidade de Santiago de Compostela, 2013.

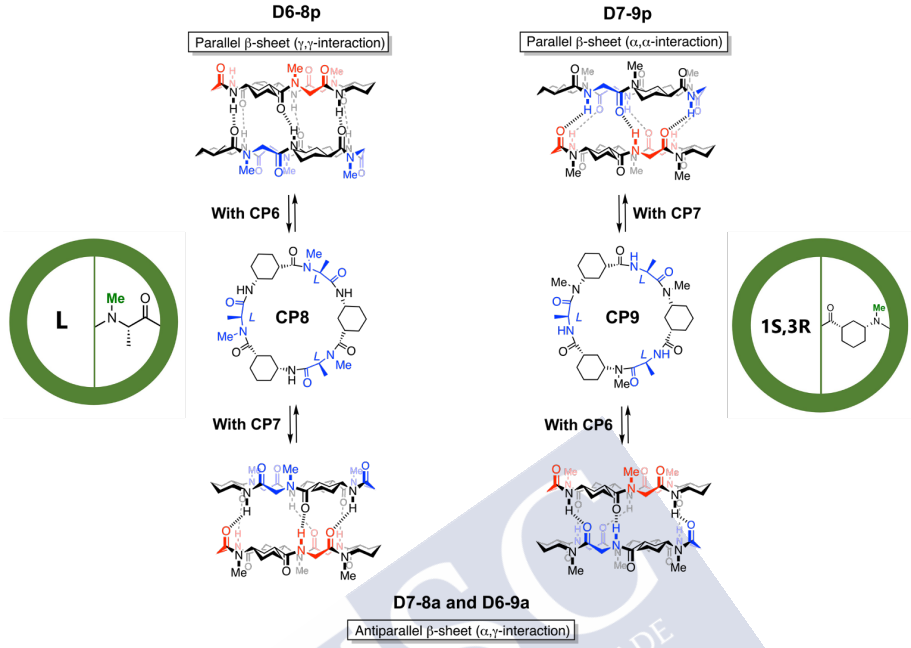

Figure 23. *Structure of the α,γ-CPs **CP8** and **CP9** together with their corresponding dimers, formed by the combinations with their enantiomers (**CP6** and **CP7**, respectively). **CP8** can from a parallel dimer that presents a γ,γ-interaction when it is combined with **CP6** (**D6-8p**), whereas **CP9** and **CP7** forms a parallel dimer through an α,α-interaction (**D7-9p**). Furthermore, two antiparallel dimers presenting an α-γ interaction emerge through the combination of **CP8** with **CP7** (**D7-8a**) and **CP9** with **CP6** (**D6-9a**). It is important to note that **D7-8a** and **D6-9a** are enantiomers and, thus, computationally equivalent. Additionally, **CP8** and **CP9** can interact between themselves, resulting in **D8a** and **D9a**, enantiomers of **D6a** and **D7a**, respectively; as well as between them, forming **D8-9p**, enantiomer of **D6-7p**. Blue (L-residues) and red (D-residues) colours are used to differentiate the chirality of the α-amino acids. The molecular viewer Dimerdice AR®, developed by us can be used for displaying **CP8** and **CP9** in AR using the trackers on the sides of the figure.*

Optimized geometries of **D6-8p**, **D7-9p** and **D6-9a** (or **D7-8a**), together with the interaction and dimerization energies obtained from the Counterpoise calculation, are presented in **Table 7**.

***Table 7.** Top: Optimized geometries of the parallel **D6-8p** and **D7-9p** as well as antiparallel **D6-9a** or **D7-8a** dimers (top and side views). For simplicity, only the polar hydrogens are displayed. The molecular viewer Dimerdice AR®, developed by us, can be used for displaying the dimers in AR using the trackers above the side views. Down: Interaction and Dimerization Energies (in kcal/mol) for the above presented α,γ-dimers.*

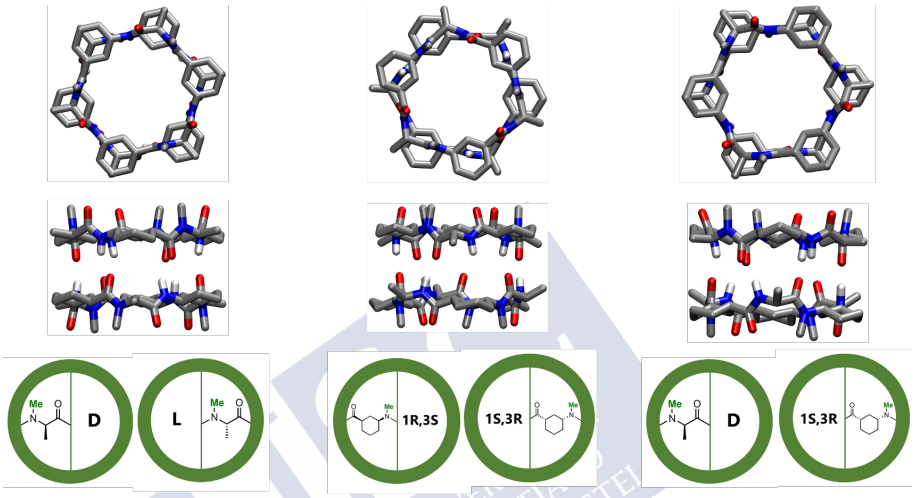

	D6-8p	**D7-9p**	**D6-9a** or **D7-8a**
	γ-γ	α-α	α-γ
Interaction Energy	-61.8	-46.6	-55.2
Dimerization Energy	-38.5	-40.4	-38.1

As can be shown in the previous table, the strongest interaction energy corresponds to the γ-γ pattern presented by the **D6-8p**, in which the carbonyl and NH groups are separated by three atoms, in a similar way that the antiparallel **D6a** (**Figure 24***A*). However, the H-bond patterns are not the same, since in the **D6-8p** dimer each γ-unit interacts with the two γ-residues which are flanking the facing α-amino acid, whereas in the dimer composed by just one enantiomer (**D6a**) each γ-

residue is interacting with the analogous of the facing CP. Nevertheless, both the interaction and dimerization energies are equal, claiming that there are no energetic differences between the dimers composed by one or two enantiomeric CPs for this kind of interaction. This **D6-8p** is almost 7 kcal/mol more stable than the antiparallel **D6-9a**, which presents an α-γ interaction, whose donor and acceptor groups are separated by three and five atoms (**Figure 24***C*). For this interaction, the energy calculations favour the dimer composed by one enantiomer, **D6-7p**, by 7 and 10 kcal/mol for the interaction and dimerization energies, respectively. The weakest interaction energy corresponds to the α-α parallel dimer (**D7-9p**), whose hydrogen donors and acceptor groups are separated by one and five atoms, the longest distance (**Figure 24***B*). Contrary, the analogous dimers composed by one enantiomer (**D7a** or **D9a**) present a separation of only one atom (**Figure 24***B*). This big separation found for **D7-9p** leads to the formation of only three H-bonds, instead the six observed in the rest of dimers. In consequence, the interaction and dimerization energies of this dimer are 13.0 and 11.4 kcal/mol, respectively, less favourable than **D7a**, suggesting a clear preference for the dimer composed by only one enantiomer. Furthermore, the interaction energy of **D7-9p** is 15.2 and 8.6 kcal/mol less favourable than **D6-8p** and **D6-9a**, respectively. However, the difference in the dimerization energy is only ~2 kcal/mol but in favour of **D7-9p**, probably due to the intramolecular H-bonds that appear between the non-methylated γ-residues in the monomers. This fact could suggest that modulating the folding properties of these CPs could provide new suitable interactions that could provide novel nanotube materials.

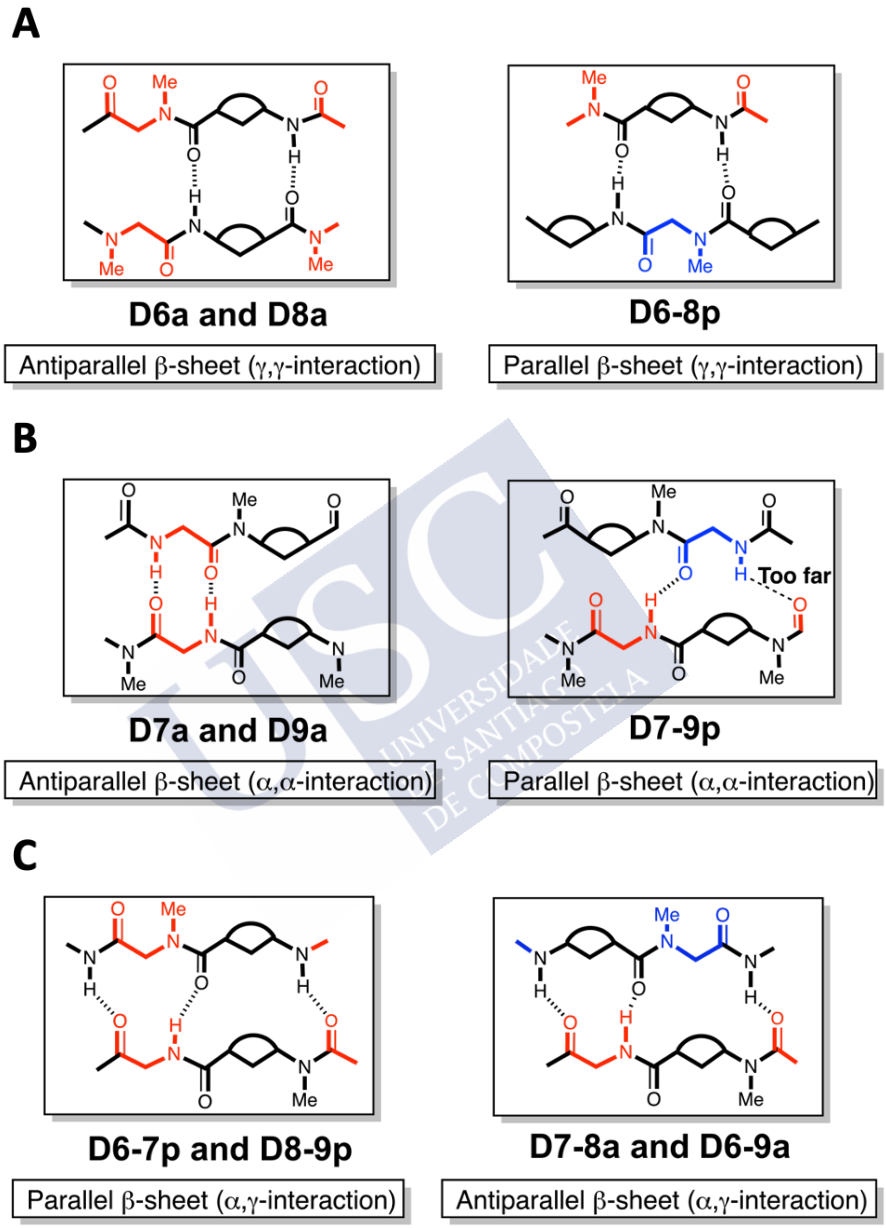

Figure 24. *Schematic representation of the different H-bond patterns of dimers composed by just one of the enantiomers or a racemic mixture, depending on the kind of interaction that they present:* ***A)*** *a* γ-γ *interaction,* ***B)*** *an* α-α *interaction and* ***C)*** *an* α-γ *interaction. Red (D-) and blue (L-)*

colours highlight the different chirality of the α-amino acids. It is important to note that only one of the possible dimers is displayed, since the analogous enantiomers are equivalent from a computational point of view.

The previous study suggests that the formation of dimers composed by only one enantiomer is favoured, with the exception of the γ-γ interaction, in which both possibilities present rather similar energies. The case of the α-α is also intriguing. If we consider the H-bonds as the prevalent interaction between CPs, those of the **D7-9p** are the strongest (46.6 kcal/mol / 3 H-bonds ≈ 15 kcal/mol per H-bond, whereas in the rest of the cases ~60 kcal/mol / 6 H-bonds ≈ 10 kcal/mol). In order to investigate this hypothesis, a study about the geometrical parameters of the H-bonds was carried out. This analysis reveals longer O···H distances for **D6-8p** and **D6-9a** compared with the analogous interactions with one enantiomer (**Figure 25** and **Figure 21**). Conversely, for the **D7-9p**, these distances are just slightly shorter (0.03 Å) than those for **D7a**. The structural analysis jut focused on the H-bond interactions obtained do not match with the conclusions obtained from the analysis of the energy calculations, since there is no explanation for the similar stability of **D6-8p** and **D6a**. Additionally, the similar values obtained for the H-bonds distances in the α-α interaction does not explain the presumably strongest H-bonds in **D7-9p**.

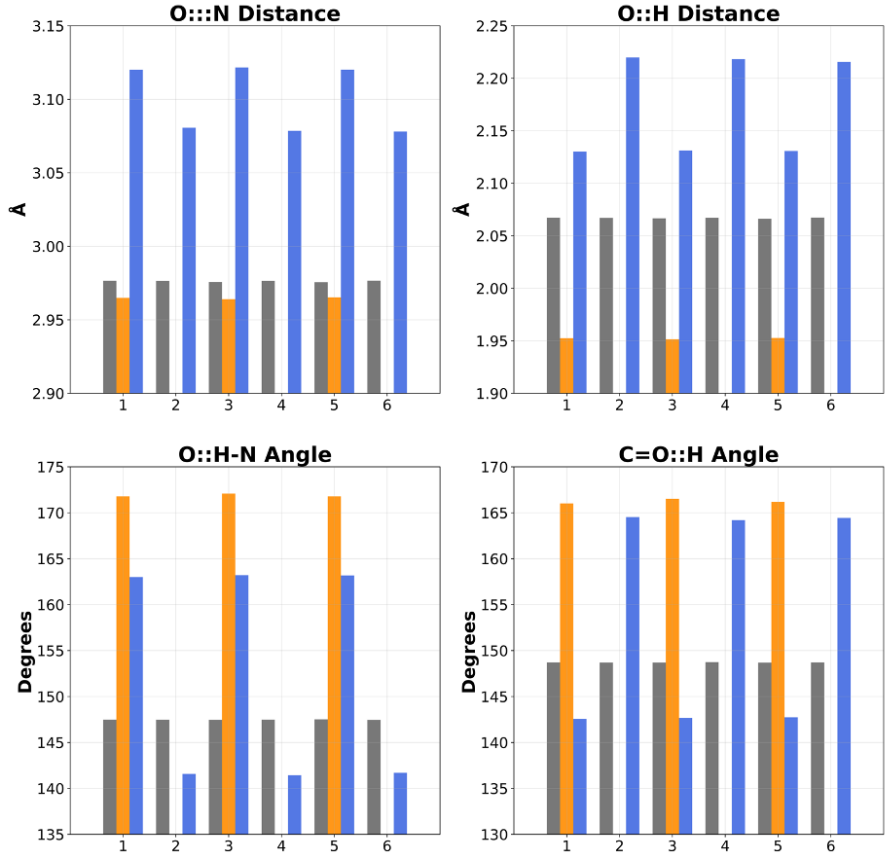

Figure 25. *H-bond distances and angles in the dimeric structures* ***D6-8p****,* ***D7-9p*** *and* ***D6-9a*** *(or* ***D7-8a****). The colour code is grey for* ***D6-8p****, orange for* ***D7-9p*** *and blue for* ***D6-9a*** *(or* ***D7-8a****). Each value of the y axis corresponds to a bond or angle between each pair of residues of the hexameric α,γ-dimer.*

In order to evaluate the strength of the H-bonds in the dimers, QTAIM calculations were carried out (**Table 8**). This method has been proven useful to the study of H-bonds, having been found a good correlation between the electron density at the BCPs and the interaction energy.[286–291] Additionally, a clear correlation between the electron density and the O···H distance has been demonstrated.[292,293]

286. Koch, U. et al. *J. Phys. Chem.* **1995**, *99* (24), 9747–9754.
287. Alkorta, I. et al. *Struct. Chem.* **1998**, *9* (4), 243–247.
288. Parthasarathi, R. et al. *J. Phys. Chem. A* **2006**, *110* (10), 3349–3351.
289. Grabowski, S. J. *J. Phys. Chem. A* **2001**, *105* (47), 10739–10746.
290. Grabowski, S. J. *J. Phys. Chem. A* **2000**, *104* (23), 5551–5557.
291. Boyd, R. J. et al. *Chem. Phys. Lett.* **1986**, *129* (1), 62–65.
292. Grabowski, S. J. *J. Mol. Struct.* **2001**, *562* (1–3), 137–143.
293. Espinosa, E. et al. *Chem. Phys. Lett.* **1998**, *285* (3–4), 170–173.

***Table 8.** Kind of interaction, interaction energy, average O···H bond distance and average electron density at the BCP of the H-bonds of the α,γ-dimers.*

	Interaction	Interaction Energy (kcal/mol)	H-bond distance (Å)		Electron density at the BCP (a.u.)	
D6a	γ-γ	-61.1	1.99		0.0209	
D7a	α-α	-59.6	1.99		0.0222	
D6-7p	α-γ	-62.5	**NH from α**	**NH from γ**	**NH from α**	**NH from γ**
			1.98	1.92	0.0208	0.0240
D6-8p	γ-γ	-61.8	2.07		0.0187	
D6-9a	α-γ	-55.2	**NH from α**	**NH from γ**	**NH from α**	**NH from γ**
			2.13	2.22	0.0163	0.0131
D7-9p	α-α	-46.6	1.95		0.0221	

The higher electron density found for the H-bonds in the dimers composed by one enantiomer suggests that this interaction is stronger than the analogous between monomers in the racemic mixture, agreeing with the longer H-bond distances (**Table 8**). Moreover, the higher electron density found for the α-α interaction in **D7a** compared to the γ-γ of **D6a**, , also matches with the observed in the literature.[116] Contrary, there is no explanation just based on the H-bonds for the similar interaction energies obtained for **D6a** and **D6-8p**. Furthermore, the electron densities of the H-bonds in the dimers presenting an α-α interaction are very similar independently of being formed by one or two enantiomers, discarding a higher strength of those from **D7-9p**. In this way, there is no reason for a difference in energy between **D7-9p** and **D7a** of only 10 kcal/mol (should be higher). These two facts open the door to the existence of other interactions between CPs which could justify the previous observations. In order to investigate it, the BCP's formed between the carbonyl groups of the CPs facing the H-bond network and other hydrogens pointing to the same face were evaluated (**Figure 26**).

For the three dimers composed by one enantiomer, a total of 6 interactions per dimer are found, although the longer distances and the smaller electron density observed suggest that they are not important (**Figure 26***ABC*). For the dimers **D6a** and **D7a**, only one kind of interaction is found: the oxygen of the carbonyl with the hydrogen of the Cα of the α-residues in **D6a** and with the hydrogen of the Cγ in **D7a** (**Figure 26***A* and **Figure 26***B*). On the contrary, for **D6-7p** two different types of contacts are observed: three interactions between the carbonyl and the hydrogen of the Cα of two γ-amino acids and another three between the carbonyl of an α-unit and an axial hydrogen of a Cβ of the γ-residues (**Figure 26***C*).

On the other hand, for the dimers composed by racemic mixtures these interactions seem to be more important. For the three different kinds of dimers, twelve interactions per dimer are observed. For **D7-9p**, three BCP's with a high electron density (0.0104 a.u.) emerge between the carbonyl group of the α-residues and the hydrogen of the

116. García-Fandiño, R. et al. *J. Phys. Chem. B* **2010**, *114* (15), 4973–4983.

tertiary Cγ of the γ-amino acids (**Figure 26***F*). These interactions could stabilize this dimer, increasing its interaction energy without the need of stronger H-bonds in the structure and justifying the unexpected higher interaction energy observed for this dimer (**Table 7**). For **D6-9a**, three interactions between the carbonyl group of an α-unit and the hydrogen of the tertiary Cγ of the γ-residues with a high electron density (0.0114 a.u.) are found (**Figure 26***E*). Moreover, another three interactions between the carbonyl group an α-amino acid and an axial hydrogen of a Cβ of the γ-residues also present a quite high electron density (0.0108). These six interactions are approximatively half as strong as those observed for the H-bonds of **D6-7p**, which suggest that they could compensate the weaker H-bonds found in **D6-9a** and justifying the similar interaction energies compared to **D6-7p**. Finally, in the case of **D6-8p**, these interactions are taking place between the carbonyl groups and the axial hydrogens of the Cβ's of the γ-residues and, although the electron densities found are clearly smaller than those observed in the H-bonds, it seems that the sum of all of them could compensate the weaker H-bonds compared to **D6a** and equalize the interaction energy (**Figure 26***D*).

A

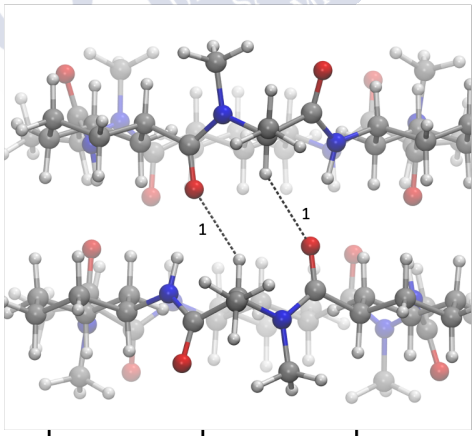

D6a	Distance (Å)	Electron density at the BCP(a.u.)	Times observed
1	2.52	0.00839	6

B

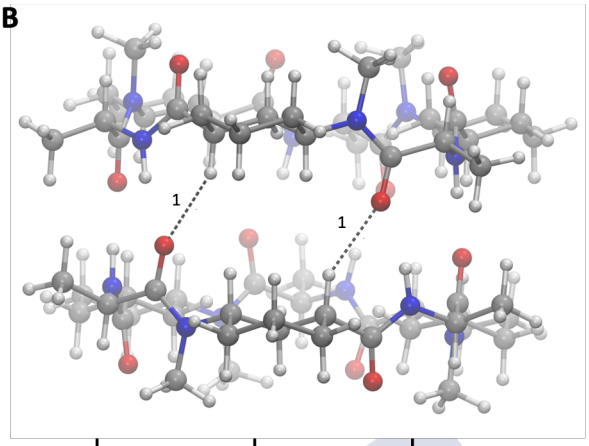

D7a	Distance (Å)	Electron density at the BCP(a.u.)	Times observed
1	2.44	0.00980	6

C

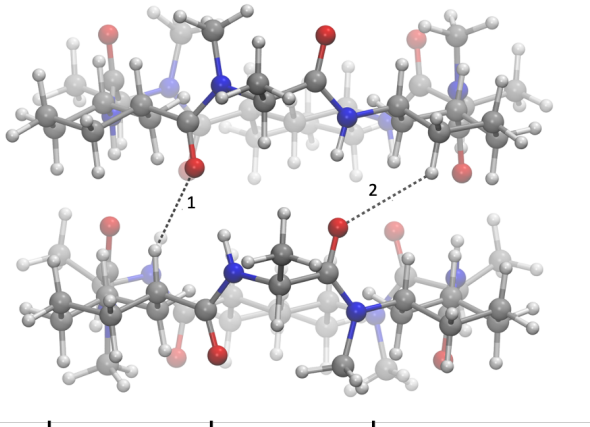

D6-7p	Distance (Å)	Electron density at the BCP(a.u.)	Times observed
1	2.54	0.00870	3
2	2.86	0.00469	3

D

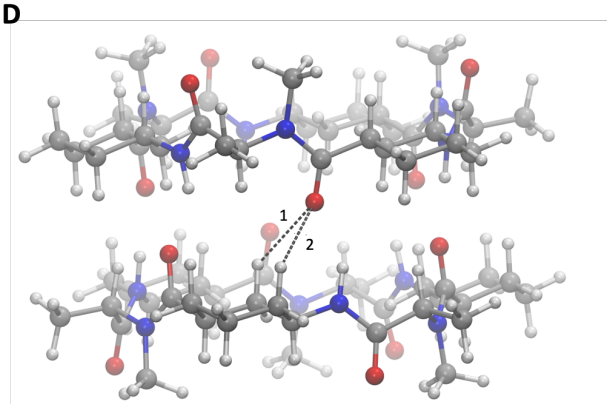

D6-8p	Distance (Å)	Electron density at the BCP(a.u.)	Times observed
1	2.62	0.00735	6
2	2.61	0.00753	6

E

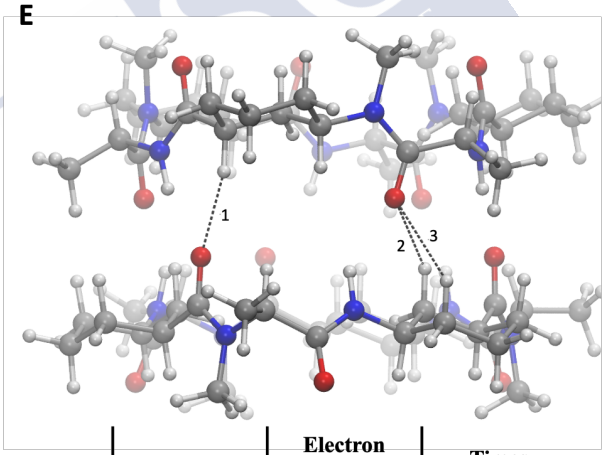

D6-9a	Distance (Å)	Electron density at the BCP(a.u.)	Times observed
1	2.38	0.0108	3
2	2.40	0.0114	3
3	2.80	0.00531	3

F

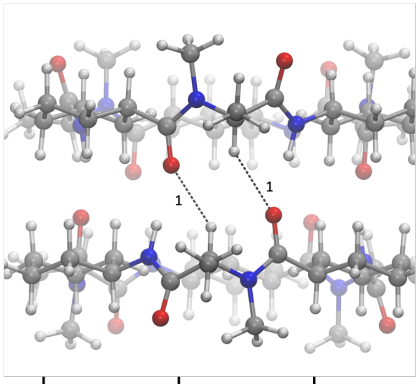

D7-9p	Distance (Å)	Electron density at the BCP(a.u.)	Times observed
1	2.38	0.0104	3
2	2.67	0.00638	3
3	2.81	0.00486	3
4	2.55	0.00846	3

Figure 26. *Interactions between the oxygen of the carbonyl groups and other hydrogens different from those which are forming H-bonds found using QTAIM for* ***A) D6a****,* ***B) D7a****,* ***C) D6-7p****,* ***D) D6-8p****,* ***E) D6-9a*** *and* ***F) D7-9p****. For each dimer, the distance between the interacting atoms, the electron density found at that BCP and the number of times which it is observed per dimer is presented.*

As it was mentioned above, the formation of dimers between enantiomers pairs leads to a deviation of the alignment between amino acids of the same nature. This fact could lead to new designs in which the side chains of the α-amino acids stand above the γ-units, leading to fancy structures as the one presented in **Figure 27**, which could present a certain helicoidal character.

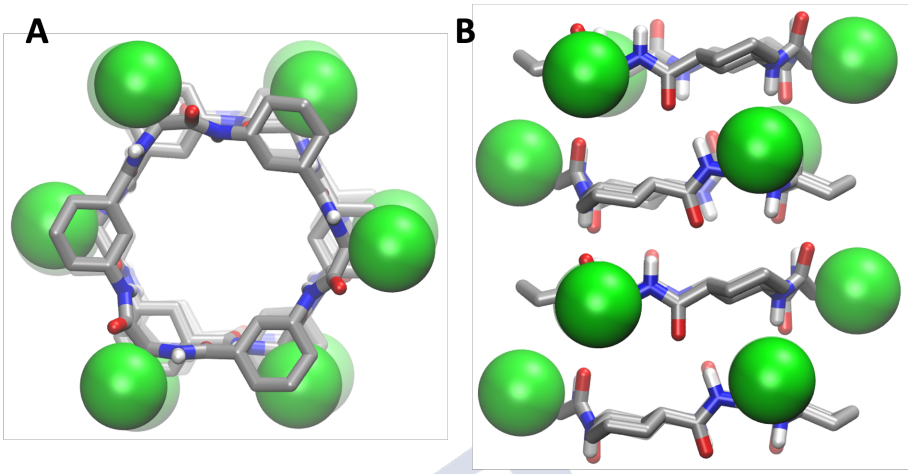

***Figure 27.** Top (**A**) and lateral (**B**) view of a SCPN model composed by mixtures of enantiomers to illustrate the "helicoidal" character of the resulting structure. The deviation of the alignment of the amino acids of the same nature results in a disposition that can infer some type of helicoidal character in the nanotube. The lateral chains of the α-amino acids are highlighted in green.*

The possible dimers that can be formed considering all the combinations among the four α,γ-CPs studied are presented in **Table 9**, in order to provide an easier comparison between the classical interactions and the new ones here proposed. Although, in general, the dimers made of one enantiomer are more favoured, the case of the γ-γ interaction deserves special attention. In this scenario, both the interaction and dimerization energies are rather similar for the dimers composed by one or two enantiomers, which suggest that a competitive experiment in presence of **CP6** and **CP8** would lead to the formation of **D6a**, **D8a** and **D6-8p** in identical proportions. This fact opens the door to a new design of these peptides, in which a parallel γ-γ interaction is formed through the combination of two α-N-methylated enantiomers. This model, similar to the SCPNs composed by enantiomeric pairs of *D*,*L*-α-CPs proposed by Prof. Undén, could provide new features thanks to the different stacking pattern

presented.[262] On the other hand, the other new interaction proposed (α-α in **D7-9p**) shows the least favoured interaction energy, probably due to the smallest number of H-bonds formed, which suggest that they are much less probable than the γ-γ **D6-8p** dimer.

Table 9. *Summary of the dimers that can be formed considering all possible combinations of the four α,γ-CPs here studied:* ***CP6****,* ***CP7****,* ***CP8*** *and* ***CP9****. For each combination, the name of the dimer and the kind of interaction are presented, as well as the interaction (in italic) and dimerization (in bold) energies (in kcal/mol). The different kind of interactions are highlighted by shadows of different colours: grey for γ-γ, blue for α-α and orange for α-γ.*

	CP6	**CP7**	**CP8**	**CP9**
CP6	**D6a** γ-γ *-61.1* **-38.6**	**D6-7p** α-γ *-62.5* **-48.4**	**D6-8p** γ-γ *-61.8* **-38.5**	**D6-9a** α-γ *-55.2* **-38.1**
CP7	**D6-7p** α-γ *-62.5* **-48.4**	**D7a** α-α *-59.6* **-51.8**	**D7-8a** α-γ *-55.2* **-38.1**	**D7-9p** α-α *-46.6* **-40.4**
CP8	**D6-8p** γ-γ *-61.8* **-38.5**	**D7-8a** α-γ *-55.2* **-39.1**	**D8a** γ-γ *-61.1* **-38.6**	**D8-9p** α-γ *-62.5* **-48.4**
CP9	**D6-9a** α-γ *-55.2* **-38.1**	**D7-9p** α-α *-46.6* **-40.4**	**D8-9p** α-γ *-62.5* **-48.4**	**D9a** α-α *-59.6* **-51.8**

262. Rosenthal-Aizman, K. et al. *J. Am. Chem. Soc.* **2004**, *126* (11), 3372–3373.

4.5. CONCLUSIONS.

In order to examine the preferred stacking properties adopted by CPs that contain aminocyclohexanecarboxylic acids, a computational study has been carried out *via* quantum (DFT and semiempirical) calculations. These flat systems made up of δ-Ach or γ-Ach residues alternated with α-residues to lead to *D*,*L*-α,δ-CPs or α,γ-CPs stack on top of each other, eventually resulting in nanotubes in which some methylene groups of the Ach residues (two for the *D*,*L*-α,*δ*-CPs and one for α,γ-CPs) are projected towards their inner cavity, providing hydrophobic properties, as well as available positions for further functionalization.

The results here obtained confirm that when only the backbone interactions are considered, the parallel β-sheet rises as the most stable for the stacking of the *D*,*L*-α,*δ*-CPs and, surprisingly, also for the α,γ-CPs, putting into question previously assumptions about these peptides. A deep structural analysis suggests that the explanation for this fact could be coming from the different disposition of the axial hydrogen atoms which are not participating in the H-bond formation, highlighting the influence of the presence of the non-natural residues. Despite this, it has been found that modifying the sequence of these CPs the preferred parallel arrangement can be switched to the antiparallel stacking by choosing residues that can establish favourable cross-strand interactions between the side chains of the α-amino acids. These findings imply a change of paradigm with respect to the designs that should be considered for future applications of nanotubes based on this type of CPs.

Furthermore, exploring the possible combinations of the four α,γ-CPs (two pair of enantiomers) here studied, two new kind of interactions have been found: one γ-γ (**D6-8p**) and one α-α (**D7-9p**), being both parallel β-sheets forming by pairs of enantiomers. Although the energetic parameters calculated for the new α-α interaction suggest that it is not significantly favourable, those for the γ-γ (**D6-8p**) seem comparable to those of the dimers made of one enantiomer. This fact suggests that, at least from the energetic point of view, a new arrangement for these systems can be proposed, enriching the possibilities for further designs.

Using QTAIM calculations, it has been demonstrated that the H-bonds of the dimers composed by only one enantiomer are stronger than those resulting from the combination of the racemic mixture, with the exception of **D7-9p**, although in this case only 3 H-bonds are formed. However, interactions between the carbonyl groups with different hydrogen atoms from the opposite face could stabilize such dimers, increasing the interaction energy.

The results presented in this chapter have led the following publications: Calvelo, M.; Lamas, A.; Guerra, A.; Amorin, M.; Garcia-Fandiño, R.; Granja, J. R. *Chem. – A Eur. J.* **2020**, *26*, 5846-5858. Moreover, another work describing the new interactions of α,γ-CPs is under preparation. Additionally, a molecular viewer for the visualization of the α,γ-CPs using AR has been developed and registered: *Dimerdice AR*®.[281] This app includes a downloadable the template for the building of a dice whose faces are trackers for the individual **CP6**, **CP7**, **CP8** and **CP9** (**Figure 28***A*). Pointing with the device to each tracker separately, an AR image of the corresponding optimized monomer is viewed (**Figure 28***C*). When the tracker images of two monomers are placed close to each other (using two dices), the structure of the dimer formed by that combination of CPs is shown (**Figure 28***D*).

281. Dimer dice - Apps on Google Play https://play.google.com/store/apps/details?id=com.mduse.DimerDice&hl=en (accessed Jun 18, 2020).

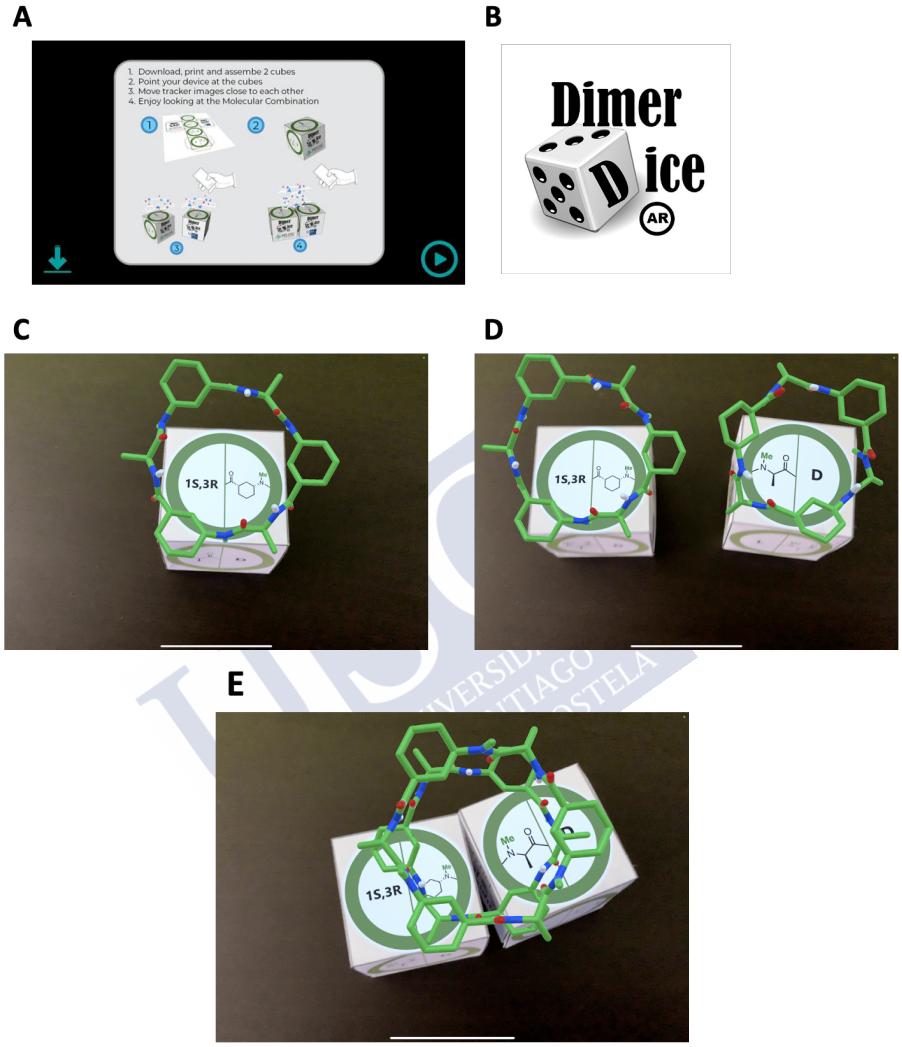

Figure 28. *Pictures of the app Dimerdice AR®.* ***A)*** *First screen of the app, in which the pattern for the dice is available, as well as instructions of use.* ***B)*** *Logo of the app Dimerdice®.* ***C)*** *Example of how the app works, using one face of the dice, the corresponding optimized monomer can be visualized in AR.* ***D)*** *Example using two dices, which leads to the visualization of a dimer composed by the selected CPs.*

USC
UNIVERSIDADE
DE SANTIAGO
DE COMPOSTELA

5. Supramolecular receptors based on SCPNs

5.1. PRECEDENTS AND MOTIVATION.

Peptide nanotubes are hollow tubular structures whose internal diameter depends on the number and type of amino acids used in the CP. The presence of this cavity has allowed to dream about their potential applications as molecular containers, in which molecules or ions are trapped or confined in their inner pore depending on their size and chemical properties. During last decades, the emergence of nanometric molecular containers has had a huge impact in a number of fields as catalysis, nanotechnology or materials science.[294–300] Advances in supramolecular chemistry have led to the development of self-assembling capsules, being the studies with cryptands of Prof. Lehn, in which crown ethers are converted into three dimensional systems,[301,302] and the spherands and carcerands developed by Prof. Cram,[303–305] the most important precedents in this area. The work of these three authors was awarded with the Nobel Prize in 1987 for "their development and use of molecules with structure-specific interactions

294. Zarra, S. et al. *Chem. Soc. Rev.* **2015**, *44* (2), 419–432.
295. Ballester, P. et al. *Chem. Soc. Rev.* **2015**, *44* (2), 392–393.
296. Smulders, M. M. J. et al. *Chem. Soc. Rev.* **2013**, *42* (4), 1728–1754.
297. Chakrabarty, R. et al. *Chem. Rev.* **2011**, *111* (11), 6810–6918.
298. Kim, H. J. et al. *Chem. Soc. Rev.* **2012**, *41* (3), 1173–1190.
299. Hasell, T. et al. *Nature Reviews Materials*. Nature Publishing Group July 26, 2016, pp 1–14.
300. Rizzuto, F. J. et al. *Nature Reviews Chemistry*. Nature Publishing Group April 1, 2019, pp 204–222.
301. Dietrich, B. et al. *Tetrahedron Lett.* **1969**, *10* (34), 2889–2892.
302. Lehn, J. M. *Acc. Chem. Res.* **1978**, *11* (2), 49–57.
303. Cram, D. J. et al. *J. Am. Chem. Soc.* **1988**, *110* (8), 2554–2560.
304. Cram, D. J. et al. *J. Am. Chem. Soc.* **1979**, *101* (22), 6752–6754.
305. Cram, D. J. et al. *J. Am. Chem. Soc.* **1985**, *107* (12), 3645–3657.

of high selectivity".[306] Since then, other supramolecular chemical principles for the formation of self-assembling capsules have been used until now, highlighting the works of Raymond, Nitschke, Rebek, Fujita or Stang, among others.[307–314]

Cyclic molecules relatively similar to CPs, such as cyclodextrins (CDs), have been also proposed for acting as molecular containers.[315,316] These ring-shaped oligosaccharides were firstly isolated by Villiers in 1891, and, since then, their use as molecular receptors was deeply studied.[22,23,317–322] CDs are known to acquire a truncated cone shape and, similarly to CPs, the size of the inner cavity is determined by the number of glucopyranoside groups: 6 (α-CD), 7 (β-CD) or 8 (γ-CD).[323] This conformation, in which all the secondary hydroxyl groups are oriented to the wide edge and the primary hydroxyls disposed towards the narrow entry, leaving an hydrophobic cavity, determines the specific properties of these molecules, making them useful for a range of applications such as drug excipients

22. Crini, G. *Chem. Rev.* **2014**, *114* (21), 10940–10975.
23. Villiers, A. *Compt. Rend. Acad. Sci* **1891**, *112*, 536–538.
306. The Nobel Prize in Chemistry 1987 - NobelPrize.org https://www.nobelprize.org/prizes/chemistry/1987/summary/ (accessed May 18, 2020).
307. Wyler, R. et al. *Angew. Chemie Int. Ed. English* **1993**, *32* (12), 1699–1701.
308. Branda, N. et al. *Science.* **1994**, *263* (5151), 1267–1268.
309. Ajami, D. et al. *Acc. Chem. Res.* **2013**, *46* (4), 990–999.
310. Cook, T. R. et al. *Chem. Rev.* **2013**, *113* (1), 734–777.
311. Harris, K. et al. *Chem. Commun.* **2013**, *49* (60), 6703–6712.
312. Fujita, D. et al. *Chem* **2016**, *1* (1), 91–101.
313. Ronson, T. K. et al. *Chem. Commun.* **2013**, *49* (25), 2476–2490.
314. Parac, T. N. et al. *Journal of the American Chemical Society*. American Chemical Society August 12, 1998, pp 8003–8004.
315. Saenger, W. *Angew. Chemie Int. Ed. English* **1980**, *19* (5), 344–362.
316. Bender, M. L. et al. *Cyclodextrin Chemistry*; Reactivity and Structure Concepts in Organic Chemistry; Springer Berlin Heidelberg: Berlin, Heidelberg, 1978; Vol. 6.
317. Del Valle, E. M. M. *Process Biochemistry*. Elsevier May 31, 2004, pp 1033–1046.
318. dos Santos, C. et al. *Curr. Opin. Food Sci.* **2017**, *16*, 106–113.
319. Marques, H. M. C. *Flavour Fragr. J.* **2010**, *25* (5), 313–326.
320. Saha, S. et al. *Sci. Rep.* **2016**, *6* (1), 1–12.
321. Rekharsky, M. V. et al. *Chem. Rev.* **1998**, *98* (5), 1875–1917.
322. F. Garrido, P. et al. *Biomolecules* **2020**, *10* (3), 431.
323. Davis, M. E. et al. *Nat. Rev. Drug Discov.* **2004**, *3* (12), 1023–1035.

or cholesterol depletion, among others.[324–328] Additionally, CDs are able to form supramolecular complex which allow to expand the possible use of these molecules.[329–333] Furthermore, the use of cucurbiturils, macrocyclics composed by units of glycoluril, has been also exploited during last years.[334–336]

Self-assembling α,γ-CPs have been already proposed as good candidates for entrapping molecules.[96,98,337–340] In this sense, it is worth to mention the capsule based on two complementary α,γ-CPs, each of them functionalized with a Zn porphyrin cap through a dynamic covalent bond, developed in our group.[341] Those porphyrin units are used for the selective recognition of guests, having been found that the affinity for these ligands showed a strong dependence on the guest length.[341] The delivery of the trapped guest could be controlled by hydrolysis of the dynamic covalent bonds that links the CPs with the porphyrin caps (**Figure 29**).

96. Reiriz, C. et al. *Org. Biomol. Chem.* **2009**, *7* (21), 4358–4361.
98. Rodríguez-Vázquez, N. et al. *Angew. Chemie Int. Ed.* **2016**, *55* (14), 4504–4508.
324. Patro, N. M. et al. *J. Incl. Phenom. Macrocycl. Chem.* **2014**, *78* (1–4), 471–483.
325. Braga, S. S. *Biomolecules* **2019**, *9* (12).
326. Ohvo, H. et al. *Biochemistry* **1996**, *35* (24), 8018–8024.
327. Uekama, K. *Chem. Pharm. Bull.* **2004**, *52* (8), 900–915.
328. Garrido, P. F. et al. *Int. J. Pharm.* **2020**, *588*, 119689.
329. Zhang, H. et al. *J. Phys. Chem. C* **2014**, *118* (13), 7163–7173.
330. Liu, Y. et al. *J. Phys. Chem. B* **2005**, *109* (9), 4129–4134.
331. Cheng, X. et al. *Dalt. Trans.* **2011**, *40* (44), 11788–11794.
332. Ji, J. et al. *J. Am. Chem. Soc.* **2019**, *141* (23), 9225–9238.
333. Messner, M. et al. *Int. J. Pharm.* **2011**, *407* (1–2), 174–183.
334. Márquez, C. et al. *J. Am. Chem. Soc.* **2004**, *126* (18), 5806–5816.
335. Barrow, S. J. et al. *Chem. Rev.* **2015**, *115* (22), 12320–12406.
336. Pichierri, F. *Dalt. Trans.* **2013**, *42* (17), 6083–6091.
337. Rodríguez-Vázquez, N. et al. *Met. Ions Life Sci.* **2016**, *16*, 485–556.
338. Rodríguez-Vázquez, N. et al. *Org. Lett.* **2017**, *19* (10), 2560–2563.
339. Pérez-Alvite, M. J. et al. *Amino Acids* **2011**, *41* (3), 621–628.
340. Panciera, M. et al. *Chem. - A Eur. J.* **2013**, *19* (15), 4826–4834.
341. Ozores, H. L. et al. *J. Am. Chem. Soc.* **2017**, *139* (2), 776–784.

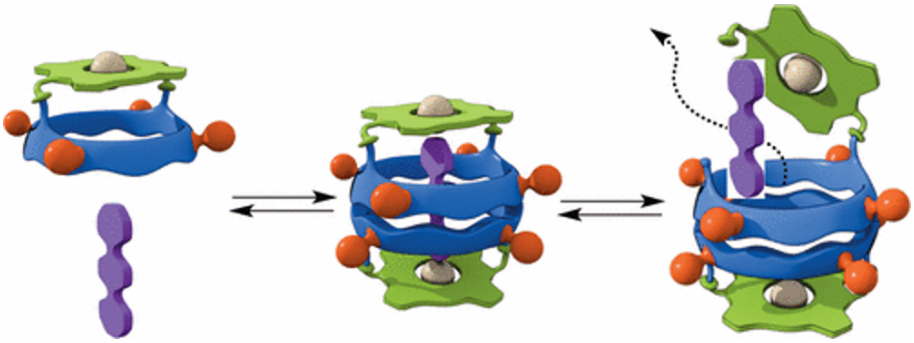

Figure 29. *Molecular capsule proposed by the group of Prof. Granja, based on a self-assembling α,γ-CPs (blue) endowed with a porphyrin cap (green). The dimerization of this peptide organizes both metalloporphyrins in a parallel manner that allow to recognize different bipyridines. the selective release of guest ligands (purple) could be controlled by reverting the dynamic covalent bonds that links the CPs with the porphyrin caps.*

More recently, α,δ-SCPNs have been considered as good candidates for the entrapment of carbon structures, as fullerenes.[107] However, due to the novelty of these peptides, no further studies have been carried out so far. In this sense, computational methods could be applied in order to perform a theoretical screening for this purpose, as previously has been done for other systems, mainly using DFT calculations.[342] This technique enables to determine the lowest energy structure, as well as it allows to discriminate between different forms depending on energetic parameters. In this way, the study of SCPN composed by different kinds of CP (α,γ- or α,δ-CPs) acting as molecular containers may be carried out.

5.2.AIM.

The self-assembly process of CPs could lead to the formation of nanotubular structures with potential application for their use as molecular containers, acting as supramolecular receptors able to trap atoms or molecules in their inner cavity. However, there is a lack of research in this field. In this way, a computational study in order to test this possible usage has been carried out. Two different kind of systems

107. Lamas, A. et al. *Chem. Sci.* **2018**, *9* (43), 8228–8233.
342. Miklitz, M. et al. *J. Phys. Chem. C* **2017**, *121* (28), 15211–15222.

based on cyclic peptides, which are expected to encapsulate distinct molecules/atoms, are considered:

A. α,γ-CP dimers for the trapping of noble gases (Kr, Xe and Rn), as well as chloroform.
B. α,δ-SCPNs for the encapsulation of carbon nanostructures: fullerene (C_{60} and C_{70}) and CNTs of different size.

Using DFT calculations, their energetic and structural properties has been evaluated.

5.3. METHODS.

All DFT calculations have been performed using the Gaussian package.[165] Geometries of the systems have been obtained from previous studies of the group as well as using chemical drawing software, as Avogadro and ChemOffice.[189,190]

For the studies about the encapsulation of noble gases, geometry optimizations were carried out at B3LYP level with the 6-31G(d) basis set for all atoms (C, N, H, O and Cl) except for Kr, Xe and Rn, in which the aug-cc-pVTZ-PP relativistic effective small-core potential (RECP) was used.[343–345] Interaction and complexation energy were evaluated following the Counterpoise approach at B3LYP level and 6-311++G(d,p) as basis set for C, N, H, O and Cl and the same basis used in the optimization for the noble gases. Dispersion was also included using the D3BJ correction. The interaction energy was defined as:

$$\boldsymbol{Interaction\ Energy} = Energy_{complex} - \left(Energy_{dimer} + Energy_{guest}\right)$$

Where *guest* corresponds to chloroform, Kr, Xe or Rn, depending on the case, and *complex* corresponds with the dimer plus the atom/molecule trapped.

165. Frisch, M. J. et al. *Gaussian, Inc., Wallingford CT,* 2016.
189. Cousins, K. R. *J. Am. Chem. Soc.* **2011**, *133* (21), 8388.
190. Hanwell, M. D. et al. *J. Cheminform.* **2012**, *4* (8), 17.
343. Peterson, K. A. et al. *J. Chem. Phys.* **2003**, *119* (21), 11113–11123.
344. Peterson, K. A. et al. *J. Phys. Chem. A* **2006**, *110* (51), 13877–13883.
345. Huang, Z. et al. *Sci. Rep.* **2017**, *7* (1), 10278.

On the other hand, the complexation energy was defined as:

$$\boldsymbol{Complexation\ Energy} = Interaction\ Energy - \left(Energy_{dimer\ isol.} + Energy_{guest\ isol.}\right)$$

Where $Energy_{dimer\ isol.}$ and $Energy_{encap.isol.}$ correspond to the energy of dimer and trapped molecule/atom when the complex (dimer + guest) is not formed. Consequently, $Energy_{guest\ isol.}$ was equal to $Energy_{encap.}$ for Kr, Xe and Rn, since the geometry of a single atom does not vary whether it was encapsulated or not. It is worth noting that this magnitude is equal to the dimerization energy defined in the previous chapter, but in this case we decided to rename it in order to facilitate the comprehension of the phenomenon studied. Additionally, in the model selected for this work the supramolecular structure (dimer or nanotube) is formed before the encapsulation of the guest. Other mechanisms of encapsulation, despite their possible interest, were not considered in this thesis in order to limit the study length. Calculation of the internal volumes has been carried out using *3V server*.[346]

For the encapsulation studies of fullerenes and carbon nanotubes, the geometry optimization was performed using PM7, due to the large number of atoms.[156] The interaction and complexation energies were evaluated at B3LYP/6-31G(d) level for the system containing fullerenes and B3LYP/6-31G(d,p) for the carbon nanotubes, including the D3BJ correction for the dispersion in both cases. It is worth to mention that a smaller basis set has been selected for the fullerene calculations due to the larger number of CPs considered in that system (six for fullerenes and two for CNTs), which obviously increases the size and thus the computational effort. The interaction and complexation energies were defined as in the noble gases study, but in this case *guest* corresponds to the carbon structure (fullerene or carbon nanotube).

156. Stewart, J. J. P. *J. Comput. Chem.* **1989**, *10* (2), 209–220.
346. Voss, N. R. et al. *Nucleic Acids Res.* **2010**, *38* (Web Server issue), W555-62.

5.4. NOBLE GAS CONFINEMENT IN CAPSULES COMPOSED BY THE SELF-ASSEMBLY OF α,γ-CPS.

Recently, the research of heavy noble gases has grown due to their possible applications in different fields.[347–349] However, for those purposes a high purity is needed, which implies the improvement of separation methods.[350,351] In this context, molecular cages have arisen as quite promising candidates for that purpose, since its efficiency has been probed in a number of works.[352–356] Since the use of amino acids for building cage-like nanostructures has been previously reported, dimers composed by the self-assembly of α,γ-CPs are proposed to act as cages for trapping noble gases.[357]

The use of a hexameric pyridyl-substituted α,γ-CPs (**Figure 30**) is selected to perform this study (**CP10**) considering the possibility of closing the dimer cavity by coordination of heterocyclic moieties with an appropriate metal ion. The self-assembling of **CP10** leads to the formation of the dimer **D10a**, which was assumed to form an antiparallel sheet through the α-faces. However, in order to simplify the model, pyridyl moieties were substituted by methylene groups, being **CP11** used for the further calculations. In addition, methyl groups (Ala) instead of the isobutyl groups (Leu) have been selected as side-chains of α-residues, reducing the number of conformational variants. This CP leads to the formation of **D11a**, analogous to **D10a** but with a simple methyl group instead of the alkynilpyridyl moieties on the γ-residues. This change should not affect to the dimension or properties of the dimer cavity. Additionally, it is worth to mention that the cyclic residue of these α,γ-CPs is, in this case, 3-aminocyclopentanecarboxylic acid

347. Schröder, L. et al. *Science.* **2006**, *314* (5798), 446–449.
348. Schröder, L. *Phys. Medica* **2013**, *29* (1), 3–16.
349. Rogers, N. J. et al. *Proc. Natl. Acad. Sci. U. S. A.* **2016**, *113* (12), 3164–3168.
350. Yang, R. T. *Gas Separation by Adsorption Processes*; Elsevier, 1987.
351. Kerry, F. G. *Industrial gas handbook: gas separation and purification. 1st ed. Boca Raton, FL: CRC Press; 2007*; CRC Press, 2007.
352. Banerjee, D. et al. *Acc. Chem. Res.* **2015**, *48* (2), 211–219.
353. Bazan, R. E. et al. *Adsorption* **2011**, *17* (2), 371–383.
354. Chen, L. et al. *Nat. Mater.* **2014**, *13* (10), 954–960.
355. Liu, Y. et al. *BMC Chem. Eng.* **2019**, *1* (1), 3.
356. Banerjee, D. et al. *Chem* **2018**, *4* (3), 466–494.
357. Wang, C. H. et al. *Org. Biomol. Chem.* **2012**, *10* (26), 5049–5054.

(γ-Acp), contrary to the six-member ring of those from the previous chapter. The use of these of this five-member ring derivatives in α,γ-CPs was also previously reported.[263]

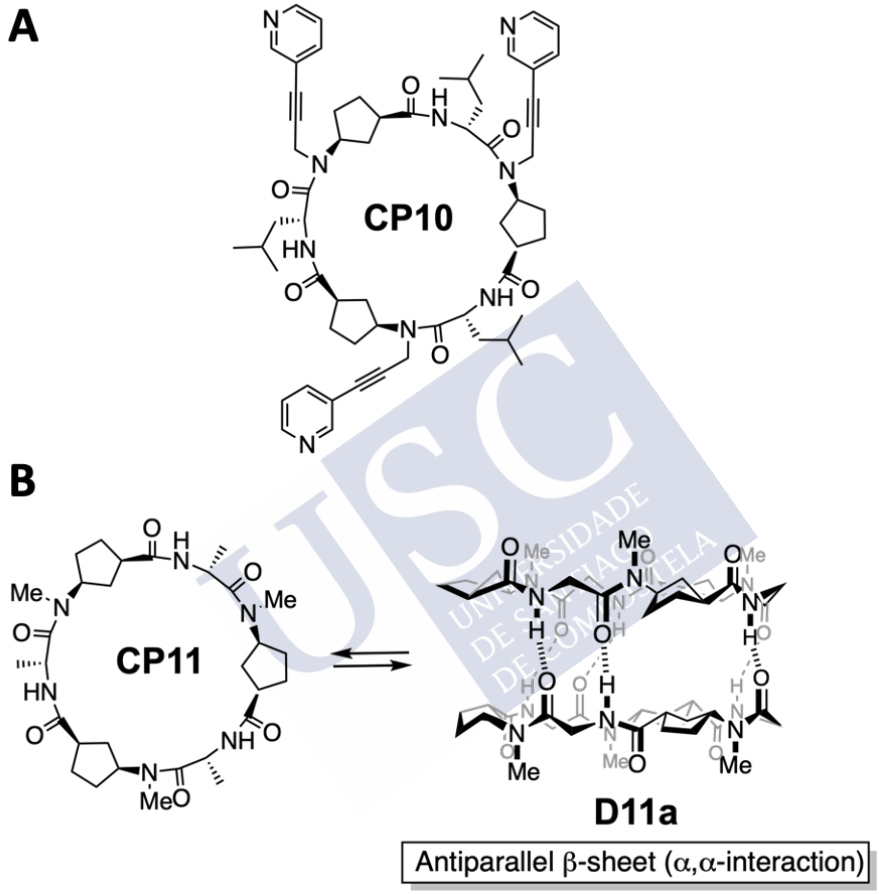

Figure 30. *Structure of the cyclic peptide used in experimental studies* ***A) CP10*** *and model used in this study* ***B) CP11*** *in equilibrium with dimer* ***D11a****.*

263. Brea, R. J. et al. *Angew. Chemie - Int. Ed.* **2005**, *44* (35), 5710–5713.

The incorporation of noble gases as Kr, Xe and Rn was evaluated, and compared with the encapsulation of chloroform, since the entrance of this molecule inside dimers or SCPNs has been previously reported.[95,358,359] Optimized geometries of the dimer **D11a**, as well as the corresponding filled structures formed by the encapsulation of chloroform or the above mentioned noble gases, are displayed in **Figure 31**. No significant structural differences are observed between the capsules and the isolated dimer **D11a**, except for slightly longer H-bond distances (**Table 10**).

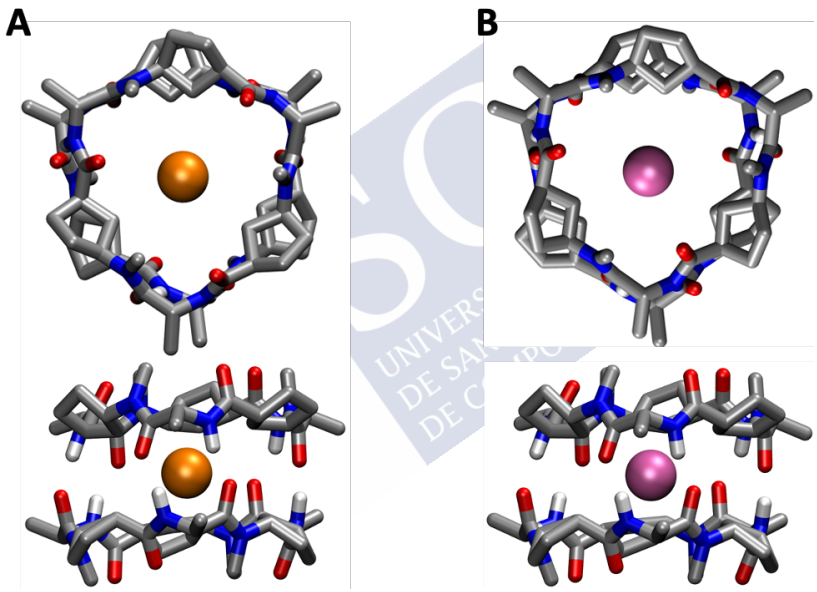

95. Amorín, M. et al. *J. Am. Chem. Soc.* **2003**, *125* (10), 2844–2845.
358. Zhao, X. et al. *J. Mol. Graph. Model.* **2018**, *83*, 74–83.
359. Li, R. et al. *J. Chem. Phys.* **2015**, *143* (1), 015101.

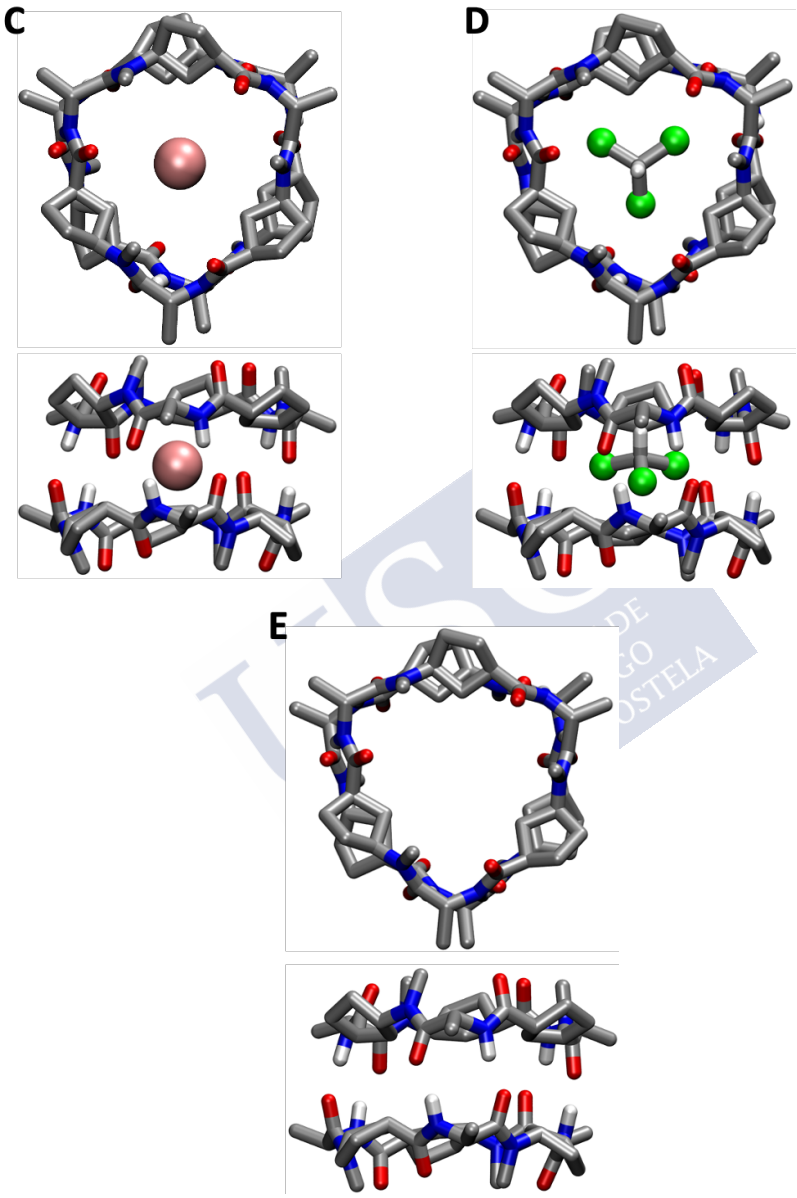

Figure 31. *Top and side view of minimized geometries of* ***D11a*** *(****E****) and the corresponding encapsulated structures:* ***A)*** *Kr (****Kr⊂D11a****),* ***B)*** *Xe (****Xe⊂D11a****),* ***C)*** *Rn (****Rn⊂D11a****) and* ***D)*** *chloroform (****$CHCl_3$⊂D11a****). For clarity, only the hydrogens involved in the H-bonding network are presented.*

***Table 10.** H-bond length (in Å) corresponding to the **D11a** and **Kr⊂D11a**, **Xe⊂D11a**, **Rn⊂D11a** or **CHCl₃⊂D11a**.*

Kr⊂D11a	Xe⊂D11a	Rn⊂D11a	$CHCl_3$⊂D11a	D11a
1.90	1.90	1.92	1.87	1.90
1.87	1.87	1.90	1.94	1.86
1.87	1.87	1.90	1.87	1.86
1.90	1.90	1.94	1.91	1.90
1.88	1.88	1.90	1.85	1.88
1.89	1.89	1.90	1.87	1.88

The comparison of the resulting structures of the dimers encapsulating Kr (**Kr⊂D11a**) and Xe (**Xe⊂D11a**) with **D11a** reveals similar H-bond lengths. In the case of Rn (**Rn⊂D11a**) and chloroform (**$CHCl_3$⊂D11a**), however, those distances are slightly distorted with respect **D11a**. Nevertheless, the interaction and complexation energies calculated using the Counterpoise approach show that the encapsulation of chloroform presents the most favourable values for both energetic parameters (interaction and complexation energies), followed by Rn (**Table 11**). This fact suggests that these supramolecular capsules are able to modify their conformation for fitting better the guest. This observation was also confirmed by the analysis of the available inner volume (**Table 12**). X-ray experiments showed that cavity internal volume of **D11a** was 147 $Å^3$, being this parameter reduced to 125 $Å^3$ for the dimers that are encapsulating a noble gas and 138 $Å^3$ when a chloroform molecule is trapped. As far as the guest molecules are concerned, their van der Waals volumes have been calculated, being 34.5 $Å^3$ for Kr, 42.2 $Å^3$ for Xe and 50.3 $Å^3$ for Rn, and significantly bigger for chloroform (72 $Å^3$). It is important to note that the bigger size of the chloroform lead to a greater internal volume of the dimer. Nevertheless, no significant differences are found for H-bond distances of the dimer, which suggests that the capsule remains formed (**Table 10**).

The internal volume of the dimer and the size of the guests can be related calculating the *Packing Coefficient* proposed by Rebek:[360]

$$Packing\ Coefficient = \frac{Volume_{guest}}{Internal\ Volume_{dimer}}$$

The packing coefficient obtained for the chloroform encapsulation is 52%, near the 55% proposed by Rebek as the most favourable, being these for the noble gases considerably smaller (between 28% and 40%).[360] This fact agrees with the interaction and complexation energies obtained, since the chloroform shows the best energetic parameters and packing coefficient.

Table 11. *Interaction and complexation Energies (in kcal/mol) for the Kr, Xe, Rn and chloroform trapped inside* ***D11a.***

Energy	Kr⊂D11a	Xe⊂D11a	Rn⊂D11a	$CHCl_3$⊂D11a
Inter.	-5.8	-7.8	-9.5	-16.8
Complex.	-4.3	-6.4	-7.7	-14.1

Table 12. *Calculated internal volumes (in Å^3) of dimers* ***D11a*** *and the volume of the guests (Kr, Xe, Rn and chloroform, in Å^3), together with packing coefficient.*

	Kr⊂D11a	Xe⊂D11a	Rn⊂D11a	$CHCl_3$⊂D11a
Guest Volume	34.5	42.2	50.3	72
Dimer Volume	125	125	125	138
Packing coefficient (%)	28	34	40	52

360. Mecozzi, S. et al. *Chem. – A Eur. J.* **1998**, *4* (6), 1016–1022.

It is worth to mention that both the interaction and complexation energy showed that encapsulation of Kr and Xe is also favourable, highlighting that these dimers could be a promising system for the capture of noble gases, showing best results to those observed for other cages, like cucurbiturils and cyclodextrins in solution.[361,362] Furthermore, it has been found that the larger the guest volume (Kr < Xe < Rn < $CHCl_3$) the better the energetic values, suggesting the importance of their size and opening the door to a deeper study of this dependency. Additionally, this work has been a complement to an experimental study, whose results agree with the ones here obtained.[363] The results presented in this chapter have led the following publications: Pizzi, A.; Ozores, H. L.; Calvelo, M.; García-Fandiño, R.; Amorín, M.; Demitri, N.; Terraneo, G.; Bracco, S.; Comotti, A.; Sozzani, P.; Bezuidenhout, C. X.; Metrangolo, P.; Granja, J. R. *Angew. Chemie - Int. Ed.* **2019**, *58* (41), 14472–14476.

361. Brotin, T. et al. *J. Am. Chem. Soc.* **2000**, *122* (6), 1171–1174.
362. Bartik, K. et al. *J. Magn. Reson. Ser. B* **1995**, *109* (2), 164–168.
363. Pizzi, A. et al. *Angew. Chemie - Int. Ed.* **2019**, *58* (41), 14472–14476.

5.5.SELF-ASSEMBLING α,δ-CPS ENCAPSULATING FULLERENES.

The use of α,δ-SCPNs for encapsulating different type of hydrophobic molecules has been proposed since the first time they were designed and synthetized by the group of Prof. Granja.[107] It is important to note that the presence of two methylene moieties per cyclic amino acid oriented inwards in the α,δ-CPs increases the hydrophobic character of its inner cavity compared to the previous α,γ-CPs, in which only one methylene per cyclic amino acid is pointing inwards (**Figure 32**). With this in mind, carbon nanostructures (fullerene, C_{60}) were proposed as potential substrates to fill the pore of SCPNs made of α,δ-CPs dodecamers, which could improve their solubilization in aqueous solution. The UV absorption experiments of fullerene suspensions confirmed their solubilization in aqueous media that contain these peptides. These experiments found an optimal proportion of one molecule of C_{60} per each twenty CPs.

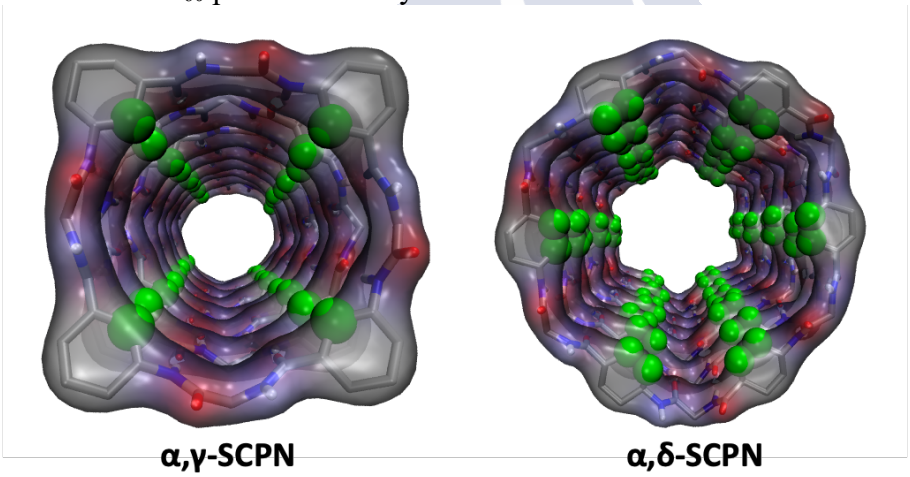

Figure 32. *Detail of the inner cavity of an α,γ- and an α,δ-SCPN, highlighting the hydrophobic moieties oriented inwards in green.*

107. Lamas, A. et al. *Chem. Sci.* **2018**, *9* (43), 8228–8233.

In order to better understand such process, we decided to carry out a computationally study with SCPNs composed by six dodecamers of α,δ-CPs encapsulating a C_{60} (**Figure 33***A*). For this task, the unmethylated **CP1** studied in the previous chapter was selected. Although the parallel arrangement was the most favourable, the antiparallel sheet was also considered, in order to elucidate the effect of entrapping the fullerene in the stability of this kind of β-sheet (**Figure 33***B*). In this way, two SCPNs were considered: **SCPN1p**, formed by three units of **D1p**; and **SCPN1a**; made of three dimers **D1a**. Therefore, each SCPN was made of six CPs. Additionally, it is important to mention that in all cases the fullerene molecule is initially placed in the central part of the SCPN pore, ensuring the peptide environment.

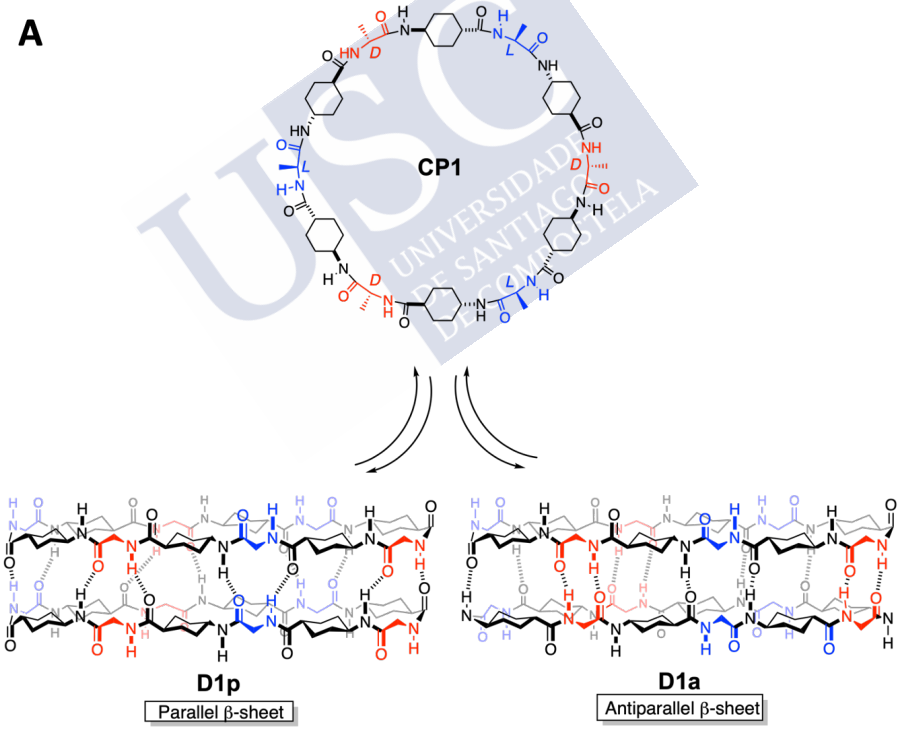

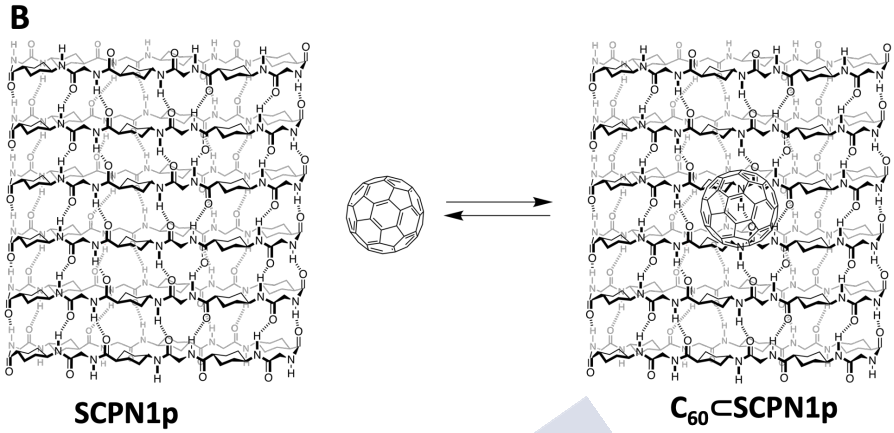

Figure 33. A) *Schematic representation of a α,δ-SCPN made of six dodecameric CPs encapsulating one C_{60} molecule (**C_{60}⊂SCPN1p**). The antiparallel nanotubes **C_{60}⊂ SCPN1a** would be analogous but changing the β-sheet packing.* ***B)*** *Structure of the basic subunit used in the formation of this nanotube (**CP1**), as well as the dimers in the parallel (**D1p**) and the antiparallel (**D1a**) forms.*

DFT was not suitable for the optimization of the geometry due to the huge number of atoms of the final structure (1140 atoms of the complex SCPN and C_{60}). Consequently, the semiempirical method PM7 was selected for this purpose. The optimized geometries of both SCPNs, the parallel and the antiparallel packing, encapsulating a C_{60} molecule, **C_{60}⊂SCPN1p** and **C_{60}⊂SCPN1a**, respectively, as well as the isolated nanotubes (**SCPN1p** and **SPCN1a**) are displayed in **Figure 34**.

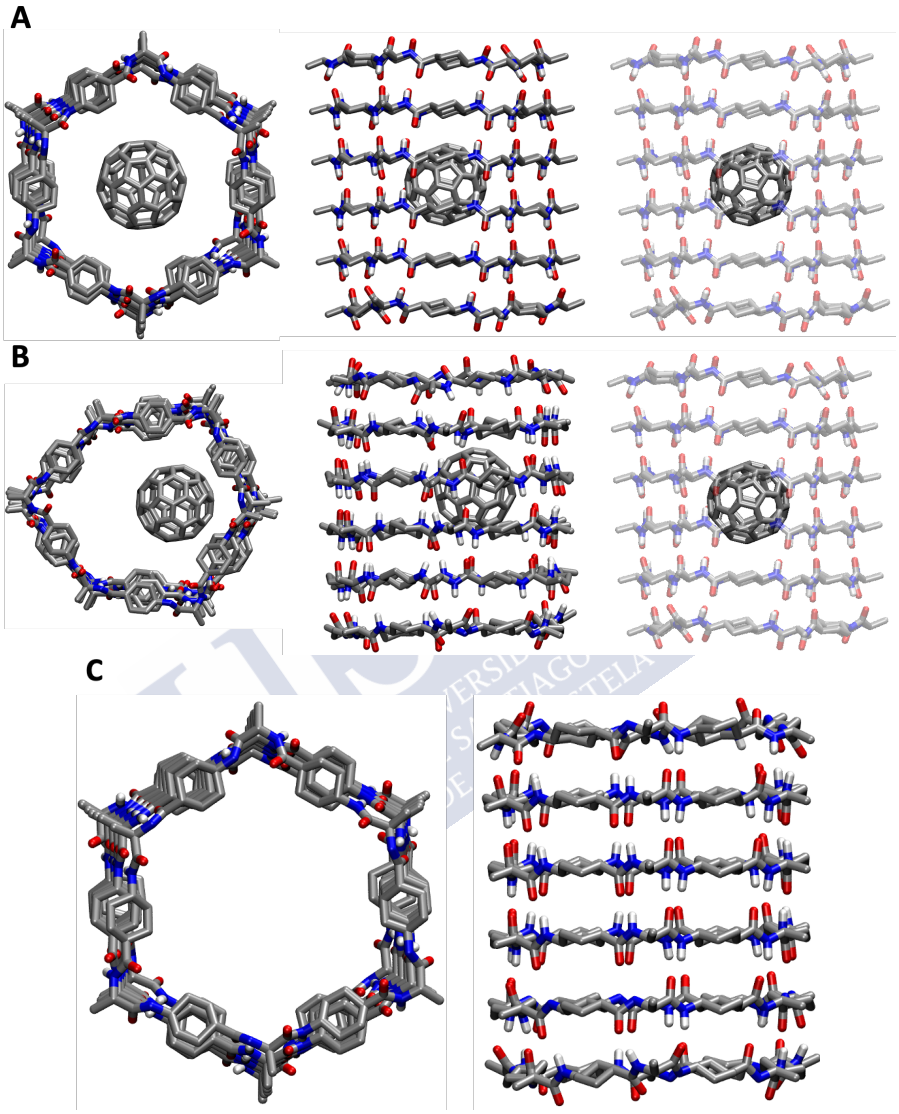
A
B
C

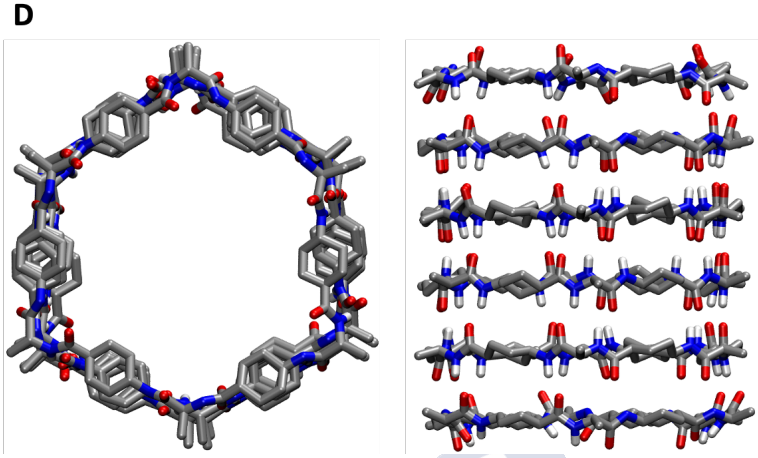

Figure 34. *Top and side views of the optimized geometry of* ***A) C_{60}⊂SCPN1p*** *and* ***B) C_{60}⊂SCPN1a*** *and the corresponding nanotubes* ***C) SCPN1p*** *and* ***D) SCPN1a****. For clarity, only the hydrogens involved in the H-bonding network are presented.*

The structural comparison of the optimized SCPNs structures with and without the fullerene moiety reveals that **SCPN1a** changes significantly its geometry when it contains the fullerene (**Figure 34***B* and **Figure 34***D*), losing the C6 geometry observed in the isolated **SCPN1a**. This distortion could be driven by a maximization of the interaction of the C_{60} with the walls of the SCPN. Contrary, **SCPN1p** preserves better its shape, there are no noteworthy changes in the nanotube with and without the C_{60} (**Figure 34***A* and **Figure 34***C*). Additionally, the C_{60} molecule remains near the centre of this nanotube.

The effect of these structural changes is reflected in the interaction energy, with a value around 10 kcal/mol more favourable for the antiparallel aggregate (**C_{60}⊂SCPN1a**), probably due to the improvement of SCPN/C_{60} interaction provided by the geometric changes (**Table 13**). However, the complexation energy shows that the confinement of fullerene in **SCPN1p** is more favourable, possibly due to the energetic cost derived from the structural deformation of **SCPN1a**. Additionally, it is important to note that whereas the difference in interaction energy is 10.4 kcal/mol more favoured to **C_{60}⊂SCPN1a**, the complexation energy only favours **C_{60}⊂SCPN1p**

by 6.2 kcal/mol. Nevertheless, the present calculations suggest that the trapping of fullerene in these systems is in both cases energetically favourable, at least following the proposed model, supporting the results obtained experimentally in the Prof. Granja's group.[107]

***Table 13.** Interaction and complexation Energies (in kcal/mol) for C_{60}⊂**SCPN1p** and C_{60}⊂**SCPN1a**.*

	C_{60}⊂SCPN1p	**C_{60}⊂SCPN1a**
Interaction Energy	-22.1	-32.5
Complexation Energy	-18.8	-12.6

The stability of the H-bonds of the β-sheet backbone were studied by calculation of the distances between the H of the amide group and the oxygen of the carbonyl (**Figure 35**). This analysis revealed that the H-bond distances between **C_{60}⊂SCPN1p** and **SCPN1p** are very similar, ranging from 1.80 to 1.95 Å for the H-bonds in which α-NH are participating and between 1.75 (1.80 for the isolated SCPN) to 1.95 Å for the H-bonds in which the amide protons correspond to δ-residues (**Figure 35***AC*). For the antiparallel nanotube the encapsulation of a C_{60} molecule does not disturb neither too much the H-bond pattern, being again the ranges of distances very similar for both structures (**Figure 35***BD*). These facts claim that differences in the energies cannot be explained by changes in the H-bond pattern, suggesting that other phenomena (as, for example, van der Waals or electrostatic interactions between the fullerene and the SCPNs or ring strains (angle or torsional) may be playing additional roles in this process.

107. Lamas, A. et al. *Chem. Sci.* **2018**, *9* (43), 8228–8233.

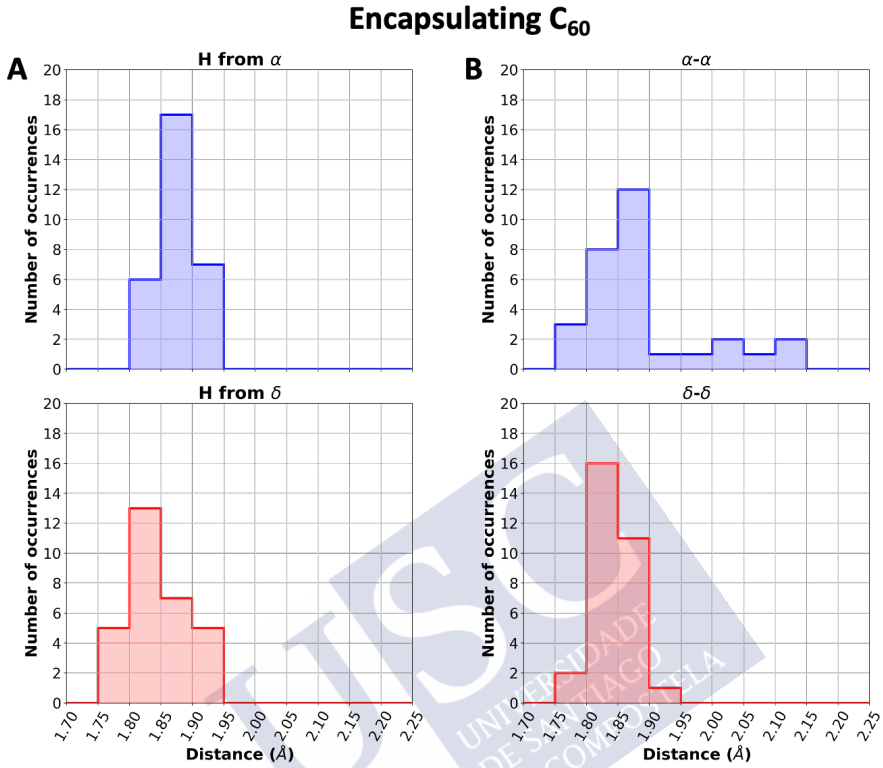
Encapsulating C_{60}
A
H from α
B
α-α
H from δ
δ-δ
Number of occurrences
Distance (Å)

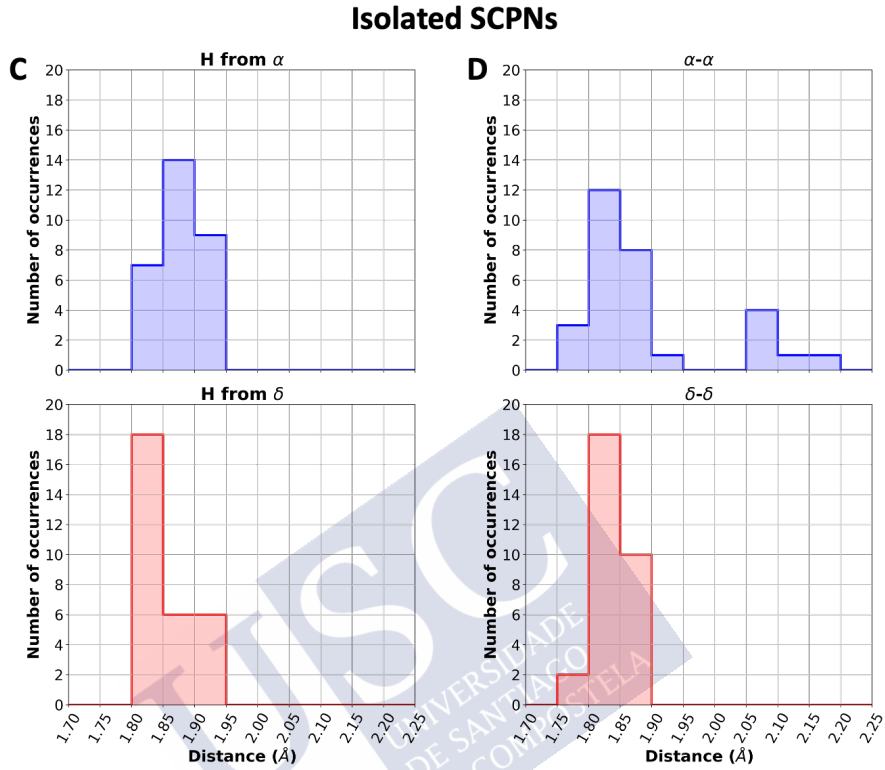

***Figure 35.** Histograms with the backbone H-bond distances of **A) C₆₀⊂SCPN1p** and **B) C₆₀⊂SCPN1a** and the corresponding empty SCPNs; **C) SCPN1p** and **D) SCPN1a**, respectively optimized at PM7 level. For the parallel nanotubes, the H-bonds formed by NH of α-residues are presented in blue, whereas those formed by NH of δ-amino acid are printed in red. For the antiparallel nanotubes, the results for the H-bonds formed between α-amino acids are presented in blue, while the results for the analogous formed between δ-residues are showed in red.*

The optimized structures obtained for the confined C_{60} in **SCPN1p** and **SCPN1a** suggest that there is some space in their cavity for the encapsulation of larger molecules. In this way, the next step was the evaluation of analogous complexes but formed with C_{70} moiety, **C_{70}⊂SCPN1p** and **C_{70}⊂SCPN1a**. Due to its rugby-ball shape, two different situations were considered: in one of them, the longest axis of C_{70} fits with the nanotube axis (**Figure 36***A*), whereas in the other the

C_{70} was disposed with its axis oriented perpendicular to the SCPN one (**Figure 36***B*). In order to explore both possibilities, calculations starting from C_{70} placed in the centre of the nanotube in both dispositions were carried out. From now, the first interaction will be named as $^{\perp}$**C$_{70}$⊂SCPN1p** and $^{\perp}$**C$_{70}$⊂SCPN1a** for the perpendicular disposition and $^{\parallel}$**C$_{70}$⊂SCPN1p** and $^{\parallel}$**C$_{70}$⊂SCPN1a** for the parallel orientation.

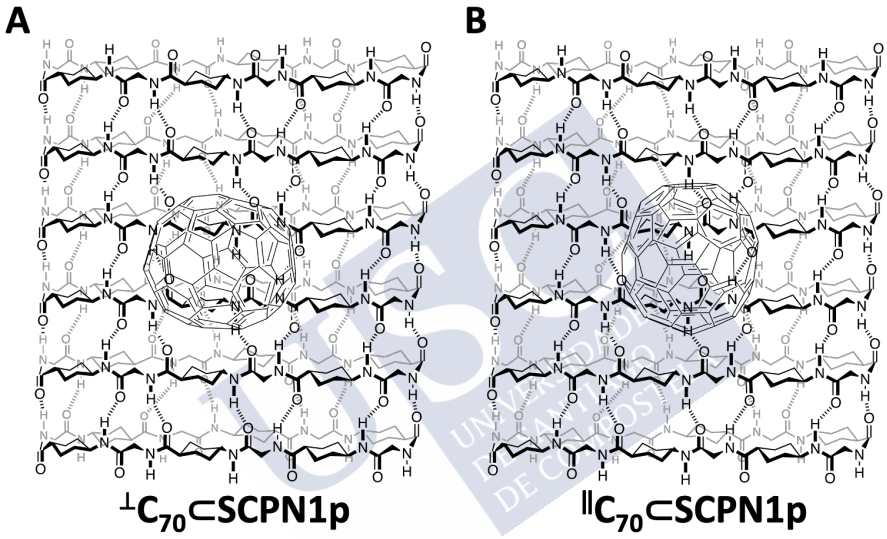

Figure 36. *Schematic representation of models with the initial orientation of the C_{70} moiety into the lumen of the nanotube,* ***A)*** *$^{\perp}$**C$_{70}$⊂SCPN1p** and* ***B)*** *of $^{\parallel}$**C$_{70}$⊂SCPN1p**. The antiparallel nanotubes $^{\perp}$**C$_{70}$⊂SCPN1a** and $^{\parallel}$**C$_{70}$⊂SCPN1a**, would be analogous to A and B but changing the β-sheet packing.*

Both SCPNs encapsulating a C_{70} molecule (**C$_{70}$⊂SCPN1p** and **C$_{70}$⊂SCPN1a**) starting from the two different initial structures were optimized at PM7 level (**Figure 37**). The results show that in all cases the nanotube conformation is distorted, except for the $^{\parallel}$**C$_{70}$⊂SCPN1p**, in which the C6 symmetry is pretty well preserved, remaining the fullerene in the centre of the *xy* plane of the CP. The rest of the nanotubes ($^{\perp}$**C$_{70}$⊂SCPN1p**, as well as $^{\perp}$**C$_{70}$⊂SCPN1a** and $^{\parallel}$**C$_{70}$⊂SCPN1a**) present a deviation of their geometry, which

presumably provokes a higher interaction energy than in the previous studies (**Table 14**). These structures show a more favourable interaction between the C_{70} molecule and the distorted nanotubes than in the case of **$^{I}C_{70}$⊂SCPNp**, highlighting the ability of these SCPNs to adapt their geometry in order to improve the confinement. Additionally, it is noteworthy that none of the C_{70} molecules change their conformation with respect the *z* axis of the SCPN, despite no restriction was added (**Figure 37**). This fact could suggest that both orientations are possible.

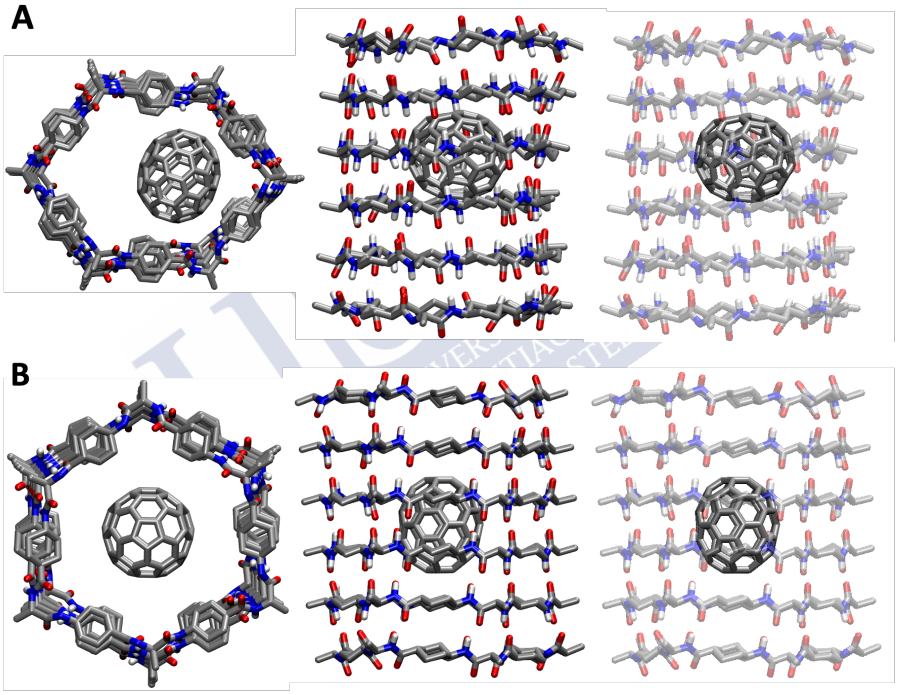

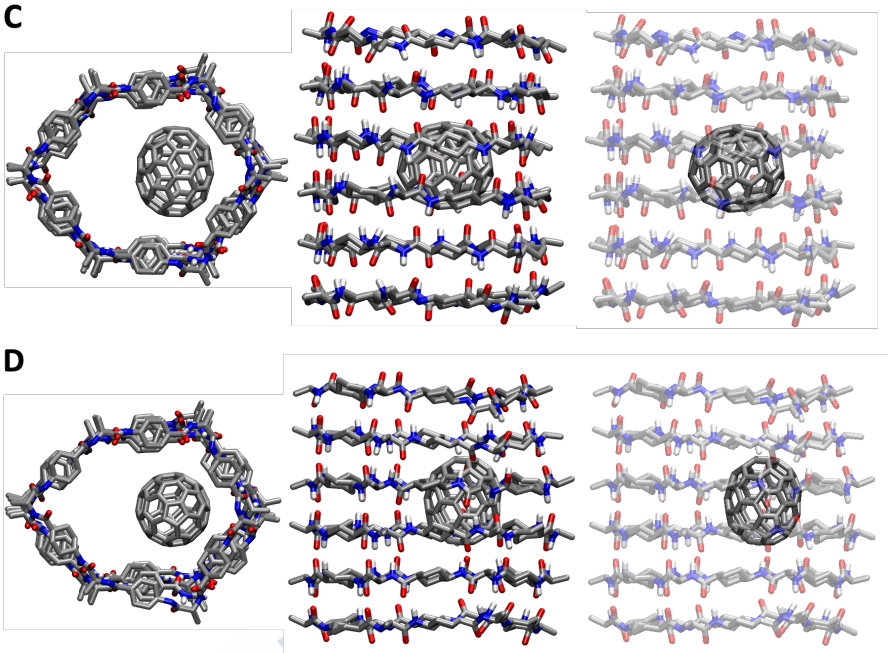

Figure 37. *Top and two side views of the optimized geometry of* ***A)*** *$^{\perp}C_{70}$⊂**SCPN1p**,* ***B)*** *$^{\parallel}C_{70}$⊂**SCPN1p**,* ***C)*** *$^{\perp}C_{70}$⊂**SCPN1a*** *and* ***D)*** *$^{\parallel}C_{70}$⊂**SCPN1a**. For clarity, only the hydrogens involved in the H-bonding network are presented.*

Table 14. *Interaction and complexation Energies (in kcal/mol) for the* ***A)*** *parallel $^{\perp}C_{70}$⊂**SCPN1p*** *and $^{\parallel}C_{70}$⊂**SCPN1p*** *and* ***B)*** *antiparallel $^{\perp}C_{70}$⊂**SCPN1a*** *and $^{\parallel}C_{70}$⊂**SCPN1a*** *complexes.*

A

Energy	$^{\perp}C_{70}$⊂SCPN1p	$^{\parallel}C_{70}$⊂SCPN1p
Inter.	-38.8	-28.3
Complex.	-13.7	-21.3

B

Energy	$^{\perp}C_{70}$⊂SCPN1a	$^{\parallel}C_{70}$⊂SCPN1a
Inter.	-39.5	-43.9
Complex.	-17.7	-12.3

The comparison among the different systems reveals a higher interaction in $^{\parallel}$**C$_{70}$⊂SCPN1a**, followed by $^{\perp}$**C$_{70}$⊂SCPN1p** and $^{\perp}$**C$_{70}$⊂SCPN1a**, which present very similar results (± 0.7 kcal/mol). As it was previously mentioned, $^{\parallel}$**C$_{70}$⊂SCPN1p** is the nanotube which presents the poorest interaction. Conversely, and as it was observed for the encapsulation of C_{60}, the most favourable complexation energy is found for this nanotube ($^{\parallel}$**C$_{70}$⊂SCPN1p**), probably due to small energy required for the deformation of the nanotube. The highest complexation energies are found for the nanotubes $^{\perp}$**C$_{70}$⊂SCPN1p** and $^{\parallel}$**C$_{70}$⊂SCPN1a**, being around 8 kcal/mol less favourable than the previous case. In between, we can find $^{\perp}$**C$_{70}$⊂SCPN1a**, being only 3.6 kcal/mol less favourable than $^{\parallel}$**C$_{70}$⊂SCPN1a**. However, the interaction in this antiparallel nanotube is 11.2 kcal/mol more advantageous. This fact, as well as the observed for the C_{60} encapsulation, suggests that a balance between these two terms should be considered.

The analysis of the H-bond distances reveals that the distortion of the nanotube is higher than in the encapsulation of C_{60} (probably due to its bigger size) with the exception of $^{\parallel}$**C$_{70}$⊂SCPN1p** (**Figure 38***B*). In this case, the H-bond distance assortments are almost the same than in the isolated parallel nanotube (**Figure 38***E* and **Figure 35***C,* in different scale): ranging from 1.80 to 1.95 Å for the H-bonds made by the NH of α-amino acids and from 1.75 (1.80 in the case of the isolated nanotube) to 1.95 Å when the H-bond is form by the amide proton of δ-residues. It is important to note that the ranges are very similar regardless if the **SCPN1p** is isolated or encapsulating a C_{60} or a C_{70} whose long axis is parallel to the nanotube. For the $^{\perp}$**C$_{70}$⊂SCPN1p** the distance ranges are slightly wider, being longer than 2.00 Å in some cases, which suggests that nanotube shape preservation depends on the conformation adopted by the guest (**Figure 38***A*). For the antiparallel nanotube the distortion is clearly more pronounced, especially in the case of the H-bonds formed by δ-amino acids (**Figure 38***CDF*). Whereas in the isolated **SCPN1a** all H-bonds distances of this type are shorter than 1.90 Å, the encapsulation of a C_{70} molecule lengthens considerably these distances. Additionally, in one case it is possible to find a distance between 2.35 and 2.40 Å, a value in which the H-bond is probably not formed.

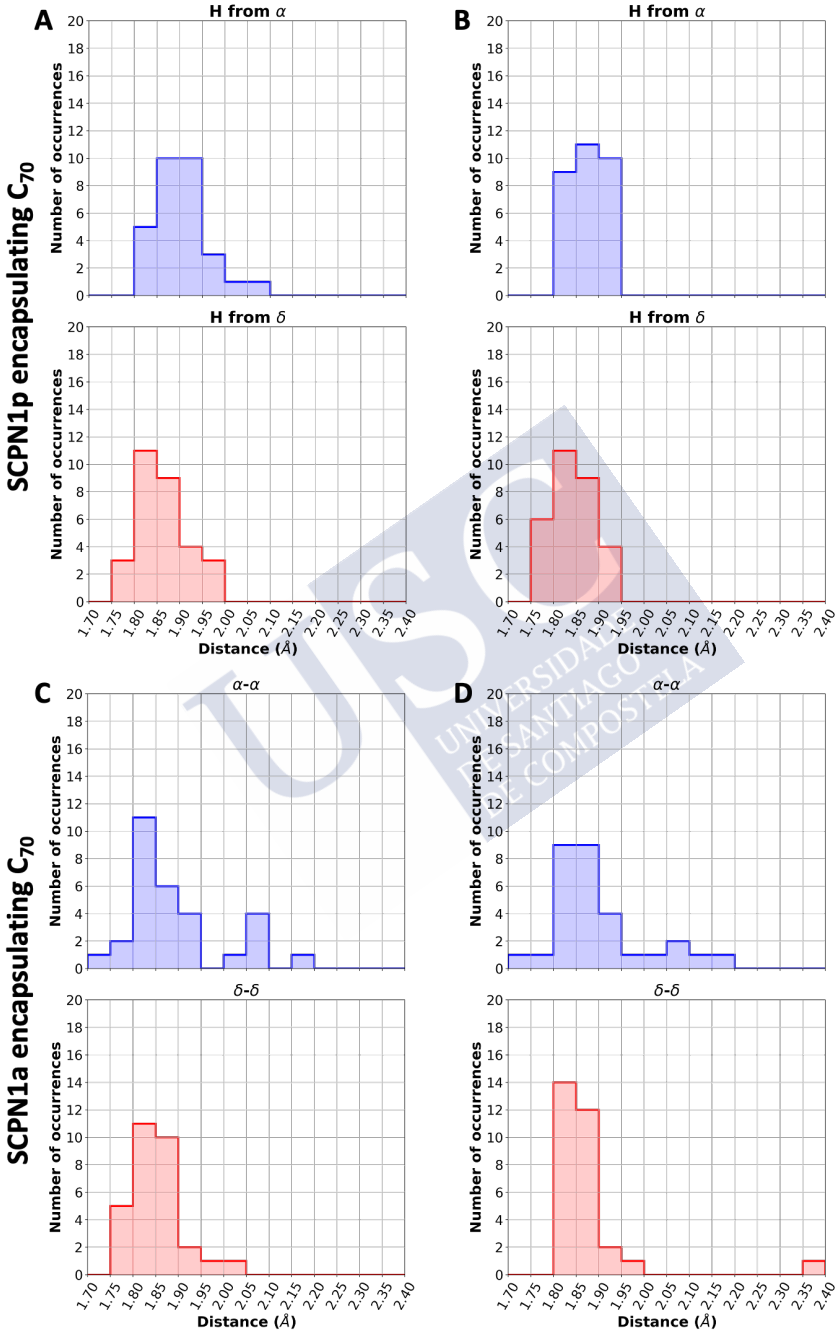
A
B
C
D
SCPN1p encapsulating C70
SCPN1a encapsulating C70
H from α
H from δ
α-α
δ-δ
Number of occurrences
Distance (Å)

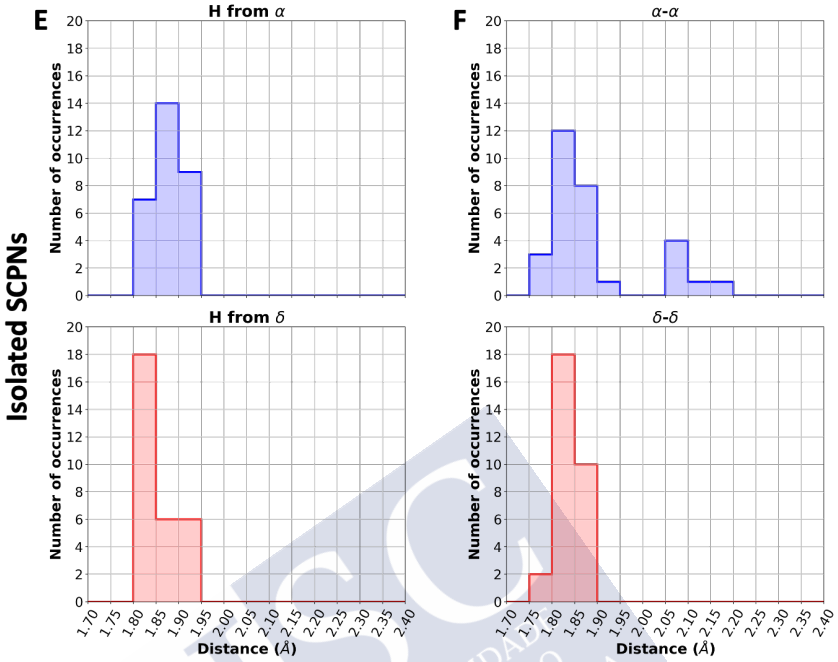

***Figure 38.** Histogram with the backbone H-bond distances of **SCPN1p** and **SCPN1a** encapsulating a C_{70} molecule in a perpendicular conformation [**A**)$^{\perp}$**C$_{70}$⊂ SCPN1p** and **C**) $^{\perp}$**C$_{70}$⊂ SCPN1a**, respectively] and parallel orientation [**B**) $^{\parallel}$**C$_{70}$⊂ SCPN1p** and **D**) $^{\parallel}$**C$_{70}$⊂ SCPN1a**] and the corresponding hosts nanotubes [**E**) **SCPN1p** and **F**) **SCPN1p**] optimized at PM7 level. For the parallel nanotubes, the H-bond distances with the amide proton (NH) of an α-residue are presented in blue, whereas the analogous with NH of the δ-amino acid are printed in red. For the antiparallel nanotubes, the results for the H-bonds formed between α-amino acids are presented in blue, while the distances for the analogous formed between δ-residues are showed in red.*

To sum up, after the PM7 geometry optimizations and DFT energy calculations, this study suggests that the encapsulation of fullerenes (C_{60} and C_{70}) inside dodecameric α,δ-CPs nanotubes is favourable in all cases, at least when a model in which the nanotube is formed before the encapsulation is considered. Further experimental evidence would be useful to validate or not these assumptions. In any case, it should be noted that quantum calculations do not consider explicit solvent and the

flexibility of the systems and these factors could have a great importance in the study of this type of complexes.

5.6. SELF-ASSEMBLING α,δ-CPS ENCAPSULATING CARBON NANOTUBES.

After the study of the entrapping of two fullerenes (C_{60} and C_{70}) inside α,δ-SCPNs, being found that it was favourable at a semiempirical level optimization and DFT calculation, we decided to extend this type of studies to the encapsulation of a carbon nanotube (CNT).

During the last decades, several interesting applications of CNTs in fields like catalysis, energy storage, electronic, biology or medicine have been proposed.[364–366] Despite them, the use of CNTs is limited due to its low solubility, self-aggregation propensity and presumable toxic character.[367,368] In order to overcome such difficulties, covalent and non-covalent modifications have been proposed as one of the most promising approach.[369–371] In this sense, the interaction between CNTs and peptides has provide useful insights in this field, being found improvements in CNTs solubilization and biocompatibility.[372–374]

One interesting approach is the threading of CNT by cyclic molecules, highlighting the works of the group of Emilio Pérez.[375–382]

364. Heister, E. et al. *ACS Appl. Mater. Interfaces* **2013**, *5* (6), 1870–1891.
365. Yan, Y. et al. *Chem. Soc. Rev.* **2015**, *44* (10), 3295–3346.
366. Baughman, R. H. et al. *Science.* **2002**, *297* (5582), 787–792.
367. Bottini, M. et al. *Toxicol. Lett.* **2006**, *160* (2), 121–126.
368. Kobayashi, N. et al. *J. Occup. Health* **2017**, *59* (5), 394–407.
369. Bianco, A. et al. *Chem. Commun.* **2005**, No. 5, 571–577.
370. Singh, P. et al. *Chem. Soc. Rev.* **2009**, *38* (8), 2214–2230.
371. Britz, D. A. et al. *Chem. Soc. Rev.* **2006**, *35* (7), 637–659.
372. Bakota, E. L. et al. *Biomacromolecules* **2009**, *10* (8), 2201–2206.
373. Antonucci, A. et al. *ACS Appl. Mater. Interfaces* **2017**, *9* (13), 11321–11331.
374. Cogan, N. M. B. et al. *J. Phys. Chem. C* **2014**, *118* (11), 5935–5944.
375. Pérez, E. M. *Chem. - A Eur. J.* **2017**, *23* (52), 12681–12689.
376. Blanco, M. et al. *Nat. Commun.* **2018**, *9* (1), 1–7.
377. López-Moreno, A. et al. *ACS Nano* **2016**, *10* (8), 8012–8018.
378. Mena-Hernando, S. et al. *Chem. Soc. Rev.* **2019**, *48* (19), 5016–5032.
379. Villalva, J. et al. *J. Phys. Chem. C* **2020**, *124* (28), 15541–15546.
380. López-Moreno, A. et al. *Chem. Commun.* **2015**, *51* (25), 5421–5424.
381. de Juan, A. et al. *Angew. Chemie* **2014**, *126* (21), 5498–5504.
382. Chamorro, R. et al. *Chem. Sci.* **2018**, *9* (17), 4176–4184.

As far as SCPNs are concerned, they could be also possible candidates for such task. Although the interaction between the side-chains of a SCPNs with CNTs has been reported in a previous work by our group using CPs bearing a pyrene moiety, threading of CNTs with the CPs results clearly interesting, since this approach may provide a higher selectivity for the type and properties of the carbon material.[102] In 2005, the group of the Prof. Gregg R. Dieckmann developed a CP constituted by alternating *D*- and *L*-, similar to those previously proposed by Prof. Ghadiri, but containing a disulfur linker between the N- and C-termini, which allows a reversible cyclization.[383] Via UV/vis/NIR and Raman spectroscopies, together with atomic force microscopy and MD simulations, the solubilization of CNTs after being threaded by these cyclic peptides was demonstrated.[384,385] Additionally, it has been claimed that this approach allows the selective encapsulation of CNTs controlling the diameter of the CPs.[384]

Years later, Prof. Kolandaivel's group carried out MD simulations of a dimer composed by *D*,*L*-α-CPs of fourteen amino acids encapsulating a CNT.[386] However, the assembly of that dimer was not observed, remaining both CPs threading the CNT but not interacting through H-bonds. Nevertheless, it may be possible that this result could be related with a not suitable fitting of the size of both components (SCPN and CNT). In this way, and as a first approximation, we proposed the study of a dimer (unmethylated **D1p**) made of two dodecameric α,δ-CPs (unmethylated **CP1**) threating armchair CNTs of different diameters: **4,4**, with a diameter of 5.4 Å; **5,5** (6.7 Å); **6,6** (8.1 Å); **7,7** (9.5 Å); and **8,8** (10.9 Å). It is important to note that the diameter is defined as the distance between the position of two carbon atoms in opposite positions, without taking into account the van der Waals radii (**Figure 39***A*). Same approach has been followed for defining the radii of the SCPN that was considered between the carbon-carbon bonds (C3-C4) of cyclohexyl moiety of Ach residues in opposite positions as illustrated in **Figure 39***B* (15.5 Å). In this study, we only

383. Ortiz-Acevedo, A. et al. *J. Am. Chem. Soc.* **2005**, *127* (26), 9512–9517.
384. Friling, S. R. et al. *Nanoscale* **2010**, *2* (1), 98–106.
385. Chiu, C. C. et al. *ACS Nano* **2010**, *4* (5), 2539–2546.

consider the threading of the previous mentioned armchair CNTs by parallel **D1p**, since it has been shown previously as the most stable.

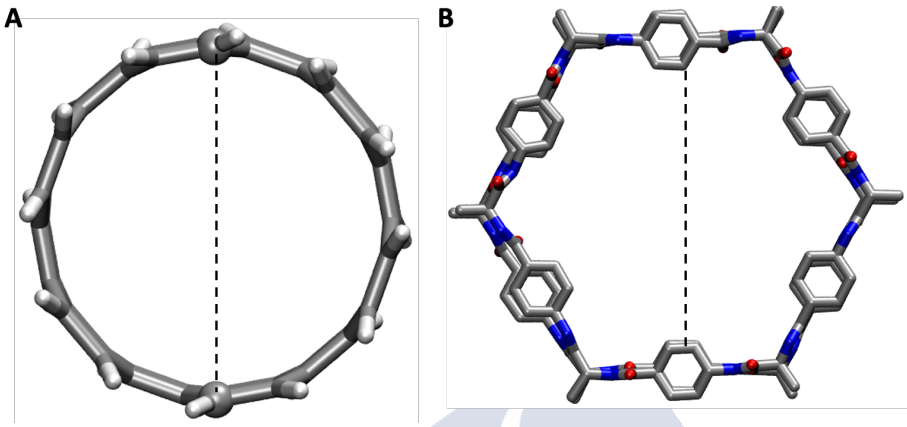

Figure 39. *Representation of how the inner diameter of* ***A)*** *CNT and* ***B) D1p*** *is defined.*

The initial structures, as well as the optimized geometries at PM7 level, are displayed in **Figure 40**. It is important to note that the calculation with the system threading the **8,8** CNT (^{8,8}**CNT⊂D1p**) did not converge, evincing that this CNT is too big for the cavity of the dimer **D1p**.

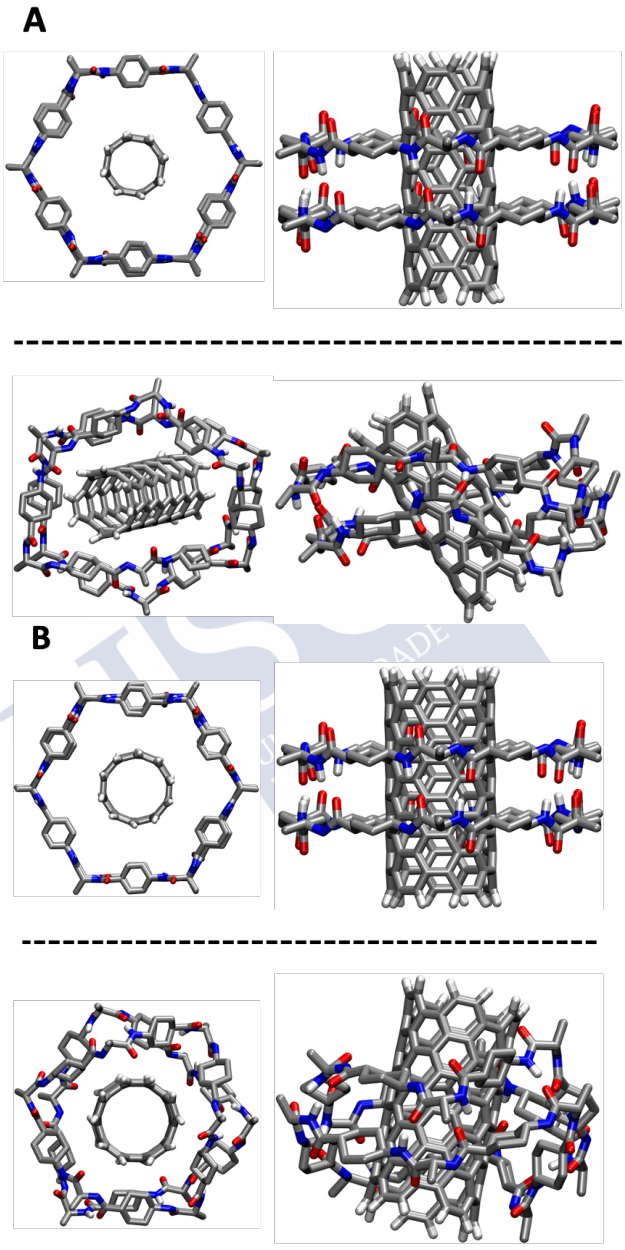
A
B

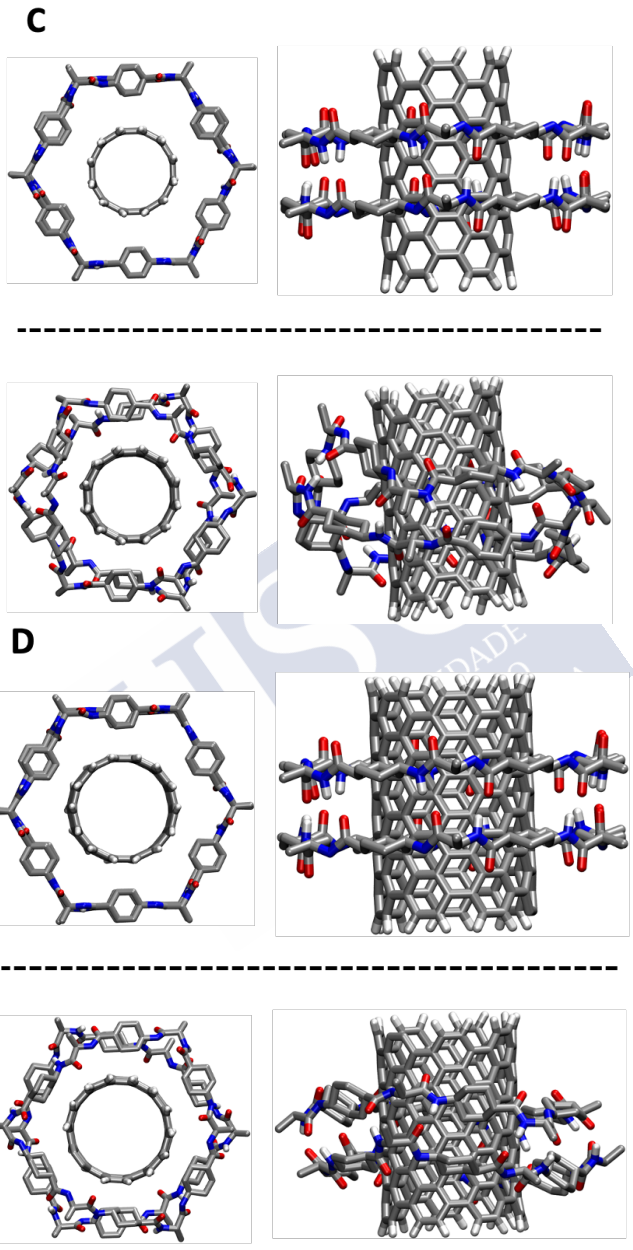
C
D

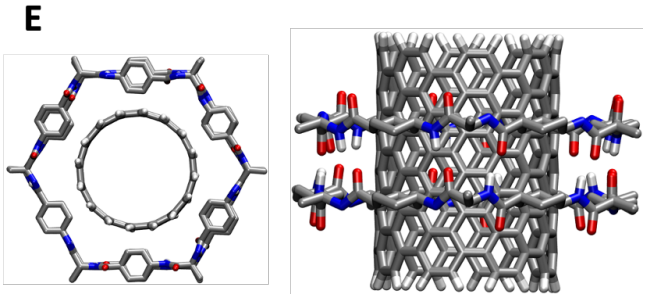

***Figure 40.** Top and side view of the initial (top) and optimized (down) geometry of **D1p** threading CNTs **A)** ^{4,4}**CNT⊂ D1p**, **B)** ^{5,5}**CNT⊂ D1p**, **C)** ^{6,6}**CNT⊂ D1p**, **D)** ^{7,7}**CNT⊂ D1p** and **E)** ^{8,8}**CNT⊂ D1p** (in this case, only the initial structure is displayed, since the geometry optimization did not converge). For clarity, only the hydrogens involved in the H-bonding network are represented.*

The optimized geometry of the two smallest CNTs (**4,4** and **5,5**) reveals a significant deformation of **D1p**, especially for ^{4,4}**CNT⊂D1p**. This effect could be due to the fact that the CNT is too small, which provokes the loss of the CP planarity after the interaction with the CNT. The pseudorotaxane structure of **6,6** and **7,7** (**^{6,6}CNT⊂D1p** and **^{7,7}CNT⊂D1p**, respectively) led to less deformed dimers, mainly for the largest one (**7,7**). This suggest that the methylene groups of the CPs like to interact with the CNT and, consequently, the bigger the CNT diameter the less the distortions, since most of these groups can already interact with the aromatic surface of the CNT. Additionally, one could speculate that the threaded CNT could prevent the deformation of the dimer due to van der Waals or electrostatic interactions, since other authors have previously reported the important role of these phenomena in these complexes.[386] Despite the interest of this hypothesis, it was not possible to go in deep into this matter.

Differences in the H-bond distances were also found (**Figure 41**). In this case it is possible to find wider distance ranges for all the structures where the dimer was encapsulating a CNT (also it is important to note that in this case the size of the bins is shorter than in

Figure 35 and **Figure 38**). However, for the **^{6,6}CNT⊂D1p** and **^{7,7}CNT⊂D1p** the ranges are clearly shorter than for **^{4,4}CNT⊂D1p** and **^{5,5}CNT⊂D1p**, which suggests again that the bigger CNTs produce the smaller distortion in the dimer.

386. Vidhyasankar, S. et al. *J. Biomol. Struct. Dyn.* **2018**, *36* (5), 1108–1117.

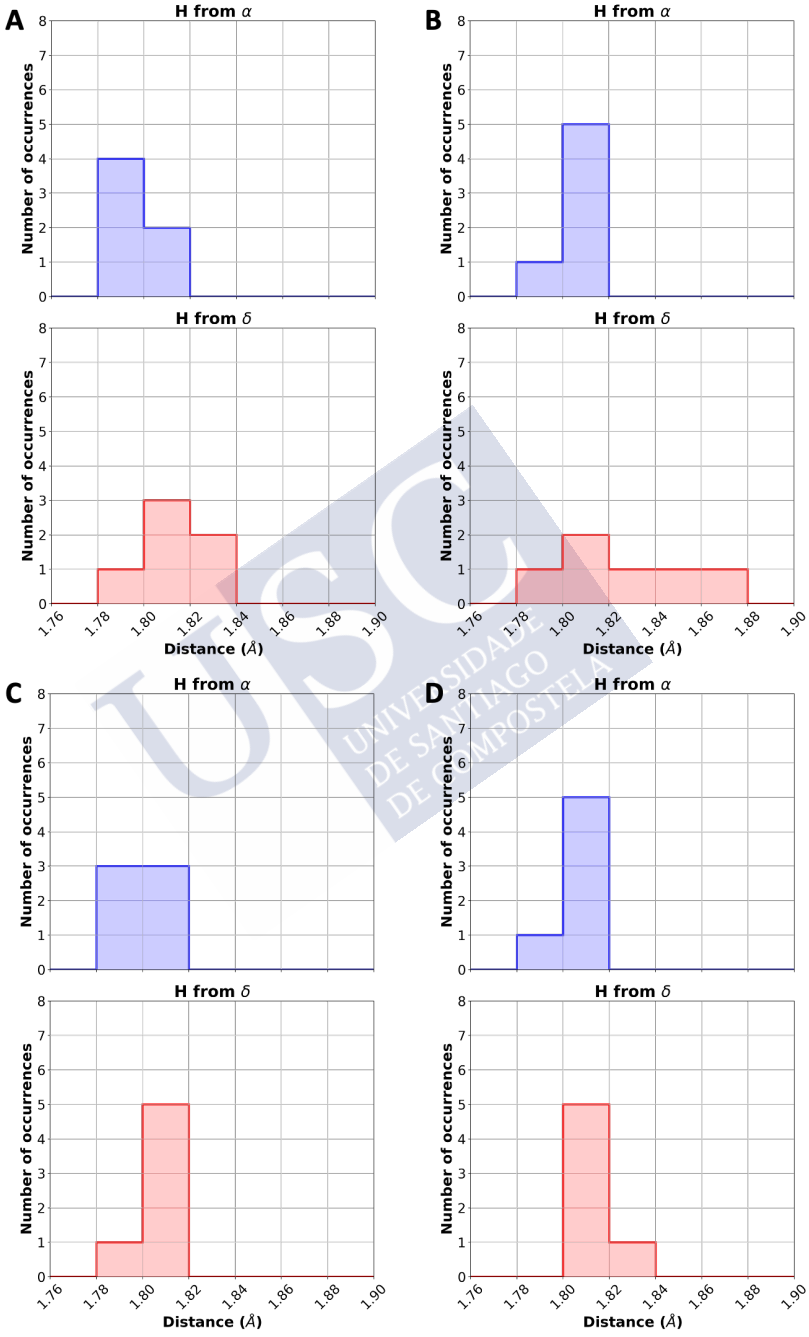
A
H from α
Number of occurrences
H from δ
Number of occurrences
Distance (Å)
B
H from α
Number of occurrences
H from δ
Number of occurrences
Distance (Å)
C
H from α
Number of occurrences
H from δ
Number of occurrences
Distance (Å)
D
H from α
Number of occurrences
H from δ
Number of occurrences
Distance (Å)

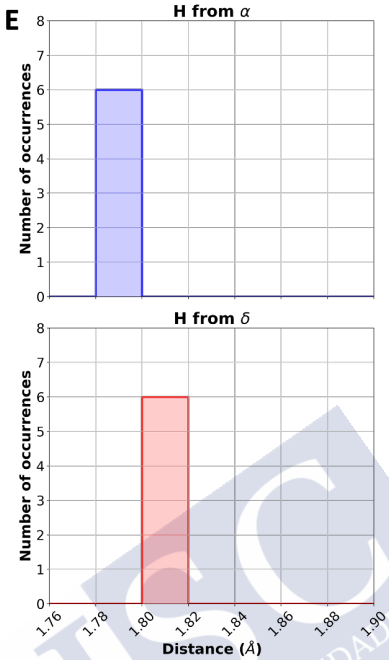

Figure 41. *Histogram with the backbone H-bond distances of* ***D1p*** *(****E****) and the corresponding threaded derivative of CNT of different sizes:* ***A)*** ^{4,4}***CNT⊂D1p, B)*** ^{5,5}***CNT⊂D1p, C)*** ^{6,6}***CNT⊂D1p*** *and* ***D)*** ^{7,7}***CNT⊂D1p****. The H-bonds made by NH group of an α-residue are presented in blue, whereas those made by the amide proton of a δ-amino acid are printed in red.*

As expected, the observed differences of optimized geometries provoke modifications in the interaction and complexation energies (**Table 15**). Despite the big distortion of the dimer, and contrary to the previously observed for the fullerene incorporation, the threading of the ^{4,4}**CNT** appears as the least favourable interaction with a difference larger than 15 kcal/mol with respect to the others. This suggests that the ^{4,4}**CNT** is too small for being favourably incorporated in the cavity of **D1p**, at least individually, compared with the rest of CNTs herein studied. The trapping of the other three CNTs shows a very similar interaction energy, being all values in a range of 3.5 kcal/mol. As it was observed for the fullerene encapsulation, the least favourable complexation energy is found for the most deformed dimers: ^{4,4}**CNT⊂D1p** and ^{5,5}**CNT⊂D1p**, whose values are -21.5 and -29.4

kcal/mol, respectively. The threading of **^{6,6}CNT** and **^{7,7}CNT**, despite showing similar interaction energies to **^{5,5}CNT**, presents a much kindlier complexation energy (-45.7 and -53.8 kcal/mol, respectively). In this way, the encapsulation of **^{7,7}CNT⊂D1p** appears as the most favourable. Nevertheless, the negative values for the complexation energies obtained for all the CNTs considered, suggest that the complex formation of the four studied CNTs would be possible.

***Table 15.** Interaction and complexation Energies (in kcal/mol) for ^{4,4}CNT⊂ D1p, B) ^{5,5}CNT⊂ D1p, C) ^{6,6}CNT⊂ D1p and D) ^{7,7}CNT⊂ D1p.*

Energy	^{4,4}CNT⊂D1p	^{5,5}CNT⊂D1p	^{6,6}CNT⊂D1p	^{7,7}CNT⊂D1p
Inter.	-58.4	-73.2	-76.7	-75.6
Complex.	-21.5	-29.4	-45.7	-53.8

5.7. CONCLUSIONS.

DFT calculations using dimers made of hexameric α,γ-CPs revealed that these systems are prone to encapsulate noble gases, in agreement with experimental observations, emerging as good candidates for their use as molecular containers. The results obtained in this chapter showed how the dimer changed its inner cavity in order to favour the gas trapping. To do this, the calculations show that small conformational changes allow varying the available volume of the dimer lumen. The trend for a more favoured encapsulation seems to be related with the size of the guest molecule, since it has been found that the higher the packing coefficient, the more preferred the trapping. Although the encapsulation of chloroform appears as the most favourable, these results open the door to a new application of these systems: the use of self-assembling cyclic oligopeptides as a simple strategy to construct porous materials using biocompatible building blocks. The results above exposed led to the following publication: Pizzi, A.; Ozores, H. L.; Calvelo, M.; García-Fandiño, R.; Amorín, M.; Demitri, N.; Terraneo, G.; Bracco, S.; Comotti, A.; Sozzani, P.; Bezuidenhout, C. X.; Metrangolo, P.; Granja, J. R. *Angew. Chemie - Int. Ed.* **2019**, *58* (41), 14472–14476.

The formation of SCPNs by the self-assembling process of α,δ-CPs to provide nanotubes that contains an internal pore with

hydrophobic properties, opens the opportunity to display new applications in delivery and extraction processes. Therefore, we decided to study the use of α,δ-SCPNs in the solubilization of different carbon allotropes in an aqueous solution. Specially, we envisaged that the encapsulation of fullerenes and carbon nanotubes of different sizes could be evaluated via computational methods. Calculations carried out with the fullerenes showed that the entrapment of a C_{60} molecule in a SCPN made of the stacking of dodecameric α,δ-CPs was favoured. The optimized geometries revealed that the antiparallel α,δ-SCPN was able to distort its shape in order to maximize the interaction with the C_{60} fullerene. However, this ability provokes that a highest energy cost has to be paid, being this reflected in a less favourable complexation energy. Similar conclusions were obtained for the interaction with a C_{70} fullerene, being again always favourable for all the scenarios considered. In addition, further calculations showed that not only the encapsulation of fullerenes in α,δ-SCPNs is favoured, but also the trapping of CNTs of different sizes.

Finally, as it was mentioned in the section *Methods*, it is crucial to note that all conclusions derived from these studies were obtained considering a model in which the peptide supramolecular structures (dimer or nanotube) were formed before the encapsulation of the guest. Other models may be also plausible, as for example the grown of a nanotube after the encapsulation of the guest in individual CPs. Nevertheless, they were not considered during the completion of this thesis, although further studies may start from this point.

II. MD simulations of SCPNs with hydrophobic sequences: studying their possible application as transmembrane channels

Cylindrical-shaped structures with inner pores could be used as transmembrane channels when they are inserted in lipid bilayers.[387–389] SCPNs have emerged as good candidates for developing this task, since it has been proposed that those CPs made up of fully hydrophobic sequences self-assemble in membranes acquiring a transmembrane-channel shape (**Figure 42**).[73,76,77,337,390–392] Some of the inherent advantages of these systems are their presumably biocompability, easy control of their inner diameter and synthetic simplicity.

73. Ghadiri, M. R. et al. *Nature* **1994**, *369* (6478), 301–304.
76. Montenegro, J. et al. *Acc. Chem. Res.* **2013**, *46* (12), 2955–2965.
77. Granja, J. R. et al. *J. Am. Chem. Soc.* **1994**, *116* (23), 10785–10786.
387. Almeida, J. G. et al. *Biochim. Biophys. Acta - Biomembr.* **2017**, *1859* (10), 2021–2039.
388. Sisson, A. L. et al. *Chem. Soc. Rev.* **2006**, *35* (12), 1269–1286.
389. Chen, L. et al. *J. Am. Chem. Soc.* **2013**, *135* (6), 2152–2155.
390. Khazanovich, N. et al. *J. Am. Chem. Soc.* **1994**, *116* (13), 6011–6012.
391. García-Fandiño, R. et al. *Chem. Sci.* **2012**, *3* (11), 3280–3285.
392. Vijayaraj, R. et al. *Phys. Chem. Chem. Phys.* **2012**, *14* (43), 15135–15144.

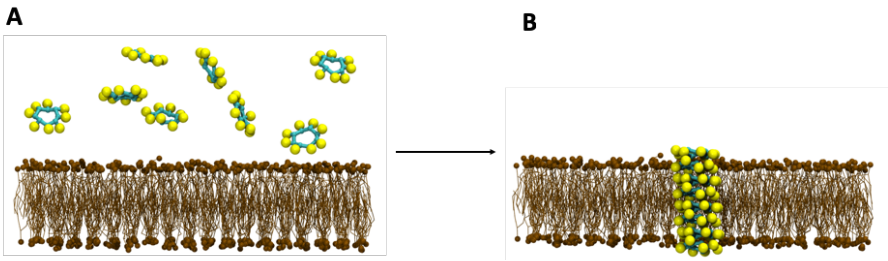

Figure 42. *Schematic representation of self-assembly process of hydrophobic CPs. In the water phase (**A**), it is expected that they are not forming nanotubes, whereas once they reach the membrane the self-assembly into SCPNs occurs (**B**). The hydrophobic lateral chains of the CPs are displayed in yellow and the membrane lipids are showed in brown. Water molecules were not displayed for clarity.*

In this section, the stacking of α,γ- or α,δ-CPs made by residues with hydrophobic side chains that should self-assemble in presence of the lipid membraned to form nanotubes that adopts a perpendicular orientation, creating a transmembrane channel, will be evaluated via All-atom MD (AA-MD) simulations. Both the stability of the nanotubes as well as their potential transport capabilities will be taken into consideration in the following chapters, trying to elucidate the performance of α,γ- and α,δ-SCPNs as transmembrane nanotubes. This study has led to the following publication: Calvelo, M.; Granja, J. R.; Garcia-Fandiño, R. *Phys. Chem. Chem. Phys.* **2019**, *21* (37), 20750–20756.

In the first of the following chapters, a doubly modulable α,γ-SCPN, formed by the stacking of internally functionalized α,γ-CPs, sensitive both to the environment (the lipid membrane, **Figure 42**) and to the pH of the media has been studied via MD simulations. At low pH values, the protonation of the inner groups (carboxylic acids) of CPs in the membrane would lead to stable SCPNs that work as aquaporins, allowing the permeation of water but not ions. However, higher pH would lead to deprotonation of the carboxylic groups at the lumen. The resulting anionic tubes disassemble, leading to an aggregate that is able to attract the ions towards the hydrophobic core of the bilayer. This process could destroy the ionic balance of the cell and ideally would

kill the target cell. The obtained results suggest that controlling not only the outer properties of nanotubes, but also the inner of the SCPNs, it can be also possible to modulate their interaction with the lipid bilayer, opening the door to new strategies for the preparation of therapeutic peptides (antimicrobial or anticancer) that interact at the membrane level.

In the next chapter, MD simulations to study water behaviour in α,γ- and α,δ-SCPNs using different water models have been carried out. Usually, the water models commonly used in MD simulations have been developed and validated by their ability to reproduce bulk water properties. However, it is not clear that these models can precisely simulate and predict the water properties in the nanoconfined conditions of a channel pore. Here, the water behaviour in the inner cavity of SCPNs was evaluated using four different water models (TIP3P, TIP4P, TIP4P/2005 and OPC). The studies showed that the dynamic behaviour of the water molecules and ions in these channels depends on the water model used, whereas the stability of the SCPNs seems to be unaffected. Additionally, it has been proven that the two more recent models (TIP4P/2005 and OPC), which are known to reproduce the experimental self-diffusion coefficient of bulk water quite well, exhibit very similar results under the nanoconfined conditions. In contrast, TIP3P and TIP4P models provide data that suggest a water behaviour with a considerably faster movement. Since none of the models studied was specifically parametrized for peptide confinement environments, this study pretends to be a point of reference for further validations. Furthermore, due to the novelty of the α,δ-SCPNs, this is the first study using MD simulations of these systems. This study has been carried out during a stay in the group of Prof. Mark S. P. Sansom, in the Oxford University, resulting in the following article: Calvelo, M.; Lynch, C.; Granja, J. R.; Sansom, M. S. P.; Garcia-Fandiño, R. *ACS Nano, accepted*.

Author affiliations:
-Calvelo, M.; García-Fandiño, R. and Granja, J. R.: Centro Singular de Investigación en Química Biolóxica e Materiais Moleculares (CiQUS), Departamento de Química Orgánica, Universidade de Santiago de Compostela, 15782 Santiago de Compostela, Spain
-Lynch, C. and Sansom, M. S. P.: Department of Biochemistry, University of Oxford, South Parks Road, Oxford OX1 3QU, United Kingdom

USC
UNIVERSIDADE
DE SANTIAGO
DE COMPOSTELA

6. Competitive double-switched SCPNs: a dual internal and external control

6.1. PRECEDENTS AND MOTIVATION.

MD simulations of SCPNs made up of an even number of alternating *D*- and *L*-α-amino acids, as the ones proposed by Ghadiri,[72] allowed a better understanding of the mechanism of cation transport across the membrane.[73,393,394] Moreover, it is quite unusual to find anions inside them, presumably because of the partial negatively character of the lumen of the SCPNs derived from the long pairs of carbonyl groups. Additionally, the transport of other positively charged molecules, as NH_4^+, has been also found in these systems.[395] Furthermore, other studies have been shown that SCPNs are able to encapsulate organic molecules, as ethanol, having been proposed to extract chloroform diluted in solution.[358,359] In this case, however, they are more prone to encapsulate rather than transport along them. On the other hand, other works have shown that they are able to transport methane and methanol, probably due to their smaller size.[396] At this respect, experimental studies shown that small polar molecules, like glucose or glutamic acid, can be transported through nanotubes formed by CPs with ten residues.[77] Another interesting feature that has been reported for *D*,*L*-α-SCPNs is their capability to discriminate between enantiomers, being able to differentiate between *R*- and *S*- lactic acid.[397] Also using MD

72. Ghadiri, M. R. et al. *Nature* **1993**, *366* (6453), 324–327.
73. Ghadiri, M. R. et al. *Nature* **1994**, *369* (6478), 301–304.
358. Zhao, X. et al. *J. Mol. Graph. Model.* **2018**, *83*, 74–83.
359. Li, R. et al. *J. Chem. Phys.* **2015**, *143* (1), 015101.
393. Song, Y. et al. *J. Phys. Chem. B* **2016**, *120* (46), 11912–11922.
394. Dehez, F. et al. *J. Phys. Chem. B* **2007**, *111* (36), 10633–10635.
395. Zhang, M. et al. *J. Mol. Model.* **2016**, *22* (10), 233.
396. Xu, J. et al. *J. Mol. Model.* **2016**, *22* (5), 1–12.
397. Farrokhpour, H. et al. *J. Phys. Chem. C* **2017**, *121* (14), 8165–8176.

simulations, transport studies of potential drug molecules, as 5-fluorouracil, have been carried out.[398]

Systems resulting from the combination of natural and non-natural amino acids, as α,γ- and α,δ-SCPNs, could result specially intriguing, since they allow to reach additional properties not found the pristine SCPNs.[95–97] In these peptides, at least one methylene group is pointing toward the lumen of the nanotube changing the pore properties (more hydrophobic) that might influence in their transport properties.[399,400] Cation transport properties of the α,γ-nanotubes developed by the group of Prof. Granja have revealed a reduced selectivity for the alkali metals studied (Li^+, Na^+, K^+ and Cs^+), but important differences were found with respect to anion (Cl^-) or divalent cations (Ca^{2+}).[391] In fact, they have been proposed as feasible calcium containers, based on the calculated PMF (*Potential Mean Force*) of Ca^{2+}, which showed a preference for encapsulation this cation in the lumen of a nanotube inserted in a lipid bilayer. Interestingly, computational studies have shown that these α,γ-SCPNs are stable in water when they encapsulate chloroform (or similar derivatives).[401] Organochloride polymers could be used to control the length of the nanotubes, which is not a trivial task.

In order to improve their selectivity, these systems allow chemical modifications of the methylene moieties of the γ-units oriented towards the lumen of the nanotube, adding internal functional groups, in a similar way than others biomimicking pores previously proposed.[57,400,402,403] In fact, our group prepared a new γ-amino acid bearing a hydroxyl group at the β-carbon and used it in the synthesis of

57. García-Fandiño, R. et al. *Proc. Natl. Acad. Sci. U. S. A.* **2012**, *109* (18), 6939–6944.
95. Amorín, M. et al. *J. Am. Chem. Soc.* **2003**, *125* (10), 2844–2845.
96. Reiriz, C. et al. *Org. Biomol. Chem.* **2009**, *7* (21), 4358–4361.
97. Rodríguez-Vázquez, N. et al. *Chem. Sci.* **2016**, *7* (1), 183–187.
391. García-Fandiño, R. et al. *Chem. Sci.* **2012**, *3* (11), 3280–3285.
398. Vijayaraj, R. et al. *Phys. Chem. Chem. Phys.* **2013**, *15* (4), 1260–1270.
399. Alsina, M. A. et al. *Phys. Chem. Chem. Phys.* **2016**, *18* (46), 31698–31710.
400. Ruiz, L. et al. *J. Phys. Chem. Lett.* **2015**, *6* (9), 1514–1520.
401. García-Fandiño, R. et al. *J. Phys. Chem. C* **2013**, *117* (19), 10143–10162.
402. Hou, X. et al. *J. Am. Chem. Soc.* **2009**, *131* (22), 7800–7805.
403. Hou, X. et al. *J. Am. Chem. Soc.* **2010**, *132* (33), 11736–11742.

CPs.[97,98] The resulting α,γ-CP presented a quite different features changing their assembling properties, requiring the presence of polar solvents to form the corresponding assembly. Owing this approach, in our group MD simulations using internally hydroxylated α,γ-SCPNs have been carried out.[404] For this study, three different models of nanotubes composed by ten units of octameric functionalized CPs were considered (**Figure 43**). In one of them, each CP contained a hydroxyl group in the β-position of all the γ-Ach moieties (c-[(*L*-Trp-*D*-γ-Ach-)$_4$], **CP$_{4OH}$**), leading to the formation of **SCPN$_{4OH}$** (**Figure 43**). In the other two models, the hydroxyl groups were introduced only on two opposite faced γ-Ach units of each CP (**CP$_{2OH}$**). The presence of two hydroxyl groups per CP produces the apparition of different possible relative orientations. Although in a nanotube composed by ten **CP$_{2OH}$** the number of possible arrangements is very large ($2^{(n-1)}$), this work was carried out with only two models: the one in which all the hydroxylated units are eclipsed, aligning all OH's along the nanotube [**SCPN$_{2OH}$(e)**]; and the other in which the functionalized γ-Ach units are alternated with respect to those in the neighbouring CPs [**SCPN$_{2OH}$(a)**] (**Figure 43**). Nevertheless, similar conclusions than those previously obtained for the non-functionalized nanotubes were obtained, with no preference observed for any particular cation. This study is part of the Master's thesis of Martín Calvelo Souto and led to the following publication: Calvelo, M.; Vázquez, S.; García-Fandiño, R. *Phys. Chem. Chem. Phys.* **2015**, *17* (43), 28586–28601.

97. Rodríguez-Vázquez, N. et al. *Chem. Sci.* **2016**, *7* (1), 183–187.
98. Rodríguez-Vázquez, N. et al. *Angew. Chemie Int. Ed.* **2016**, *55* (14), 4504–4508.
404. Calvelo, M. et al. *Phys. Chem. Chem. Phys.* **2015**, *17* (43), 28586–28601.

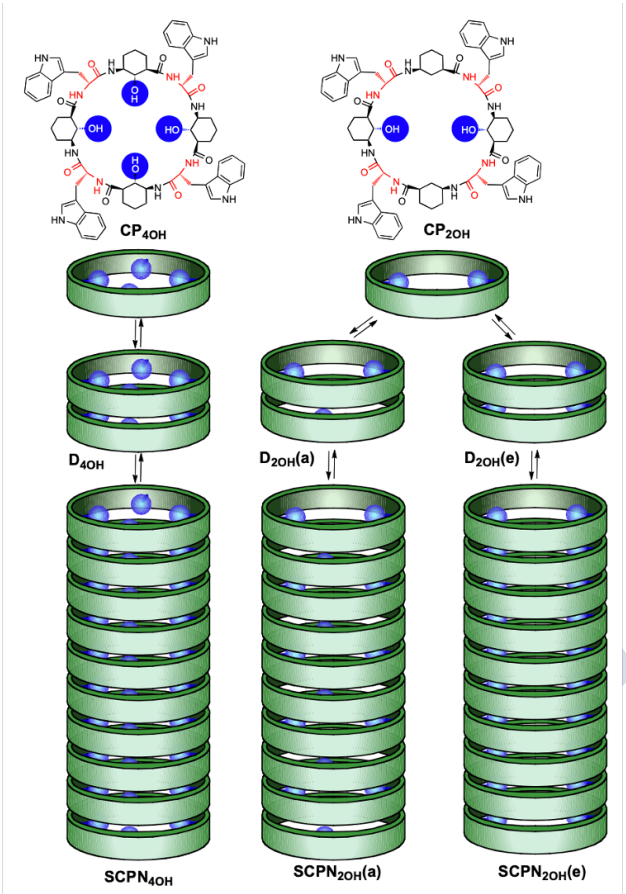

Figure 43. *Schematic models of the internally hydroxylated α,γ-SCPNs studied, highlighting the position of the hydroxyl groups (in blue), leading to* ***SCPN4OH*** *from* ***CP4OH*** *and alternated [****SCPN2OH(a)****] or eclipsed [****SCPN2OH(e)****] structures from the* ***CP2OH****.*

So, given that, it seems that the next step for improving the selectivity could be the introduction of charged residues, mimicking pores presented in Nature.[405–407] Additionally, the group was able to show that CP having a γ-residue with a carboxylate moiety could

405. Green, W. N. et al. *Annu. Rev. Physiol.* **1991**, *53*, 341–359.
406. DeCaen, P. G. et al. *Proc. Natl. Acad. Sci. U. S. A.* **2009**, *106* (52), 22498–22503.
407. Subramanyam, P. et al. *J. Mol. Biol.* **2015**, *427* (1), 190–204.

encapsulate Pt complexes that have shown a good anticancer activity.[338]

Moreover, α,γ-SCPNs not only could be internally functionalized with moieties with capacity of enhancing their transport properties, but also open the door to the use of "responsive" groups that allow the modulation of the nanotube behaviour depending on external stimulus.[408,409] The use of these "intelligent" materials that form the active species only under some specific conditions provides new tools for developing regulated systems for biomedical applications and material sciences. This strategy has the advantage that the biologically active supramolecular entities could be controlled or induced by the environmental conditions, leading to a more efficient mechanism of action.

6.2. AIM.

A systematic atomistic MD study of a transmembrane nanotube with functionalized internal cavity is proposed. Since previous simulations with non-functionalized and internally hydroxylated α,γ-SCPNs have shown no preference for any cation, MD simulations of α,γ-SCPNs inserted in a DOPC (1,2-dioleoyl-sn-glycero-3-phosphocholine) membrane and functionalized with carboxylic groups were carried out, expecting that the introduction of negatively charged amino acids could help to overcome the lack of discrimination.[391,404] Some natural proteins have carboxylates groups at the selective filter of the channel to improve the cation selectivity.[410–412] In general, a release mechanism has been proposed for this kind of channels. The spatial organization of the carboxylate resembles in some sense the organization of the nanotube made of CPs having carboxylate groups on the γ-residues. To carry out this study, two protonated states were evaluated in order to test their reaction to a stimulus (pH), mimicking natural pores which

391. García-Fandiño, R. et al. *Chem. Sci.* **2012**, *3* (11), 3280–3285.
338. Rodríguez-Vázquez, N. et al. *Org. Lett.* **2017**, *19* (10), 2560–2563.
404. Calvelo, M. et al. *Phys. Chem. Chem. Phys.* **2015**, *17* (43), 28586–28601.
408. Urban, M. W. *Handbook of stimuli-responsive materials*; John Wiley & Sons, 2011.
409. Li, Q. et al. *Adv. Opt. Mater.* **2019**, *7* (16), 1901160.
410. Li, Y. et al. *PLoS One* **2016**, *11* (9).
411. Flood, E. et al. *PLoS Comput. Biol.* **2018**, *14* (9).
412. Csányi, É. et al. *Biochim. Biophys. Acta - Biomembr.* **2012**, *1818* (3), 592–600.

are found to show sensitiveness to external boosts.[413–416] The introduction of pH sensitive functional groups into the inner cavity of a membrane nanotube allows the creation of a double modulable system responsive both to the nature of the environment (controllable by the outer of the nanotube) and also to the local pH condition (controllable by the internal groups). Those studies are expected to bring light to the availability of the introduction of negatively charged functional groups in their lumen, as well as to the use of responsive groups in order to create easily modulated SCPNs.

6.3.METHODS.

The parametrization of the atoms of the CPs (considering one CP as a single residue) and the DOPC were obtained using the tool antechamber, using RESP/6-31G(d) charges and the van der Waals parameters of the GAFF Force Field.[417–420] The water SPC/E water model was selected, together with the parameters published by Joung *et al.* for the ions in order to prevent the crystallization previously reported at high concentrations.[421,422] Starting geometries were constructed from previous works.[282,391,404] Nanotubes were inserted in the corresponding membranes, removing the water from the hydrophobic region of the bilayer, so that the channel was completely dry at the beginning of the simulation. The resulting systems were ionized using different salts solutions (LiCl, NaCl, KCl, CsCl and $CaCl_2$ at 0.5 M) in such way that the total net charge of the whole systems was always zero. Every system was partially optimized, thermalized and equilibrated, followed by an unrestrained production

282. Calvelo, M. et al. *Chem. – A Eur. J.* **2020**, *26* (26), 5846–5858.
391. García-Fandiño, R. et al. *Chem. Sci.* **2012**, *3* (11), 3280–3285.
404. Calvelo, M. et al. *Phys. Chem. Chem. Phys.* **2015**, *17* (43), 28586–28601.
413. Fyles, T. M. et al. *New J. Chem.* **2007**, *31* (5), 655–661.
414. Tarek, M. et al. *Acc. Chem. Res.* **2013**, *46* (12), 2755–2762.
415. Reyes, R. et al. *J. Biol. Chem.* **1998**, *273* (47), 30863–30869.
416. Schneider, F. et al. *Biophys. J.* **2013**, *105* (1), 91–100.
417. Wang, J. et al. *J. Comput. Chem.* **2004**, *25* (9), 1157–1174.
418. Wang, J. et al. *J. Mol. Graph. Model.* **2006**, *25* (2), 247–260.
419. Wang, J. et al. *J. Comput. Chem.* **2004**, *25* (9), 1157–1174.
420. Wang, J. et al. *J. Am. Chem. Soc* **2001**, *222*, U403.
421. Berendsen, H. J. C. et al. *J. Phys. Chem.* **1987**, *91* (24), 6269–6271.
422. Joung, I. S. et al. *J. Phys. Chem. B* **2008**, *112* (30), 9020–9041.

step with a time step of two fs. The constant pressure and temperature NPT ensemble were employed with a pressure of 1 bar, controlled using a semi-isotropic Parrinello–Rahman barostat, and a temperature of 300 K, which was imposed by a V-rescale thermostat.[215,423] The LINCS algorithm was employed to remove the bond vibrations.[194] The Particle Mesh Ewald method coupled to periodic boundary conditions was used to treat the long-range electrostatics using a direct-space cut-off of 1.0 nm and a grid spacing of 0.12 nm.[211] The van der Waals interactions were computed using PBC coupled to a spherical cut-off of 1.4 nm. All MD simulations were performed using the package GROMACS.[424]

Some of the analysis carried out, as root-mean-square-deviation (RMSD), number of H-bonds and density maps, were calculated using tools available in GROMACS. For the RMSD, the initial structure of the nanotube, which presents an ideal tubular shape, was selected as reference. Pore analysis were carried out using the program CHAP.[425] The rest of analysis were performed executing written code using the python MDAnalysis library.[426] Graphs were plotted using the python Matplotlib library, whereas pictures of the molecules were obtained with VMD.[231,427]

6.4. Results

MD simulations of a transmembrane nanotube with functionalized internal cavity have been carried out in order to evaluate the introduction of pH sensitive functional groups (**Figure 44**). For this purpose, we have selected the two more drastic stages of protonation of the carboxyl groups in the lumen (fully protonated and fully deprotonated) to try to understand how the system would behave under these extreme conditions. The proposed sequence was based on an α,γ-CP made by four Trp to ensure the solubilization in the lipidic media of

194. Hess, B. et al. *J. Comput. Chem.* **1997**, *18* (12), 1463–1472.
211. Essmann, U. et al. *J. Chem. Phys.* **1995**, *103* (19), 8577–8593.
215. Parrinello, M. et al. *J. Appl. Phys.* **1981**, *52* (12), 7182–7190.
231. Humphrey, W. et al. *J. Mol. Graph.* **1996**, *14* (1), 27-28,33-38.
423. Bussi, G. et al. *J. Chem. Phys.* **2007**, *126* (1), 014101.
424. Abraham, M. J. et al. *SoftwareX* **2015**, *1–2*, 19–25.
425. Klesse, G. et al. *J. Mol. Biol.* **2019**, *431* (17), 3353–3365.
426. Michaud-Agrawal, N. et al. *J. Comput. Chem.* **2011**, *32* (10), 2319–2327.
427. Hunter, J. D. *Comput. Sci. Eng.* **2007**, *9* (3), 99–104.

the nanotube ensemble and four γ-Ach that contain a carboxylic group at the β-position (Ach_{COOH}). To avoid that these β-carboxy groups could prevent the nanotube formation, they should be *trans* oriented with respect to the amino and carbonyl groups. The chair conformation of the cyclohexyl moiety would dispose all these groups in the equatorial orientation, inducing to the CP adoption of the flat conformation required for the nanotube formation. The resulting CP was studied in the nanotube structure forming two classes of SCPN models: the deprotonated stage **$SCPN_{4COO-}$**, in which each cyclic unit contributes with four negative charges to the inner pore, and the protonated stage **$SCPN_{4COOH}$**, in which all the carboxylate groups are protonated. It is important to note that in order to facilitate the identification of these nanotubes, the nomenclature of the CPs is different from that of the rest of the chapters.

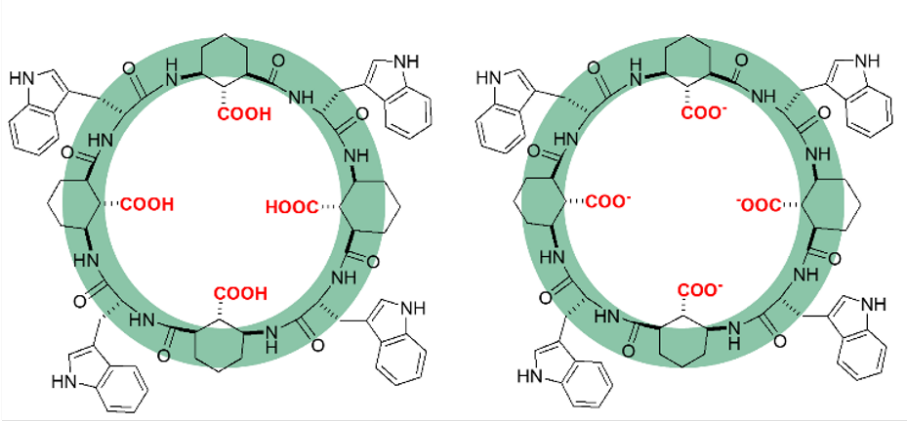

Figure 44. *Functionalized CPs studied in this work, highlighting the position of the carboxylic/carboxylate groups in the inner cavity. Left (**CP_{4COOH}**) corresponds with the basic subunit used for obtaining **$SCPN_{4COOH}$**, whereas right (**CP_{4COO-}**) would assemble into **$SCPN_{4COO-}$**.*

Both **$SCPN_{4COO-}$** and **$SCPN_{4COOH}$** consist of 10 units of an octameric CP (c-{[*L*-Trp-D-γ-Ach(COOH)-]$_4$}, **CP_{4COOH}**), analogous to a non-functionalized system that was previously used in computational studies, but in which the equatorial hydrogen of β-

carbon of the Ach moiety is replaced by the carboxylic group in the two protonated stages (**Figure 44**).[391,404] Those nanotubes were stacked in an antiparallel fashion. Each SCPN structure was embedded in a lipid bilayer (formed by the phospholipid DOPC), solvated with different salt compositions (LiCl, NaCl, KCl, CsCl and $CaCl_2$ 0.5M, respectively) and simulated atomistically for at least 100 ns.

The presence of the carboxylic/carboxylate groups, as well as increasing the hydrophilic character of the internal cavity of the CPs, led to the decrease of the internal net volume of the channels. The effective radii of the functionalized pores were estimated both before and after the MD simulations. In all cases, the effective radius locates in the plane of the CP whereas the maximum radius is placed in the region between the two planes of the rings. The smallest radii before simulation corresponded to the planes of the CPs, leading to values of 0.8 and 2.2 Å for **SCPN$_{4COOH}$** and **SCPN$_{4COO-}$**, respectively (**Figure 45**). The radii for **SCPN$_{4COO-}$** was similar to a previous studied SCPN with four hydroxyl groups per CP (**SCPN$_{4OH}$**).[404] Relaxation of the initial structures along the MD simulations resulted into a reduction of the differences between the intra and inter CPs for **SCPN$_{4COOH}$**, being, in general, the minimum radii slightly wider than in the initial structure, while the simulation of **SCPN$_{4COO-}$** led, as expected, to the nanotube disassembled. Additionally, it can be observed that the water number density of the inter-CP region (minimums in **Figure 46**) is pretty similar than the observed experimentally for the bulk water. In the plane of the CPs (maximums in **Figure 46**), conversely, the water number density is higher, although a smaller number of waters is expected to be found. However, this phenomenon can be explained for the quite small radii of those regions. This fact also leads to extremely high water number density values in the regions in which, due to the movement of the CPs, the channel is partially closed, which reduces the radius size even more.

391. García-Fandiño, R. et al. *Chem. Sci.* **2012**, *3* (11), 3280–3285.
404. Calvelo, M. et al. *Phys. Chem. Chem. Phys.* **2015**, *17* (43), 28586–28601.

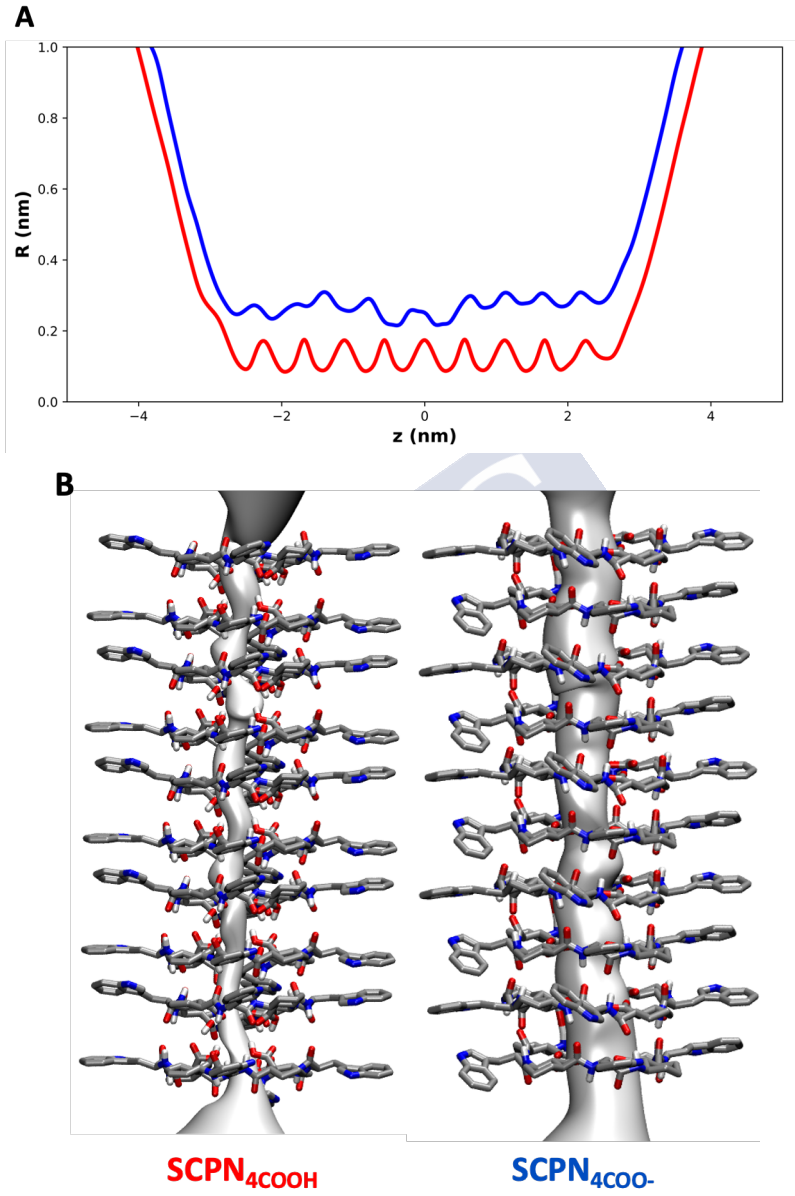

Figure 45. A) *Minimum radius of* ***SCPN$_{4COOH}$*** *(red) and* ***SCPN$_{4COO-}$*** *(blue) and* ***B)*** *graphical comparison between them along the principal axis before MD simulations.*

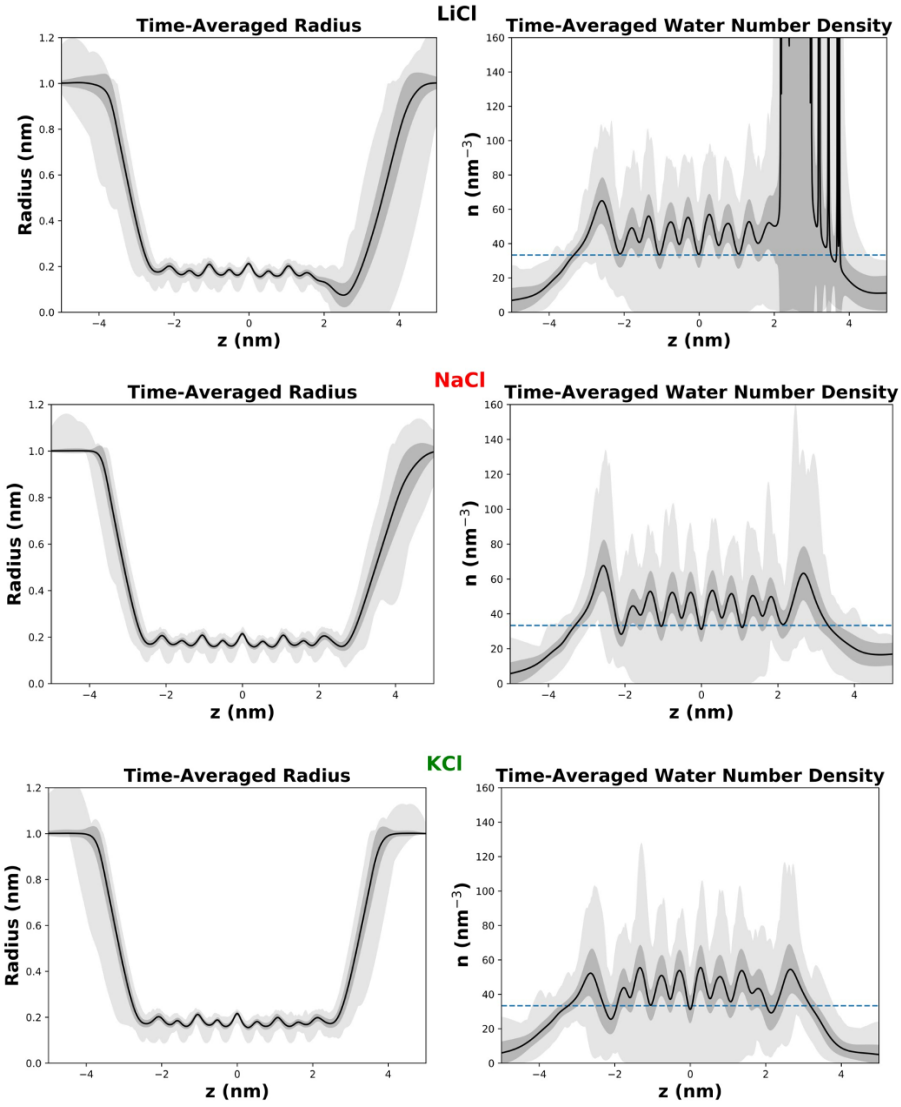
LiCl
Time-Averaged Radius
Radius (nm)
z (nm)
Time-Averaged Water Number Density
n (nm^{-3})
z (nm)
NaCl
Time-Averaged Radius
Radius (nm)
z (nm)
Time-Averaged Water Number Density
n (nm^{-3})
z (nm)
KCl
Time-Averaged Radius
Radius (nm)
z (nm)
Time-Averaged Water Number Density
n (nm^{-3})
z (nm)

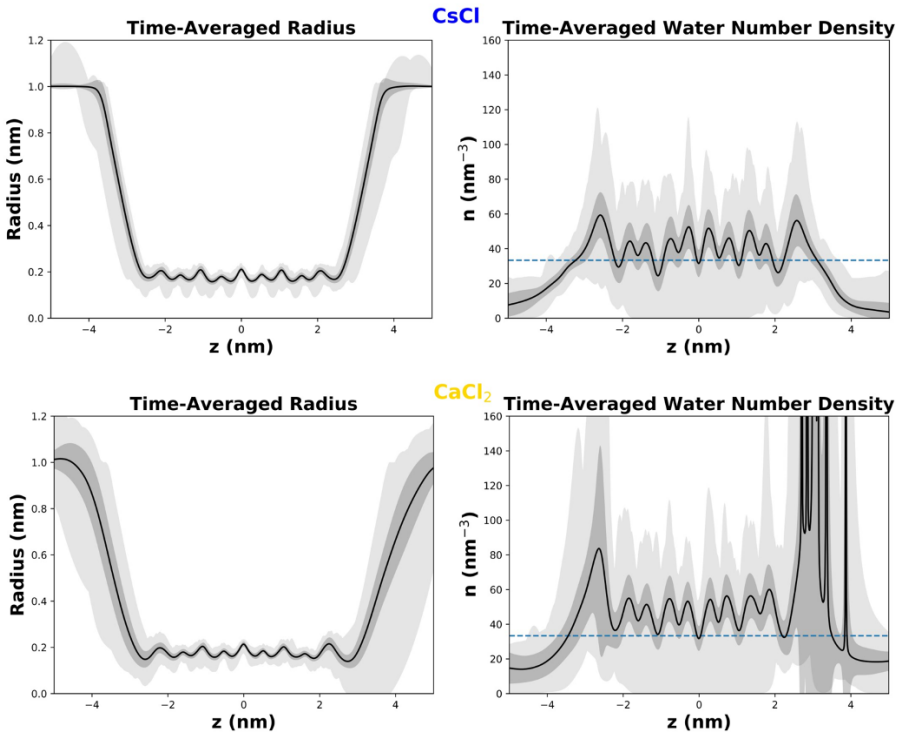

Figure 46. *Minimum radius of* ***SCPN$_{4COOH}$*** *(left) and the water number density (right) averaging during the 200ns of MD simulation. The blue dashed line represents the experimental bulk water density.*

MD simulations of the nanotube at low pH (**SCPN$_{4COOH}$**) inserted into a lipid bilayer and using different salt compositions show that the channel structure is well preserved, as it can be observed in the snapshots at 200 ns presented in **Figure 47**. On the other hand, the alkalinization of the media would deprotonate the COOH groups and form **SCPN$_{4COO-}$**, which led to the loss of CP planarity (probably due to the presence of 4 negative charges in the lumen of the pore) and to the rapid disassembly of the channel in all studied conditions (**Figure 47**).

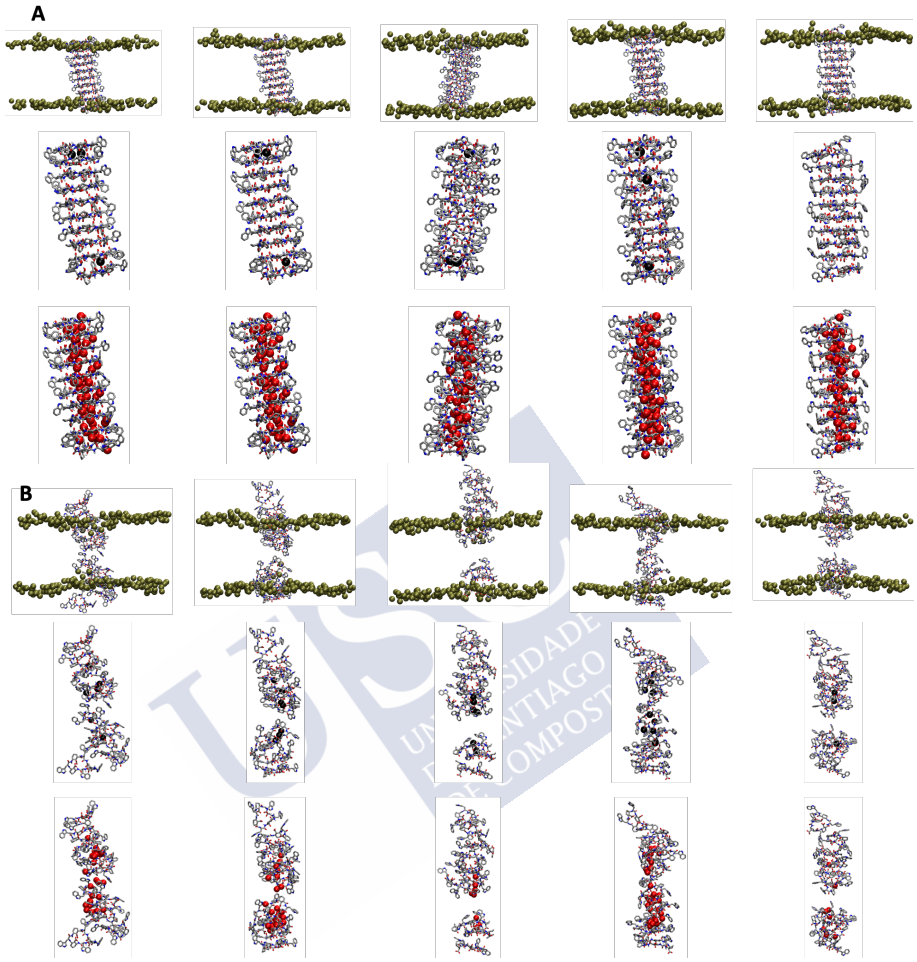

Figure 47. *Snapshots of the two simulated* ***A) SCPN$_{4COOH}$*** *and* ***B) SCPN$_{4COO^-}$****, in LiCl, NaCl, KCl, CsCl and $CaCl_2$ 0.5M electrolyte solutions after 200 ns of simulation. Lipids, water and external ions have been removed for clarity. Brown spheres correspond to the phosphorous atoms from the lipids, black circles are the corresponding ions, and red spheres correspond to the oxygen of water molecules. For clarity, only the hydrogens involved in the H-bonding network are displayed.*

In order to have clearer evidence of the nanotube integrity of **SCPN$_{4COOH}$**, the RMSD were calculated (**Figure 48**). The quite stable shape of the graph together with the low values (less than 0.5 nm) suggest again the stability of these nanotubes. Additionally, the extension of one of these simulations up to 640 ns shows that even at this time scale the tubular structure is pretty well preserved, highlighting the stability of these SCPNs (**Figure 49**). Opposite behaviour is observed for **SCPN$_{4COO-}$**, in which bigger fluctuations as well as the higher values confirm the disassembly of the nanotube. In addition, this process seems to be extremely fast, the RMSD values rise until high values just at the very beginning of the simulation, just during the first picoseconds of the trajectory. Furthermore, during the minimization of the **SCPN$_{4COO-}$** was possible to find the disruption of H-bonds between different units of CPs that support the tubular structure, which probes again the high speed of such process (**Figure 50**). This must be related with the repulsion generated by the negative charges, which could distort the flat rings and orient the carboxylate groups towards the mouth of the SCPN (**Figure 50**). After the destruction of the tubular structure, CPs aggregate to form negatively charged clusters, which potentially could open a pore in the membrane. This aggregate remains in the membrane region during the whole trajectory and, even after the extension of one of the simulations up to 640 ns (the one in presence of NaCl), it does not leave the lipid bilayer (**Figure 49**).

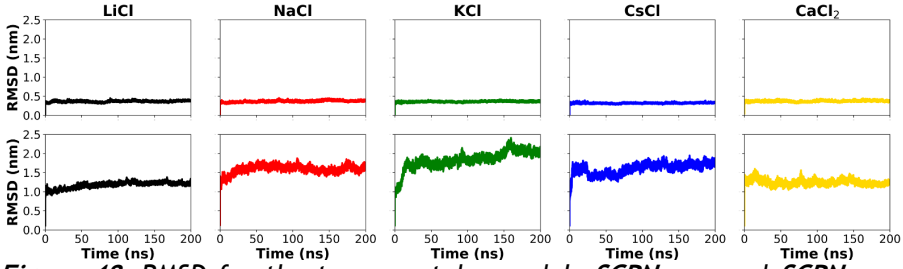

Figure 48. *RMSD for the two nanotube models* ***SCPN$_{4COOH}$*** *and* ***SCPN$_{4COO-}$****, simulated in different salt solutions for 200 ns and considering all atoms of the SCPN. Top: results for S* ***SCPN$_{4COOH}$****. Down: results for* ***SCPN$_{4COO-}$****.*

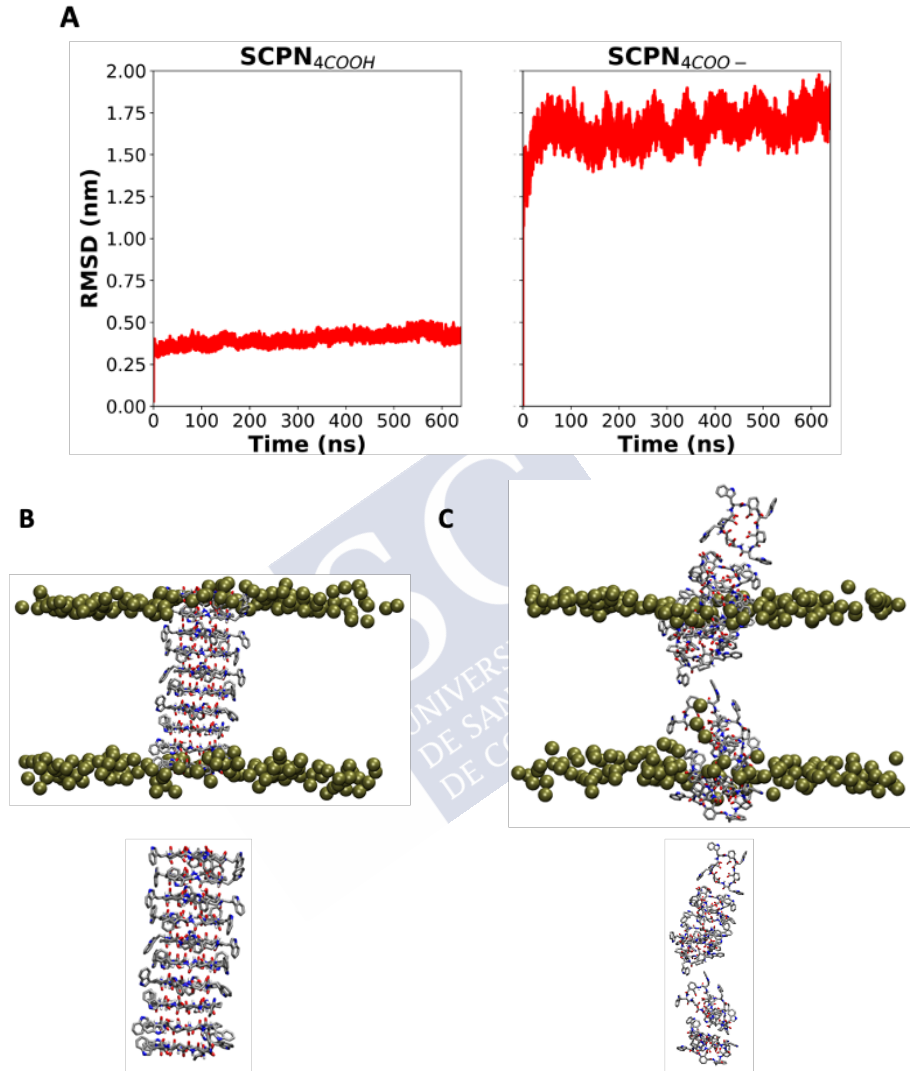

***Figure 49. A)** RMSD of two extended simulations of both nanotubes up to 640 ns. Snapshot of **B)** the **SCPN**$_{4COOH}$ and **C) SCPN**$_{4COO-}$ at the end of the extended simulations (t = 640 ns). Brown spheres represent the phosphorous atoms of the lipid bilayer.*

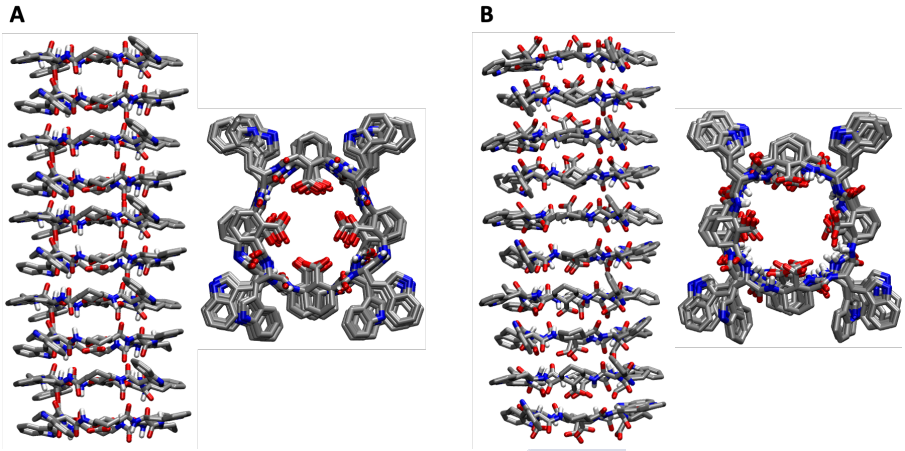

Figure 50. *Snapshot of **A)** the initial structure of **SCPN$_{4COO^-}$** and **B)** the same structure after minimization. It can be noticed that the H-bonding network is slightly distorted just after this step.*

An analysis of the number of H-bonds that maintain the tubular structure during the simulations was performed (**Table 16**). Although the theoretical maximum number of H-bonds considering only the groups of the backbone is 72, almost 20% of the H-bonds can get lost during the calculations, with a number ranging between 58 and 69 for the **SCPN$_{4COOH}$**, depending on the salt composition. This reduction could come from the competition with water molecules and, to a lesser extent, with the lipids (**Table 16**). It is worth to mention that, in general, the carboxylic moieties do not interact with the groups of the backbone, being only possible to observe one H-bond at most, probably because they are too far. However, they are able to interact among themselves, forming between 2 and 4 H-bonds. For the **SCPN$_{4COO^-}$**, the number of H-bonds between the backbone groups and carboxylate moieties is significantly smaller for all salt compositions (a range between 28 and 39), showing again the reduced stability of the tubular structure of this nanotube. This disassembly allows the interaction between the carboxylate and peptide backbone groups, appearing between 19 and 27 H-bonds. Regarding the interaction with water, it is possible to observe that the simulations with **SCPN$_{4COOH}$** lead to a range between 106 and 127 H-bonds, much smaller than in the case of **SCPN$_{4COO^-}$**. In

these simulations the number of H-bonds observed rises up to 246, due to the flexibility of the non-stacked CPs, which facilitates the interaction with water molecules. This fact suggests that the loss of the backbone H-bonding network is compensated by interactions between the CPs and the water molecules. Additionally, the number of H-bonds between the CPs and the lipids is pretty similar for both states, showing no dependence on the pH. Nevertheless, this number is not so big, suggesting that this is not an important interaction to drive the process towards the nanotube disassemble.

***Table 16.** Mean and standard deviation of the number of H-bonds between different components of the simulated systems in different salt solutions for 200 ns. Standard deviations are presented between parentheses.*

		CP-CP	**CP-COO(H)**	**CP-water**	**CP-lipids**	**COO(H)-COO(H)**
SCPN$_{4COOH}$	LiCl	62 (3)	1 (1)	113 (6)	5 (2)	2 (1)
	NaCl	66 (3)	1 (1)	111 (6)	4 (2)	2 (1)
	KCl	65 (3)	-	109 (6)	3 (1)	2 (1)
	CsCl	69 (3)	-	106 (7)	3 (1)	4 (1)
	$CaCl_2$	58 (3)	0 (1)	127 (8)	3 (2)	2 (2)
SCPN$_{4COO-}$	LiCl	31 (4)	26 (3)	212 (10)	2 (1)	
	NaCl	33 (3)	22 (2)	188 (12)	5 (2)	
	KCl	33 (3)	24 (3)	220 (10)	2 (1)	
	CsCl	28 (3)	19 (3)	246 (11)	6 (2)	
	$CaCl_2$	39 (4)	27 (2)	171 (8)	5 (1)	

The number of waters and ions inside the **SCPN$_{4COOH}$** channel was analysed for each salt composition (**Table 17**). In general, the water molecules content is quite homogenous in all simulations (between 35 and 37). The interplanar region is the area in which more water molecules are found, as it can be observed in the time-averaged water number density profiles of the **Figure 46**, where the maximum peaks tend to match with the region between CPs. Density maps of

hydrophobic region of the membrane reveal that water molecules are only present in the nanotube area, suggesting that these peptides could as water channels (**Figure 51**). Additionally, in the deprotonated **SCPN$_{4COO-}$** it is also possible to find waters in the hydrophobic region, coordinated to the disassembled aggregate but, in any case, only in contact with the CPs (**Figure 47**).

Table 17. *Mean and standard deviation of the number of ions and water molecules inside the nanotubes, simulated for different salt solutions for 200 ns.*

	SCPN$_{4COOH}$			**SCPN$_{4COO-}$**		
	Cations	**Anions**	**Water**	**Cations**	**Anions**	**Water**
LiCl	1 (0)	-	35 (4)	7 (1)	-	22 (3)
NaCl	1 (1)	-	37 (4)	7 (1)	-	24 (3)
KCl	2 (1)	-	37 (4)	7 (1)	-	14 (5)
CsCl	2 (1)	-	36 (4)	9 (1)	-	41 (6)
$CaCl_2$	-	-	36 (4)	4 (1)	-	11 (2)

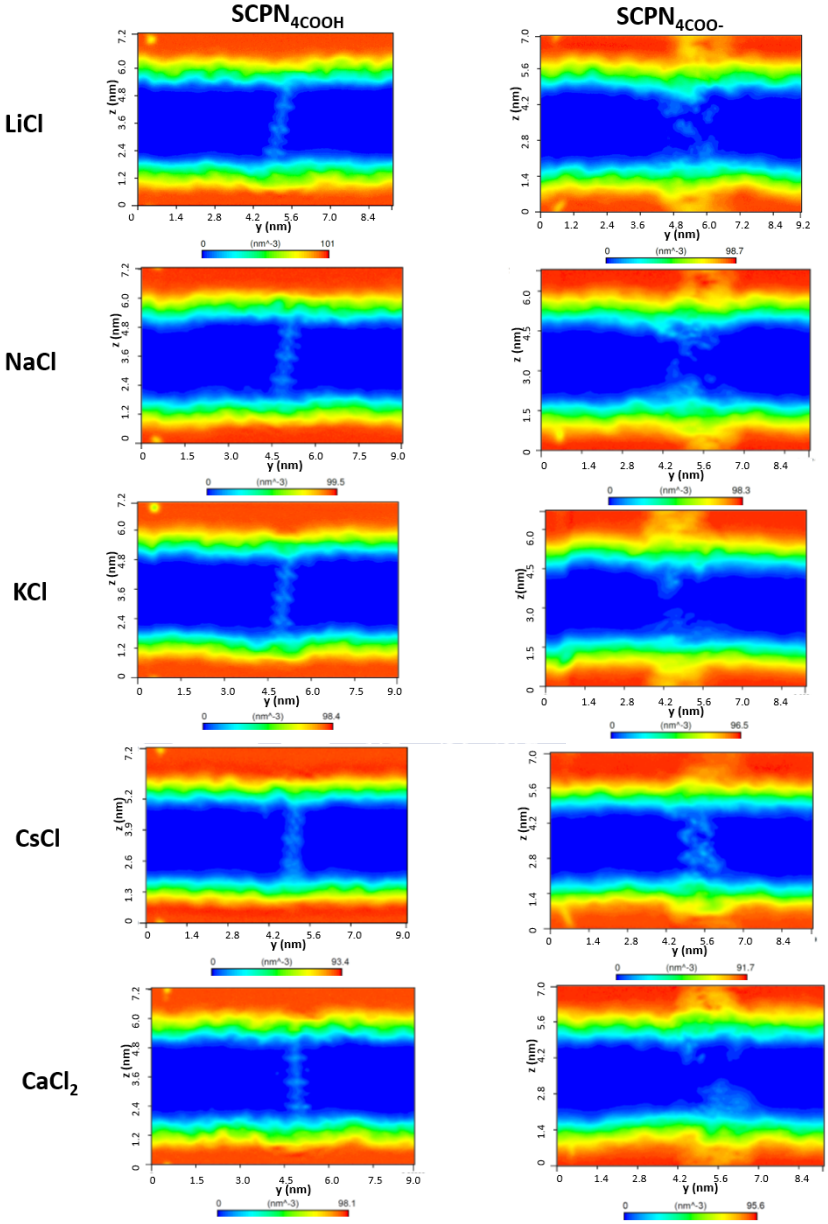

***Figure 51.** Water 2D-density map along the yz plane for the system **SCPN**$_{4COOH}$ and **SCPN**$_{4COO^-}$ simulated in different salt concentrations, averaged from 200 ns of MD simulation. The more populated regions are displayed in red, whereas the small water densities are coloured in blue.*

Regarding cation localization, the z-coordinate analysis reveals that some ions approximate to the edge of the nanotube (**SCPN$_{4COOH}$**) although no one enters deeply inside the channel (**Figure 52**). This fact suggests that the introduction of four carboxylic groups per CP reduces the inner radii, precluding the infiltration of the cations, even for a small ion as Li^+. Interestingly, a deeper penetration is observed for Cs^+, being the only ion that is able to reach the centre of the channel. Contrary, the divalent cation (Ca^{2+}) is not able to even approximate to the entrance of the nanopore.

For the deprotonated system, the disassembly of **SCPN$_{4COO^-}$** leads to the formation of an amorphous negatively charged aggregate placed in the membrane. However, this accumulation of CPs is able to attract cations to the hydrophobic region of the lipid bilayer, entering much deeper than in the simulations with the protonated nanotube (**Figure 52**). The access for monovalent cations seems to be quite favourable, being possible to find 7 atoms of Li^+, Na^+ and K^+ and up to 9 of Cs^+ in the membrane, whereas for Ca^{2+} the number is smaller (4). This fact, together with the conclusions obtained for this cation in the **SCPN$_{4COOH}$** channel, suggest that the permeability of Ca^{2+} is not favoured. Furthermore, it is relevant to note that no net flux of ions is observed in any sample. These results suggest that the kinetics of the ions trapped both in the protonated SCPNs or in the aggregate form by the deprotonated systems is very slow. Even extending the MD simulations up to 640 ns does not lead to any displacement of those ions, suggesting that much longer simulation times would be needed to appreciate the diffusion of these ions, if it would take place at larger scales (**Figure 53**).

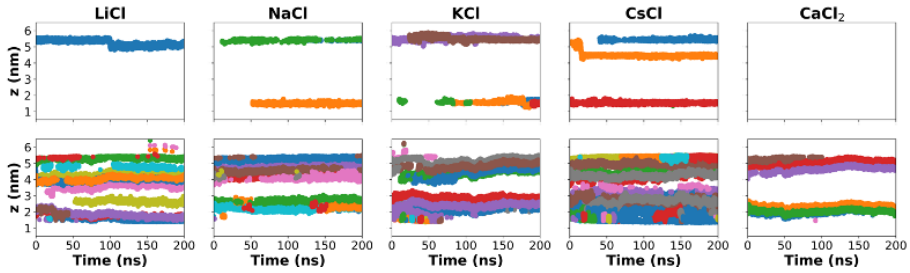

***Figure 52.** Z-coordinate (being z the perpendicular axis to the membrane) for each of the cations inside the simulated peptide nanotubes along the 200 ns trajectory. The nanotube z-region is comprehended between the region ≈1-6 nm. Each colour corresponds to a different ion. Top: results for **SCPN**$_{4COOH}$. Down: results for **SCPN**$_{4COO^-}$.*

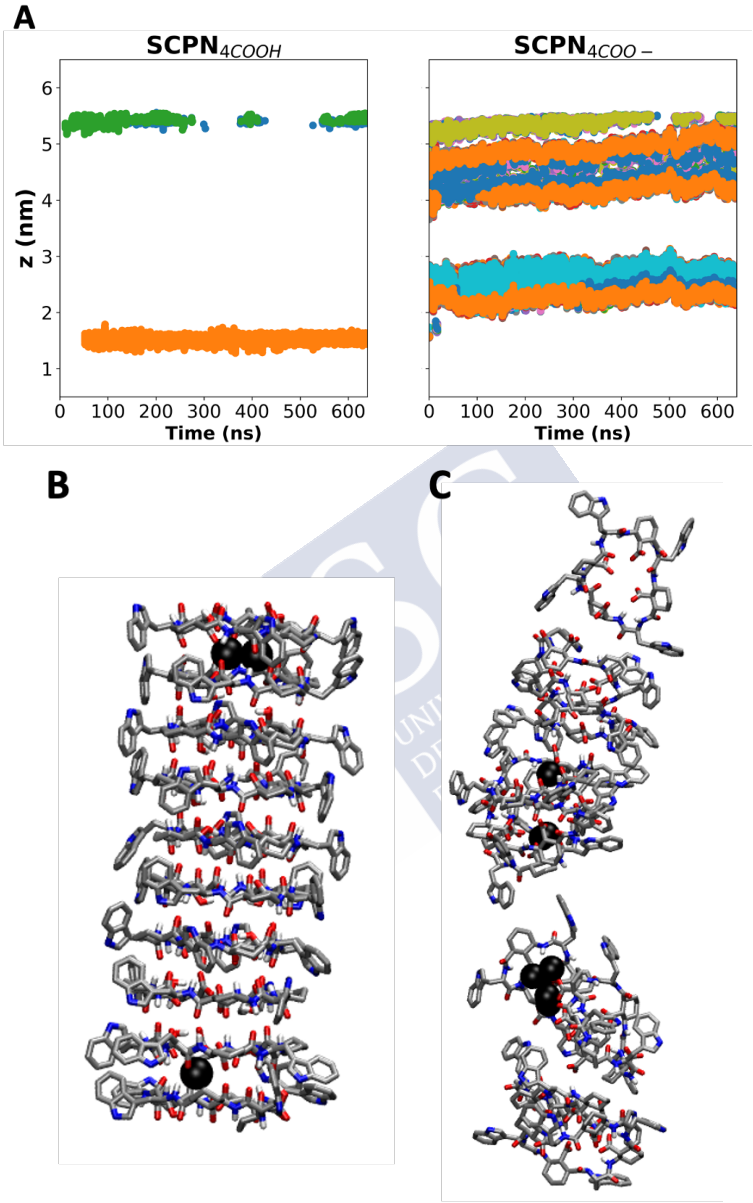

Figure 53. A) *Z-coordinate of Na+ ions from the two extended simulations of both nanotubes up to 640 ns. Snapshot of* ***B)*** *the* ***SCPN$_{4COOH}$*** *and* ***C) SCPN$_{4COO-}$*** *at the end of the extended simulations (t = 640 ns). Black spheres represent the cations (Na^+).*

In contrast to the behaviour observed in the protonated nanotube, the number of waters inside the pore is not constant for **SCPN$_{4COO^-}$** (**Table 17**). This variation could be related with the number of molecules coordinated to the cations. With that purpose, the number of oxygens from waters, carbonyl groups of the backbone and carboxylates inside the first sphere of coordination of the cations were evaluated (**Table 18**). For Cs^+, a higher number of waters coordinated is observed, which could explain the greater number of waters inside the channel. Moreover, the coordination of Ca^{2+} involved the presence of at least two units of CPs monomers, since each ion coordinates to 7 carboxylate groups. Contrary to previous results obtained with CPs composed by non charged functionalized γ-Achs, where Ca^{2+} seemed to maintain the hydration shell, the presence of carboxylates in the lumen seems to favour the water replacement by some of their oxygen atoms.[404]

***Table 18.** Mean and standard deviation of the number of oxygens coordinated to the cations inside **SCPN$_{4COO^-}$** in the first coordination sphere. Oxygen atoms from different sources (water, C=O from the backbone and the introduced COO^- groups). Values averaged over 200ns.*

	SCPN$_{4COO^-}$		
	O (H_2O)	**O (C=O)**	**O (COO^-)**
LiCl	1 (0)	-	3 (0)
NaCl	2 (0)	1 (0)	3 (0)
KCl	2 (0)	1 (0)	3 (0)
CsCl	5 (0)	1 (0)	2 (0)
$CaCl_2$	1 (1)	1 (0)	7 (0)

After all, the present study has shown that at low pH values, the protonation of the carboxylic acids would lead to a SCPN in a lipid environment, stable, permeable to water, but not permeable to ions due to the small internal diameter. By contrast, at higher pH the deprotonation of these groups would lead to the presence of four net

404. Calvelo, M. et al. *Phys. Chem. Chem. Phys.* **2015**, *17* (43), 28586–28601.

charges in the CP, which would induce the disassembly of the nanostructure on account of the loss of the planarity of the CPs. Additionally, the resulting negatively charged assembly attract ions towards the hydrophobic core of the bilayer that ideally facilitate their translocation, ideally killing in that way, the targeted malignant cell.

Considering partial deprotonation of the CPs (1, 2 or 3 carboxylic groups) would be also interesting. However, the possible rotation of the CPs around the nanotube axis, together with the introduction of asymmetry in the inner cavities of the CPs and the ability to exchange protons between carboxylic groups, would be translated into an intractable number of nanotubular structures for each of the intermediate protonation states along the SCPN (**Figure 54**). Trying to find an affordable approach that could shed light on these partially protonated states, MD studies have been carried out with nanotubes composed by CPs having two carboxyl groups (Ach_{COOH}), considering again both protonates states (**Figure 55**). These residues were placed in opposite positions in the CPs, which leads to the appearance of two rotamers every two CP forming the SCPN: in one of them, the carboxyl/carboxylates groups are paired forming an eclipsed dimer that could be extended all through the nanotube; whereas in the other form these groups would be organized in an alternated structure in which the Ach_{COOH} residues would be paired with the amino acids without the carboxylate moiety (**Figure 55**). In this case, taking into account that this study is a proof of concept, only NaCl 0.5M was selected as salt composition.

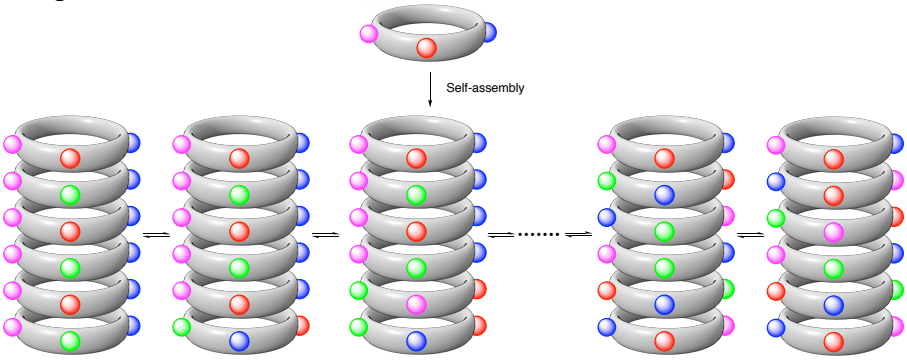

Figure 54. *Illustration of the multiple possibilities of organization of the charged groups along the SCPN due to freedom of rotation among the CPs.*

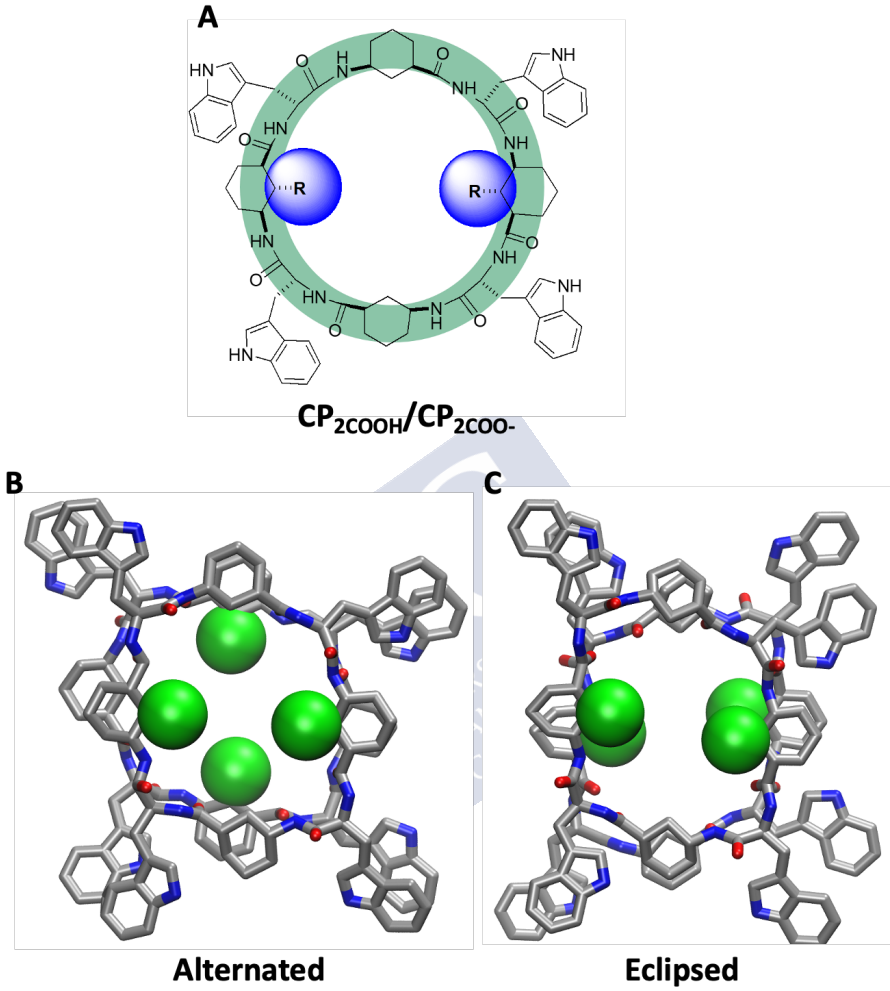

***Figure 55.** A) Schematic representation of the CP decorated with 2 carboxylic/carboxylate groups (**CP_{2COOH}**/**CP_{2COO-}**). R corresponds to the COOH/COO^- group. Representation of the **B)** alternated and **C)** eclipsed packing, in which the carboxylate/carboxylic groups are highlighted in green.*

Thus, a total of four new nanotubes were evaluated depending on the protonation states of carboxylates and their relative orientation: **$^{a}SCPN_{2COOH}$** and **$^{e}SCPN_{2COOH}$**, for the protonated alternated and eclipsed channels, respectively, and **$^{a}SCPN_{2COO-}$** and **$^{e}SCPN_{2COO-}$** for

the analogous deprotonated tubes. MD simulations in presence of a solution of 0.5 M NaCl with the four SCPNs lead to very similar conclusions than in the previous cases, being found the destruction of the anionic nanotubes, for both orientations, within 50 ns of simulation (**Figure 56**). This fact suggests that just the half of the total negative charge is enough for disassembling the nanotube, highlighting the importance of these unfavourable repulsive interactions. On the other hand, as in the previous simulations, the trajectories with the protonated nanotubes reveal the high stability of the channel in this time scale (50 ns) (**Figure 56**). RMSD calculations of these systems agree with the previous observations, being the values for the deprotonated tubes much higher (**Figure 57**). Regarding the different orientations, it seems that the RMSD values for the alternated SCPNs are slightly higher, which could mean less stable systems. Nevertheless, the differences are very small, making it hard to draw any conclusion.

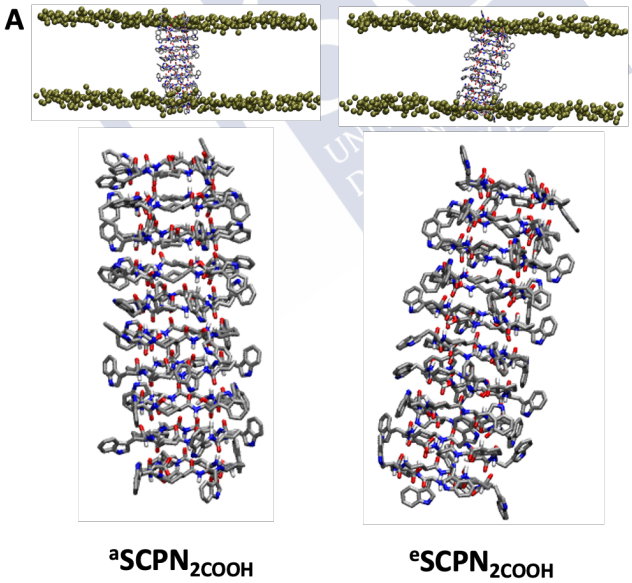

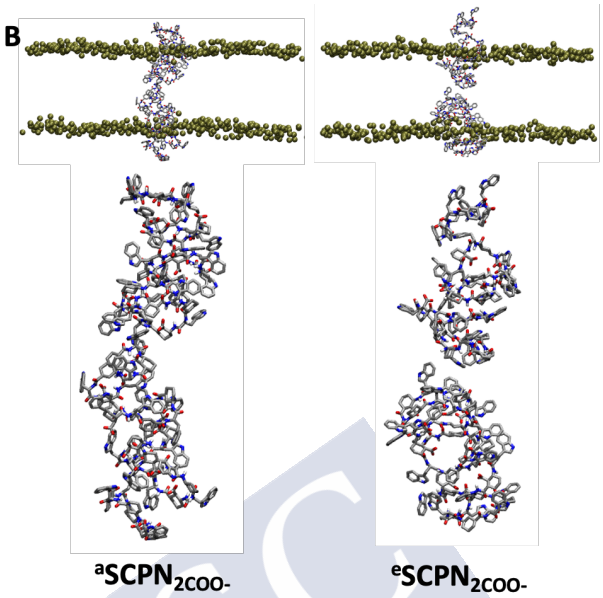

***Figure 56.** Snapshots at t = 50 ns of simulations with the **A)** protonated **$SCPN_{2COOH}$** and **B)** deprotonated **$SCPN_{2COO-}$** nanotubes, considering both conformations (alternated and eclipsed) in NaCl 0.5 M. Brown spheres represent the phosphorous atoms of the lipid bilayer.*

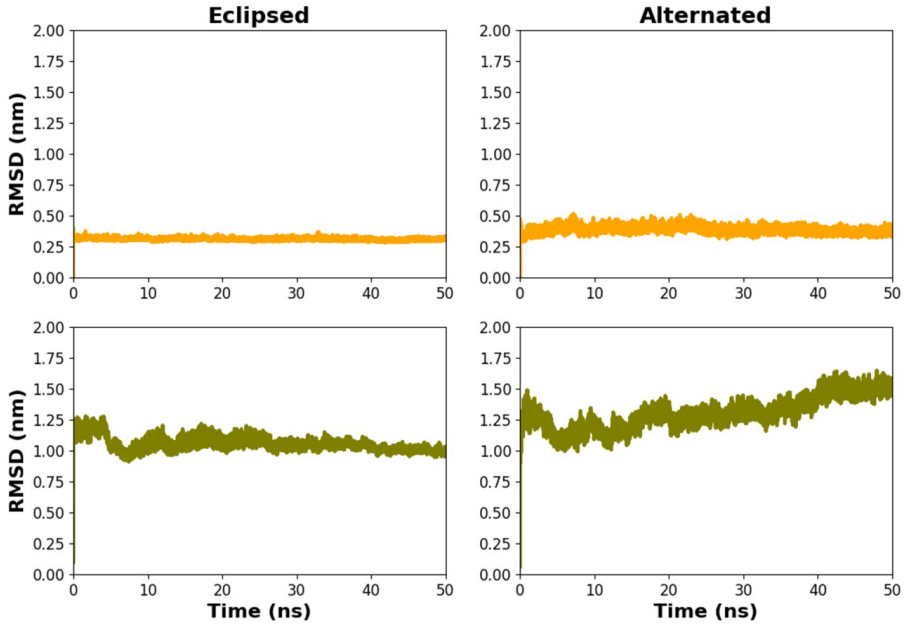

Figure 57. *RMSD of the simulated peptide nanotubes* ***^{e}SCPN$_{2COOH}$*** *and* ***^{a}SCPN$_{2COOH}$*** *(top) and* ***^{e}SCPN$_{2COO-}$*** *and* ***^{a}SCPN$_{2COO-}$*** *(bottom) in NaCl 0.5 M along the 50 ns of trajectory.*

Again, the high density of negative charges of the CPs is able to attract cations towards the membrane region (**Figure 58**). These results suggest that the behaviour of these intermediate systems is quite similar to that of the fully protonated/deprotonated **SCPN$_{4COOH}$**/**SCPN$_{4COO-}$**. However, it seems that in the simulations with the protonated **^{a}SCPN$_{2COOH}$** and **^{e}SCPN$_{2COOH}$** tubes the cations enter deeper into the nanopore (**Figure 58**), claiming that the radius of these channels is not small enough for blocking the pass of ions, as happened when the CPs are bearing four carboxylic groups (**SCPN$_{4COOH}$**).

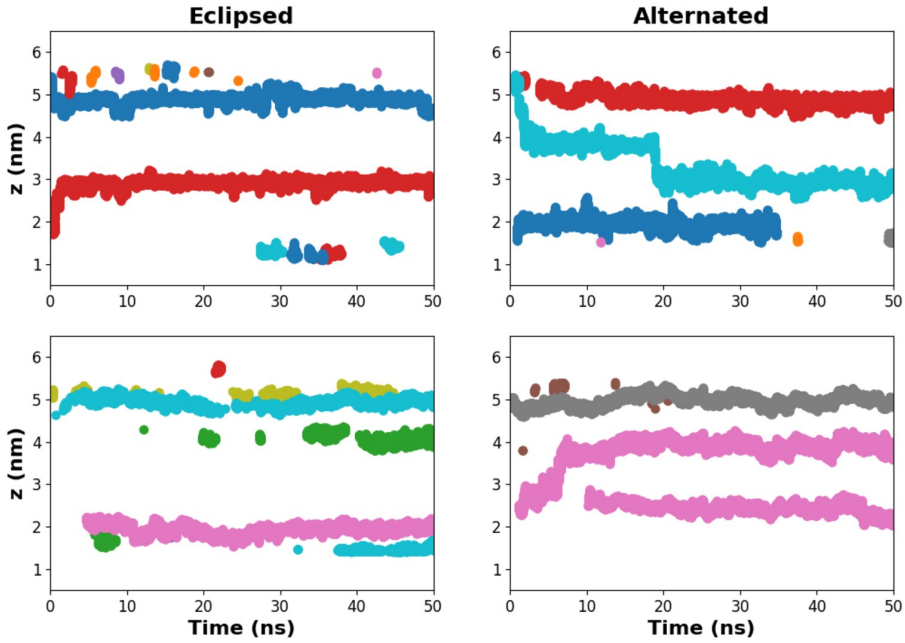

***Figure 58.** Z-coordinate for each of the Na+ inside the simulated peptide nanotubes ^{e}**SCPN**$_{2COOH}$ and ^{a}**SCPN**$_{2COOH}$ (top) and ^{e}**SCPN**$_{2COO-}$ and ^{a}**SCPN**$_{2COO-}$ (bottom) along the 50 ns of trajectory.*

6.5. CONCLUSIONS.

In this work, we have designed and investigated, using AA-MD simulations, a doubly modulable nanotube formed by the self-assembly of cyclic peptides sensitive to both the presence of a lipid membrane and the pH of the aqueous media. In this system, the control of the nanotube orientation in the membrane is determined by the outer groups of the nanotube (side chain of the α-amino acids), thanks to their sensitiveness to the presence of lipids, whereas the inner groups can control the stability of the tubular shape, depending on the pH of the media. For that purpose, we have selected two classes of SCPN models representing two extreme protonation states: one composed by CPs inner-decorated with 4 negative charges (4COO-), **SCPN$_{4COO-}$**, and another with all the carboxylate groups protonated (4COOH), **SCPN$_{4COOH}$**. At higher pH values, the repulsion among the negatively charged carboxylates provokes the SCPN disassemble, attracting ions

to the hydrophobic environment of the bilayer. Similar conclusions were obtained with SCPNs with a smaller amount of negative charge (just two carboxylic/carboxylate groups instead of four). However, despite the collapse of the tubular structure, the charged CPs remain aggregated at the membrane and attract cations into the hydrophobic interior of the bilayer, potentially facilitating its translocation. This fact could suggest that this new interaction with membranes could also lead to a dissipation of the membrane potential causing their instability, or cell death in case of biological membranes of living cells. Contrary, at lower pH values the protonation of the carboxylate groups of the CP leads to nanotubes that are stable in a lipid environment. The resulting hollow structure is partially able to permeate monovalent cations but unable to permeate Ca^{2+} ions.

These findings open the door, at least conceptually, to another mechanism of interaction of CPs with cell membranes, different from those known up to the moment: the modulation of the external surface of the CP (amino acid sequence) is not the unique parameter that can be modified to control the assembly of the nanotube in the membrane. As it was previously mentioned, the interaction of SCPNs and the membrane, as well as other proteins, are based on the external hydrophobicity of the side chains.[392] It is well known that modifications on the external surface of CPs (amino acid sequence) can be used to control the orientation, stability and so the permeation of the membrane nanotube. SCPNs formed by hydrophobic CPs are typically oriented perpendicular to the lipid bilayer, whereas amphiphilic CPs adopt the parallel disposition. Such orientation determines the response caused in the lipid membrane. Hydrophobic CPs form transmembrane channels that can efficiently transport ions and small polar molecules. On the other hand, amphipathic nanotubes show disruptive properties of the membrane that make then useful as antimicrobial agents. All the previously reported mechanisms proposed for the interaction of SCPNs and membranes (barrel pore, carpet-like, toroidal, etc) are based on the external properties of the nanotube. In this work, it has been demonstrated that the control of the inner properties of the SCPNs provides an additional way of controlling the disposition of the CPs at

392. Vijayaraj, R. et al. *Phys. Chem. Chem. Phys.* **2012**, *14* (43), 15135–15144.

the membrane, influencing also in their mechanism of interaction, providing an additional regulatory level able to affect the SCPN behaviour. Modulating the load of the functional groups inside the channel seems ideally possible to pass from an aggregated structure of CPs negatively charged to a tubular structure with neutral groups, and *vice versa* (**Figure 59**). Additionally, whereas the tubular conformation blocks the pass of ions through it, the disassembly of the SCPN forms a negatively charged aggregate that is able to attract cations to the hydrophobic region of the membrane (**Figure 59**). In this way, the ionic balance of target cells could be potentially destroyed by modulating the conformation of the CPs varying the pH, showing up new approaches for the preparation of antimicrobial peptides whose mode of action is at the membrane level and following a different mechanism of action than other antimicrobial amphipathic peptides.[428–430]

428. J. Bond, P. et al. *Protein Pept. Lett.* **2012**, *17* (11), 1313–1327.
429. Shai, Y. *Biopolym. - Pept. Sci. Sect.* **2002**, *66* (4), 236–248.
430. Kumar, P. et al. *Biomolecules* **2018**, *8* (1), 4.

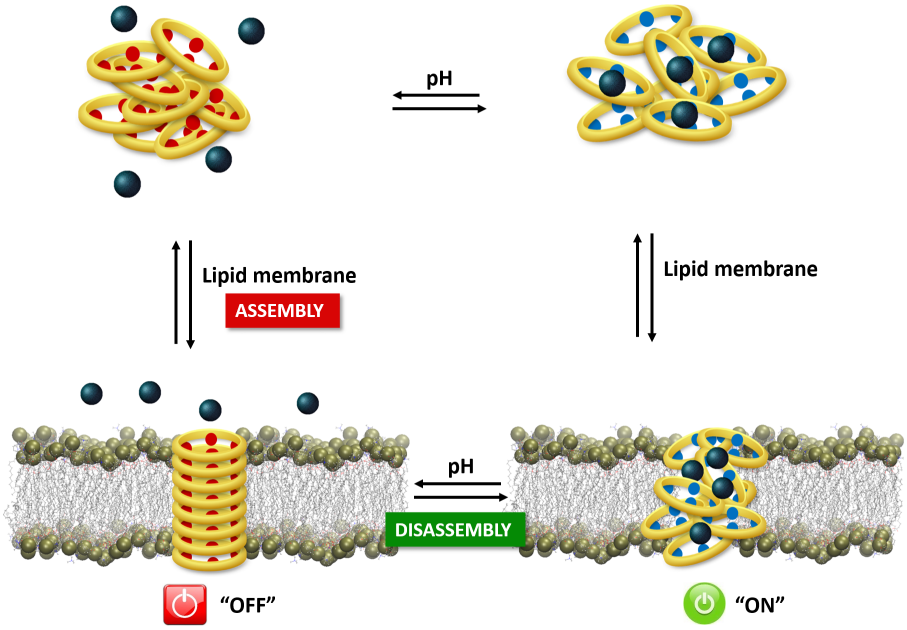

Figure 59. *Schematic concept of a doubly modulable self-assembled cyclic peptide nanotubes: pH sensitive inside and environmental/lipid sensitive outside: In a lipid environment low pH values would lead to the assembly of the CPs into a nanotube not permeant to ions, whereas alkaline conditions would lead to the disassembly that would attract ions towards the hydrophobic core of the membrane.*

This study resulted in the following publication: Calvelo, M.; Granja, J. R.; Garcia-Fandiño, R. *Phys. Chem. Chem. Phys.* **2019**, *21* (37), 20750–20756.[431]

431. Calvelo, M. et al. *Phys. Chem. Chem. Phys.* **2019**, *21* (37), 20750–20756.

7. Effect of water models on transmembrane SCPNs

7.1. PRECEDENTS AND MOTIVATION.

Water is one of the most studied molecules due to its fundamental importance in all aspect of our life, from biological point of view to other areas including nanoscience, technology and industrial applications.[432] The diverse and unique properties of this solvent in the bulk solution, in nanoconfined environments, in solvation shells around other molecules, and at interfaces between media of different polarity have inspired the development of many water models for computational simulation studies to explain all the properties.[433] Despite the pioneering development of a realistic interaction potential for water by Bernal-Fowler in 1933,[434] it was not until almost 40 years later that the first computer calculation was carried out by Barker and Watts.[435] Since then, more than a hundred different water models have been developed, in an effort to reproduce a number experimental properties such as density, vaporization enthalpy, interfacial tension and molar heat capacity.[436–439]

Water molecules in the nanoconfined environment provided by natural or artificial membrane channels deserve special attention, since they are expected to behave significantly differently from those in bulk solution and at interfaces.[433,440] Simplified models of nanotubes and

432. Franks, F. et al. *Water a Comprehensive Treatise. Volume 1.The Physics and Physical Chemistry of Water.*; Springer New York, 1972; Vol. 1.
433. Lynch, C. et al. *Chem. Rev.* **2020**, *120*, 10298–10335.
434. Bernal, J. D. et al. *J. Chem. Phys.* **1933**, *1* (8), 515–548.
435. Barker, J. A. et al. *Chem. Phys. Lett.* **1969**, *3* (3), 144–145.
436. Guillot, B. *J. Mol. Liq.* **2002**, *101* (1), 219–260.
437. Jorgensen, W. L. et al. *Proc. Natl. Acad. Sci. U. S. A.* **2005**, *102* (19), 6665 LP – 6670.
438. Cisneros, G. A. et al. *Chem. Rev.* **2016**, *116* (13), 7501–7528.
439. Water models http://www1.lsbu.ac.uk/water/water_models.html (accessed Apr 30, 2020).
440. Baaden, M. et al. *Faraday Discuss.* **2018**, *209* (0), 205–229.

nanopores have been extensively studied in terms of the behaviour of nanoconfined water within their cavities, using both continuum fluid dynamic (CFD) theory and MD simulations.[441–448] Maybe surprisingly, continuum models (modified by insights from AA-MD simulations) have also afforded significant knowledge into the behaviour of water in simple nanopores. Even with continuum models, the strong influence of the internal shape and hydrophobicity of the channels has been also demonstrated.[449–451] For example, studies carried out by Gravelle et al. with Aquaporins concluded that the internal geometry of the channel is also playing a role, suggesting that those which reduce the surface friction, as the hourglass shape, favours the water permeability compared with cylindrical channels.[452,453] However, it has been proven that the accuracy of the continuum models depends on the hydrophobicity and size of the pore, being the water flow underestimated for small hydrophobic pores (< 1 nm).[433,454] For small pores, the structural and dynamical properties of water are strongly influenced by interactions with the pore-lining interfaces and thus the detailed chemical properties of the pores may be important in determining water behaviour. It is likely that for the design of novel nanopores and in order to understand complex biological nanopores, accurate atomistic simulations of water properties are required. In this context, MD simulations emerge as a good alternative for studying pores with a small radii (< 1 nm).[433]

433. Lynch, C. et al. *Chem. Rev.* **2020**, *120*, 10298–10335.
441. Wu, K. et al. *Langmuir* **2019**, *35* (26), 8867–8873.
442. Detcheverry, F. et al. *Phys. Rev. E - Stat. Nonlinear, Soft Matter Phys.* **2013**, *88* (1), 012106.
443. Fayer, M. D. et al. *Annu. Rev. Anal. Chem.* **2010**, *3* (1), 89–107.
444. Collins, M. D. et al. *Proc. Natl. Acad. Sci. U. S. A.* **2005**, *102* (46), 16668–16671.
445. Rasaiah, J. C. et al. *Annu. Rev. Phys. Chem.* **2008**, *59*, 713–740.
446. Beckstein, O. et al. *Proc. Natl. Acad. Sci. U. S. A.* **2003**, *100* (12), 7063–7068.
447. Sisan, T. B. et al. *Microfluid. Nanofluidics* **2011**, *11* (6), 787–791.
448. Walther, J. H. et al. *Nano Lett.* **2013**, *13* (5), 1910–1914.
449. Kashiwagi, K. et al. *Nanoscale* **2018**, *10* (24), 11657–11669.
450. Lu, P. et al. *Micromachines* **2017**, *8* (6).
451. Liu, J. et al. *J. Comput. Phys.* **2010**, *229* (20), 7834–7847.
452. Gravelle, S. et al. *Proc. Natl. Acad. Sci. U. S. A.* **2013**, *110* (41), 16367–16372.
453. Gravelle, S. et al. *J. Chem. Phys.* **2014**, *141* (18), 18C526.
454. Schaschke, C. *A Dictionary of Chemical Engineering*; Oxford University Press, 2014.

MD studies have shown that the behaviour of different biological structures can depend on the water model employed. For example, Anandakrishnan et al. have recently shown the importance of the water model in the calculations of protein folding landscapes[455] and similar conclusions have been obtained for RNA.[456] Additionally, host-guest binding energy differences for supramolecular complexes based on cyclodextrins have proved to depend significantly on the water model.[457] Some computational studies with cylindrical systems embedded in lipid bilayers, acting as transmembrane channels, also suggest differences depending on the selected water model.[458–461] For example, the extensive work of Kassinos et al. on carbon nanotubes (CNTs) show differences in water density, self-diffusivity, and even in the stability of CNTs.[458–460] Liu et al. investigated pressure driven flow rates of water through a **6,6** CNT for the TIP3P, SPC/E, and TIP4P/2005 water models, finding a high dependence of the flow rates on the water model, with TIP3P showing the fastest flow and TIP4P/2005 the slowest.[462] In contrast to larger (**8,8** and **9,9**) CNTs considered in earlier works, the different flow rates cannot be attributed to different model-dependent water structures within the nanotubes but to differing bulk mobilities of the water models affecting the rate of entry into the nanotube.[463] A recent extensive survey of simulations of water behaviour in nanopores and channels also reveals a number of cases where the choice of water model influences on the results regarding the behaviour of water in a nanopore environment, especially in hydrophobic gating of ion channels.[433,461] Thus, the selection of water model for such simulations deserves particular scrutiny. This is because water models are typically parameterized and evaluated by how well they can reproduce the properties of bulk water, and the extent

433. Lynch, C. et al. *Chem. Rev.* **2020**, *120*, 10298–10335.
455. Anandakrishnan, R. et al. *J. Chem. Theory Comput.* **2019**, *15* (1), 625–636.
456. Bergonzo, C. et al. *J. Chem. Theory Comput.* **2015**, *11* (9), 3969–3972.
457. Henriksen, N. M. et al. *J. Chem. Theory Comput.* **2017**, *13* (9), 4253–4269.
458. Kassinos, S. *Mol. Simul.* **2008**, *34* (7), 671–678.
459. Alexiadis, A. et al. *Chem. Eng. Sci.* **2008**, *63* (10), 2793–2797.
460. Alexiadis, A. et al. *Chem. Rev.* **2008**, *108* (12), 5014–5034.
461. Klesse, G. et al. *J. Am. Chem. Soc.* **2020**, *142* (20), 9415–9427.
462. Liu, L. et al. *J. Chem. Phys.* **2016**, *144* (18), 184502.
463. Liu, L. et al. *J. Chem. Phys.* **2014**, *141* (18), 18C518.

of transferability of such water models to nanoconfined water remains unclear. Furthermore, experimental data are not available for these systems. Therefore, to date, the best practice for MD simulations involving water in confined systems is to compare results obtained with different water models.

Recent studies have shown that the presence of hydrophobic regions in different membrane channel proteins can play an important role in controlling the transport of ions, water, and other solutes.[464–468] These regions can be wetted upon application of an electric field, and then de-wetted after the field removal, facilitating the translocation of small charged species, such as some DNA sequences.[465] Thus, the study of artificial hydrophobic nanopores that could mimic the behaviour of the natural channels has attracted growing interests in using them as novel platforms for many technological applications including those where nanopores are used as sensors, such DNA sequencing devices.[463] As it has been mentioned previously, SCPNs are hollow cylindrical-shaped structures.[67–69,252] As a result of their biocompatibility, the tuneability of their diameters and the range of possibilities for functionalizing their inner cavities, SCPNs have emerged as potential candidates for functional transmembrane channels.[60,67–69,95–98,269,469–473]

60. Bong, D. T. et al. *Angew. Chemie Int. Ed.* **2001**, *40* (6), 988–1011.
67. Rodríguez-Vázquez, N. et al. *Org. Biomol. Chem.* **2017**, *15* (21), 4490–4505.
68. Brea, R. J. et al. *Chem. Soc. Rev.* **2010**, *39* (5), 1448–1456.
69. Chapman, R. et al. *Chem. Soc. Rev.* **2012**, *41* (18), 6023–6041.
95. Amorín, M. et al. *J. Am. Chem. Soc.* **2003**, *125* (10), 2844–2845.
96. Reiriz, C. et al. *Org. Biomol. Chem.* **2009**, *7* (21), 4358–4361.
97. Rodríguez-Vázquez, N. et al. *Chem. Sci.* **2016**, *7* (1), 183–187.
98. Rodríguez-Vázquez, N. et al. *Angew. Chemie Int. Ed.* **2016**, *55* (14), 4504–4508.
252. Bong, D. T. et al. *Angew. Chem. Int. Ed. Engl.* **2001**, *40* (6), 988–1011.
269. Seebach, D. et al. *Helv. Chim. Acta* **1997**, *80* (1), 173–182.
463. Liu, L. et al. *J. Chem. Phys.* **2014**, *141* (18), 18C518.
464. Jiang, Y. et al. *Nature* **2003**, *423* (6935), 33–41.
465. Haynes, T. et al. *ACS Nano* **2018**, *12* (8), 8208–8213.
466. Song, C. et al. *J. Phys. Chem. B* **2009**, *113* (21), 7642–7649.
467. Dixit, M. et al. *J. Chem. Phys.* **2020**, *153* (5), 054101.
468. Shen, J. et al. *J. Am. Chem. Soc.* **2020**, *142* (22), 10050–10058.
469. Hourani, R. et al. *J. Am. Chem. Soc.* **2011**, *133* (39), 15296–15299.
470. Clark, T. D. et al. *J. Am. Chem. Soc.* **1998**, *120* (35), 8949–8962.
471. Kobayashi, K. et al. *Angew. Chemie Int. Ed. English* **1995**, *34* (1), 93–95.
472. Horne, W. S. et al. *J. Am. Chem. Soc.* **2003**, *125* (31), 9372–9376.
473. Leclair, S. et al. *Angew. Chemie Int. Ed.* **2004**, *43* (3), 349–353.

However, whilst the interaction and transport of water by SCPNs composed by the classical *D*,*L*-α-CPs have already been studied, no comparable characterizations have been performed in systems using non-standard amino acids that might lead to structures with new properties.[110,474–477] A good understanding of the behaviour of these SCPNs might provide useful information for the design and optimization of new artificial nanopores, as well as for the further improvement of water models and the understanding of their interactions with biological systems. In addition, the present study will also shed light on the structural stability and dynamical behaviour of a new class of peptide nanotubes: α,δ-SCPNs, previously studied by Quantum methods in *Section I*.

110. Tarek, M. et al. *Biophys. J.* **2003**, *85* (4), 2287–2298.
474. Liu, J. et al. *J. Phys. Chem. B* **2010**, *114* (38), 12183–12192.
475. Liu, J. et al. *J. Phys. Chem. A* **2010**, *114* (6), 2376–2383.
476. Comer, J. et al. *J. Phys. Chem. C* **2013**, *117* (50), 26797–26803.
477. Tiangtrong, P. et al. *Appl. Nanosci.* **2016**, *6* (3), 345–357.

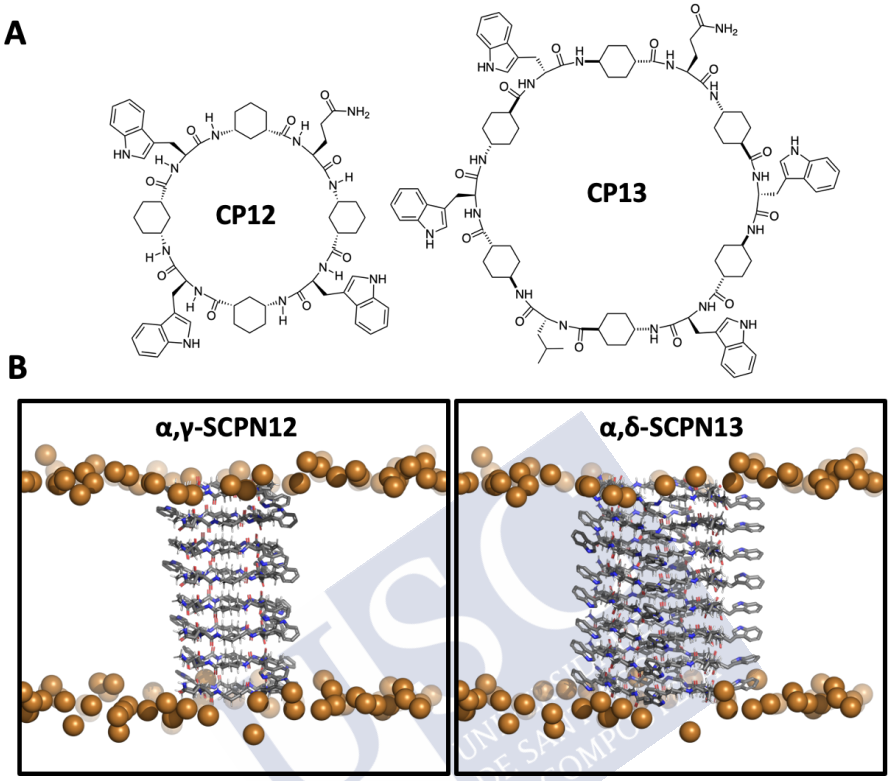

Figure 60. ***A)*** *CP sequences studies in this work. Left: α,γ-CP (**CP12**); Right: α,δ-CP (**CP13**).* ***B)*** *Initial structures for the MD simulations of **α,γ-SCPN12** (left) and **α,δ-SCPN13** (right). For clarity, only the SCPN and the phosphorus atoms of the lipid molecules forming the bilayer (brown spheres) are represented.*

7.2.AIM.

In this study we describe in detail the structural stability of two kinds of SCPNs inserted into a phospholipid bilayer (**α,γ-SCPN12** and **α,δ-SCPN13**, **Figure 60**), together with the analysis of their interactions with four water models, two of which (TIP3P, TIP4P) have been used previously in many studies of biomolecules and nanopores, as well as

two more recently developed water models (TIP4P/2005 and OPC).[478–481] Whereas the **α,γ-SCPN12** is composed of eight residue-long CPs (four α- and four γ-amino acid), the α,δ-CP precursor of the latter SCPN is a dodecamer (six of each α- and δ-amino acids). Taken together, these studies provide a systematic comparison of the water behaviour depending on the different water models in MD simulations of nanoconfined water in two different sizes of SCPNs.

7.3. METHODS.

The starting geometries of the employed cyclic peptides were taken from previous works.[282] For the standard amino acids and the ions, the parameters from the Amber99SB-ILDN Force Field were used.[482] The non-standard amino acids (δ and γ residues), were parametrized using the tool *Antechamber*.[418,420] For the POPC 2-oleoyl-1-palmitoyl-sn-glycero-3-phosphocholine lipids, the parameters derived by Joakim Jambeck (Lipidbook) were used.[483–485] In all simulations, the water molecules in the hydrophobic region of the lipids, together with the waters of the inner cavity of the nanotube, were removed prior to the start of the simulation. In the first step of the simulation, the SCPN lumen was therefore completely dry. A solution of 0.15M NaCl was added in all cases. The initial size of the simulation box for all cases was 12.7x13.4x8.5 nm^3, and contained 131 Na^+, 131 Cl^- and ~24000 water molecules. The number of lipids differed depending on the nanotube: for the α,δ-SCPN, the simulation box contained 407 lipids, whereas for the α,γ-SCPN, it contained 479 lipids. This variation arises from the difference in the diameter of the SCPNs.

282. Calvelo, M. et al. *Chem. – A Eur. J.* **2020**, *26* (26), 5846–5858.
418. Wang, J. et al. *J. Mol. Graph. Model.* **2006**, *25* (2), 247–260.
420. Wang, J. et al. *J. Am. Chem. Soc* **2001**, *222*, U403.
478. Jorgensen, W. L. et al. *J. Chem. Phys.* **1983**, *79* (2), 926–935.
479. Abascal, J. L. F. et al. *J. Chem. Phys.* **2005**, *123* (23), 234505.
480. Izadi, S. et al. *J. Phys. Chem. Lett.* **2014**, *5* (21), 3863–3871.
481. Madura, J. D. *Mol. Phys.* **1985**, *56* (6), 1381–1392.
482. Lindorff-Larsen, K. et al. *Proteins Struct. Funct. Bioinforma.* **2010**, *78* (8), 1950–1958.
483. Jämbeck, J. P. M. et al. *J. Phys. Chem. B* **2012**, *116* (10), 3164–3179.
484. Jämbeck, J. P. M. et al. *J. Chem. Theory Comput.* **2012**, *8* (8), 2938–2948.
485. Klauda, J. B. et al. *J. Phys. Chem. B* **2010**, *114* (23), 7830–7843.

All simulations were performed with the GROMACS 2018.3 package.[424] All systems were partially firstly minimized, followed by an unrestrained production run of 50 ns, with a time step of 2 fs. No restrictions were applied to the peptides at any step, allowing the free movement of all atoms. Five replicas, starting from the same coordinates but differing in the initial velocities, which were randomly assigned from a Boltzmann distribution in the first step of the production, were made for each system, bringing the total number of simulations to forty: twenty for each nanotube, with five for each water model (TIP3P, TIP4P, TIP4P/2005 and OPC). An NPT ensemble (constant pressure and temperature) was employed at one bar pressure, using the semi-isotropic Parrinello-Rahman barostat, and a temperature of 300K, using a V-rescale thermostat (i.e. temperature coupling using velocity rescaling with a stochastic term).[215,423] In all simulations, all bond vibrations were removed employing the LINCS algorithm.[194] For treating the long-range electrostatics, the Particle Mesh Ewald method (PME) was used, using a direct-space cutoff of 1.0 nm and a grid spacing of 0.12 nm.[211] The van der Waals interactions were calculated using a cutoff of 1.0 nm. The data obtained in the simulations were analysed using GROMACS tools and locally written code using the Python MDAnalysis library.[426,486] The molecular graphic pictures of the systems were prepared using the molecular visualizer VMD and PyMOL, and the pore size was calculated using the package CHAP.[231,232,425]

194. Hess, B. et al. *J. Comput. Chem.* **1997**, *18* (12), 1463–1472.
211. Essmann, U. et al. *J. Chem. Phys.* **1995**, *103* (19), 8577–8593.
215. Parrinello, M. et al. *J. Appl. Phys.* **1981**, *52* (12), 7182–7190.
231. Humphrey, W. et al. *J. Mol. Graph.* **1996**, *14* (1), 27-28,33-38.
232. DeLano, W. L. *CCP4 Newsletter On Protein Crystallography*. 2002.
423. Bussi, G. et al. *J. Chem. Phys.* **2007**, *126* (1), 014101.
424. Abraham, M. J. et al. *SoftwareX* **2015**, *1–2*, 19–25.
425. Klesse, G. et al. *J. Mol. Biol.* **2019**, *431* (17), 3353–3365.
426. Michaud-Agrawal, N. et al. *J. Comput. Chem.* **2011**, *32* (10), 2319–2327.
486. Gowers, R. J. et al. In *Proceedings of the 15th Python in Science Conference*; Benthall, S. et al., Eds.; 2016; pp 98–105.

The RMSD calculations were carried out using the GROMACS tool. The initial frame of the trajectory was taken as the reference point, as in this case the tubular shape was expected to be perfectly formed. In order to avoid fluctuations provoked by the side-chains, only the backbone was considered.

The tilt angle was defined as the angle between the normal of the membrane and a vector which links the centre of the CPs of the edges of the nanotube. For calculation of the mean displacements, 160 windows of 100 ps were defined starting at different points of the simulations. For each window, the total amount of movement of each water molecule was calculated, averaging over all these molecules. Only the waters which were inside the nanotube during the whole window were considered. The probability distributions (*P*) presented for these two magnitudes were calculated using the python library Numpy.[487]

The survival probability of the waters inside the nanotube represents the likelihood of one water molecule to remain encapsulated after a certain time, following the approach described by Liu et al.[488] The autocorrelation function for the H-bond lifetime has been obtained using the description proposed by Rapaport, being here presented the intermittent H-bonds.[489] These two calculations are available in the *Water Dynamics Analysis* section of MDAnalysis.[490]

For the water density maps, a grid in the *xy* or *xz* planes were defined, counting the number of times that a water molecule was presented in each position. In order to obtain a proper comparison, the results were normalized by taking the most populated point of all simulations as a reference point.

The z-coordinate representation of the ions, as well as the total number of cations which enter in the nanotube and the number of molecules coordinated to them, were obtained using local Python code.

487. Harris, C. R. et al., *Nature* **2020**, *585* (7825), 357–362.
488. Liu, P. et al. *J. Phys. Chem. B* **2004**, *108* (21), 6595–6602.
489. Rapaport, D. C. *Mol. Phys.* **1983**, *50* (5), 1151–1162.
490. 4.8.3. Water dynamics analysis — MDAnalysis.analysis.waterdynamics — MDAnalysis 0.20.2-dev0 documentation https://www.mdanalysis.org/mdanalysis/documentation_pages/analysis/waterdynamics.html (accessed Apr 28, 2020).

The coordination numbers of the cations inside the SCPN were calculated by counting the number of oxygens at a distance smaller than a defined cut-off, which was the end of the first coordination layer of the Na^+ (approx. 3.2 Å). This value was obtained from the RDF calculation of oxygen of the waters taking as reference all the cations (also those outside the nanotube), using the GROMACS tool.

In order for the nanotube to be long enough to traverse the membrane, and following previous studies, an α,γ-SCPN structure composed of eight CPs was built, with four α-amino acid and four γ-Ach residues (*c*-[*L*-Gln-*D*-γ-Ach-(*L*-Trp-*D*-γ-Ach-)$_3$], **CP12**) in each ring, leading to the formation of **α,γ-SCPN12**.[110,264,391,404,431] The α,δ-SCPN structure was also composed of eight CPs, but in this case each ring was made up of six α-amino acids and six δ-Ach resiudes (*c*-[*L*-Gln-δ-Ach-(*L*-Trp-δ-Ach-)$_2$*L*-Leu-δ-Ach-(*L*-Trp-δ-Ach-)$_2$], **CP13**), resulting in **α,δ-SCPN13**. Note that in this case the prefix α,γ- or α,δ- is added to the nomenclature of the SCPNs in order to facilitate the differentiation of the nanotubes. The antiparallel and parallel β-sheet-like interactions were chosen for the α,γ- and α,δ-SCPN, respectively. Due to the different number of amino acids, the initial minimum internal radii for the α,γ- and α,δ-SCPN were 0.34 and 0.53 nm respectively (**Figure 61***A*). The different number of methylene groups oriented inwards leads to a more hydrophobic cavity for the **α,δ-SCPN13** (**Figure 61***B*).

Four water models (TIP3P, TIP4P, TIP4P/2005 and OPC) were used to describe the water properties in the lumen of these SCPNs embedded in a POPC membrane (**Figure 60***BC*).[478–480] TIP3P is a 3-point model, i.e. it is composed of three particles—two positive point charges on the hydrogen sites and one negative point charge on the oxygen site.

110. Tarek, M. et al. *Biophys. J.* **2003**, *85* (4), 2287–2298.
264. Amorín, M. et al. *Chem. - A Eur. J.* **2008**, *14* (7), 2100–2111.
391. García-Fandiño, R. et al. *Chem. Sci.* **2012**, *3* (11), 3280–3285.
404. Calvelo, M. et al. *Phys. Chem. Chem. Phys.* **2015**, *17* (43), 28586–28601.
431. Calvelo, M. et al. *Phys. Chem. Chem. Phys.* **2019**, *21* (37), 20750–20756.
478. Jorgensen, W. L. et al. *J. Chem. Phys.* **1983**, *79* (2), 926–935.
479. Abascal, J. L. F. et al. *J. Chem. Phys.* **2005**, *123* (23), 234505.
480. Izadi, S. et al. *J. Phys. Chem. Lett.* **2014**, *5* (21), 3863–3871.

Each site also has a Lennard-Jones potential to describe the non-directional interactions of the atoms. By contrast, TIP4P, and the more recently developed TIP4P/2005 and OPC models, are 4-point models. In this case the Lennard-Jones potential remains on the oxygen site, but the negative charge is displaced from the oxygen site towards the hydrogen sites. The geometries, Lennard-Jones parameters and charges also differ between the models.[433,439,491]

All the simulations were performed in the presence of NaCl (0.15 M). For each system, five MD trajectories of 50 ns were generated (giving a total of 250 ns per system).

433. Lynch, C. et al. *Chem. Rev.* **2020**, *120*, 10298–10335.
439. Water models http://www1.lsbu.ac.uk/water/water_models.html (accessed Apr 30, 2020).
491. Onufriev, A. V. et al. *Wiley Interdiscip. Rev. Comput. Mol. Sci.* **2018**, *8* (2), e1347.

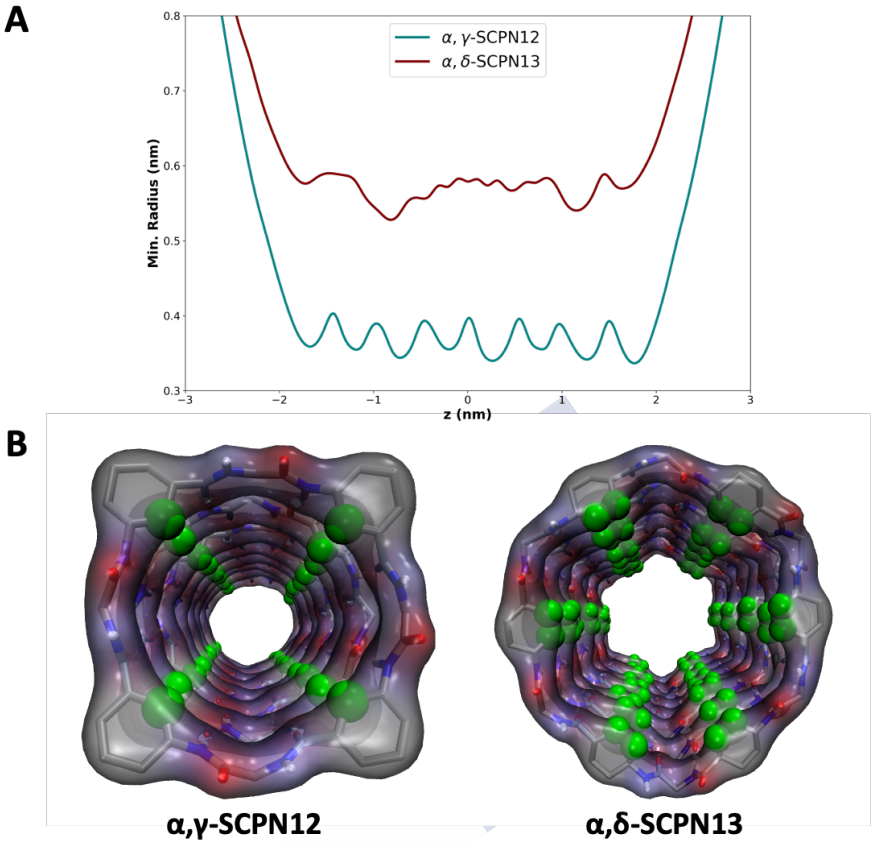

Figure 61. A) *Minimum Inner Radius of the* ***α,γ-SCPN12*** *and* ***α,δ-SCPN13*** *at the beginning of the simulation (t = 0).* ***B)*** *Detail of the inner cavity of both SCPNs, highlighting the hydrophobic moieties oriented inwards in green.*

7.4. RESULTS.

Previous studies with α,γ-SCPNs composed of *c*-[(*L*-Trp-*D*-γ-Ach-)$_4$] (**α,γ-SCPN2**) have shown that they are stable in a lipid bilayer environment, forming nanopores.[391,404,492] α,δ-SCPNs as transmembrane channels when they are inserted in a lipid bilayer have not yet been studied previously, so no evidences on their structural

391. García-Fandiño, R. et al. *Chem. Sci.* **2012**, *3* (11), 3280–3285.
404. Calvelo, M. et al. *Phys. Chem. Chem. Phys.* **2015**, *17* (43), 28586–28601.
492. Garcia-Fandiño, R. et al. *ACS Nano* **2016**, *10* (3), 3693–3701.

stability in a lipidic environment exists.

Both the bilayer and nanotubes were stable in the forty MD trajectories (two different nanotubes, **α,γ-SCPN12** and **α,δ-SCPN13**, each simulated with the four water models, with five replicas for each simulation), claiming that α,γ-SCPNs are stable under this environment, as previously observed, and indicating for the first time that α,δ-SCPNs can function as transmembrane channels (**Figure 62**). The tubular shape is well preserved during the simulation time, with the average RMSD values for the **α,γ-SCPN12** being slightly smaller than the ones for the **α,δ-SCPN13** (**Figure 63**). No significant differences in pore model stability are found between the trajectories using different water models. The RMSD analysis by CP position in the nanotube also demonstrated the stability of the nanotube, although, as expected, the CPs at either end of the nanotubes exhibit a slightly larger movement than the others as a consequence of their reduced packing interactions in one solvent exposed face (**Figure 64**).

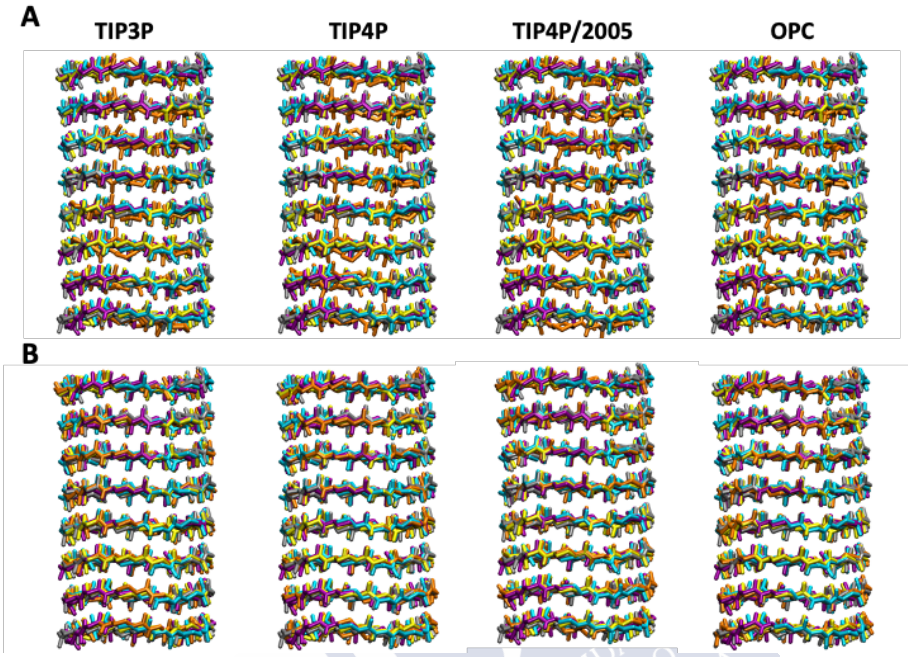

Figure 62. *Snapshots of the backbone of a simulated* ***A) α,γ-SCPN12*** *and* ***B) α,δ-SCPN13*** *(B) after 50 ns of simulation. The final structure of each replica is represented in a different colour (5 replicas per water model, 5 colours).*

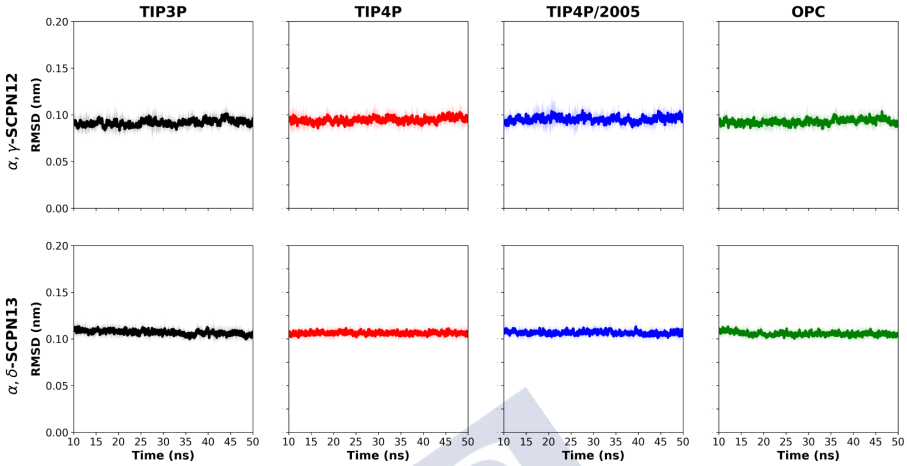

Figure 63. *Average backbone RMSD among the five replicas of both SCPNs in TIP3P, TIP4P, TIP4P/2005 and OPC, respectively. Each water model is displayed with a different colour. Standard deviations are shown in a paler colour.*

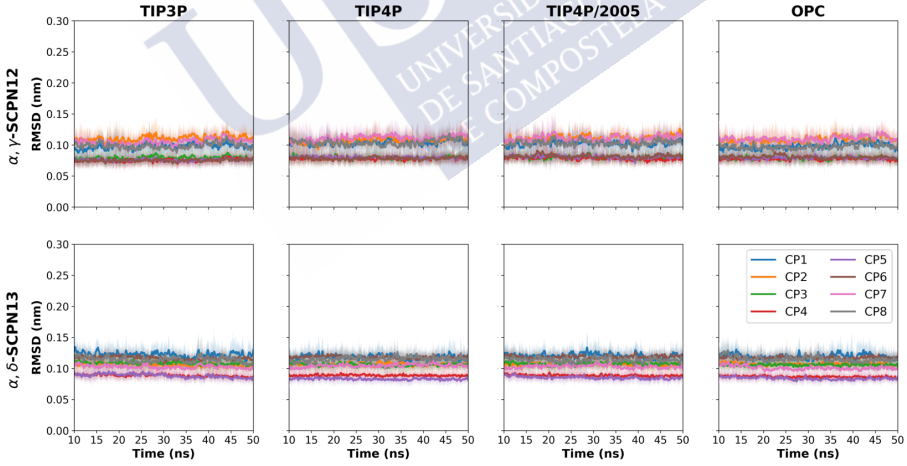

Figure 64. *Average backbone RMSD among the five replicas of both SCPNs split by CP in TIP3P, TIP4P, TIP4P/2005 and OPC. Standard deviations are shown in a paler colour.*

The number of H-bonds is directly related to the stability of the nanotube. In the case of **α,γ-SCPN12**, the number of H-bonds between CPs (49 ± 2, **Figure 65***A*) is close to the maximum possible (56, 8 per CP and 7 pairs of CPs), whereas for **α,δ-SCPN13** the number of H-bonds is 72 ± 3 (compared to the maximum of 84, 12 per CP x 7 pairs of CPs) (**Figure 65***A*). These results show that the sacrifice of almost 15% of the inter-backbone H-bonds, probably due to competition with the water molecules, is not enough to disrupt the tubular structure. In addition, some extra H-bonds (around 6-7) are formed between glutamine side-chains that form a continuing net along the nanotube (see atomistic detail in **Figure 65***B*). These interactions are present in both nanotubes. Regarding the comparison between the water models employed, no significant differences are found apart from a slightly increased number of H-bonds in the nanotube network for the **α,δ-SCPN13** in TIP3P (**Figure 65***A*), and an increase in the number of H-bonds between the nanotube and water in both nanotubes when using TIP4P/2005 (**Figure 65***A*).

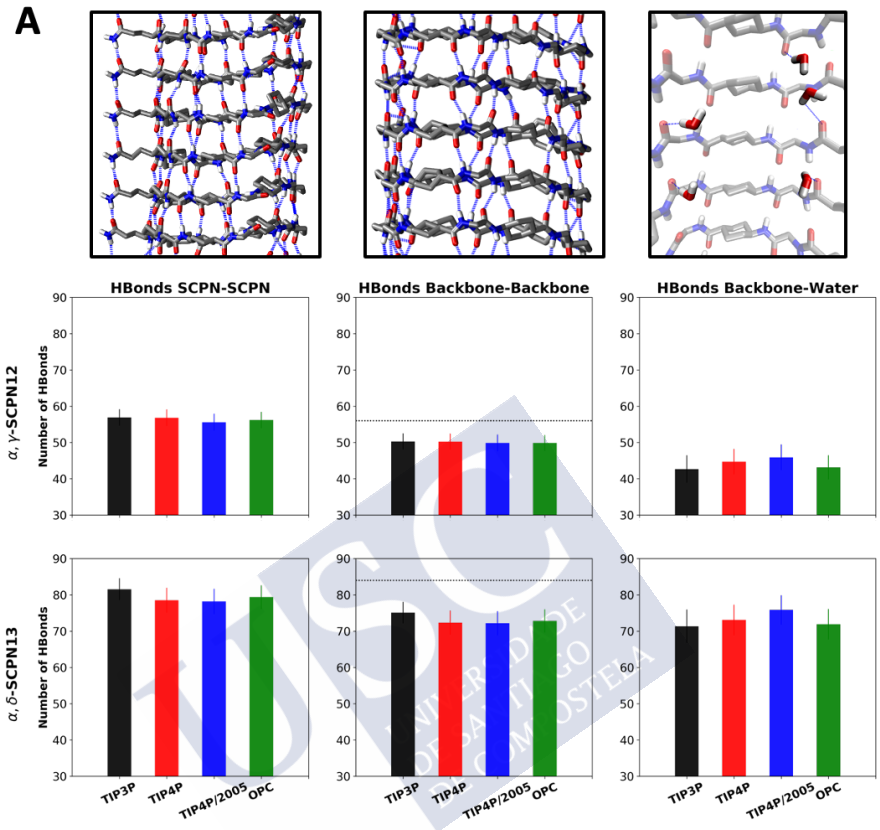
A
HBonds SCPN-SCPN
HBonds Backbone-Backbone
HBonds Backbone-Water
α, γ-SCPN12
α, δ-SCPN13
Number of HBonds
TIP3P
TIP4P
TIP4P/2005
OPC

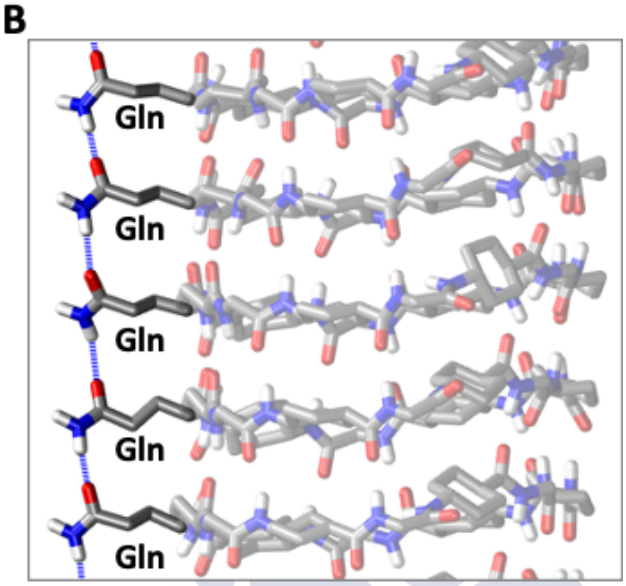

Figure 65. A) *Number of H-bonds between the different parts of the system (among the different CPs—as a whole or just considering the backbone—and between the CPs and the water), averaged over the last 40 ns of the simulation, and over all replicas. Standard deviations are also shown as error bars. A detail of each type of interaction is shown in the figures at the top. The maximum number of H-bonds that can be formed among the backbone of all CPs is displayed with a dashed line.* ***B)*** *Detail of the Gln-Gln H-bonds, shown as broken blue lines.*

The stability of the pore radii is a crucial issue from the point of view of studying the water and ion channels. The average values of the minimum radius during the last 40 ns of the five replicas shows a quite constant inner size, with very similar values to the initial radius (**Figure 66**). This stability suggests that these pores remain in an open state throughout the entirety of their trajectories, which corresponds to relatively long-lived channel openings observed experimentally.[76,391]

76. Montenegro, J. et al. *Acc. Chem. Res.* **2013**, *46* (12), 2955–2965.
391. García-Fandiño, R. et al. *Chem. Sci.* **2012**, *3* (11), 3280–3285.

The effective radius, as previously observed for the **α,γ-SCPN12**, is situated in the plane of the CP whereas the maximum radius is located in the region between the two planes of the rings (**Figure 66***B*).[391,404] The smallest radii that correspond to the plane of the CPs alternate from smaller to bigger values from one CP to the next along the nanotube. The same trend is found for the **α,δ-SCPN13** (**Figure 66***B*). These differences in the size of the inner cavity could potentially lead to different transport behaviours and water confinement patterns (*vide infra*).

391. García-Fandiño, R. et al. *Chem. Sci.* **2012**, *3* (11), 3280–3285.
404. Calvelo, M. et al. *Phys. Chem. Chem. Phys.* **2015**, *17* (43), 28586–28601.

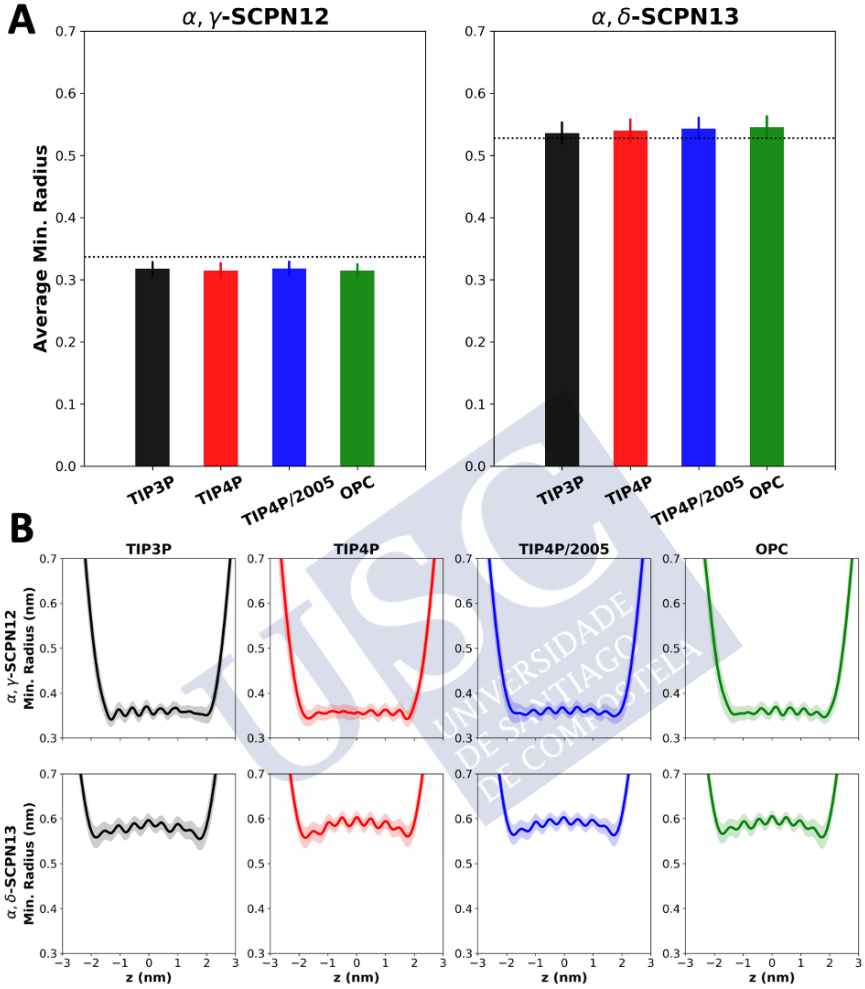

Figure 66. *Minimum Inner Radius averaged over the five replicas, as well as the standard deviation, for both SCPNs in TIP3P, TIP4P, TIP4P/2005 and OPC presented as* ***A)*** *a histogram and* ***B)*** *along the z axis of the nanotube.*

Given the unequal internal radii and hydrophobic character of both nanotubes, differences in the entrance of molecules inside of the channels can be anticipated (**Figure 61**). The study of the filling of both channels reveals a faster process for TIP3P than for the other three water models, with the channel being completely filled within the first 0.2 ns (**Figure 67**). Additionally, and especially in the **α,δ-SCPN13**, it is possible to observe that OPC waters need more time for a complete filling of the nanotube, suggesting that the diffusion of this water model within the pore may be slower than the others (**Figure 67**). TIP4P and TIP4P/2005 also show unequal behaviours, being TIP4P more similar to TIP3P and TIP4P/2005 to OPC.

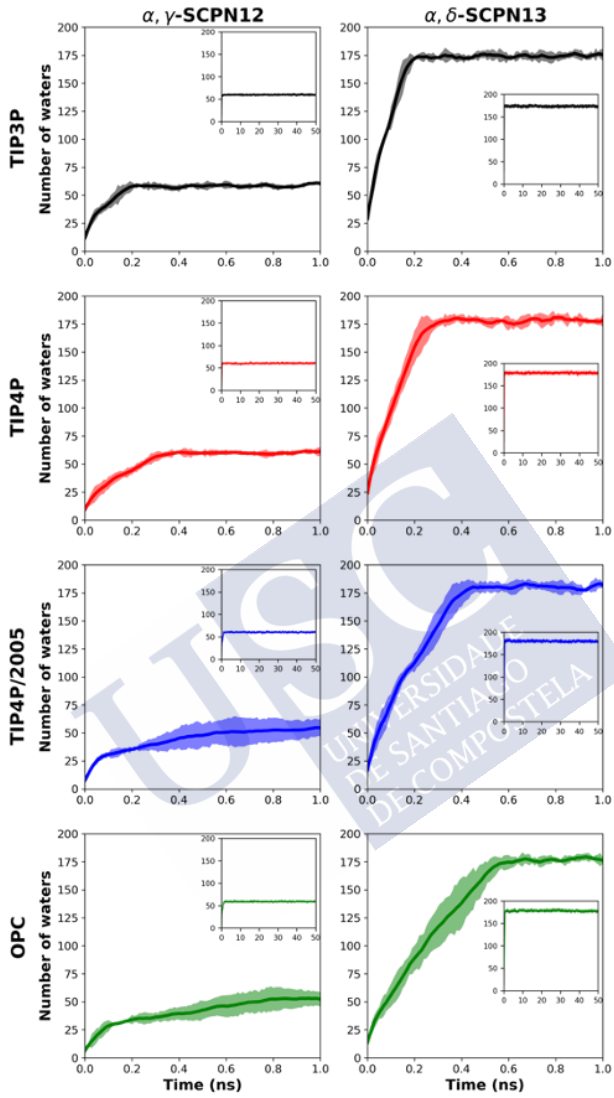

Figure 67. *Number of waters entering* ***α,γ-SCPN12*** *(left) and* ***α,δ-SCPN13*** *(right) during the first 1 ns of each MD simulation. Each colour corresponds to a different water model averaged over the five replicas. Standard deviations are shown in a paler colour. The number of waters inside the nanotube over the total 50 ns of simulation is presented in the small insets.*

The average number of waters inside the channel of **α,γ-SCPN12** is significantly smaller (more than 100 molecules less) due to its smaller radius compared to **α,δ-SCPN13** (**Figure 68**). For both channels, simulations with TIP4P and TIP4P/2005 led to the inclusion of more water molecules than with the other models. This may explain the higher number of H-bonds between the nanotubes and the water molecules (**Figure 65***A*). Surprisingly, in the wider nanotube (**α,δ-SCPN13**), TIP3P model gives a smaller number of water molecules inside the pore, despite being the water model that predict the fastest filling of the nanotube. This behaviour is not observed for the **α,γ-SCPN12**, where the differences between all water models are no significant. These observations suggest that there is no correlation between filling rates and the number of waters within the channel, suggesting that the number of waters inside is an equilibrium property and does not simply reflect differences in filling rates of the pores.

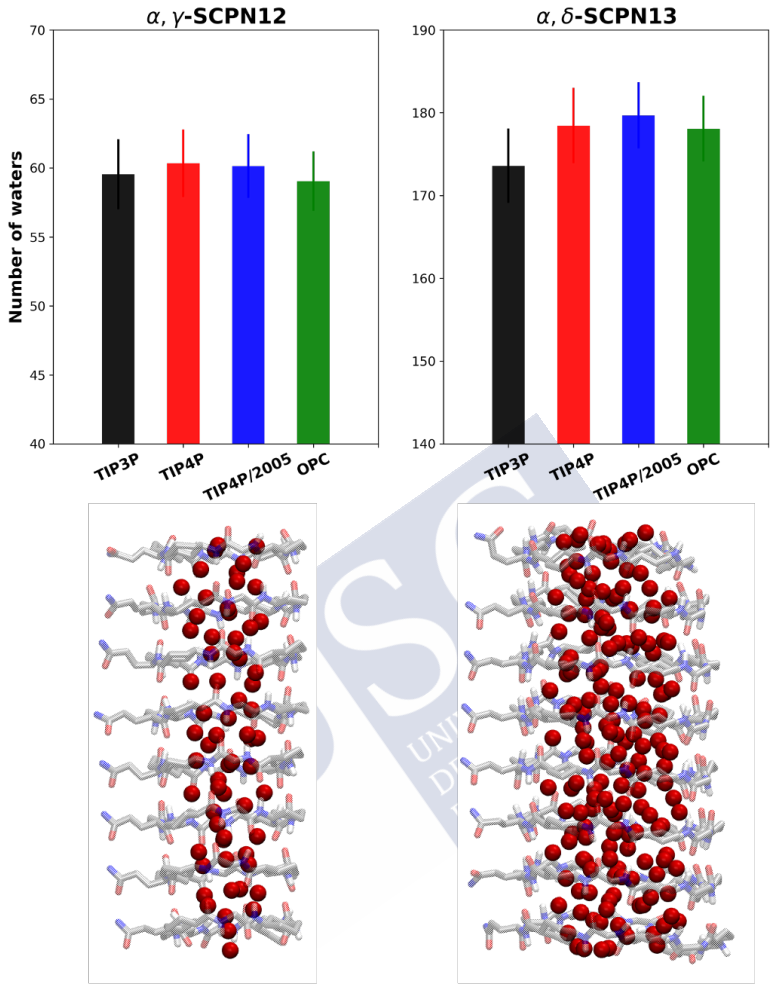

Figure 68. *Number of waters inside* ***α,γ-SCPN12*** *and* ***α,δ-SCPN13****, averaged over the last 40 ns of the simulation, and over all replicas. Each colour corresponds to a different water model. A picture of each channel with water inside (red spheres correspond to the water oxygen atoms) is shown for each SCPN. Standard deviations are also shown as error bars.*

The velocity of water molecules inside both nanotubes was analysed by calculating the mean square deviation (MSD) of all the encapsulated molecules during a time window of 100 ps (**Figure 69**). These results show that the water molecules of TIP3P model move more than the others in the same time interval, being, therefore, the fastest followed by TIP4P. On the other hand, TIP4P/2005 and OPC models predict significantly slower kinetics than the other models. The velocity exhibited by these two parameterizations is very similar in both nanotubes. This trend reflects the self-diffusion in bulk water of the different models (D = 5.5, 3.2, 2.1 and 2.4 x 10^9 m^2 s^{-1} for TIP3P, TIP4P, TIP4P/2005 and OPC respectively, compared to 2.3 x 10^9 m^2 s^{-1} experimentally).[478–480,493,494] Similar trends were also observed for studies of pressure-induced flow through CNTs with radii between ∼0.4 and ∼0.9 nm, suggesting a nearly 3-fold difference between, for example, TIP3P and TIP4P/2005.[495] Thus, TIP4P/2005 and OPC, which have very similar self-diffusion coefficients in bulk water (in good agreement with the experimental value), keep this similarity when the water is confined in a SCPN. TIP3P, in which water molecules are known to diffuse in the bulk too quickly compared with experimental values, is also predicting the fastest diffusion in this confined environment. Finally, an intermediate behaviour is exhibited by TIP4P. Larger differences are found for **α,δ-SCPN13** than **α,γ-SCPN12**, being possible to observe a small overlapping between the different water models in the narrower nanotube, especially for TIP3P and TIP4P. Furthermore, the same conclusion is obtained when longer time windows (200 and 500 ps) are defined (**Figure 69***BC*). Additionally, and due to the larger inner radii, the water MSDs are greater for **α,δ-SCPN13** (**Figure 69**).

478. Jorgensen, W. L. et al. *J. Chem. Phys.* **1983**, *79* (2), 926–935.
479. Abascal, J. L. F. et al. *J. Chem. Phys.* **2005**, *123* (23), 234505.
480. Izadi, S. et al. *J. Phys. Chem. Lett.* **2014**, *5* (21), 3863–3871.
493. Mills, R. *J. Phys. Chem.* **1973**, *77* (5), 685–688.
494. Krynicki, K. et al. *Faraday Discuss. Chem. Soc.* **1978**, *66* (0), 199–208.
495. Liu, L. et al. *J. Chem. Phys.* **2017**, *146* (7), 074502.

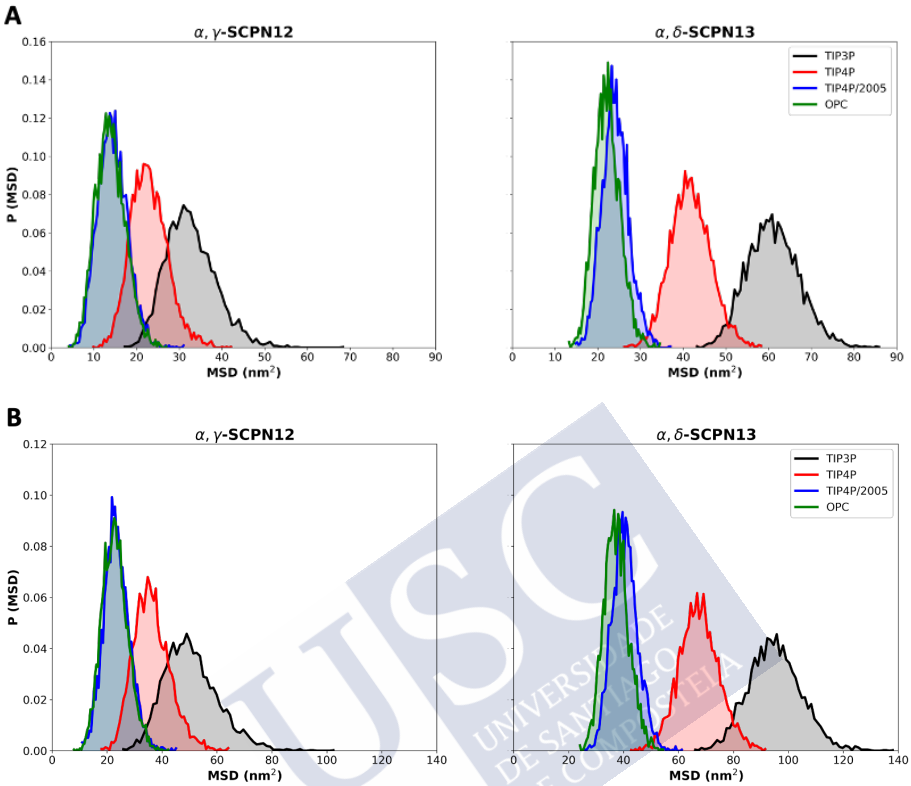
A
α, γ-SCPN12
α, δ-SCPN13
TIP3P
TIP4P
TIP4P/2005
OPC
P (MSD)
MSD (nm²)
B
α, γ-SCPN12
α, δ-SCPN13
TIP3P
TIP4P
TIP4P/2005
OPC
P (MSD)
MSD (nm²)

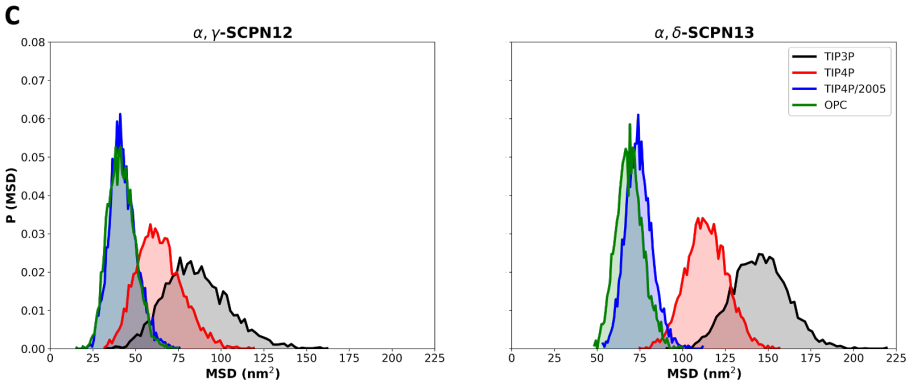

***Figure 69.** Probability distribution of the MSD of waters inside **α,γ-SCPN12** and **α,δ-SCPN13** during windows of **A)**100 ps, **B)** 200 ps and **C)** 500 ps along the last 40 ns of all replicas for the different water models studied. Each water model is displayed with a different colour (TIP3P in black, TIP4P in red, TIP4P/2005 in blue and OPC green).*

Differences between water models also appear when the water-peptide interaction strength is considered. Despite the similarity in the number of H-bonds between the nanotube and water (**Figure 65**), the lifetime of these bonds is longer in TIP4P/2005 and OPC models, which could slow down their movement inside the SCPN (**Figure 70**). The H-bonds with the waters of TIP3P model are the most short-lived, followed by TIP4P. These results suggest a relation between the diffusion of the water molecules in the SCPN and the life-time of the interaction with the peptide. Moreover, the obtained trend is also reflected in the survival probability of the waters inside the SCPN, in which the waters of TIP4P/2005 and OPC models are retained for longer time in the lumen of the nanotube than those of TIP3P and TIP4P models (**Figure 71**).

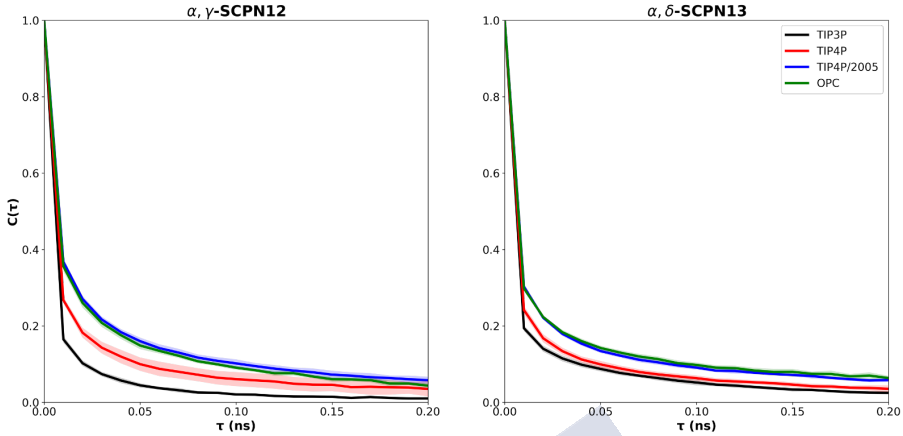

Figure 70. *H-bond lifetime between both SCPNs and water molecules in TIP3P, TIP4P, TIP4P/2005 and OPC, averaged over the five replicas. Each water model is displayed in a different colour (TIP3P in black, TIP4P in red, TIP4P/2005 in blue and OPC green). Standard deviations are shown in a paler colour.*

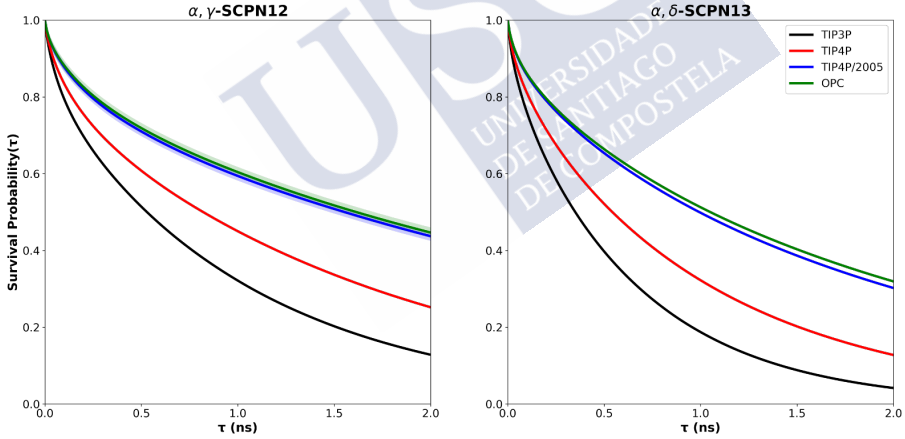

Figure 71. *Survival probability of water molecules inside both SCPNs in TIP3P, TIP4P, TIP4P/2005 and OPC, averaged over the five replicas. Each water model is displayed in a different colour (TIP3P in black, TIP4P in red, TIP4P/2005 in blue and OPC green). Standard deviations are shown in a paler colour.*

The different inner radii of the nanotubes also lead to an unequal pattern of water distribution in the pores. The density of the encapsulated waters projected onto the membrane plane reveals a pattern with approximately six-fold rotational symmetry for the nanotube derived from the dodecameric CP (**α,δ-SCPN13**) (**Figure 72**). These peaks correspond with the region of the Cα of the α-amino acids, probably due to the proximity of the amino and carboxyl groups that generates a hydrophilic environment. The presence of the two methylene groups of the cyclohexyl moieties results in a dry region (hydrophobic) next to them, where the water density is practically cero. Additionally, water seems to be more likely situated near the backbone than in the centre of the pore, probably induced again by the influence of the polar character of the peptide bonds. The water density shows an approximately two-fold rotational symmetry for the nanotube derived from the octapeptide (**α,γ-SCPN12**), with three columns following a pattern wet-dry-wet (**Figure 72***A*). This anisotropic profile is quite surprising given that the lumen of this hollow structure has a four-fold rotational symmetry. Interestingly, the origin of this asymmetry in the inner water density seems to come from the presence of Gln in the sequence, which induces an asymmetric outer surface of the channel. The replacement of the Gln by a Trp (**α,γ-SCPN14**), revealed a much more symmetric profile (**Figure 73**), confirming this hypothesis and highlighting that the exterior of the channel can influence the internal water arrangement. This can derive from the modifications of the heads of phospholipids organization that might influence on the water structure at the entrance of the pore and therefore on the alignment in the channel. A similar effect is also observed for the **α,δ-SCPN13**, since the densities are not exactly 6-fold symmetric either, however it is not so marked, probably due to the larger size and the above mentioned remarked preference of water molecules close to the peptide bonds. A related phenomena has been previously observed in a CNT, being the flow increased by the insertion of a point charge just outside the nanotube.[496]

496. Li, J. et al. *Proc. Natl. Acad. Sci. U. S. A.* **2007**, *104* (10), 3687–3692.

As already found before, the water profile along the z-coordinate reveals for both nanotubes a higher density in the region between the CP planes, (**Figure 72***B*) that is explained by the larger radius found in this region (**Figure 66***B*). It is important to note that the same density pattern is reproducible regardless of the water model. However, the colours are slightly more intense following the sequence: TIP3P < TIP4P < TIP4P/2005 ≈ OPC, probably due to the differences in water diffusion mentioned above. These patterns suggest that water positions are related to the same principle, possibly trying to stablish the maximum number of interactions per water. Consequently, the water molecules rarely occupy some positions (non colour) while are mainly placed in other positions (darker blue). This is quite obvious in the **α,δ-SCPN13**, in which the inter-disc areas close to the amide bonds are always occupied by water molecules and this already fix the positions of the neighbour waters, while the central part is more disperse with almost no predeterminate positions for the water molecules. This is also visualized in the symmetric pattern observed for the **α,γ-SCPN14**, in which water is clearly distributed following the symmetry element C4, forming a cross shape in the centre of the nanotube (**Figure 73**). This confirms that water molecules do not like to be close to the methylene group of the Ach group, which must organize the rest of the molecules.

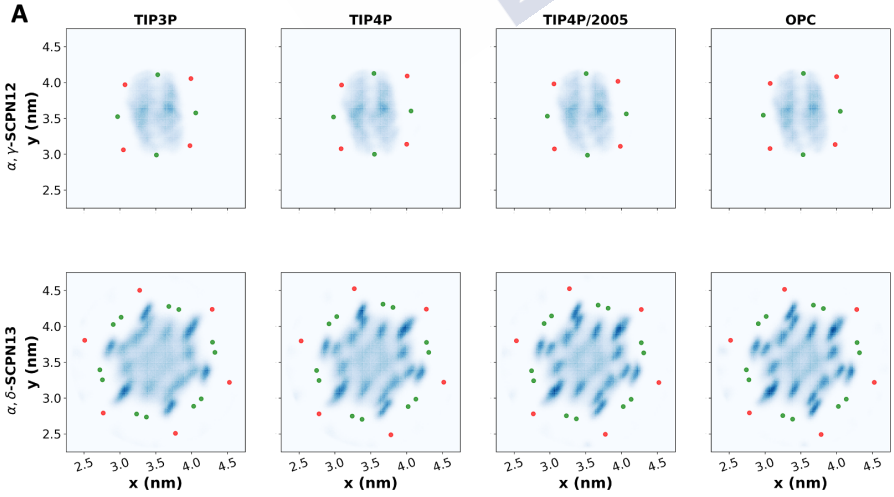

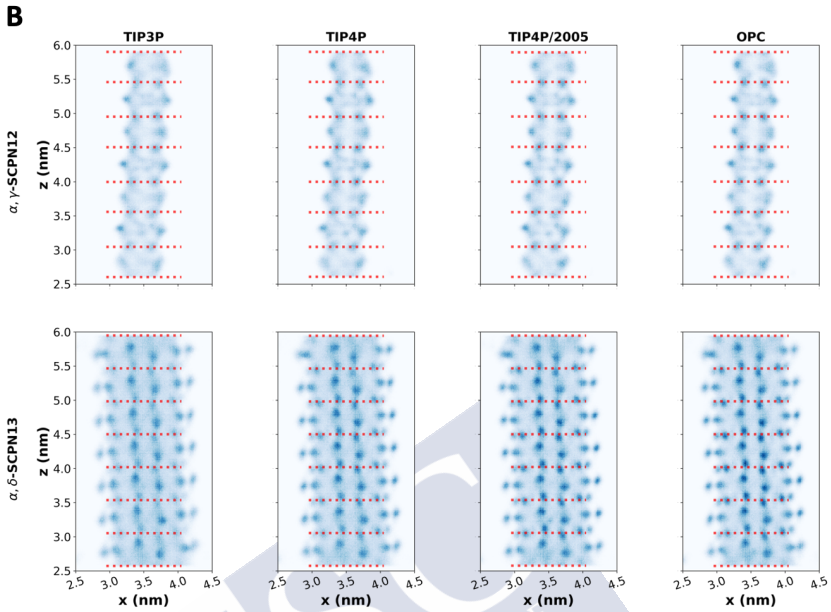

***Figure 72. A)** XY-Density profile of the water molecules inside both nanotubes. The averaged positions Cα of the α-amino acids and the C of the inwards methylenes of the non-natural residues are highlighted in red and green, respectively. **B)** Z-Density profile of the water molecules inside both nanotubes. The averaged Z-coordinates of the Cα of each CP are highlighted with a red dashed line.*

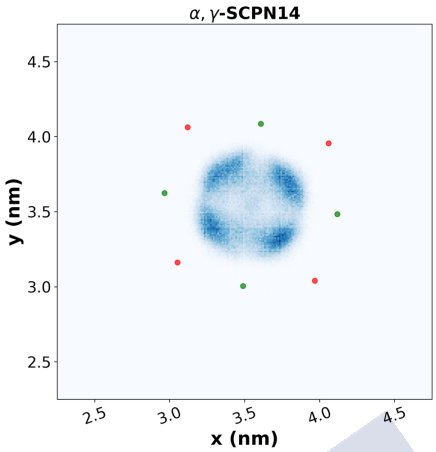

Figure 73. *XY-Density profile of the water molecules inside of the symmetric channel* ***α,γ-SCPN14****, using the TIP3P model. The averaged positions Cα of the α-amino acids and the C of the inwards methylenes of the non-natural residues are highlighted in red and green, respectively.*

As mentioned above, one of the most important applications of these systems is their insertion into a lipid bilayer in order to act as transmembrane ion channels. As it has been found with similar nanotubes, and commented in the previous chapter, there is a strong selectivity for cations in the **α,γ-SCPN12**, attributed to the negatively-charged carbonyl oxygens and the consequently organization of the hydrogen-bonded water molecules inside this type of channel (**Figure 74***A*, **Figure 75***A*).[391,404] For the **α,δ-SCPN13** this cation selectivity is less pronounced, as indicated by the presence of both cations (Na^+) and anions (Cl^-) in the nanotube region (**Figure 74***B*, **Figure 75***B*). This may be due to the increase in nanotube diameter as well as the greater exposure of hydrophobic groups to the lumen of the pore, since it has been suggested that hydrophobic contacts, van der Waals and C-H···Cl hydrogen bonds, may favour chloride over cations.[461,497] However, the number of cations inside remains considerably higher than that of

391. García-Fandiño, R. et al. *Chem. Sci.* **2012**, *3* (11), 3280–3285.
404. Calvelo, M. et al. *Phys. Chem. Chem. Phys.* **2015**, *17* (43), 28586–28601.
461. Klesse, G. et al. *J. Am. Chem. Soc.* **2020**, *142* (20), 9415–9427.
497. Lisbjerg, M. et al. *J. Am. Chem. Soc.* **2015**, *137* (15), 4948–4951.

anions. It is also noticeable that most of the anions entering **α,δ-SCPN13** are paired with the corresponding cation, as indicated by the z-coordinates of those ions from **Figure 74** and **Figure 75**. Globally, there is also a difference in the number of cations inside each of the nanotubes, being higher for those containing δ-residues, in agreement with their larger diameter. Focusing on water models, in the simulations with TIP3P the number of different cations entering the nanotube is significantly higher, which could suggest a correlation between the water diffusion and the number of ions entering the nanotube (**Figure 76**). No large differences have been found among the remaining models, with the number of cations always being smaller than those found for the TIP3P model.

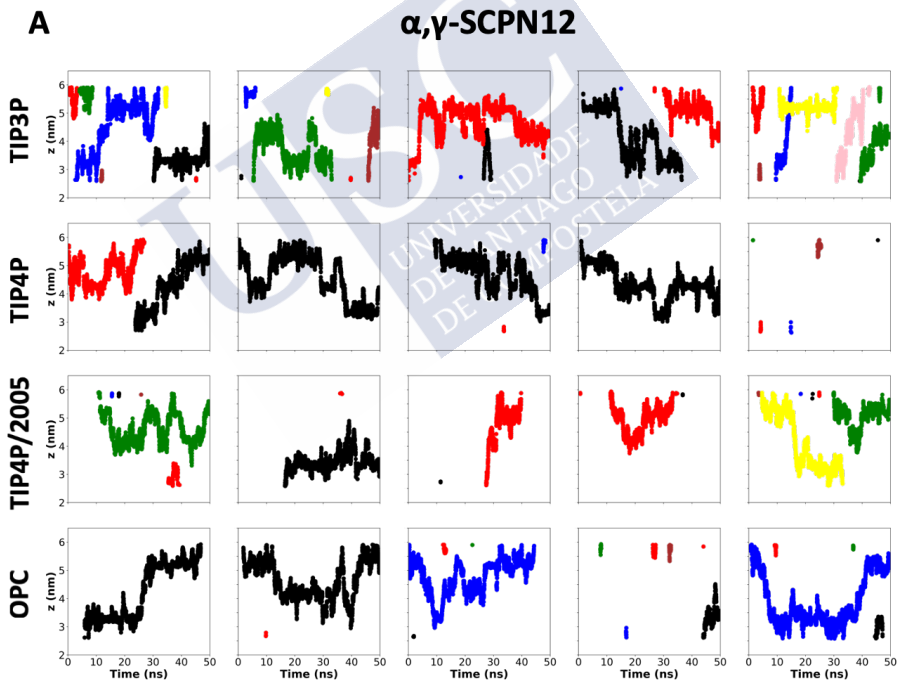

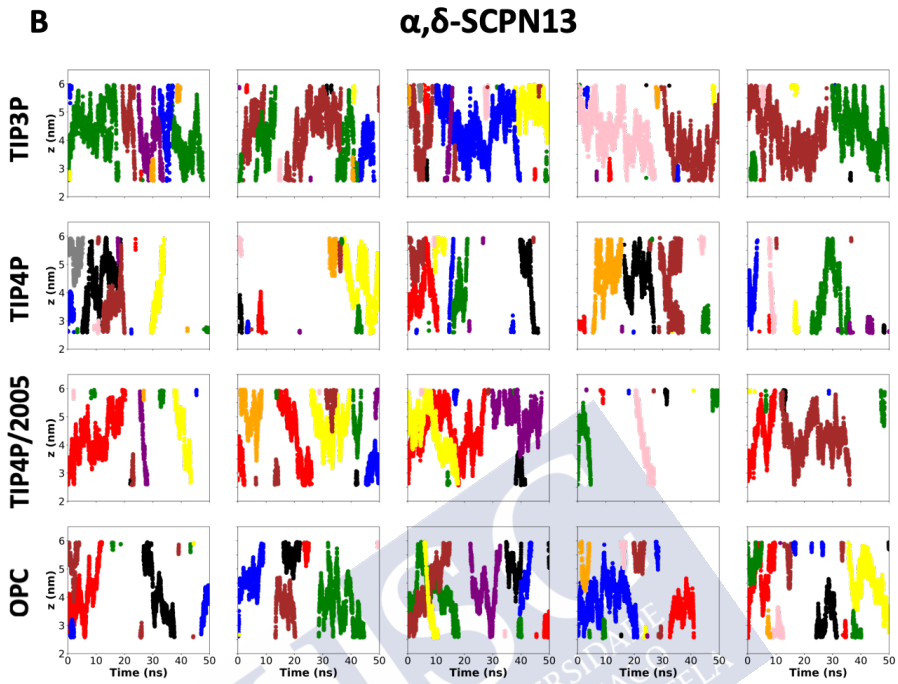

Figure 74. *Z-coordinate for each of the cations inside the* ***A) α,γ-SCPN12*** *and* ***B) α,δ-SCPN13*** *along the 50 ns trajectory. The nanotube z-region is taken between ≈2-6 nm. Each column corresponds to a different replica. Each colour corresponds to a different ion.*

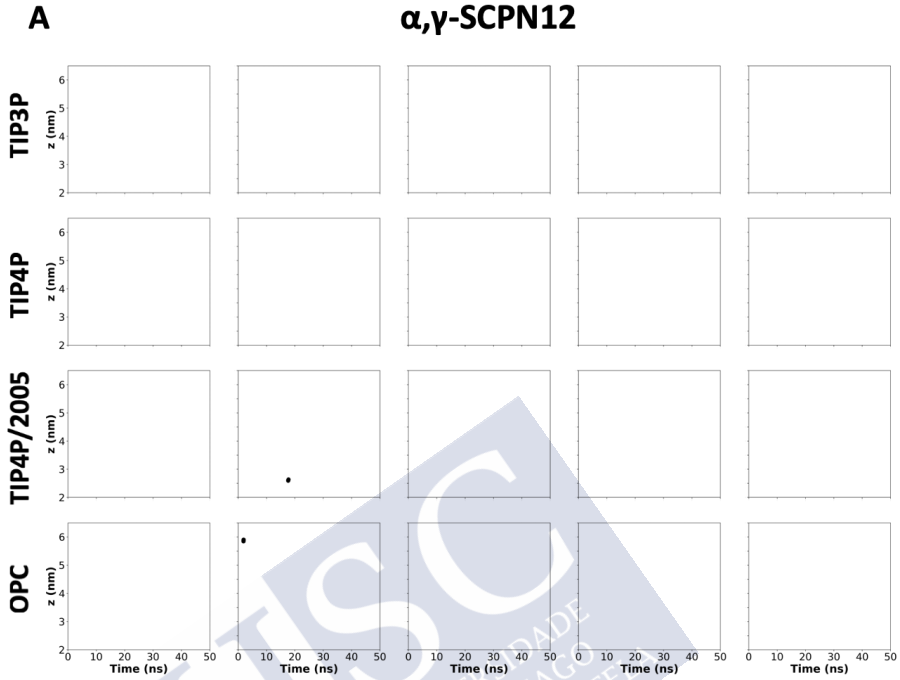
A
α,γ-SCPN12
TIP3P
TIP4P
TIP4P/2005
OPC
z (nm)
Time (ns)

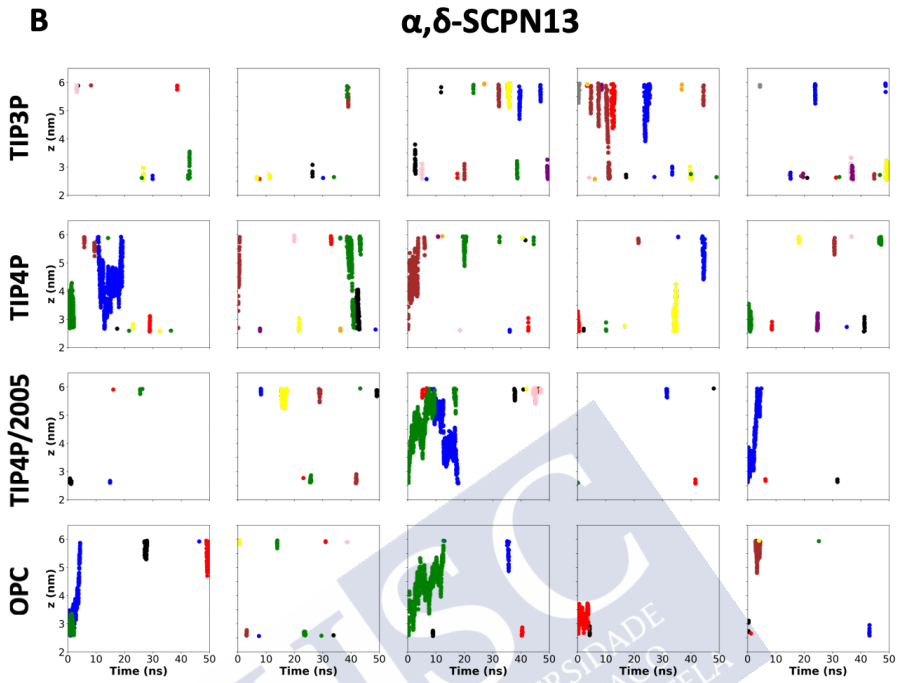

Figure 75. *Z-coordinate for each of the cations inside the* ***A) α,γ-SCPN12*** *and* ***B) α,δ-SCPN13*** *B) along the 50 ns trajectory. The nanotube z-region is taken to be between ≈2-6 nm. Each column corresponds to a different replica. Each colour corresponds to a different ion.*

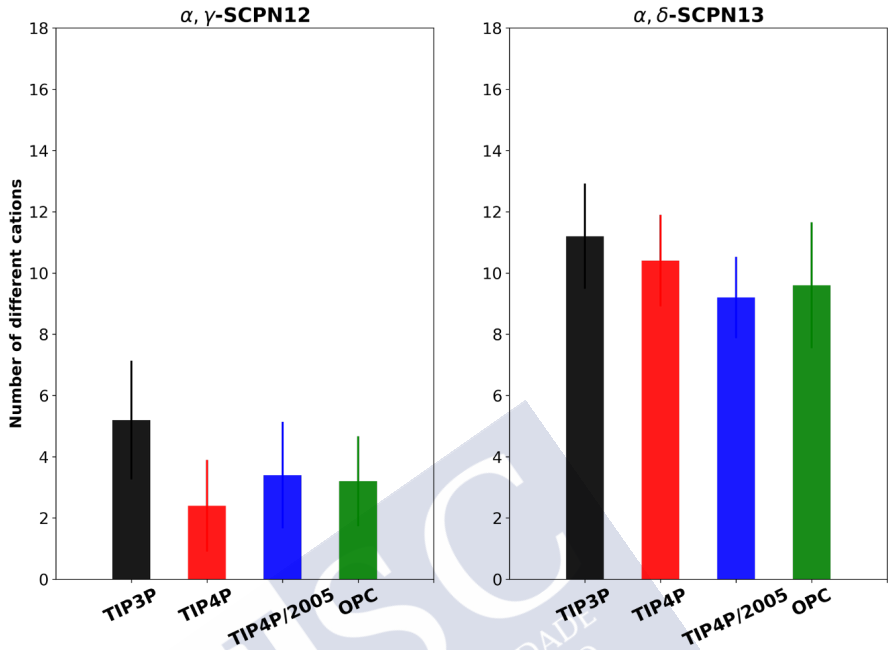

***Figure 76.** Total number of different cations which enter inside both nanotubes along the 50 ns of simulation averaged over the five replicas in TIP3P, TIP4P, TIP4P/2005 and OPC. Standard deviations are given as error bars.*

Finally, the coordination of the cations inside the nanotube was evaluated by analysing the number of oxygen atoms within their first coordination layer (**Figure 77**). This calculation shows that for both nanotubes a number of water molecules are coordinated to the cations when they are inside the SCPN, finding no differences between the different water models. Additionally, although the same coordination number is observed for both peptides (6), the oxygens come from different molecules depending on the type of SCPN. For the **α,δ-SCPN13**, it has been found that the six interactions correspond to water molecules. Contrary, in the case of the **α,γ-SCPN12**, the cations are coordinated to five water molecules and one carbonyl group, probably due to the smaller radius of this SCPN.

A

	α,γ-SCPN12		α,δ-SCPN13	
	Water	C=O (BB)	Water	C=O (BB)
TIP3P	5±1	1±1	6±1	0
TIP4P	5±1	1±1	6±1	0
TIP4P/2005	5±1	1±1	6±1	0
OPC	5±1	1±1	6±1	0

B

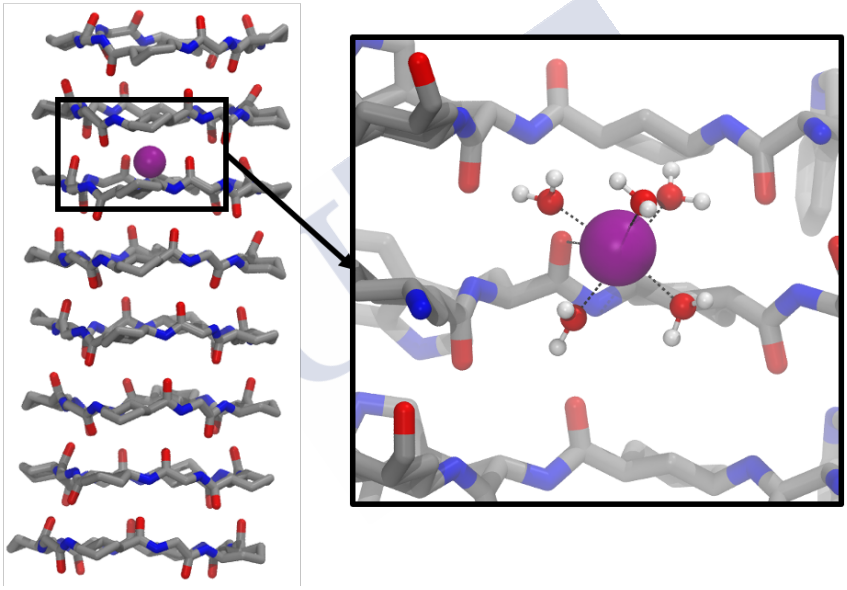

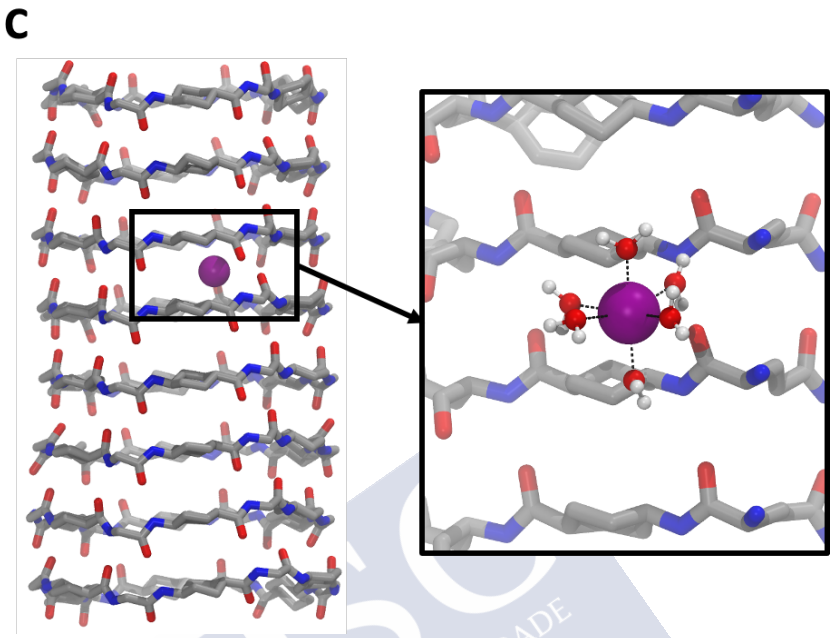

***Figure 77. A)** Averaged number of oxygen atoms from the water and the carbonyl groups of the amino acids of the backbone of the SCPNs coordinated to the cations inside the nanotube. This number was defined as the number of oxygen atoms within a cut-off of 3.2 Å (approx. the end of the first coordination sphere observed in the RDF calculation. **B)** Detail of the coordination pattern of a cation inside the **α,γ-SCPN12**, in which 5 waters and 1 carbonyl group are coordinated to a cation (purple sphere). **C)** Detail of the coordination pattern of a cation inside the **α,δ-SCPN13**, in which 6 waters are coordinated to a cation (purple sphere).*

7.5. CONCLUSIONS.

A systematic AA-MD simulation study comparing the behaviour of four water models (TIP3P, TIP4P, TIP4P/2005 and OPC) inside two sizes of self-assembled cyclic peptide nanotubes (**α,γ-SCPN12** and **α,δ-SCPN13**) has been carried out. This has enabled us to investigate how water models affect the behaviour of supramolecular tubes acting as transmembrane channels. All the SCPNs preserve their tubular structure across all the trajectories, independently of the water model selected. However, the results show that the dynamics of the water

molecules, and their interactions with the cyclic peptides present in the nanopores depend on the water model employed.

TIP3P exhibits the fastest dynamics, as indicated by the higher mean displacement values and significantly shorter nanotube filling times, followed by TIP4P. Interestingly, the two more modern water models OPC and TIP4P/2005, which both provide good results in bulk water, show quite similar dynamic properties, as can be concluded from the analysis of the velocities of the encapsulated waters, from the survival probability inside the nanotube and from the H-bond lifetimes with the SCPN. The velocity of the water molecules confined inside the channel was TIP3P > TIP4P > TIP4P/2005 ≈ OPC, independently of the nanotube model. This trend is in accordance with that for bulk water, indicating that the confined environment studied here did not have a significant impact on this overall trend.

The density of the water inside the channels is quite similar for all the water models. Interestingly, we have found that the side-chain properties of the CPs that form the SCPNs (outer properties) can influence the inner water arrangement, and thus in the internal behaviour of transmembrane channel. This finding opens the door to the modulation of channel permeability by modifying its external surface when inserted into a lipid bilayer.

Furthermore, both nanotubes exhibit a selectivity for cations over anions, although this is more pronounced for the **α,γ-SCPN12** as it completely blocks the passage of chloride ions. In the case of **α,δ-SCPN13**, some anions enter the channel, probably due to its higher internal radii and the greater exposure of hydrophobic residues towards the inner cavity and the possibility of entering as an ion pairs. Additionally, the choice of water model also affects the number of ions found inside the channels. The simulations with TIP3P exhibit a higher number of cations entering the nanotube, highlighting the role of the water model in ion transport properties. Furthermore, it has been proven that the cations inside the channel are coordinated to water molecules (6 in the case of **α,δ-SCPN13**, 5 for **α,γ-SCPN12**), with no differences between the water models. For the narrower nanotube, the vacant coordination position is fulfilled with an oxygen from the carbonyl groups of the skeleton of the peptide, suggesting that the pore size of

such SCPN is not enough for transporting Na^+ preserving its whole first coordination layer.

The significance of this study resides in the importance of research into transmembrane ion channels formed by cyclic peptides. Our results show that ion and water transport rates depend on the water model employed for the simulations. The obtained results follow the expected trend for bulk properties. However, it is important to note that none of these models was specifically designed for simulations of water in nanotubes and, in the absence of wet-lab experimental structural and dynamic data of water in SCPNs, it is not possible to assess which of them predict more accurately the water reality in the channel. We therefore propose that this data set could be used as a point of reference for wet-lab experiments. Such a comparison is important for the validation of water models in confined systems. This study was carried out during a predoctoral stay at the group of Prof. Mark S. P. Sansom (Oxford University) and resulted in the following publication: Calvelo, M.; Lynch, C.; Granja, J. R.; Sansom, M. S. P.; Garcia-Fandiño, R. *ACS Nano, accepted*.

USC
UNIVERSIDADE
DE SANTIAGO
DE COMPOSTELA

III. MD simulations of SCPNs with amphipathic sequences: exploring their antimicrobial capabilities

Although the antimicrobial action mechanism of amphipathic Ghadiri's SCPNs is not fully understood,[78,79,498] it has been proposed that CPs would assemble in the bilayer forming nanotubes with a parallel orientation to the membrane, exposing the hydrophobic face towards the lipids and the polar one towards the interface and the aqueous environment (**Figure 78)**. Individual CPs (as they are in the water phase), if designed properly, should not present toxicity, and only once they reach the membrane and start to self-assemble should adopt the active form, the SCPN. This new action mechanism, distinct to the one exhibited by most of the commercial antimicrobial agents of the market, which usually target proteins, is expected to help to provide new strategies for overcoming the acquired resistance of bacterial organism, one of the biggest worldwide problems nowadays.[499,500] Although this mechanism is similar to those proposed for membrane active antimicrobial peptides (AMPs),[428–430] it should be expected than the higher hierarchical mechanism of the CPs (stacking on nanotubes, formation of 2D-plates on the membrane and membrane disruption) should provide lowers toxicity and higher selectivity than natural AMPs.

78. Danial, M. et al. *Org. Biomol. Chem.* **2015**, *13* (8), 2464–2473.
79. Fernandez-Lopez, S. et al. *Nature* **2001**, *412* (6845), 452–455.
428. J. Bond, P. et al. *Protein Pept. Lett.* **2012**, *17* (11), 1313–1327.
429. Shai, Y. *Biopolym. - Pept. Sci. Sect.* **2002**, *66* (4), 236–248.
430. Kumar, P. et al. *Biomolecules* **2018**, *8* (1), 4.
498. Fu, Y. et al. *J. Phys. Chem. B* **2017**, *121* (38), 9006–9012.
499. Antimicrobial resistance https://www.who.int/en/news-room/fact-sheets/detail/antimicrobial-resistance.
500. Lack of new antibiotics threatens global efforts to contain drug-resistant infections https://www.who.int/news-room/detail/17-01-2020-lack-of-new-antibiotics-threatens-global-efforts-to-contain-drug-resistant-infections.

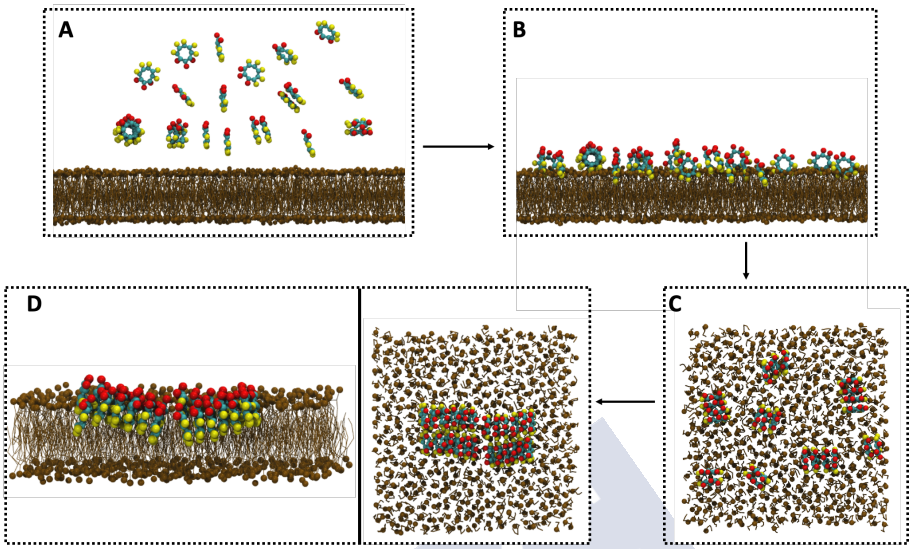

Figure 78. *Schematic representation of the proposed mechanism of action of CPs with an amphiphilic sequence. In the water phase (**A**), it is expected that they were not interacting or just forming small aggregates (dimers/trimers), whereas in presence of a target membrane (**B**), the insertion of the CPs into the lipid bilayer takes place. Once they reach the membrane, they would self-assemble into SCPNs (**C**). It is expected that several SCPNs also assemble, resulting in the formation of 2D-plates and producing the cell lysis (**D**). The hydrophobic lateral chains of the CPs are displayed in yellow, whereas those with a hydrophilic character are printed in red. The membrane lipids are showed in brown. Water molecules were not displayed for clarity.*

A detailed understanding of the molecular details of the membrane permeabilization process would allow the rational design of new molecules with the same mechanism of action, but with improved activity, selectivity, and bioavailability. Computer simulations can provide valuable insights in the field, especially shedding light about the conformation and secondary structure of the peptides, adsorption processes onto membrane surfaces, spontaneous assembly of multiple peptides and mechanisms that they follow until reach the membrane

lysis, for example.[428,501–503] Due to that most of the previous events occur at time scales longer that those reachable for AA resolution, Coarse Grained MD (CG-MD) simulations have emerged as a good alternative for the study of these systems.[504,505] In this way, during the next chapter, the use of two amphipathic CPs with proven antimicrobial properties will be tested under different lipid membrane environments, aiming at understanding their mechanism of action.

The obtained results revealed different orientations that the SCPNs adopt in the membrane depending on the negative character of the lipids. Additionally, the tubular structure stability also depends on the kind of the lipid present in the bilayer. These insights could be the first steps in the design of new antibiotic agents based on CPs that target selectively specific lipid compositions. This study is included in in Claro, B.; González-Freire, E.; Calvelo, M.; Bessa, L. J.; Goormaghtigh, E.; Amorín, M.; Granja, J. R.; Gracia-Fandiño, R.; Bastos, M. *Colloids and Surfaces B: Biointerfaces* **2020**, *196*, 111349.

Furthermore, in this chapter has been also included the validation of a new tool for the conversion of CG structures into AA coordinates, called *GADDLE Maps* and developed by the group of Prof. Luis Miguel Varela Cabo, from the University of Santiago de Compostela. The work carried out has been published in Otero-Mato, J. M.; Montes-Campos, H.; Calvelo, M.; García-Fandiño, R.; Gallego, L. J.; Pineiro, Á.; Varela, L. M. *J. Chem. Theory Comput.* **2018**, *14* (2), 466-478.

428. J. Bond, P. et al. *Protein Pept. Lett.* **2012**, *17* (11), 1313–1327.
501. Matyus, E. et al. *Curr. Med. Chem.* **2007**, *14* (26), 2789–2798.
502. Arasteh, S. et al. *Methods Mol. Biol.* **2017**, *1548*, 103–118.
503. Cirac, A. D. et al. *Biophys. J.* **2011**, *100* (10), 2422–2431.
504. Balatti, G. E. et al. *J. Mol. Model.* **2018**, *24* (8), 208.
505. Balatti, G. E. et al. *Molecules* **2017**, *22* (10).

Author affiliations:
-Calvelo, M.; Lamas, A.; Guerra, A.; Amorín, M; García-Fandiño, R.; Granja, J. R. and González-Freire, E.: Centro Singular de Investigación en Química Biolóxica e Materiais Moleculares (CiQUS), Departamento de Química Orgánica, Universidade de Santiago de Compostela, 15782 Santiago de Compostela, Spain
-Claro, B. and Bastos, M.: CIQUP, Centro de Investigação em Química, Departamento de Química e Bioquímica, Faculdade de Ciências, Universidade do Porto, Porto, Portugal
-Bessa, L. J.: LAQV/Requimte, Departamento de Química e Bioquímica, Faculdade de Ciências da Universidade do Porto, Porto, Portugal
-Goormaghtigh, E.: Structure and Function of Biological Membranes, Center for Structural Biology and Bioinformatics, ULB, Brussels, Belgium
-Otero-Mato, J. M.; Montes-Campos, H.; Gallego, L. J. and Varela, L. M.: Nanomaterials, Photonics and Soft Matter Group, Departamento de Física de Partículas y Departamento de Física Aplicada, Facultade de Física, Universidade de Santiago de Compostela, 15782 Santiago de Compostela, Spain
-Piñeiro, Á.: Soft Matter and Molecular Biophysics Group, Departamento de Física Aplicada, Facultade de Física, Universidade de Santiago de Compostela, 15782 Santiago de Compostela, Spain

8. Antimicrobial SCPNs targeting lipid membrane compositions

8.1. PRECEDENTS AND MOTIVATION.

Bacterial resistance is a natural life mechanism to ensure survival of life. However the acquired resistance has been exacerbated since the discovery of antibiotics due to their abuse and misuse to the point that *World Health Organization* (WHO) has declared some bacterial organism as one of the biggest challenges which mankind needs to face.[499,500] In order to overcome such problem, an intensive research in this area is required looking for new antibiotic paradigms.[506,507] In this sense, AMPs, especially those with an hydrophobic/cationic character, appeared as a promising alternative to conventional therapeutics, thanks to the fact that they are supposed to target bacterial membranes (partially negative charged), contrary to classical antibiotic agents, which are focused in other elements, as transmembrane proteins, for example.[508–511] These compounds, which are present in the innate immune system of most organism for pathogen inactivation, have interesting antimicrobial activity against different cell lines, including Gram-positive and Gram-negative bacteria.[511–515]

499. Antimicrobial resistance https://www.who.int/en/news-room/fact-sheets/detail/antimicrobial-resistance.
500. Lack of new antibiotics threatens global efforts to contain drug-resistant infections https://www.who.int/news-room/detail/17-01-2020-lack-of-new-antibiotics-threatens-global-efforts-to-contain-drug-resistant-infections.
506. Payne, D. J. *Science.* **2008**, *321* (5896), 1644–1645.
507. Bassetti, M. et al. *Ann. Clin. Microbiol. Antimicrob.* **2013**, *12* (1), 1–15.
508. da Cunha, N. B. et al. *Drug Discov. Today* **2017**, *22* (2), 234–248.
509. Fjell, C. D. et al. *Nat. Rev. Drug Discov.* **2012**, *11* (1), 37–51.
510. Mahlapuu, M. et al. *Front. Cell. Infect. Microbiol.* **2016**, *6* (12), 194.
511. Silva, T. et al. *Biochim. Biophys. Acta - Biomembr.* **2013**, *1828* (5), 1329–1339.
512. Pasupuleti, M. et al. *Crit. Rev. Biotechnol.* **2012**, *32* (2), 143–171.
513. Wiesner, J. et al. *Virulence* **2010**, *1* (5), 440–464.
514. Yeung, A. T. Y. et al. *Cell. Mol. Life Sci.* **2011**, *68* (13), 2161–2176.
515. Zasloff, M. *Nature* **2002**, *415* (6870), 389–395.

On the other hand, one of the biggest limitations of these systems is that their mechanism is not completely clear, which limits the design of synthetic peptides.[516] Nonetheless, it is supposed that the aggregation of these peptides could open membrane pores that potentially disrupt the electric potential, killing the cell.[517–519]

Cyclic AMPs have also been proposed as potential antibiotic candidates based on their promising antimicrobial activity.[520–522] Additionally, it has been reported that, in some cases, the cyclic structure presented better results than the analogous linear sequence.[523,524] Some of the most famous cyclic AMPs, such as Gramicidin S, are able to self-assembly and form β-structures and, eventually, result in nanotubes.[525,526] The adoption of such a strong secondary structure provides interesting features to these molecules, since it could prevent them to protease degradation.[523] It is not difficult to establish a relation between these systems with *D,L*-α-CP,[72] since they present quite similar features. Actually, antimicrobial activity has been already proved in amphipathic *D,L*-α-CP, showing high results against Gram-positive and Gram-negative bacteria and low activity against mammalian cells.[79,80] Furthermore, very recently it has been demonstrated that these CPs are able to remodel the mouse gut microbiome, inhibiting the development of atherosclerosis[527]

During last decades, the importance of bacterial membrane compositions has been clearly revealed, having been found that a same peptide could interact differently depending on the presence of certain

72. Ghadiri, M. R. et al. *Nature* **1993**, *366* (6453), 324–327.
79. Fernandez-Lopez, S. et al. *Nature* **2001**, *412* (6845), 452–455.
80. Dartois, V. et al. *Antimicrob. Agents Chemother.* **2005**, *49* (8), 3302–3310.
516. Wimley, W. C. et al. *J. Membr. Biol.* **2011**, *239* (1–2), 27–34.
517. Leontiadou, H. et al. *J. Am. Chem. Soc.* **2006**, *128* (37), 12156–12161.
518. Jean-François, F. et al. *Biophys. J.* **2008**, *95* (12), 5748–5756.
519. Regen, S. L. *JACS Au* **2020**, jacsau.0c00037.
520. Wu, M. et al. *Antimicrob. Agents Chemother.* **1999**, *43* (5), 1274–1276.
521. Jelokhani-Niaraki, M. et al. *J. Pept. Res.* **2002**, *60* (1), 23–36.
522. Qian, Z. et al. *Biochemistry* **2016**, *55* (18), 2601–2612.
523. Mika, J. T. et al. *Biochim. Biophys. Acta - Biomembr.* **2011**, *1808* (9), 2197–2205.
524. Ongwae, G. M. et al. *ACS Infect. Dis.* **2020**, *6* (6), 1427–1435.
525. Mihailescu, D. et al. *J. Phys. Chem. B* **1999**, *103* (9), 1586–1594.
526. Mihailescu, D. et al. *Biophys. J.* **2000**, *79* (4), 1718–1730.
527. Chen, P. B. et al. *Nat. Biotechnol.* **2020**, *38*, 1288–1297.

lipids.[528–530] The behaviour exhibited by a specific AMP in presence of bilayers with different lipid composition could be extrapolated to its potential antimicrobial activity against diverse cell lines. Additionally, a link between the peptide sequence also influences critically to their binding to essential components of bacterial membranes.[531] In this way, studying a wide range of lipid compositions as well as a number of peptide sequence appears as decisive for a deep understanding of these systems, something absolutely necessary for a proper *bottom-up* design of synthetic AMPs.

Previous works evaluating the interaction between *D,L*-α-CPs and a lipid membrane have been reported.[79,111–113] Using CG and AA-MD simulations, Hwang studied the orientation of hydrophobic SCPNs in a membrane, being able to observe the spontaneous insertion of the nanotube into the membrane, adopting a channel structure.[111] Also Tarek was able to extract similar conclusions working with a CP composed by Trp and Leu.[112] Additionally, this author has also reported studies using an amphiphilic sequence, whose antimicrobial activity had been previously demonstrated by the group of Ghadiri (**CP15**, **Figure 79**).[79,113] In this work, CG-MD simulations performed at various concentrations of **CP15** interacting with membranes made by POPE:POPG (3:1) have suggested a type of mechanism in which the peptides first self-assemble at the membrane interface, forming amphipathic nanotubes with the hydrophilic surface pointing towards the water phase. Those results were reproduce independently on the starting structure (individual randomly distributed CPs, pre-assembled SCPNs,…) suggesting that the interaction with the membrane is triggered by strong electrostatic interactions between the charged peptides and the lipid head groups.

79. Fernandez-Lopez, S. et al. *Nature* **2001**, *412* (6845), 452–455.
111. Hwang, H. et al. *J. Phys. Chem. A* **2009**, *113* (16), 4780–4787.
112. Khalfa, A. et al. *Chem. Phys.* **2009**, *358* (1–2), 161–170.
113. Khalfa, A. et al. *J. Phys. Chem. B* **2010**, *114* (8), 2676–2684.
528. Cheng, J. T. J. et al. *Biochim. Biophys. Acta - Biomembr.* **2011**, *1808* (3), 622–633.
529. Hancock, R. E. W. et al. *FEMS Microbiol. Lett.* **2002**, *206* (2), 143–149.
530. Li, X. et al. *J. Phys. Chem. B* **2019**, *123* (49), 10433–10440.
531. Schmitt, P. et al. *Biochim. Biophys. Acta - Biomembr.* **2016**, *1858* (5), 958–970.

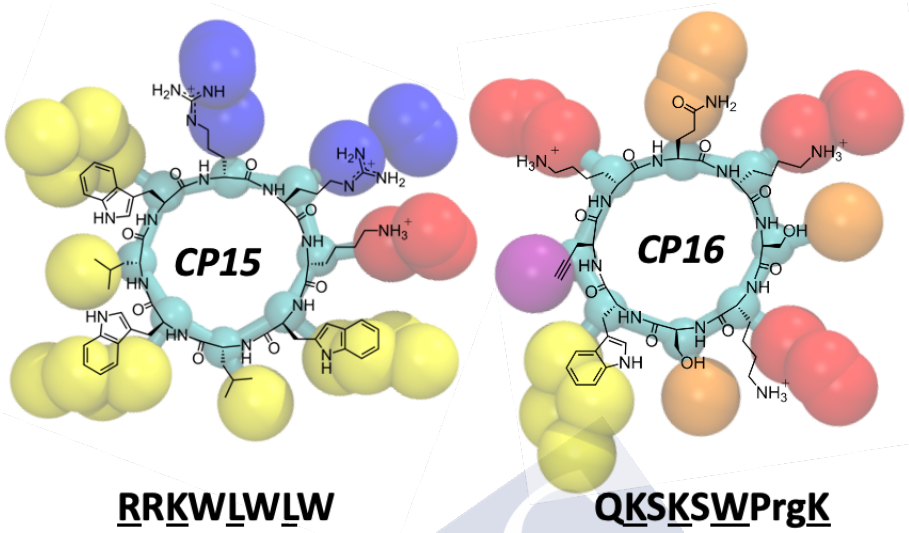

Figure 79. *2D and 3D structures of peptides **CP15** and **CP16** used in this study, together with their sequence, in which the underlined amino acids are D-residues. Lys are represented in red, Arg in blue, orange was used for the non-charged polar residues (Gln and Ser) and purple represents the alkyne moiety. The rest of the residues of the SCPN are shown in yellow. *Prg in sequence of **CP16** means propargylglycine. Considering all Arg and Lys protonated, each CP has an overall charge +3.*

8.2.AIM.

As it was mentioned in the introduction of this section, amphipathic *D,L*-α-CPs have been proposed to self-assemble in membranes leading to SCPNS following an antiparallel β-sheet structure, and oriented in parallel to the membrane, leaving the hydrophobic residues pointing the lipids and the hydrophilic units towards the water phase. Thus, in order to elucidate the mechanism of action of this kind of CPs, the orientation of two SCPNs (**SCPN15** and **SCPN16**, each composed by eight units of **CP15** and **CP16**, **Figure 79**) in different lipid bilayers (DMPC, DMPC/DMPG 3:1, DMPE/DMPG 3:1 and DMPE/DMPG 1:9) was evaluated. For that, MD simulations of pre-assembled nanotubes starting in water were carried out, evaluating their self-insertion in a range of different bacterial membrane models as well as the dispositions that they adopted. Due to the presumable unreachable time scale for simulations using AA resolution, CG-MD calculations were

carried out, since this resolution allows to perform simulations during longer times. Nevertheless, we have to consider the loss of accuracy inherent to the simplifications made in the model. In this way, and trying to overcome this situation, the performance of an algorithm for backmapping CG structures into AA coordinates will be tested.

It is expected that this study provides useful insights about the action mechanism of these potential antibiotic candidates, having in mind the developing of peptides that attack selectively specific lipid membrane compositions. The results obtained may bring useful information that could help to a more rational design of antimicrobial SCPNs.

8.3. METHODS.

Coarse-grained molecular dynamics (CG-MD) simulations of **SCPN15** and **SCPN16** interacting with different lipid bilayers were carried out. It is important to note that in these simulations all Arg and Lys residues will be treated as protonated residues considering that at physiological pH both groups are protonated, which leads to a charge +3 per CP. As models for bacterial membranes we used anionic 1,2-dimyristoyl-*sn*-glycero-3-phosphoethanolamine (DMPE) and 1,2-dimyristoyl-*sn*-glycero-3-phospho-(1'-*rac*-glycerol) (DMPG), since phosphoethanolamine (PE) and phospho-(1'-*rac*-glycerol) (PG) derivatives are known to be the main constituents of Gram negative (e.g., in E. coli there are 25% PG and 75% PE) and PG is the main component of Gram positive (57% in S. aureus and 70% in B. subtilis) plasma membranes.[530,532] In order to vary significantly the negative content of the membranes, to span a wide range of pathogens mimics and understand the role of membrane charge in the antimicrobial mechanism, we used mixtures of DMPE:DMPG at different molar ratios (3:1, 1:9). Neutral DMPC (1,2-dimyristoyl-*sn*-glycero-3-phosphocholine) lipid has been selected due to its regular presence in

530. Li, X. et al. *J. Phys. Chem. B* **2019**, *123* (49), 10433–10440.
532. Malanovic, N. et al. *Biochim. Biophys. Acta - Biomembr.* **2016**, *1858* (5), 936–946.

mammalian cells and absence in bacterial.[533] In this way, in order to elucidate the role of membrane composition in the antimicrobial mechanism, the different mixtures have been used were: pure DMPC, DMPC:DMPG (3:1), DMPE:DMPG (3:1), DMPE:DMPG (1:9).

The standard simulation parameters corresponding to the polarizable Martini Force Field (Martini v2.2P), together with the additional distance restraints (1000 $kJ \cdot mol^{-1} \cdot nm^{-2}$) between all the backbone particles, were used.[534,535] This approach allowed the spontaneous insertion and reorientation of the SCPNs into the lipid bilayer preserving their cylindrical shape, since it has been demonstrated that SCPNs in water are less stable than in a non-polar environment.[536] The CG topologies for the CPs were built using the martinize.py tool.[534] The bonds and charges of the CPs were manually modified to create the cycles. P5 type particles were used for describing the backbone of each amino acid. Additionally, in order to keep the characteristic cylindrical shape of these nanotubes, distance restraints ($k = 1000\ kJ \cdot mol^{-1} \cdot nm^{-2}$) were added for all the P5-P5 pairs. Subsequent CG-MD simulations of the pre-formed nanotubes in the membrane, releasing the restraints and limiting them to those necessary to maintain the CP opened and plane, were also carried out, following the strategy proposed by Tarek´s group.[113] Thus, for describing P5-P5 bond interactions, a harmonic potential was used, defining the equilibrium distance at 3.8 Å and a force constant of 6275 $kJ \cdot mol^{-1} \cdot nm^{-2}$. The P5-P5-P5 angle was described using a harmonic angle potential with θ_0 of 135° and a force constant of 627 $kJ \cdot mol^{-1} \cdot rad^{-2}$. In order to keep the planarity of the lateral chains, the $P5_1$-$P5_2$-$P5_3$-(lateral chain particle)$_2$ improper dihedral was described using a harmonic potential with ξ_0= 180° and a force constant of 418 $kJ \cdot mol^{-1} \cdot rad^{-2}$.

113. Khalfa, A. et al. *J. Phys. Chem. B* **2010**, *114* (8), 2676–2684.
533. Yeagle, P. L. et al. *Membr. Cells* **2016**, 189–218.
534. De Jong, D. H. et al. *J. Chem. Theory Comput.* **2013**, *9* (1), 687–697.
535. Yesylevskyy, S. O. et al. *PLoS Comput. Biol.* **2010**, *6* (6), e1000810.
536. Vijayakumar, V. et al. *J. Mol. Model.* **2016**, *22* (11), 1–12.

The membrane structures were prepared using the CHARMM membrane builder.[537–539] The parameters for DMPC, DMPE and DMPG were the standard provided for the Martini developers.[540] Each membrane was composed by ∼500 lipids and was inserted in a simulation box of 12.5 x 12.5 x 15 nm^3. In order to neutralize the charges of the anionic lipids and the SCPNs, the minimum of ions needed for compensating them were added. The CG calculations were carried out at 300 K using the V-rescale thermostat and the Parrinello−Rahman barostat with semi-isotropic pressure coupling.[215,423] A time step of 25 fs was used for all simulations. At least 1 μs was carried out in each case. All the simulations were done using GROMACS 2018.3.[424]

For the backmapping simulations, the tool GADDLE Maps has been developed and tested for switching the CG system into AA resolution. 150 ns of CG-MD simulations were performed using the non-polarizable Martini Force Field v2.2 following the same conditions above mentioned.[534,538,541] The system was mapped to AA and extended during 20 ns using OPLS-AA as Force Field.[542,543]

The tilt and the number of contacts have been calculated using written code using the python MDAnalysis library.[426] Graphs were plotted using the python Matplotlib library, whereas pictures of the molecules were obtained with VMD.[231,427]

215. Parrinello, M. et al. *J. Appl. Phys.* **1981**, *52* (12), 7182–7190.
231. Humphrey, W. et al. *J. Mol. Graph.* **1996**, *14* (1), 27-28,33-38.
423. Bussi, G. et al. *J. Chem. Phys.* **2007**, *126* (1), 014101.
424. Abraham, M. J. et al. *SoftwareX* **2015**, *1–2*, 19–25.
426. Michaud-Agrawal, N. et al. *J. Comput. Chem.* **2011**, *32* (10), 2319–2327.
427. Hunter, J. D. *Comput. Sci. Eng.* **2007**, *9* (3), 99–104.
534. De Jong, D. H. et al. *J. Chem. Theory Comput.* **2013**, *9* (1), 687–697.
537. Jo, S. et al. *J. Comput. Chem.* **2008**, *29* (11), 1859–1865.
538. Hsu, P.-C. C. et al. *J. Comput. Chem.* **2017**, *38* (27), 2354–2363.
539. Wu, E. L. et al. *J. Comput. Chem.* **2014**, *35* (27), 1997–2004.
540. Marrink, S. J. et al. *J. Phys. Chem. B* **2004**, *108* (2), 750–760.
541. Monticelli, L. et al. *J. Chem. Theory Comput.* **2008**, *4* (5), 819–834.
542. Siu, S. W. I. et al. *J. Chem. Theory Comput.* **2012**, *8* (4), 1459–1470.
543. Robertson, M. J. et al. *J. Chem. Theory Comput.* **2015**, *11* (7), 3499–3509.

8.4.RESULTS OF CG-MD SIMULATIONS WITH SCPN15 AND SCPN16. Tarek's studies showed a great tendency of **CP15** for aggregating onto the hydrophilic surface of a POPE:POPG (3:1) membrane.[113] Thus, CG-MD simulations of preassembled nanotubes composed by eight subunits of **CP15** and **CP16**, resulting in **SCPN15** and **SCPN16**, respectively, were carried out in presence of different membrane compositions (see *Methods*): DMPC, DMPC:DMPG (3:1), DMPE:DMPG (3:1) and DMPE:DMPG (1:9). Among the possible relative orientations that the CPs can adopt along the nanotube, an antiparallel β-sheet structure was assumed, since it has been shown as the most stable favourable for *D*,*L*-α-SCPNs.[258] Moreover, for **SCPN15** we decided to align all Trp units along the nanotube, defining clearly a hydrophobic face (**Figure 80***A*). In the antiparallel **SCPN16** the Trp would be alternated with the Lys, stablishing a cation-π interaction as driving force,[544] while all the Prg would be aligned along the nanotube (**Figure 80***B*). The final aim of this study is to understand the basis of the initial interaction of each nanotube with the different membrane compositions. Consequently, only one SCPN was simulated in each calculation without paying attention to concentration depending factors. Furthermore, initial simulations were carried out adding distance restraints between the particles of the backbone in order to ensure that the tubular shape of the nanotube (See *Methods*).

113. Khalfa, A. et al. *J. Phys. Chem. B* **2010**, *114* (8), 2676–2684.
258. Kobayashi, K. et al. *Angew. Chemie Int. Ed. English* **1995**, *34* (1), 95–98.
544. Gallivan, J. P. et al. *Proc. Natl. Acad. Sci. U. S. A.* **1999**, *96* (17), 9459–9464.

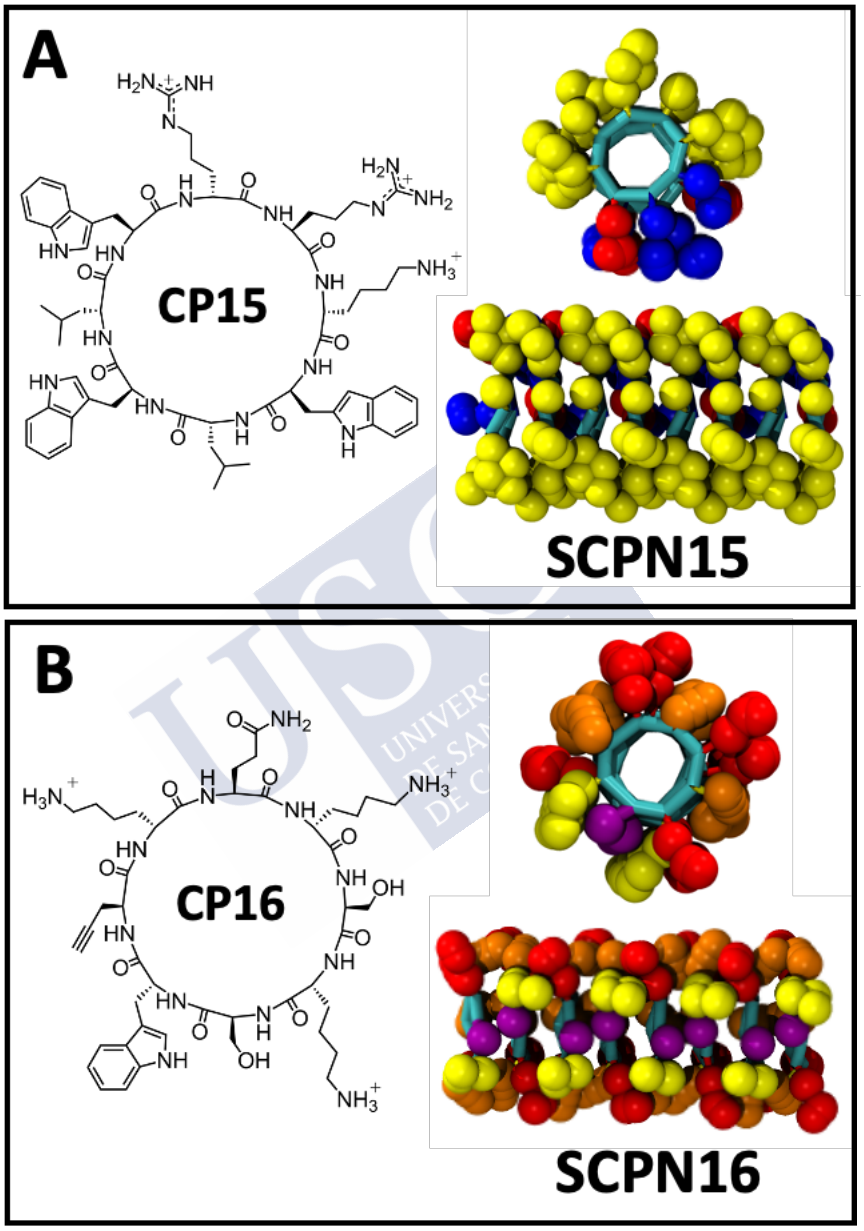
A
CP15
SCPN15
B
CP16
SCPN16

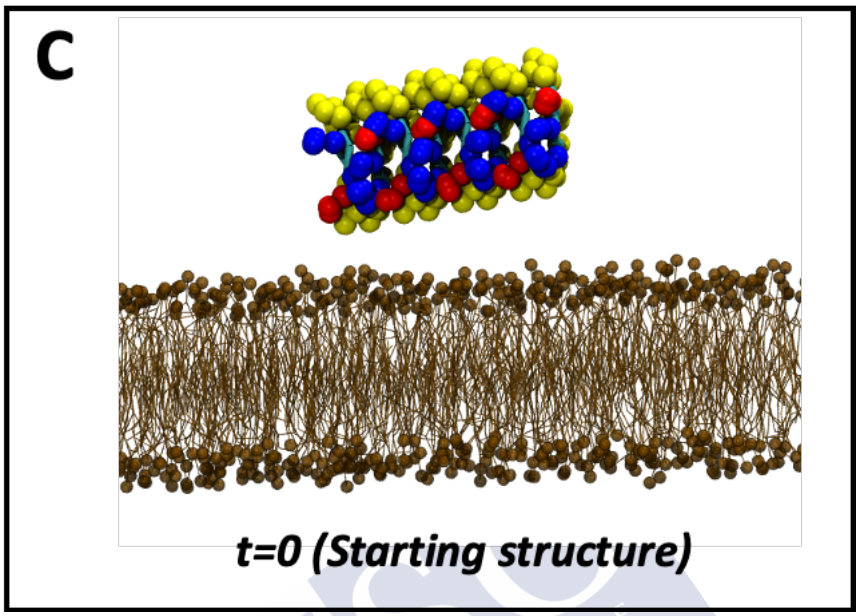

Figure 80. *2D and 3D CG-structure for* ***A) CP15*** *and* ***B) CP16*** *forming the corresponding SCPNs (****SCPN15*** *and* ***SCPN16****, respectively). Lys are represented in red, Arg in blue and purple represents the alkyne moiety. The polar non-charged amino acids (Ser and Gln) are displayed in orange. The rest of the residues of the SCPN are shown in yellow. In the initial structure (****C****) the SCPN is placed outside the membrane.*

Both SCPNs were placed initially in the vicinity of the membrane in a random orientation. A rapid spontaneous adsorption to the membrane interface was observed in all cases (**Figure 81**). In the case of **SCPN16**, the nanotube interacts with the membrane throughout its alkyne region, leaving these groups and the pair Trp/Lys in contact with the surface of the bilayer, while the remaining charged and polar groups are pointing towards the water phase, independently of the membrane composition. For **SCPN15** in DMPC, DMPC:DMPG (3:1) and DMPE:DMPG (3:1), it was found that the hydrophobic core (Trp-Leu-Trp-Leu-Trp) of the nanotube is deeply inserted in the membrane, being able to interact even with the lipids of the opposite leaflet, while the hydrophilic amino acids (Lys and Arg) remain in contact with the

water phase (**Figure 81**). This remarkable insertion of **SCPN15** could mean that **SCPN16** is less prone to interact with membranes, supporting this fact the invariance of the Differential Scanning Calorimetry (DSC) and its lower toxicity.[545] However, for the anionic membrane model with highest PG content, DMPE:DMPG (1:9), a twist of **SCPN15** has been observed. In this membrane model the SCPN adopts an orientation in which the Arg and Lys units are pointing towards the headgroups of the phospholipids, while the rest of hydrophobic core is exposed to the aqueous media. Although this disposition must have a higher energetic cost due to the exposition of the non-polar region towards the aqueous layer, the strong electrostatic interactions between the negative-charged head groups of PG and the positively charged residues of the SCPN must compensate it. It should be pointed out that the artificial restraints applied to maintain the nanotube force the positive charge residues of each CP to stay together. This computational gadget might lead to a possible overestimation of the electrostatic contributions. Additionally, in this membrane model **SCPN15** was not so deeply inserted into the bilayer compared to the other lipid compositions, probably as a consequence of exposing the hydrophobic Trp and Leu units towards the water phase.

545. Claro, B. et al. *Colloids Surfaces B Biointerfaces* **2020**, *196*, 111349.

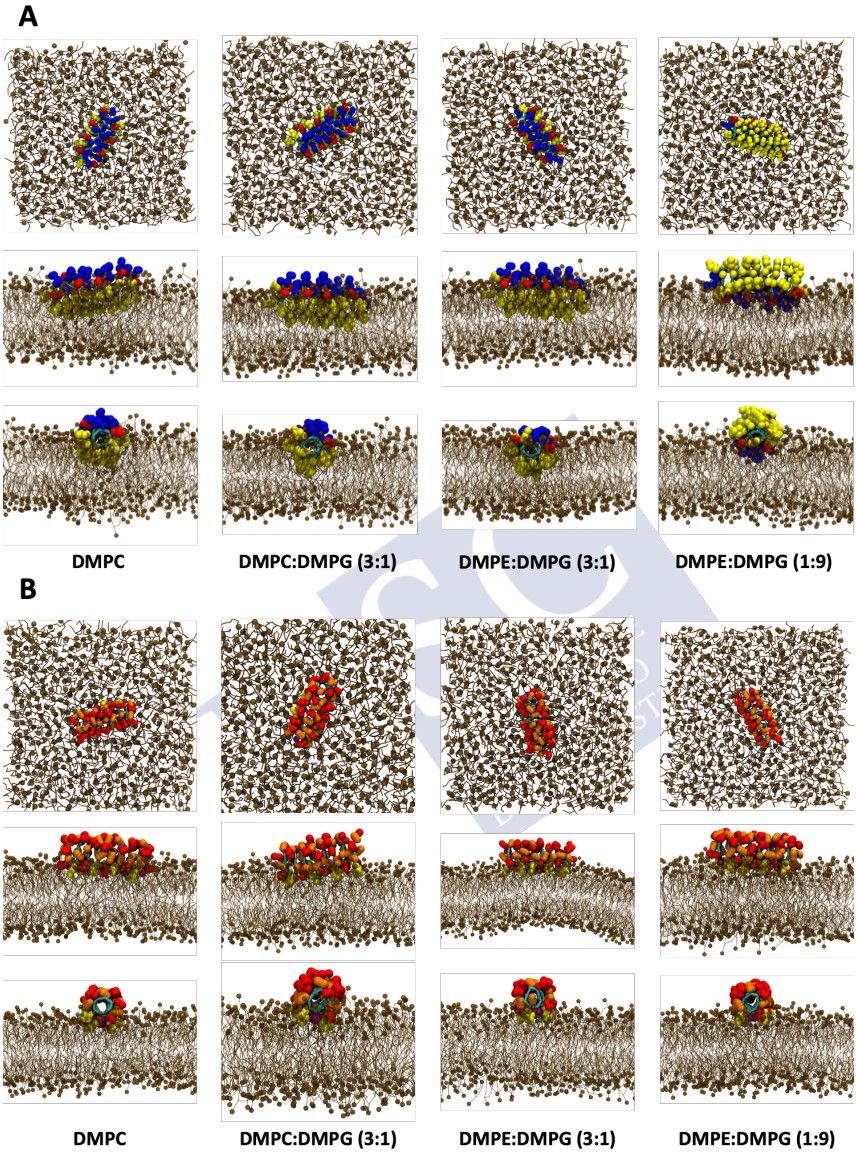

Figure 81. *Snapshots at t=1 μs for the CG-MD simulations of* ***A) SCPN15*** *and* ***B) SCPN16*** *in presence of different model membrane systems. In these computational studies, restraints to force the nanotube tubular shape preservation were used. One top (xy plane, top) and two lateral views [xz (middle) and yz (down)] are displayed for each nanotube and membrane*

composition. Lys are represented in red, Arg in blue, orange was used for the non-charged polar residues (Gln and Ser) and purple represents the alkyne moiety. The rest of the residues of the SCPN are shown in yellow. Water molecules have been removed for clarity.

The analysis of the tilt angles of the nanotubes, calculated with respect to the perpendicular axis of the membrane, exhibited more homogenous values for **SCPN16** than for **SCPN15** (**Figure 82**). Additionally, the most probable angles for **SCPN16** seem to be very close to 90º, which agrees with the parallel disposition with respect to the membrane proposed through the visualization of the last structures of the trajectories. **SCPN15**, however, showed slightly higher values, except for the simulation in DMPE:DMPG (1:9). This small increasement could be produced by the deeper insertion of this nanotube into the membranes. Similar results were obtained independently on the membrane, except for the previous mentioned **SCPN15** in DMPE:DMPG (1:9), in which the twist of the nanotube gives rise smaller angles.

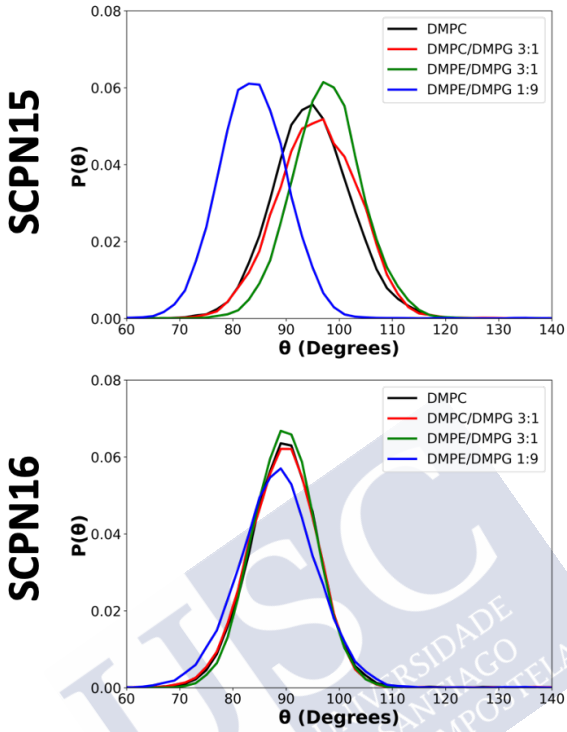

Figure 82. *Probability distribution of the tilt angles for the corresponding SCPNs (**SCPN15** and **SCPN16**) with respect to the z-axis of the membrane. (DMPC in black, DMPC:DMPG (3:1) in red, DMPE:DMPG (3:1) in green and DMPE:DMPG (1:9) in blue)*

To further improve characterization, CG-MD simulations during additional 500 ns starting from the structures generated after 1 μs were carried out but removing most of the nanotube restraints except those needed to keep the flat conformation of CPs. These calculations with **SCPN15** showed that the nanotube structures were only maintained for the experiments carried out with the membranes lacking PE, whereas with **SCPN16** the tubular shape was preserved for all membrane compositions (**Figure 83**). In DMPE:DMPG (3:1), **SCPN15** disassembled to form a shorter nanotube while the rest of CPs did not show any interactions among them. On the other hand, three small clusters are formed in DMPE:DMPG (1:9). Moreover, in this last case

the CPs changed its orientation, disposing their hydrophobic components embedded on the membrane.

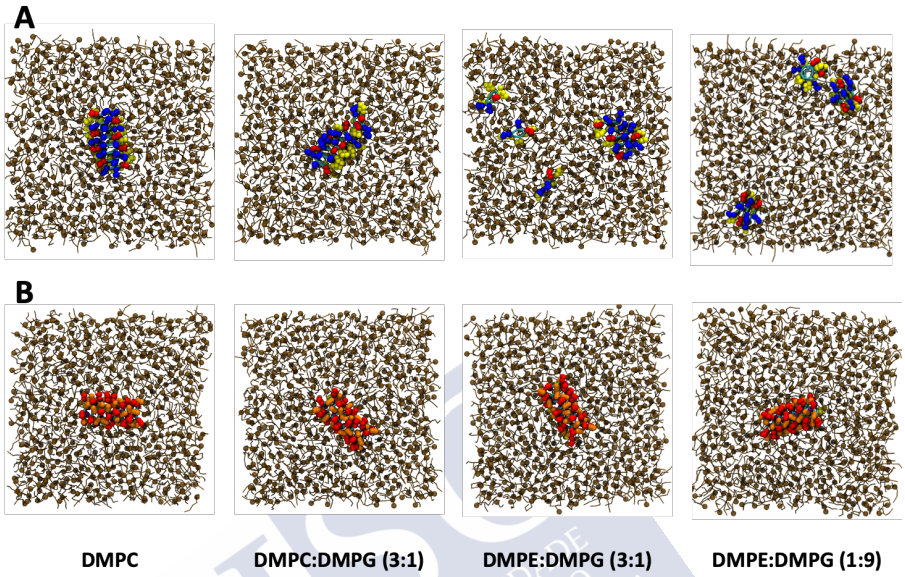

***Figure 83.** Top view snapshots at t=1.5 μs for **A) SCPN15** and **B) SCPN16** (B), in which the last 500 ns were carried out just keeping the restraints necessary to maintain the CP in the flat conformation. Lys are represented in red, Arg in blue, orange was used for the non-charged polar residues (Gln and Ser) and purple represents the alkyne moiety. The rest of the residues of the SCPN are shown in yellow. Water molecules have been removed for clarity.*

The number of contacts between lipids and peptides increased in the simulations where **SCPN15** was destroyed [DMPE:DMPG (3:1) and (1:9), **Figure 84**]. This occurs contrary to what was observed in the membranes containing PC, where the number of contacts between the CPs and the lipids is very similar after the releasing of the nanotube restraints. Thus, the releasing of the restraints that maintain the nanotube shape led to a better accommodation of the CPs and, consequently, an increase of the contacts of the CPs with lipids derived from ethanolamine (PE) and glycerol (PG). Therefore, these structural changes resulted in the destabilization of the nanotube. For **SCPN16**,

no significative changes were observed after releasing the nanotube's restraints.

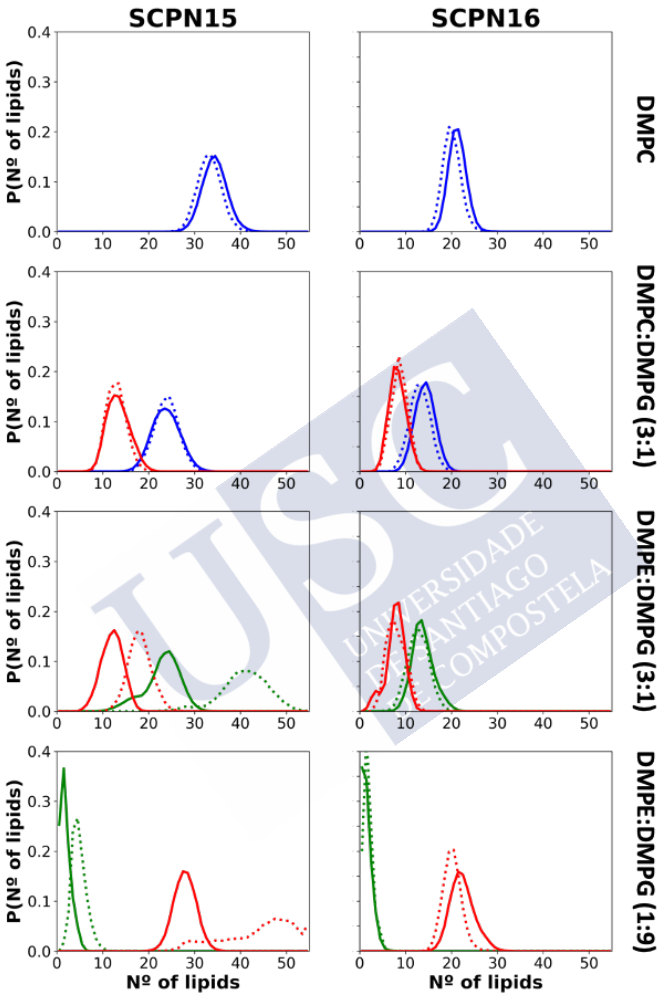

Figure 84. *Probability distribution of the number of contacts between the different lipids composing the membrane: blue for DMPC, red for DMPG and green for DMPE* ***and SCPN15*** *(top) and* ***SCPN16*** *(down), respectively. Dashed lines correspond to the CG-MD simulations after the releasing of the nanotube restraints.*

In order to check the reproducibility of the obtained results for **SCPN15** in membranes containing PE, two new replicas following the same protocol were performed in each one of those bilayers (**Figure 85**). These simulations revealed similar conclusions than those exposed previously. In presence of DMPE:DMPG (3:1), the restrained **SCPN15** was inserted in the membrane exposing the hydrophobic residues towards the lipidic environment leaving the hydrophilic core exposed to the aqueous media. After releasing the restraints, the CPs disassembled, as it had been seen previously. The simulations with DMPE:DMPG (1:9) also led to the same structure than before, with the hydrophobic amino acids in contact with the water molecules when the nanotube restraints were included. The following unrestrained calculation conduced again to the loss of the tubular shape, although in one of the replicas this fact was no so clear as in the other two simulations. Nonetheless, visualizing its trajectory it can be observed that the tubular shape is hugely distorted, which could suggest that the extension of the simulation time may lead to the disassembly of the nanotube.

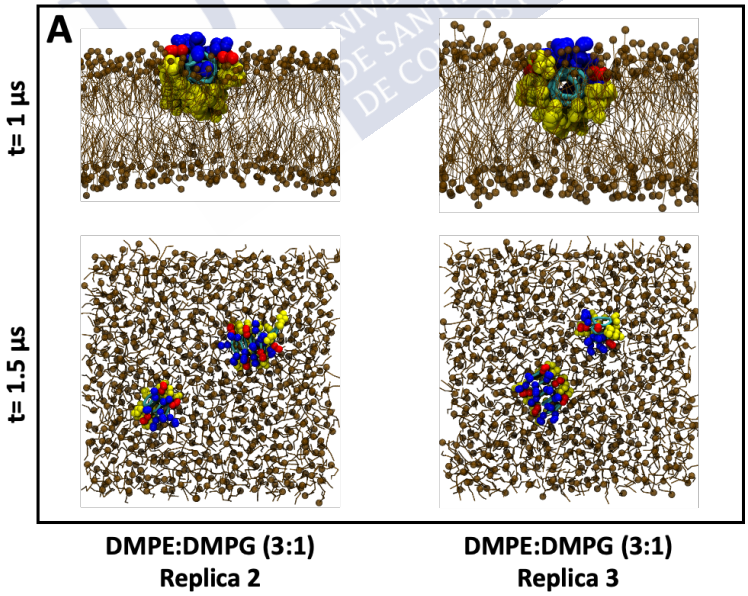

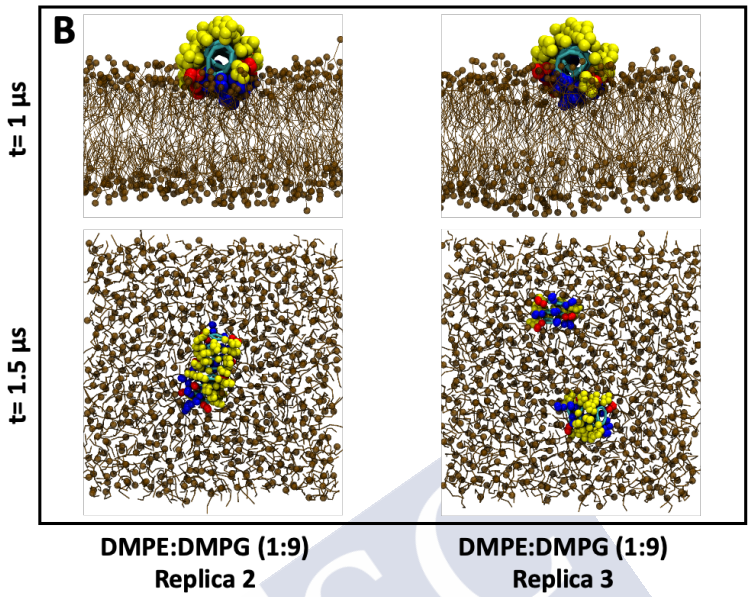

Figure 85. *Lateral view snapshots at t=1 µs for the two additional replicas of* ***SCPN15*** *applying restraints (top row) and top view snapshots at t=1.5 µs after extending the previous simulations for 500 ns but after removing the nanotube restraints (down row) in* ***A)*** *DMPE:DMPG (3:1) and* ***B)*** *DMPE:DMPG (1:9). Restraints needed for preserving the flat conformation of the CPs were kept. Lys are represented in red and Arg in blue. The rest of the residues of the SCPN are shown in yellow. Water molecules have been removed for clarity.*

With respect to the obtained results with **SCPN15** in DMPE:DMPG (1:9), it seems than once the restraints were removed, the tubular structure couldn´t be maintained because of the exposition of the hydrophobic surface to aqueous region, in which water molecules can start to compete for the backbone interactions while the non-polar residues try to reach the lipidic media of the membrane. In order to investigate the stability of the twisted SCPN, where the hydrophobic residues are forced to interact with the hydrophobic core of the membrane, a new simulation for **SCPN15** in presence of DMPE:DMPG (1:9) was performed but starting from a structure at *t*=1 µs but after rotating the nanotube to immerse the non-polar residues into the hydrophobic region of the membrane (**Figure 86**). In this case,

the restrained nanotube after 1 μs of simulation preserved this orientation, leading to a similar structure found with the other membranes, being also possible to find the interaction of the SCPN with the lipids of the opposite leaflet. However, the following 500 ns simulation in which the restrains were released gives rise again to the nanotube destruction, as in the previous cases.

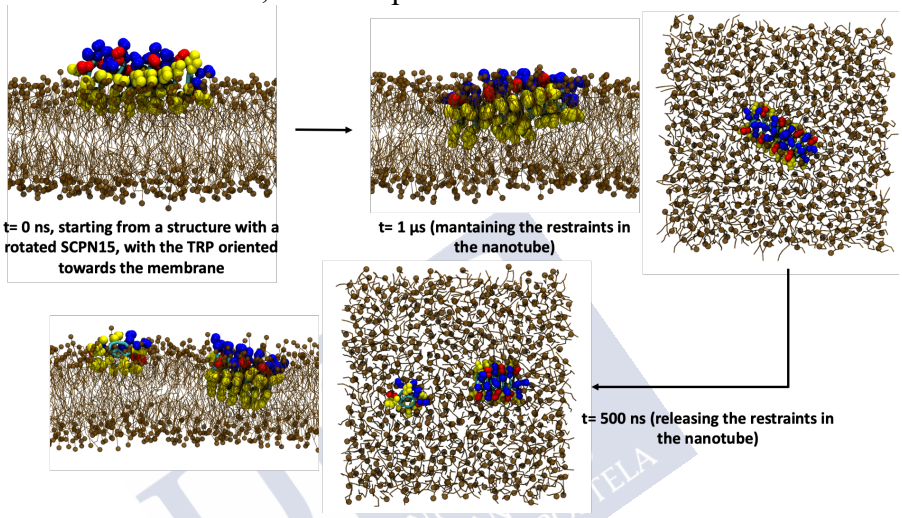

***Figure 86.** Snapshots resulting from the CG-MD simulation of DMPE:DMPG (1:9) and **SCPN15**, starting from a structure in which the nanotube was oriented with the hydrophobic residues inserted in the membrane. After 1 μs, the nanotube is immersed deeper in the membrane (centre and right in top line). After this time, the restraints were removed and the MD simulations were run for additional 500 ns. After this time, the tubular structure is destroyed (bottom pictures). Lys are represented in red and Arg in blue. The rest of the residues of the SCPN are shown in yellow. Water molecules have been removed for clarity.*

The influence of the concentration of CPs was also investigated performing analogous CG-MD simulations including four **SCPN15** units at the same time (**Figure 87**). We only carried out the simulation with **SCPN15** in membranes containing PE, since only in the presence of this lipid the nanotube lost its tubular structure. After 1 μs, the restrained nanotubes adopt the same orientation than in the previous cases. It is worth mentioning that in the simulation with 3:1 mixture of

DMPE:DMPG one nanotube is immersed deeply allowing the communication between both leaflets. In the presence of DMPE:DMPG (1:9), the nanotubes retain the previously observed arrangement for this media in which their hydrophobic part was exposed towards the aqueous phase. Interestingly under these conditions, it seems that the SCPNs tended to aggregate, forming cluster of nanotubes in a kind of reverse carpet-like structure.

As in previous studies, after this initial simulation a second calculation for 500 ns was carried out but after releasing the restraints. Once again, the resulting structure did not retain the nanotubular shape (**Figure 87**). This fact was clearer for the DMPE:DMPG (3:1) membrane, being also possible to observe some CPs deeply immersed in the hydrophobic region of the membrane. In the other membrane model, DMPE:DMPG (1:9), the nanotube also disassembled but the hydrophobic residues of the aggregate were disposed towards the aqueous environment.

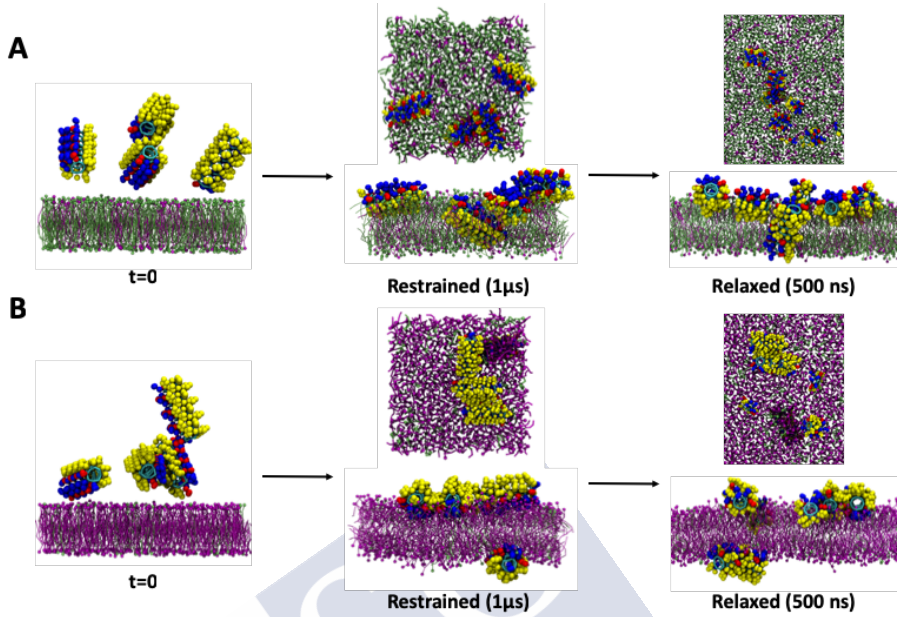

***Figure 87.** Snapshots of the CG-MD simulations using four **SCPN15**; on the left the initial input, in the centre the top and side view after 1 µs of simulation applying restraints to the nanotube and on the right top and side view of the output after 500ns of simulation of the nanotube without restraints in **A)** DMPE:DMPG (3:1) and **B)** DMPE:DMPG (1:9). DMPE lipids are displayed in green and DMPG in purple. Lys are represented in red and Arg in blue. The rest of the residues of the SCPN are shown in yellow. Water molecules have been removed for clarity.*

As it was mentioned, whereas the orientation of **SCPN15** in DMPE:DMPG (1:9), leaving the hydrophobic residues towards the water phase was stable and maintained when the nanotube was restrained, the release of the restraints led to the partial disassembly of **SCPN15**. The restraints applied to maintain the nanotube force the positively charged CPs to be artificially closer than they prefer to be. This is why when they are free to move, they apart from each other to avoid electrostatic repulsion, some of them rotate and the nanotube is disassembled. However, the conformation selected for this study, in which the Trp are all aligned (see *Methods*), is not the only one that can be adopted by the SCPN. Actually, there is a free rotation among all the

CPs and other orientations may be more favourable. With the aim of studying the effect of a different conformation, where the positively charged residues are not forced to be so near, we select a new CP organization (**SCPN15b**), in which one of the Trp was piled on top of a Arg residue, considering the previously mentioned cation-π interaction used in the **SCPN16** (**Figure 88***AB*).[544] Therefore, for each CP two Trp maintain the π-π stacking, while the third one is forming the cation-π pairing. Additionally, one Leu residue was also paired with a Lys. This new orientation preserves part of the amphipathic character of the nanotube, but place some of hydrophobic residues closer to the hydrophilic ones (**Figure 88***B*). CG-MD simulations during 1 μs applying restrains in order to keep the tubular shape led to similar structures than those obtained with the previous packing studied in **SCPN15**, with the hydrophobic face of the peptide oriented towards the membrane in all cases except for the DMPE:DMPG (1:9) system, in which cationic residues are paired with anionic phospholipids and consequently non-polar residues are oriented towards the water (**Figure 88***C*). Nevertheless, the SCPNs were less immersed into the membrane, and consequently they are not interacting with the opposite lipid leaflet. Next 500 ns simulations keeping only the restraints needed for preserving the flat conformation of the CPs showed again the destruction of the nanotube in the 3:1 DMPE:DMPG system, whereas the tubular shape was conserved in the simulation with DMPE:DMPG (1:9), contrary to the previously observed. This result reveals the important influence of the nanotube rotamers (the different tubular structures derived by the relative rotation of one CP with respect to the paired CPs) that appears as a key factor in their interaction with membranes. It is very likely that the different relative orientations of the CPs that constitute the nanotube could be determined by the membrane composition. These could open the door to a mechanism of adaptability of these systems to the environment through alternative rotations, in order to maximize the favourable interactions with the lipids. For this purpose, a new computational tool that could allow to evaluate a different number of supramolecular derivatives generated by simple rotational isomers in the presence of specific environments

544. Gallivan, J. P. et al. *Proc. Natl. Acad. Sci. U. S. A.* **1999**, *96* (17), 9459–9464.

would be required. This method could be a very valuable tool for searching for new supramolecular therapeutic strategies, prebiotic or abiotic systems or evolving materials. Finally, it is worth to mention that no differences were observed in the simulations in presence of PC after the releasing of the nanotube restraints, highlighting the huge stability of these structures in this kind of membranes.

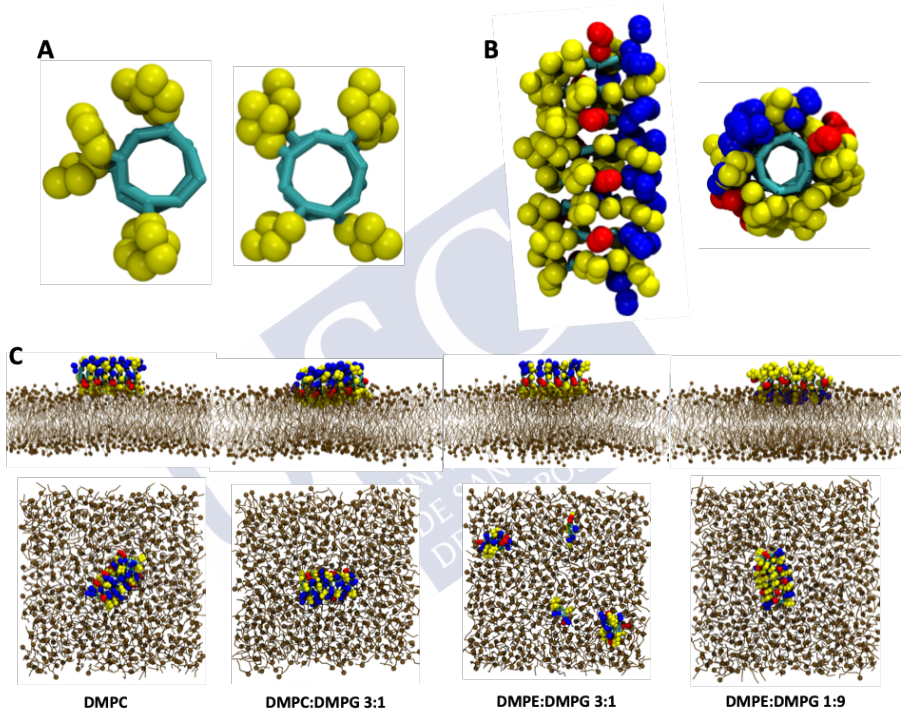

***Figure 88. A)** Schematic representation of two dimers of **CP15** in which only the Trp residues are represented, in order to highlight the difference between **SCPN15** and **SCPN15b**. **B)** Lateral and top view of the initial structure of **SCPN15b**. **C)** Results of the MD simulation starting from a structure with a different conformation of **SCPN15** (**SCPN15b**) where the Trp are not all aligned, in different membrane compositions. Top: Snapshots after 1 μs of simulation applying restraints to the nanotube. Down: Snapshots after 500 ns of simulation releasing the restraints and limiting them to those necessary to maintain the CP opened and plane. Lys are represented in red and Arg in blue. The rest of the residues of the SCPN are shown in yellow. Water molecules have been removed for clarity.*

8.5. COMING BACK TO AA RESOLUTION.

Thanks to CG methods, in which groups of atoms are represented by single particles, reducing the total number of degrees of freedom, the size of systems as well as the total time of MD simulations can be increased by more than two order of magnitudes.[540] This fact allows the study of processes which involve longer timescales than those available using classical atomistic resolution, as the assembly of nanotubes into membranes exposed above. However, this approximation involves a loss of accuracy due to lack of structural information provoked by this method in which not all the atoms are considered. This leads in some cases to the generation of some artefacts that provoke misunderstanding of the real behaviour of the studied system. In the case of SCPNs, for example, the use of CG implies that H-bonds are not explicitly considered. That is not a trivial issue, since the driven force for the assembly of these nanotubes is precisely the formation of H-bonds between the NH and C=O of peptide bonds. This interaction is treated in the Martini Force Field as an electrostatic interaction between the particles which corresponds to the backbone of the amino acids, leading to the loss of the directionality among other features of real H-bonds. Consequently, this fact avoids us distinguishing between parallel and antiparallel β-sheets, since each amino acid can form H-bonds across both faces at a time. It is worth to mention that some methods developed by other authors could help to overcome this problem, as the one suggested by Prof. Pavan.[546] In this approach, he proposed the use of polarizable particles in order to fill the lack of directionality of the H-bonds, reproducing the self-assembly of a water-soluble supramolecular polymer via CG-MD simulations maintaining a remarkably consistency with AA models.

540. Marrink, S. J. et al. *J. Phys. Chem. B* **2004**, *108* (2), 750–760.
546. Bochicchio, D. et al. *ACS Nano* **2017**, *11* (1), 1000–1011.

One alternative could be the use of *Multiscale Simulations*, that is, simulations considering more than one resolution, in an analogous way than QM/MM calculations. For example, it could be possible to perform MD simulations of solvated proteins treating the amino acids at AA level while the interactions with the solvent are carried out using CG. This approach should reduce considerably the number of particles which composes the system of study, enabling to reach longer time scales than using AA resolution, but without losing accuracy in the treatment of the protein. This approach has already been implemented quite successfully, although its application is not so straightforward as a fully AA or CG-MD calculation.[547–550] Additionally, the different cut-off used for the non-bonded interactions as well as the possible different functional form for the Coulomb and Lennard-Jones interactions used for AA and CG Force Fields, which is the case for Martini and OPLS-AA, could lead to unreal results, as an incorrect density of the Martini water, for example. Although these limitations can be overcome, the obtained results suggested that is still necessary a greater development of this approach before spreading its use.

The use of consecutive simulations at different resolutions has emerged as an interesting option.[551] This approach consists of performing a lengthy CG-MD simulation, which should describe processes that imply longer time scales, followed by an AA simulation. This combination allows to get further details at atomistic level. The bottleneck in this method is the *mapping* that imply the switch between CG and AA coordinates. Different tools have been proposed for an automatic conversion; so far, as the one developed by the group of Rzepiela.[552] Unfortunately, this method has the inconvenience that the equivalence between each CG particle in AA resolutions has to be known previously. Other two methods have been proposed by the Brocos' and Wassenaar's groups, being their use restricted to a series

547. Rzepiela, A. J. et al. *Phys. Chem. Chem. Phys.* **2011**, *13* (22), 10437–10448.
548. Wassenaar, T. A. et al. *J. Phys. Chem. B* **2013**, *117* (13), 3516–3530.
549. Sharp, M. E. et al. *J. Chem. Theory Comput.* **2019**, *15* (5), 3306–3315.
550. Goga, N. et al. *J. Chem. Theory Comput.* **2015**, *11* (4), 1389–1398.
551. Wassenaar, T. A. et al. *J. Chem. Theory Comput.* **2014**, *10* (2), 676–690.
552. Rzepiela, A. J. et al. *J. Comput. Chem.* **2010**, *31* (6), 1333–1343.

of molecules present in their corresponding libraries.[553,554] Furthermore, it is also worth to mention the tool developed by Stansfeld and Sansom, which was especially designed for the mapping of lipids.[555] However, these methods tend to be significatively complex, being their implementation to new molecules usually complicated.

Under this scenario, in collaboration with the group of Prof. Luis Miguel Varela Cabo, from the University of Santiago de Compostela, we participated in the validation of a new tool called *GADDLE Maps* (General Algorithm for Discrete object Deformations based on Local Exchange Maps), which has emerged as a good alternative to the previous mentioned methods.[556] The method is based on a Monte Carlo procedure and it is expected to be fully general. This would allow to convert any CG structure into AA coordinates without any additional code nor libraries, just a series of files (AA topology and coordinates) needed anyway for a classical MD simulation.

The whole algorithm is displayed in **Figure 89**. It works for any type of mapping, and thus it can be used for CG<->AA conversion. The information required for initiation the code is: (i) the CG coordinates of the system which is wanted to be mapped; (ii) the CG and AA topology files for each one of the compounds which are going to be mapped and (iii) one arbitrary AA coordinate file of one molecule of each one of the compounds to be mapped. Since these files are absolutely needed for any MD simulation, the general character of the tool is preserved.

553. Brocos, P. et al. *Soft Matter* **2012**, *8* (34), 9005–9014.
554. Wassenaar, T. A. et al. *J. Chem. Theory Comput.* **2014**, *10* (2), 676–690.
555. Stansfeld, P. J. et al. *J. Chem. Theory Comput.* **2011**, *7* (4), 1157–1166.
556. Otero-Mato, J. M. et al. *J. Chem. Theory Comput.* **2018**, *14* (2), 466–478.

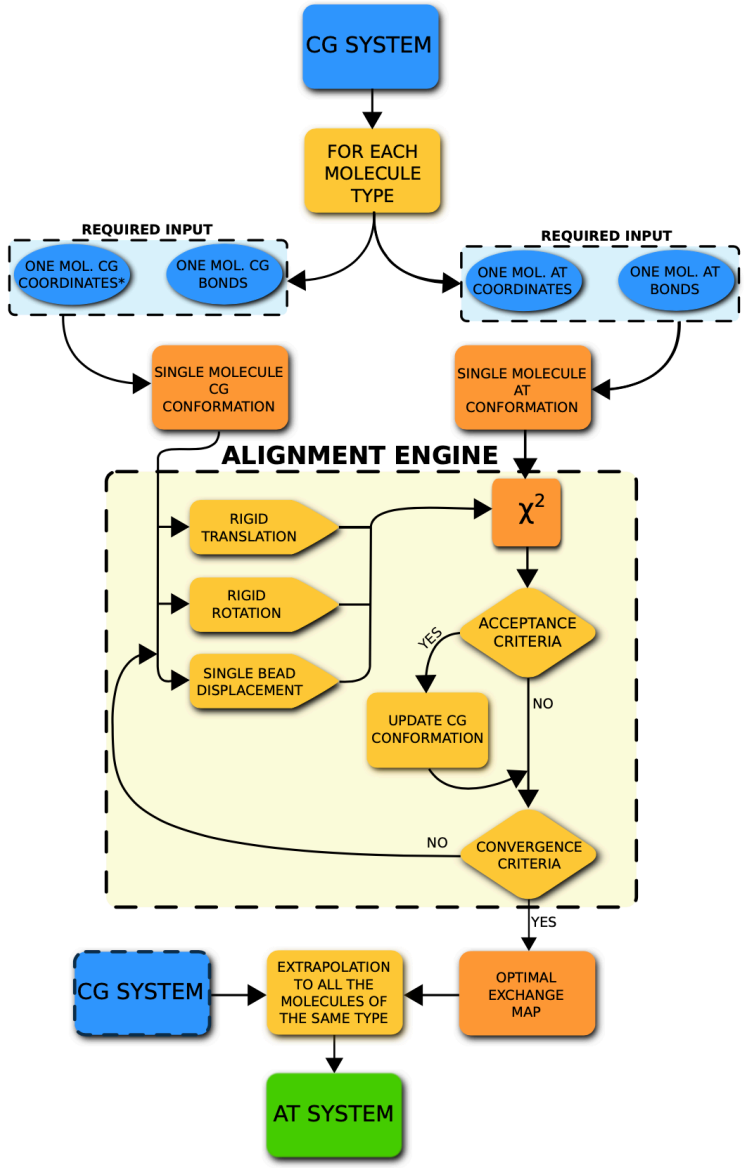

***Figure 89.** Schematic workflow of the GADDLE Maps algorithm.*

Once the files are provided, one CG molecule (of each type of compound) is randomly selected and overlaid on the AA structure

provided, minimizing the distance between the CG particles and the closets set of AA particles. For that, CG beads can be moved through in different ways: (i) translating the whole CG molecule; (ii) counter-clockwise rotations or (iii) displacing single particles. The movements are selected randomly.

After each step, in order to evaluate the CG-AA equivalence, the distance between each one of the AA atoms and its corresponding closest CG bead is calculated, providing us a distance between the CG and AA structures:

$$d^2 = \sum_{i \in AA} \left| \vec{r}_i^{AA} - \vec{r}_i^{CG} \right|^2$$

Where $\vec{r}_i^{AA}$ corresponds to the coordinates of each atom of the AA molecule and $\vec{r}_i^{CG}$ the coordinates of its closest CG particle. Assuming that the atoms are independently and normally distributed around the nearest CG particles (and vice versa) and that the standard deviation (σ) is equal for every atom (since the bond lengths are rather similar for all of them) the probability of finding a certain configuration of AA structure with respect to a CG one can be expressed as:

$$\mathrm{P} = \mathrm{e}^{-\frac{1}{2\sigma_i^2} d^2}$$

Since this probability would be maxima when the average positions of the AA atoms were those of the CG beads, this algorithm is based on the optimization of the CG structure trying to maximize P. In order to work with an expression directly proportional to d^2, we can rewrite the previous expression:

$$\chi^2 = \frac{1}{\sigma^2} \sum_{i \in AA} \left| \vec{r}_i^{AA} - \vec{r}_i^{CG} \right|^2$$

In this case, the minimization of χ^2 would provide the best fitting of the CG structure into the AA coordinates. Additionally, given that an optima mapping must consider all CG particles, an external penalty is added in order to avoid those configurations in which at least one CG bead were not included.

After each alignment, the following acceptation criterion has been defined in order to accept or discard the new CG configuration generated: if the ratio between χ^2 before (χ^2_{before}) and after (χ^2_{after})

the modification of the CG geometry is higher than one, the new configuration will be always accepted. Otherwise, the new configuration would be only accepted if this ratio divided by 100 is higher than a number between 0 and 1 randomly chosen:

$$\left(\frac{\chi^2_{before}/\chi^2_{after}}{100}\right) > 0\ to\ 1$$

If the new CG configuration is accepted, this conformation will be aligned again with the AA structure and modified following the previous mentioned allowed movements. If not, the previous CG configuration will be realigned applying different movements. This process is repeated iteratively until reaching a predefined convergence criterion, that in this case is after 5000 steps in which any of the proposed CG structures has had a smaller value than the lowest χ^2.

Once the previous cycle has provided a proper alignment, the CG beads which are closest to a group of AA atoms have been identified. This information can be extrapolated to the rest of these molecules, allowing a fast mapping. The previous whole process is repeated for each one of the different types of molecules which forms the system.

We have tested GADDLE maps for different cases, as ionic liquids, cyclodextrins, cell-penetrating peptides, lipid membranes, vesicles, organic molecules, DNA, solvated proteins, and of course SCPNs, the aim of this thesis.[556] Specifically, the results obtained from the studies with **SCPN15** in presence of a POPC membrane could be implemented using this methodology. For that purpose, the same strategy used in the previous section will be applied in this hybrid method. We started again with the restrained nanotube in the water phase (see previous section) and after 150 ns of simulation, **SCPN15** was spontaneously inserted in the lipid bilayer aligned parallel to the surface of the membrane and with the hydrophobic surface exposed to the membrane, as it was expected (**Figure 90***A*).

Using GADDLE maps, this system was mapped to AA resolution (**Figure 90***B*, **Figure 91**). The quality of the mapping of the SCPN was checked by the representation of the CG conformation with the lowest value of χ^2 overlapping the corresponding AA structure, proving

556. Otero-Mato, J. M. et al. *J. Chem. Theory Comput.* **2018**, *14* (2), 466–478.

the accuracy of the algorithm (**Figure 91**). The mapped system was simulated during 20 ns more (**Figure 90***C*). The adopted orientation of the SCPN in the membrane was preserved during the simulation time. However, the tubular structure seems to start to disassemble into smaller units, although this effect is not related with the mapping process (**Figure 90***D*).

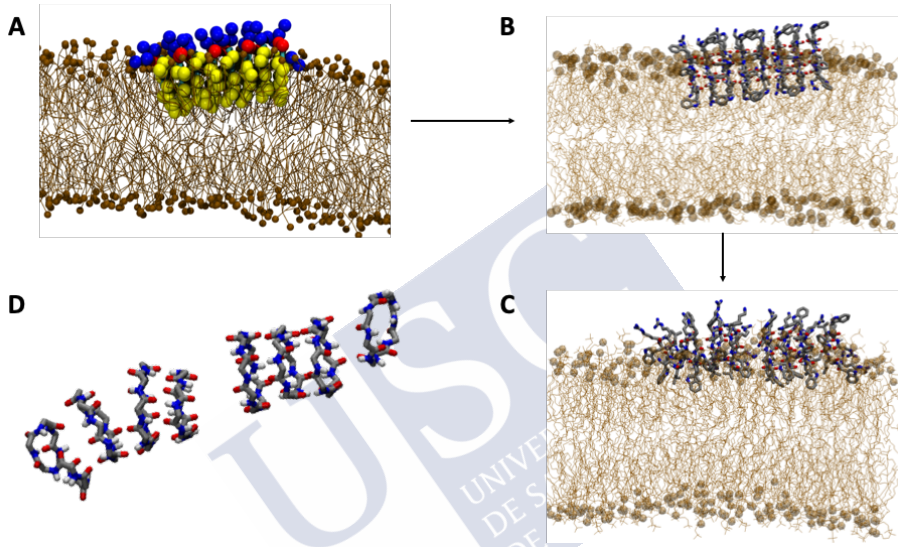

Figure 90. A) *Snapshots of last structure (t= 150 ns) resulting from the CG-MD simulation with* ***SCPN15*** *in presence of a POPC bilayer. Hydrophobic residues are displayed in yellow, Arg in blue and Lys in red.* ***B)*** *Initial (t=0 ns) and* ***C)*** *final (t= 20 ns) structures at AA resolution. In both resolutions the lipids are showed in brown, highlighting the phosphorous atoms using the Van der Waals representation. For simplicity, waters were not printed.* ***D)*** *Snapshot at t = 20 ns of the backbone of* ***SCPN15*** *at AA resolution.*

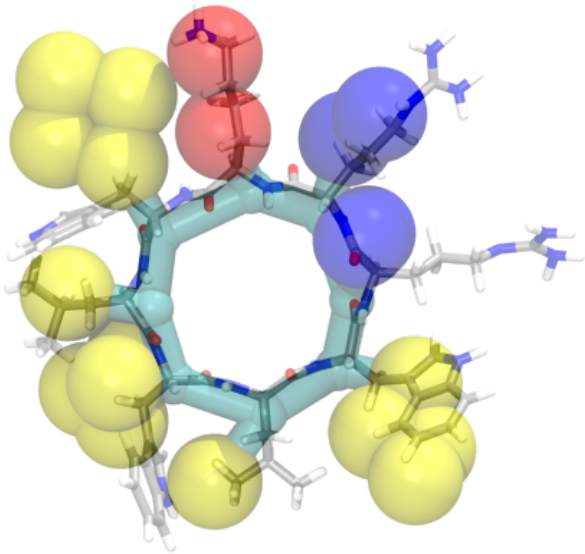

***Figure 91.** 3D structures in CG (transparent) and AA resolutions, in which the overlapping between both representations is highlighted.*

These results demonstrate the efficiency of GADDLE maps for complex supramolecular systems and facilitates the use of consecutive MD simulations at different resolutions as a good multiscale protocol. Since it does not require new codes nor direct dependency on pre-existing libraries, this algorithm is a very useful tool for the mapping of any molecule, as long as the files needed for performing a MD simulation using both resolutions (coordinates and topologies) are available. Moreover, it is worth to mention that this method can be applied to any pair of Force Fields, since the topologies are provided as inputs by the user. Regarding its computational cost, it is also remarkable that GADDLE maps is notably efficient for large systems, since the computational effort is focused on the alignment of a single molecule of each type. Once the CG beads–AA particles equivalence is identified, the full mapping is almost instantaneous. Given that, this algorithm is especially suitable for monocomponent systems, regardless of its size (within certain logical limits).

In order to better identify the previous mapping of SCPN inserted in membrane, an app for visualizing it using AR has been developed,

which is available for Android and iOS (*GADDLE MAPS AR*, **Figure 92**).[557,558]

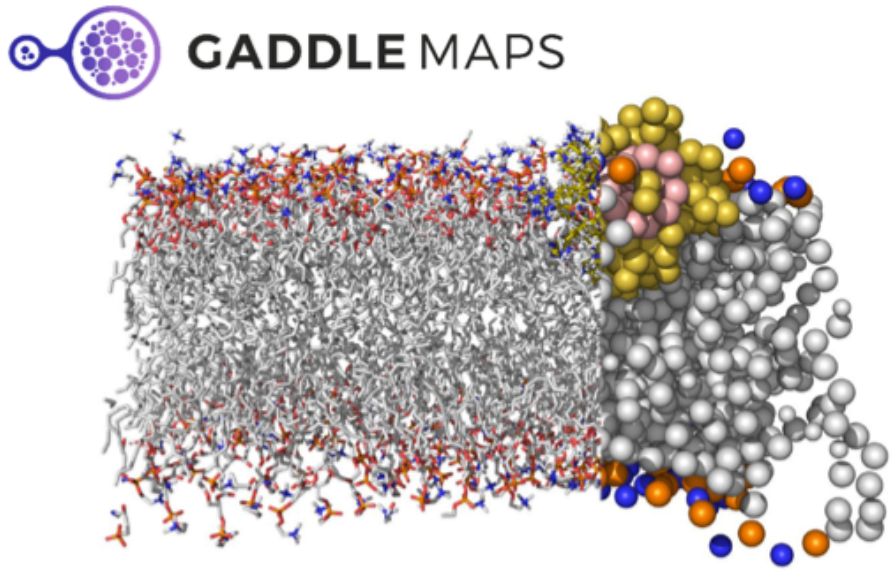

Figure 92. *AR-Pattern for being visualized using the app "GADDLE MAPS AR". Download the App, point the mobile and have fun!*

557. GADDLE MAPS AR - Apps on Google Play https://play.google.com/store/apps/details?id=com.mduse.GADDLEMAPS&hl=en.
558. Gaddle maps AR on the App Store https://apps.apple.com/ca/app/gaddle-maps-ar/id1311726695.

8.6. CONCLUSIONS.

In order to evaluate the interaction between amphipathic *D*,*L*-α-CPs (**CP15** and **CP16**) with a number of bilayers with different lipid composition that mimic natural mammal and bacteria membranes (pure DMPC, DMPC:DMPG (3:1), DMPE:DMPG (3:1) and DMPE:DMPG (1:9)), CG-MD simulations have been carried out. These calculations starting with the corresponding pre-formed SCPNs made by eight CPs (**SCPN15** and **SCPN16**) in the water media led to their spontaneous insertion in the lipid bilayer along the simulation time, orienting in parallel to the membrane surface. This result is in good agreement with experimental results and with those proposed by Tarek, suggesting that the electrostatic interactions between the CPs and the bilayers are the driven force for this assembly.[113] It is important to note that distance restraints were applied between the particle of the SCPN in order to ensure the preservation of their tubular shape.

All simulations showed that the hydrophobic amino acids tend to immerse in the lipidic media, with the exception of those with **SCPN15** in DMPE:DMPG (1:9), in which, surprisingly, they were exposed towards the aqueous phase. In this structure, the cationic units are oriented towards the anionic heads of phospholipids, most probably being this interaction the driving force that stabilize this structure. This different mechanism suggests a possible application of SCPN15 for recognizing highly negatively charged lipid bilayers. However, following CG-MD simulations removing the distance restraints, except those need for maintain the CPs flat conformation, led to the destruction of the tubular assemblies of **SCPN15** in the presence of PE. In all other simulations, in which the hydrophobic units were oriented towards the lipids, the tubular shape of the nanotubes was well preserved for both **SCPN15** and **SCPN16**. In this case, the number of contacts was found not to be increased after the releasing of the restraints, supporting that the formation of the assembly is stable. Additionally, it was found that **SCPN15**, as expected considered the larger number of hydrophobic residues, was deeply inserted in the membrane compared with **SCPN16**, being even possible to observe the interaction with lipids of the opposite leaflet. This fact suggests that **SCPN15** is more active

113. Khalfa, A. et al. *J. Phys. Chem. B* **2010**, *114* (8), 2676–2684.

against those membranes as antimicrobial agents.

After all, these results could support the use of amphipathic cationic CPs as precursors of SCPN as potential antimicrobial agents, since its interaction with membranes it was probed. However, in these studies was not possible to visualize translocation or formation of open pores, even though more than one nanotube at a time was considered. It is worth to mention that the experiments carried out in these cases were not able to retain the tubular structure of SCPN reducing the possibility of forming carpet-like structures. Consequently, a better understanding of their mechanism of action is needed, which could help to a smarter design. Given that in this work we started from a pre-formed nanotube, the next step could be the study of "free" CPs, which could assist to the understanding their assembly into nanotubes. This approach would also allow the formation of different rotamers that could interconvert to achieve the more favourable structure. Part of the results here described have resulted in the following publication: Claro, B.; González-Freire, E.; Calvelo, M.; Bessa, L. J.; Goormaghtigh, E.; Amorín, M.; Granja, J. R.; Gracia-Fandiño, R.; Bastos, M. *Colloids and Surfaces B: Biointerfaces* **2020**, *196*, 111349.

Additionally, the use of GADDLE Maps as useful tool for backmapping from CG to AA resolution has been demonstrated and validated. This fact could facilitate the use of multiscale simulations (long CG-MD simulations following for shorter AA-MD simulations) as a promising protocol for the study of these systems. More info can be found in the following publication in collaboration with the group of Prof. L. M. Varela and L. J. Gallego, from the University of Santiago de Compostela: Otero-Mato, J. M.; Montes-Campos, H.; Calvelo, M.; García-Fandiño, R.; Gallego, L. J.; Pineiro, Á.; Varela, L. M. *J. Chem. Theory Comput.* **2018**, *14* (2), 466-478.

9. General Conclusions

Throughout the present memory, a detailed study of SCPNs through a computational chemical approach has been carried out. Using *in silico* methods at different levels of calculation, structural parameters of the peptides nanotubes as well as their dynamic activity in different scenarios were evaluated, trying to elucidate some of the main basis that dominate the behaviour of these promising systems.

During the **first section** of this dissertation, in *Chapter 4*, the preferred orientation of different types of CPs when forming the SCNPs (parallel or antiparallel β-sheet) as well as their possible application as molecular containers were evaluated through quantum methods. Our results suggest that α, δ-CPs are more prone to self-assemble forming a parallel β-sheet when only the CP backbone interactions are considered. This tendency may be explained by the better packing of the facing hydrogens that are not involved in the H-bond network in the parallel arrangement, in contrast to the presumably disfavoured overlapping found for the antiparallel orientation. Nevertheless, this trend can be reversed by modulating the side chains interactions of the α-amino acids of the CP. Our calculations show that the antiparallel β-sheet can be the most favourable if the interactions between the lateral chains are optimized. In view of these results, we decided to extend our study to α,γ-CPs, in which the antiparallel arrangement was supposed to be the preferred. Contrary to the expected, our calculations show that the parallel β-sheet is the most favoured when only the backbone is considered. Again, the preference for this arrangement could be explained by the better packing of the facing hydrogens that are not participating in the H-bond network. Furthermore, in our study we present for the first time, as far as we know, new models of dimers arising from the combination of α,γ-CP isomers, which had never been considered through rational design. The calculations suggest that at least one of these new species is energetically feasible, and open the

door to experiments to validate these hypothesis. All the α,γ-dimers studied in this chapter can be visualized using AR using the app **Dimerdice**, available for Android and iOS, developed by us. The results presented in this Chapter have led to the following publication: Calvelo, M.; Lamas, A.; Guerra, A.; Amorin, M.; Garcia-Fandiño, R.; Granja, J. R. *Chem. – A Eur. J.* **2020**, *26*, 5846-5858.

In the next chapter of the first section, *Chapter 5*, and also using quantum methods, we evaluate the use of α,γ- and α,δ-dimers as molecular containers, taking advantage of their inner cavity. Our results suggest that the entrapping of a number of noble gases (Kr, Xe and Rn) by a dimer composed by hexameric α,γ-CPs (**D11a**) is energetically feasible. Additionally, the encapsulating of chloroform is also favoured, opening the door to the use of these dimers as molecular cages. This study is included in Pizzi, A.; Ozores, H. L.; Calvelo, M.; García-Fandiño, R.; Amorín, M.; Demitri, N.; Terraneo, G.; Bracco, S.; Comotti, A.; Sozzani, P.; Bezuidenhout, C. X.; Metrangolo, P.; Granja, J. R. *Angew. Chemie - Int. Ed.* **2019**, *58* (41), 14472–14476. Then, and taking advantage of the higher hydrophobicity of the inner cavity of α,δ-SCPNs, due to the presence of two methylenes groups per cyclohexyl residue pointing inwards in each CP, the entrapping of carbon allotropes (C_{60}, C_{70} and CNTs of different sizes) was also explored. In all cases, our results suggest that the encapsulation of such molecules is possible.

In the **second section**, the behaviour of transmembrane SCPNs made of α,γ- or α,δ-CPs in which the side chains of the α-amino acids are hydrophobic was evaluated via *All-atom* Molecular Dynamics. In the first of these chapters, *Chapter 6*, an AA-MD study on internally functionalized peptide nanotubes composed of α- and γ-amino acids self-assembled in lipid bilayers is presented. One of the main advantages of peptide nanotubes composed of γ-amino acids is that the properties of their inner cavities can be tuned by introducing different functions on β-carbon of the γ-amino acid. In the work described here we studied the effect of the presence of different numbers of hydroxyl groups in different positions in the lumen of these channels when they are inserted into a lipid bilayer and assessed how they affect the structural and dynamic behaviour of the modified peptide nanotubes as

well as the transmembrane transport of different ions. In order to enhance the selectivity in the cation transport of α,γ-SCPNs, AA-MD simulations with a nanotube composed by eight CPs functionalized with four carboxylic/carboxylate groups per cycle and in presence of different salt solutions (LiCl, NaCl, KCl, CsCl and $CaCl_2$) were carried out. Two different extreme protonated states were considered: all the carboxyl groups protonated (neutral SCPN) and all of them deprotonated (negatively charged SCPN). Our simulations demonstrate that the protonated SCPN preserve the tubular structure, but the reduction of the pore size due to the introduction of the carboxyl groups blocks the pass of cations through it. On the other hand, although the deprotonation of the carboxyl groups led to the loss the nanotube shape in all simulations carried out, the amorphous aggregate, negatively charged, remains in the hydrophobic region of the membrane, being able to attract cations to him. In light of these results, we can purpose a doubly modulable nanotube formed by the self-assembly of cyclic peptides sensitive to both the presence of a lipid membrane and the pH of the aqueous media. The cyclic peptides are designed to self-assemble into peptide nanotubes in the presence of a lipid bilayer and at low pH values. Under these conditions, the residual side chains point outside the cyclic peptides, being exposed to the lipid bilayer, and the inner groups (carboxylic acids) are protonated, thus allowing the permeation of water and preventing that of ions. Higher pH values are expected to create carboxylate groups at the lumen of the peptides, leading to the disassembly of the nanotube, the attraction and translocation of ions towards the hydrophobic core of the bilayer, and eventually killing the target malignant cells. Our results suggest that by introducing a second switch in a membrane sensitive system, it is possible to modulate its interaction with the lipid bilayer. This opens the door to new strategies for the preparation of antimicrobial peptides that interact at the membrane level. The results presented in this Chapter have led to a publication: Calvelo, M.; Granja, J. R.; Garcia-Fandiño, R. *Phys. Chem. Chem. Phys.* **2019**, *21* (37), 20750–20756.

In *Chapter 7*, the behaviour of one α,γ- and one α,δ-SCPN inserted in a lipid membrane and in presence of different water models (TIP3P, TIP4P, TIP4P/2005 and OPC) was tested. Our simulations led to stable

nanotubes, being probed for the first time that α,δ-SCPNs could act as transmembrane channels. Additionally, our results show that the water model selected does not affect the stability of the nanotube. However, the dynamic behaviour of the water molecules inside the SCPNs was different, being the movement of the TIP3P and TIP4P waters clearly faster than the two more modern models (TIP4P/2005 and OPC), following the same trend found in bulk. The results presented in this Chapter have been carried out during a predoctoral stay in the group of Prof. Mark S. P. Sansom and have led to the following publication: Calvelo, M.; Lynch, C.; Granja, J. R.; Sansom, M. S. P.; Garcia-Fandiño, R. *ACS Nano, accepted*.

Finally, in **Section III**, the interaction of SCPNs made of positively charged amphipathic α-CPs with membranes with different lipid compositions was evaluated via *Coarse-Grained* Molecular Dynamics. In *Chapter 8*, the spontaneous assembly of two SCPNs composed by two different CPs with probed antimicrobial behaviour (**CP15** and **CP16**) was observed at the beginning of the performed simulations. Our results show that the conformation adopted by the nanotube depends on the CP sequence, being the insertion of **CP15** more deeply, which could be related with its higher antimicrobial activity. In general, the SCPNs oriented the hydrophobic residues towards the membrane, leaving the charged residues towards the water. However, **SCPN16** in presence of a negatively charged membrane (DMPE:DMPG 1:9) was rotated, disposing the hydrophobic core to the aqueous media and the positively charged residues to the lipids. This fact may suggest a dependency on the lipid composition of the membrane. This result opens the door to the use of these SCPNs as antimicrobial agents that target specific membranes depending on the lipid composition. This action mechanism, different from that of most of the antibiotics available nowadays, could be the first step to help to overcome the acquired resistance to antibiotics found in some bacteria. Additionally, the use of the algorithm GADDLE Maps as useful tool for backmapping from CG to AA resolution has been demonstrated and validated. This fact could support facilitate the use of multiscale simulations (long CG-MD simulations following for shorter AA-MD simulations) as a promising protocol for the study of these systems The

results presented in this Chapter have led to two publications: **1)** Claro, B.; González-Freire, E.; Calvelo, M.; Bessa, L. J.; Goormaghtigh, E.; Amorín, M.; Granja, J. R.; Gracia-Fandiño, R.; Bastos, M. *Colloids and Surfaces B: Biointerfaces* **2020**, *196*, 111349, and **2)** Otero-Mato, J. M.; Montes-Campos, H.; Calvelo, M.; García-Fandiño, R.; Gallego, L. J.; Pineiro, Á.; Varela, L. M. *J. Chem. Theory Comput.* **2018**, *14* (2), 466-478.

To sum up, the results obtained in this PhD dissertation are expected to help in the future design of models based on SCPNs and in the better understanding of how they work when used in different applications, such as molecular cages, transmembrane channels or antimicrobial materials. The combination of different computational techniques is nowadays the only alternative to obtain structural and dynamic information at the level of resolution presented here, and has demonstrated to be a very useful tool in this area.

USC
UNIVERSIDADE
DE SANTIAGO
DE COMPOSTELA

10. References

1. Feynman, R. In *Engineering and Science*; 1959; Vol. 23 (5), pp 22–36.
2. Taniguchi, N. In *Proceedings of the International Conference on Production Engineering, Tokyo, Part II, Japan Society of Precision Engineering*; 1974; pp 18–23.
3. Drexler, K. E. *Proc. Natl. Acad. Sci. U. S. A.* **1981**, *78* (9 I), 5275–5278.
4. Binnig, G.; Rohrer, H. *Surf. Sci.* **1983**, *126*, 236–244.
5. Binnig, G.; Quate, C. F.; Gerber, C. *Phys. Rev. Lett.* **1986**, *56* (9), 930–933.
6. Kroto, H. W.; Heath, J. R.; O'Brien, S. C.; Curl, R. F.; Smalley, R. E. *Nature* **1985**.
7. Hashemi, P. *Gate-All-Around Silicon Nanowire MOSFETs: Top-down Fabrication and Transport Enhancement Techniques*; Massachusetts Institute of Technology, 2010.
8. Kanani, N. *Electroplating: Basic Principles, Processes and Practice*; Elsevier Ltd, 2005.
9. Pauling, L. *J. Am. Chem. Soc.* **1931**, *53* (4), 1367–1400.
10. Muller, P. *Pure Appl. Chem.* **1994**, *66* (5), 1077–1184.
11. Autumn, K.; Liang, Y. A.; Hsieh, S. T.; Zesch, W.; Chan, W. P.; Kenny, T. W.; Fearing, R.; Full, R. J. *Nature* **2000**, *405* (6787), 681–685.
12. Autumn, K.; Sitti, M.; Liang, Y. A.; Peattie, A. M.; Hansen, W. R.; Sponberg, S.; Kenny, T. W.; Fearing, R.; Israelachvili, J. N.; Full, R. J. *Proc. Natl. Acad. Sci. U. S. A.* **2002**, *99* (19), 12252–12256.
13. Mascal, M.; Armstrong, A.; Bartberger, M. D. *J. Am. Chem. Soc.* **2002**, *124* (22), 6274–6276.
14. Metrangolo, P.; Resnati, G. *Science.* **2008**, *321* (5891), 918–919.
15. Gilday, L. C.; Robinson, S. W.; Barendt, T. A.; Langton, M. J.; Mullaney, B. R.; Beer, P. D. *Chem. Rev.* **2015**, *115* (15), 7118–7195.
16. Benz, S.; Mareda, J.; Besnard, C.; Sakai, N.; Matile, S. *Chem. Sci.* **2017**, *8* (12), 8164–8169.
17. Pyykkö, P. *Chem. Rev.* **1997**, *97* (3), 597–636.
18. Yoon, J.; Czarnik, A. W. *J. Am. Chem. Soc.* **1992**, *114* (14), 5874–5875.
19. Louzao, I.; García-Fandiño, R.; Montenegro, J. *J. Mater. Chem. B* **2017**, *5* (23), 4426–4434.
20. Partington, J. R. *Nature* **1933**, *131* (3306), 348–350.
21. Fischer, E. *Berichte der Dtsch. Chem. Gesellschaft* **1894**, *27* (3), 3479–3483.
22. Crini, G. *Chem. Rev.* **2014**, *114* (21), 10940–10975.

23. Villiers, A. *Compt. Rend. Acad. Sci* **1891**, *112*, 536–538.
24. Whitesides, G. M.; Grzybowski, B. *Science.* **2002**, *295* (5564), 2418–2421.
25. Franklin, B.; Brownrigg, W.; Mr. Farish. *Philos. Trans. R. Soc. London* **1774**, *64*, 445–460.
26. Whitesides, G. M.; Mathias, J. P.; Seto, C. T. *Science.* **1991**, *254* (5036), 1312–1319.
27. Mann, S. *Angew. Chemie - Int. Ed.* **2008**, *47* (29), 5306–5320.
28. Kent, S. B. H. *Chem. Soc. Rev.* **2009**, *38* (2), 338–351.
29. Hughes, A. B. *Amino Acids, Peptides and Proteins in Organic Chemistry*; Hughes, A. B., Ed.; Wiley-VCH: Weinheim, Germany, 2011; Vol. 5.
30. Kuan, S. L.; Bergamini, F. R. G.; Weil, T. *Chem. Soc. Rev.* **2018**, *47* (24), 9069–9105.
31. Yuan, C.; Ji, W.; Xing, R.; Li, J.; Gazit, E.; Yan, X. *Nat. Rev. Chem.* **2019**, *3* (10), 567–588.
32. Sitaram, N.; Nagaraj, R. *Curr. Pharm. Des.* **2002**, *8* (9), 727–742.
33. Papagianni, M. *Biotechnol. Adv.* **2003**, *21* (6), 465–499.
34. Chen, C. H.; Lu, T. K. *Antibiotics* **2020**, *9* (1).
35. Kang, X.; Dong, F.; Shi, C.; Liu, S.; Sun, J.; Chen, J.; Li, H.; Xu, H.; Lao, X.; Zheng, H. *Sci. data* **2019**, *6* (1), 148.
36. Chierotti, M. R.; Gobetto, R. *Supramolecular Chemistry: From Molecules to Nanomaterials*; 2012.
37. Choi, W.; Ulissi, Z. W.; Shimizu, S. F. E.; Bellisario, D. O.; Ellison, M. D.; Strano, M. S. *Nat. Commun.* **2013**, *4* (1), 1–8.
38. Farshad, M.; Rasaiah, J. C. *J. Phys. Chem. B* **2020**, *124* (6), 937–943.
39. Kang, S.; Herzberg, M.; Rodrigues, D. F.; Elimelech, M. *Langmuir* **2008**, *24* (13), 6409–6413.
40. Madani, S. Y.; Naderi, N.; Dissanayake, O.; Tan, A.; Seifalian, A. M. *Int. J. Nanomedicine* **2011**, *6*, 2963–2979.
41. Ye, Y.; Geng, B. *Crit. Rev. Solid State Mater. Sci.* **2012**, *37* (2), 75–93.
42. Lamanna, G.; Garofalo, A.; Popa, G.; Wilhelm, C.; Bégin-Colin, S.; Felder-Flesch, D.; Bianco, A.; Gazeau, F.; Ménard-Moyon, C. *Nanoscale* **2013**, *5* (10), 4412–4421.
43. Yan, Y.; Miao, J.; Yang, Z.; Xiao, F. X.; Yang, H. Bin; Liu, B.; Yang, Y. *Chem. Soc. Rev.* **2015**, *44* (10), 3295–3346.
44. Karatas, A.; Algan, A. *Curr. Top. Med. Chem.* **2017**, *17* (13), 1555–1563.
45. Jiao, Y.; Mukhopadhyay, A.; Ma, Y.; Yang, L.; Hafez, A. M.; Zhu, H. *Adv. Energy Mater.* **2018**, *8* (15), 1702779.
46. Jawed, A.; Saxena, V.; Pandey, L. M. *J. Water Process Eng.* **2020**, *33*, 101009.
47. Kashiwagi, D.; Sim, S.; Niwa, T.; Taguchi, H.; Aida, T. *J. Am. Chem. Soc.* **2018**, *140* (1), 26–29.
48. Thomas, F.; Dawson, W. M.; Lang, E. J. M.; Burton, A. J.; Bartlett, G. J.; Rhys, G. G.; Mulholland, A. J.; Woolfson, D. N. *ACS Synth. Biol.* **2018**, *7* (7), 1808–1816.

49. Song, L.; Hobaugh, M. R.; Shustak, C.; Cheley, S.; Bayley, H.; Gouaux, J. E. *Science.* **1996**, *274* (5294), 1859–1866.
50. Szewczyk, A. *Mol. Membr. Biol.* **1998**, *15* (2), 49–58.
51. Fairman, J. W.; Noinaj, N.; Buchanan, S. K. *Curr. Opin. Struct. Biol.* **2011**.
52. Noinaj, N.; Kuszak, A. J.; Gumbart, J. C.; Lukacik, P.; Chang, H.; Easley, N. C.; Lithgow, T.; Buchanan, S. K. *Nature* **2013**, *501* (7467), 385–390.
53. Day, R. E.; Kitchen, P.; Owen, D. S.; Bland, C.; Marshall, L.; Conner, A. C.; Bill, R. M.; Conner, M. T. *Biochim. Biophys. Acta - Gen. Subj.* **2014**.
54. Verkman, A. S.; Anderson, M. O.; Papadopoulos, M. C. *Nat. Rev. Drug Discov.* **2014**, *13* (4), 259–277.
55. Matile, S. *Chem. Soc. Rev.* **2001**, *30* (3), 158–167.
56. Fyles, T. M. *Chem. Soc. Rev.* **2007**, *36* (2), 335–347.
57. García-Fandiño, R.; Sansom, M. S. P. *Proc. Natl. Acad. Sci. U. S. A.* **2012**, *109* (18), 6939–6944.
58. Alfonso, I.; Quesada, R. *Chem. Sci.* **2013**, *4* (8), 3009–3019.
59. Chen, J. Y.; Hou, J. L. *Org. Chem. Front.* **2018**, *5* (10), 1728–1736.
60. Bong, D. T.; Clark, T. D.; Granja, J. R.; Ghadiri, M. R. *Angew. Chemie Int. Ed.* **2001**, *40* (6), 988–1011.
61. García-Fandiño, R.; Amorín, M.; Granja, J. R. In *Supramolecular Chemistry*; John Wiley & Sons, Ltd: Chichester, UK, 2012.
62. Shimizu, L. S.; Hughes, A. D.; Smith, M. D.; Davis, M. J.; Zhang, B. P.; Zur Loye, H. C.; Shimizu, K. D. *J. Am. Chem. Soc.* **2003**, *125* (49), 14972–14973.
63. Balakrishnan, K.; Datar, A.; Zhang, W.; Yang, X.; Naddo, T.; Huang, J.; Zuo, J.; Yen, M.; Moore, J. S.; Zang, L. *J. Am. Chem. Soc.* **2006**, *128* (20), 6576–6577.
64. Frischmann, P. D.; Guieu, S.; Tabeshi, R.; MacLachlan, M. J. *J. Am. Chem. Soc.* **2010**, *132* (22), 7668–7675.
65. Yun, M.; Park, C.; Lee, J.; Kim, C. *J. Polym. Sci. Part A Polym. Chem.* **2010**, *48* (3), 730–734.
66. Hamley, I. W. *Angew. Chemie - Int. Ed.* **2014**, *53* (27), 6866–6881.
67. Rodríguez-Vázquez, N.; Amorín, M.; Granja, J. R. *Org. Biomol. Chem.* **2017**, *15* (21), 4490–4505.
68. Brea, R. J.; Reiriz, C.; Granja, J. R. *Chem. Soc. Rev.* **2010**, *39* (5), 1448–1456.
69. Chapman, R.; Danial, M.; Koh, M. L.; Jolliffe, K. A.; Perrier, S. *Chem. Soc. Rev.* **2012**, *41* (18), 6023–6041.
70. Hsieh, W. H.; Liaw, J. *J. Food Drug Anal.* **2019**, *27* (1), 32–47.
71. De Santis, P.; Morosetti, S.; Rizzo, R. *Macromolecules* **1974**, *7* (1), 52–58.
72. Ghadiri, M. R.; Granja, J. R.; Milligan, R. A.; McRee, D. E.; Khazanovich, N. *Nature* **1993**, *366* (6453), 324–327.
73. Ghadiri, M. R.; Granja, J. R.; Buehler, L. K. *Nature* **1994**, *369* (6478), 301–304.
74. Kim, H. S.; Hartgerink, J. D.; Ghadiri, M. R. *J. Am. Chem. Soc.* **1998**, *120*

(18), 4417–4424.
75. Sánchez-Quesada, J.; Isler, M. P.; Ghadiri, M. R. *J. Am. Chem. Soc.* **2002**, *124* (34), 10004–10005.
76. Montenegro, J.; Ghadiri, M. R.; Granja, J. R. *Acc. Chem. Res.* **2013**, *46* (12), 2955–2965.
77. Granja, J. R.; Ghadiri, M. R. *J. Am. Chem. Soc.* **1994**, *116* (23), 10785–10786.
78. Danial, M.; Perrier, S.; Jolliffe, K. A. *Org. Biomol. Chem.* **2015**, *13* (8), 2464–2473.
79. Fernandez-Lopez, S.; Kim, H. S.; Choi, E. C.; Delgado, M.; Granja, J. R.; Khasanov, A.; Kraehenbuehl, K.; Long, G.; Weinberger, D. A.; Wilcoxen, K. M.; Ghadiri, M. R. *Nature* **2001**, *412* (6845), 452–455.
80. Dartois, V.; Sanchez-Quesada, J.; Cabezas, E.; Chi, E.; Dubbelde, C.; Dunn, C.; Granja, J.; Gritzen, C.; Weinberger, D.; Ghadiri, M. R.; Parr, T. R. *Antimicrob. Agents Chemother.* **2005**, *49* (8), 3302–3310.
81. Motiei, L.; Rahimipour, S.; Thayer, D. A.; Wong, C. H.; Ghadiri, M. R. *Chem. Commun.* **2009**, No. 25, 3693–3695.
82. Huang, M. L.; Benson, M. A.; Shin, S. B. Y.; Torres, V. J.; Kirshenbaum, K. *European J. Org. Chem.* **2013**, *2013* (17), 3560–3566.
83. Richman, M.; Wilk, S.; Chemerovski, M.; Wärmländer, S. K. T. S.; Wahlström, A.; Gräslund, A.; Rahimipour, S. *J. Am. Chem. Soc.* **2013**, *135* (9), 3474–3484.
84. Hartgerink, J. D.; Granja, J. R.; Milligan, R. A.; Ghadiri, M. R. *J. Am. Chem. Soc.* **1996**, *118* (1), 43–50.
85. Xu, T.; Zhao, N.; Ren, F.; Hourani, R.; Lee, M. T.; Shu, J. Y.; Mao, S.; Helms, B. A. *ACS Nano* **2011**, *5* (2), 1376–1384.
86. De La Rica, R.; Pejoux, C.; Matsui, H. *Adv. Funct. Mater.* **2011**, *21* (6), 1018–1026.
87. Chen, J.; Zhang, B.; Xia, F.; Xie, Y.; Jiang, S.; Su, R.; Lu, Y.; Wu, W. *Nanoscale* **2016**, *8* (13), 7127–7136.
88. Larnaudie, S. C.; Brendel, J. C.; Romero-Canelón, I.; Sanchez-Cano, C.; Catrouillet, S.; Sanchis, J.; Coverdale, J. P. C.; Song, J.-I. I.; Habtemariam, A.; Sadler, P. J.; Jolliffe, K. A.; Perrier, S.; Romero-Canelo, I.; Sanchez-Cano, C.; Catrouillet, S.; Sanchis, J.; C Coverdale, J. P.; Song, J.-I. I.; Habtemariam, A.; Sadler, P. J.; Jolliffe, K. A.; Perrier, bastien. *Biomacromolecules* **2017**, *19* (1), 239–247.
89. Zhao, Y.; Leman, L. J.; Search, D. J.; Garcia, R. A.; Gordon, D. A.; Maryanoff, B. E.; Ghadiri, M. R. *ACS Cent. Sci.* **2017**, *3* (6), 639–646.
90. Fuertes, A.; Juanes, M.; Granja, J. R.; Montenegro, J. *Chem. Commun.* **2017**, *53* (56), 7861–7871.
91. Drienovská, I.; Roelfes, G. *Nat. Catal.* **2020**, *3* (3), 193–202.
92. Danial, M.; Tran, C. M. N.; Jolliffe, K. A.; Perrier, S. *J. Am. Chem. Soc.* **2014**, *136* (22), 8018–8026.
93. Danial, M.; My-Nhi Tran, C.; Young, P. G.; Perrier, S.; Jolliffe, K. A. *Nat.*

Commun. **2013**, *4* (1), 1–13.
94. Li, M.; Ehlers, M.; Schlesiger, S.; Zellermann, E.; Knauer, S. K.; Schmuck, C. *Angew. Chemie Int. Ed.* **2016**, *55* (2), 598–601.
95. Amorín, M.; Castedo, L.; Granja, J. R. *J. Am. Chem. Soc.* **2003**, *125* (10), 2844–2845.
96. Reiriz, C.; Amorín, M.; García-Fandiño, R.; Castedo, L.; Granja, J. R. *Org. Biomol. Chem.* **2009**, *7* (21), 4358–4361.
97. Rodríguez-Vázquez, N.; García-Fandiño, R.; Amorín, M.; Granja, J. R. *Chem. Sci.* **2016**, *7* (1), 183–187.
98. Rodríguez-Vázquez, N.; Amorín, M.; Alfonso, I.; Granja, J. R. *Angew. Chemie Int. Ed.* **2016**, *55* (14), 4504–4508.
99. Guerra, A.; Brea, R. J.; Amorín, M.; Castedo, L.; Granja, J. R. *Org. Biomol. Chem.* **2012**, *10* (44), 8762–8766.
100. Rodriguez-Vazquez, N.; Ozores, H.; Guerra, A.; Gonzalez-Freire, E.; Fuertes, A.; Panciera, M.; Priegue, J.; Outeiral, J.; Montenegro, J.; Garcia-Fandino, R.; Amorin, M.; Granja, J. *Curr. Top. Med. Chem.* **2015**, *14* (23), 2647–2661.
101. Reiriz, C.; Brea, R. J.; Arranz, R.; Carrascosa, J. L.; Garibotti, A.; Manning, B.; Valpuesta, J. M.; Eritja, R.; Castedo, L.; Granja, J. R. *J. Am. Chem. Soc.* **2009**, *131* (32), 11335–11337.
102. Montenegro, J.; Vázquez-Vázquez, C.; Kalinin, A.; Geckeler, K. E.; Granja, J. R. *J. Am. Chem. Soc.* **2014**, *136* (6), 2484–2491.
103. Cuerva, M.; García-Fandiño, R.; Vázquez-Vázquez, C.; López-Quintela, M. A.; Montenegro, J.; Granja, J. R. *ACS Nano* **2015**, *9* (11), 10834–10843.
104. Fuertes, A.; Ozores, H. L.; Amorín, M.; Granja, J. R. *Nanoscale* **2017**, *9* (2), 748–753.
105. Kubik, S.; Goddard, R.; Kirchner, R.; Nolting, D.; Seidel, J. *Angew. Chem. Int. Ed. Engl.* **2001**, *40* (14), 2648–2651.
106. Burade, S. S.; Saha, T.; Bhuma, N.; Kumbhar, N.; Kotmale, A.; Rajamohanan, P. R.; Gonnade, R. G.; Talukdar, P.; Dhavale, D. D. *Org. Lett.* **2017**, *19* (21), 5948–5951.
107. Lamas, A.; Guerra, A.; Amorín, M.; Granja, J. R. *Chem. Sci.* **2018**, *9* (43), 8228–8233.
108. Fraser, J. S.; Lindorff-Larsen, K.; Bonomi, M. *J. Chem. Inf. Model.* **2020**, *60* (5), 2410–2412.
109. Chen, G.; Su, S.; Liu, R. *J. Phys. Chem. B* **2002**, *106* (7), 1570–1575.
110. Tarek, M.; Maigret, B.; Chipot, C. *Biophys. J.* **2003**, *85* (4), 2287–2298.
111. Hwang, H.; Schatz, G. C.; Ratner, M. A. *J. Phys. Chem. A* **2009**, *113* (16), 4780–4787.
112. Khalfa, A.; Treptow, W.; Maigret, B.; Tarek, M. *Chem. Phys.* **2009**, *358* (1–2), 161–170.
113. Khalfa, A.; Tarek, M. *J. Phys. Chem. B* **2010**, *114* (8), 2676–2684.
114. Song, X.; Fan, J.; Liu, D.; Li, H.; Li, R. *J. Mol. Model.* **2013**, *19* (10), 4271–4282.

115. García-Fandiño, R.; Granja, J. R.; D'Abramo, M.; Orozco, M. *J. Am. Chem. Soc.* **2009**, *131* (43), 15678–15686.
116. García-Fandiño, R.; Castedo, L.; Granja, J. R.; Vázquez, S. A. *J. Phys. Chem. B* **2010**, *114* (15), 4973–4983.
117. The poems of John Godfrey Saxe/The Blind Men and the Elephant - Wikisource, the free online library https://en.wikisource.org/wiki/The_poems_of_John_Godfrey_Saxe/The_Blind_Men_and_the_Elephant (accessed Jun 15, 2020).
118. Nasica-Labouze, J.; Nguyen, P. H.; Sterpone, F.; Berthoumieu, O.; Buchete, N. V.; Coté, S.; De Simone, A.; Doig, A. J.; Faller, P.; Garcia, A.; Laio, A.; Li, M. S.; Melchionna, S.; Mousseau, N.; Mu, Y.; Paravastu, A.; Pasquali, S.; Rosenman, D. J.; Strodel, B.; Tarus, B.; Viles, J. H.; Zhang, T.; Wang, C.; Derreumaux, P. *Chem. Rev.* **2015**, *115* (9), 3518–3563.
119. Sperger, T.; Sanhueza, I. A.; Schoenebeck, F. *Acc. Chem. Res.* **2016**, *49* (6), 1311–1319.
120. Sugimoto, Y.; Pou, P.; Abe, M.; Jelinek, P.; Pérez, R.; Morita, S.; Custance, O. *Nature* **2007**, *446* (7131), 64–67.
121. Gross, L.; Mohn, F.; Moll, N.; Liljeroth, P.; Meyer, G. *Science.* **2009**, *325* (5944), 1110–1114.
122. Gross, L.; Mohn, F.; Moll, N.; Schuler, B.; Criado, A.; Guitián, E.; Peña, D.; Gourdon, A.; Meyer, G. *Science.* **2012**, *337* (6100), 1326–1329.
123. Hanssen, K. Ø.; Schuler, B.; Williams, A. J.; Demissie, T. B.; Hansen, E.; Andersen, J. H.; Svenson, J.; Blinov, K.; Repisky, M.; Mohn, F.; Meyer, G.; Svendsen, J.-S.; Ruud, K.; Elyashberg, M.; Gross, L.; Jaspars, M.; Isaksson, J. *Angew. Chemie Int. Ed.* **2012**, *51* (49), 12238–12241.
124. Watson, J. D.; Crick, F. H. C. *Nature* **1953**, *171* (4356), 737–738.
125. Turing, A. M. *Proc. London Math. Soc.* **1937**, *s2-42* (1), 230–265.
126. Moore, G. E. *IEEE Solid-State Circuits Soc. Newsl.* **2006**, *11* (3), 33–35.
127. Benioff, P. *J. Stat. Phys.* **1980**, *22* (5), 563–591.
128. Arute, F.; Arya, K.; Babbush, R.; Bacon, D.; Bardin, J. C.; Barends, R.; Biswas, R.; Boixo, S.; Brandao, F. G. S. L.; Buell, D. A.; Burkett, B.; Chen, Y.; Chen, Z.; Chiaro, B.; Collins, R.; Courtney, W.; Dunsworth, A.; Farhi, E.; Foxen, B.; Fowler, A.; Gidney, C.; Giustina, M.; Graff, R.; Guerin, K.; Habegger, S.; Harrigan, M. P.; Hartmann, M. J.; Ho, A.; Hoffmann, M.; Huang, T.; Humble, T. S.; Isakov, S. V.; Jeffrey, E.; Jiang, Z.; Kafri, D.; Kechedzhi, K.; Kelly, J.; Klimov, P. V.; Knysh, S.; Korotkov, A.; Kostritsa, F.; Landhuis, D.; Lindmark, M.; Lucero, E.; Lyakh, D.; Mandrà, S.; McClean, J. R.; McEwen, M.; Megrant, A.; Mi, X.; Michielsen, K.; Mohseni, M.; Mutus, J.; Naaman, O.; Neeley, M.; Neill, C.; Niu, M. Y.; Ostby, E.; Petukhov, A.; Platt, J. C.; Quintana, C.; Rieffel, E. G.; Roushan, P.; Rubin, N. C.; Sank, D.; Satzinger, K. J.; Smelyanskiy, V.; Sung, K. J.; Trevithick, M. D.; Vainsencher, A.; Villalonga, B.; White, T.; Yao, Z. J.; Yeh, P.; Zalcman, A.; Neven, H.; Martinis, J. M. *Nature* **2019**, *574* (7779), 505–510.

129. Barberousse, A.; Franceschelli, S.; Imbert, C. *Synthese* **2009**, *169*, 557–574.
130. Schlick, T. *Molecular Modeling and Simulation*; Interdisciplinary Applied Mathematics; Springer New York: New York, NY, 2002; Vol. 21.
131. Fernández, I.; Cossío, F. P. *Chem. Soc. Rev.* **2014**, *43* (14), 4906–4908.
132. Christensen, A. S.; Kubař, T.; Cui, Q.; Elstner, M. *Chem. Rev.* **2016**, *116* (9), 5301–5337.
133. Jones, L. O.; Mosquera, M. A. M. A.; Schatz, G. C.; Ratner, M. A. *J. Am. Chem. Soc.* **2020**, *142* (7), 3281–3295.
134. Entel, P.; Adeagbo, W. A.; Sugihara, M.; Rollmann, G.; Zayak, A. T.; Kreth, M.; Kadau, K. In *Computational Materials Science*; Springer, Berlin, Heidelberg, 2004; pp 177–206.
135. Grimaldo, M.; Roosen-Runge, F.; Zhang, F.; Schreiber, F.; Seydel, T. *Q. Rev. Biophys.* **2019**, *52*, E7.
136. Alder, B. J.; Wainwright, T. E. *J. Chem. Phys.* **1959**, *31* (2), 459–466.
137. Harrison, R. L. *AIP Conf. Proc.* **2009**, *1204*, 17–21.
138. Chen, J. *IOP Conf. Ser. Earth Environ. Sci* **2018**, *128*, 12110.
139. Rahman, A. *Phys. Rev.* **1964**, *136* (2A), 405–411.
140. Stillinger, F. H.; Rahman, A. *J. Chem. Phys.* **1974**, *60* (4), 1545–1557.
141. Karplus, M.; McCammon, J. A. *Nat. Struct. Biol.* **2002**, *9* (9), 646–652.
142. Karplus, M.; Kuriyan, J. *Proc. Natl. Acad. Sci. U. S. A.* **2005**, *102* (19), 6679–6685.
143. Childers, M. C.; Daggett, V. *Mol. Syst. Des. Eng.* **2017**, *2* (1), 9–33.
144. Sponer, J.; Bussi, G.; Krepl, M.; Banas, P.; Bottaro, S.; Cunha, R. A.; Gil-Ley, A.; Pinamonti, G.; Poblete, S.; Jurečka, P.; Walter, N. G.; Otyepka, M. *Chem. Rev.* **2018**, *118* (8), 4177–4338.
145. Marrink, S. J.; Corradi, V.; Souza, P. C. T.; Ingólfsson, H. I.; Tieleman, D. P.; Sansom, M. S. P. *Chem. Rev.* **2019**, *119* (9), 6184–6226.
146. Bissaro, M.; Sturlese, M.; Moro, S. *Front. Chem.* **2020**, *8*, 107.
147. Rapaport, D. C. *J. Biol. Phys.* **2018**, *44* (2), 147–162.
148. Schlick, T. In *Molecular Modeling and Simulation: An Interdisciplinary Guide*; 2010; pp 1–40.
149. The Royal Swedish Academy of Sciences. *Press. Press release* **2013**.
150. Stone, A. *The Theory of Intermolecular Forces*; Oxford University Press, 2013.
151. Frenkel, D.; Smit, B. *Understanding molecular simulation. From Algorithms to Applications*; Elsevier: San Diego, 2002.
152. Senftle, T. P.; Hong, S.; Islam, M. M.; Kylasa, S. B.; Zheng, Y.; Shin, Y. K.; Junkermeier, C.; Engel-Herbert, R.; Janik, M. J.; Aktulga, H. M.; Verstraelen, T.; Grama, A.; Van Duin, A. C. T. *npj Comput. Mater.* **2016**, *2* (1), 1–14.
153. Meuwly, M. *Wiley Interdiscip. Rev. Comput. Mol. Sci.* **2019**, *9* (1), e1386.
154. Van Der Kamp, M. W.; Mulholland, A. J. *Biochemistry* **2013**, *52* (16), 2708–2728.
155. Hartree, D. R.; Hartree, W. *Proc. R. Soc. London. Ser. A - Math. Phys. Sci.*

1935, *150* (869), 9–33.
156. Stewart, J. J. P. *J. Comput. Chem.* **1989**, *10* (2), 209–220.
157. Thiel, W. *Wiley Interdiscip. Rev. Comput. Mol. Sci.* **2014**, *4* (2), 145–157.
158. Hohenberg, P.; Kohn, W. *Phys. Rev.* **1964**, *136* (3B), B864.
159. Kohn, W.; Sham, L. J. *Phys. Rev.* **1965**, *140* (4A), A1133.
160. Raghavachari, K. *Theor. Chem. Acc.* **2000**, *103* (3–4), 361–363.
161. Cohen, A. J.; Mori-Sánchez, P.; Yang, W. *Chem. Rev.* **2012**, *112* (1), 289–320.
162. Mardirossian, N.; Head-Gordon, M. *Mol. Phys.* **2017**, *115* (19), 2315–2372.
163. Becke, A. D. *J. Chem. Phys.* **1993**, *98* (7), 5648–5652.
164. Zhao, Y.; Truhlar, D. G. *Theor. Chem. Acc.* **2008**, *120* (1–3), 215–241.
165. Frisch, M. J.; Trucks, G. W.; Schlegel, H. E.; Scuseria, G. E.; Robb, M. A.; Cheeseman, J. R.; Scalmani, G.; Barone, V.; Petersson, G. A.; O., F.; Foresman, J. B.; Fox, J. D. *Gaussian, Inc., Wallingford CT,* 2016.
166. Jones, R. O. *Rev. Mod. Phys.* **2015**, *87* (3), 897–923.
167. In *A Chemist's Guide to Density Functional Theory*; Wiley, 2001; pp 117–118.
168. Sperger, T.; Sanhueza, I. A.; Kalvet, I.; Schoenebeck, F. *Chem. Rev.* **2015**, *115* (17), 9532–9586.
169. Weijing, D.; Weihong, Z.; Xiaodong, Z.; Baofeng, Z.; Lei, C.; Laizhi, S.; Shuangxia, Y.; Haibin, G.; Guanyi, C.; Liang, Z.; Ge, S. *Energy Procedia* **2018**, *152*, 997–1002.
170. Cortese, R.; Schimmenti, R.; Prestianni, A.; Duca, D. *Theor. Chem. Acc.* **2018**, *137* (4).
171. Riley, K. E.; Pitoňcák, M.; Jurecčka, P.; Hobza, P. *Chem. Rev.* **2010**, *110* (9), 5023–5063.
172. Antony, J.; Grimme, S.; Liakos, D. G.; Neese, F. *J. Phys. Chem. A* **2011**, *115* (41), 11210–11220.
173. Yilmazer, N. D.; Korth, M. *J. Phys. Chem. B* **2013**, *117* (27), 8075–8084.
174. González, J.; Baños, I.; León, I.; Contreras-García, J.; Cocinero, E. J.; Lesarri, A.; Fernández, J. A.; Millán, J. *J. Chem. Theory Comput.* **2016**, *12* (2), 523–534.
175. Petelski, A. N.; Peruchena, N. M.; Pamies, S. C.; Sosa, G. L. *J. Mol. Model.* **2017**, *23* (9).
176. González-Díaz, N. E.; López-Rendón, R.; Ireta, J. *J. Phys. Chem. C* **2019**, *123* (4), 2526–2532.
177. Tsuzuki, S.; Lüthi, H. P. *J. Chem. Phys.* **2001**, *114* (9), 3949–3957.
178. Allen, M. J.; Tozer, D. J. *J. Chem. Phys.* **2002**, *117* (24), 11113–11120.
179. Zimmerli, U.; Parrinello, M.; Koumoutsakos, P. *J. Chem. Phys.* **2004**, *120* (6), 2693–2699.
180. Grimme, S.; Antony, J.; Ehrlich, S.; Krieg, H. *J. Chem. Phys.* **2010**, *132* (15), 154104.
181. Grimme, S.; Ehrlich, S.; Goerigk, L. *J. Comput. Chem.* **2011**, *32* (7), 1456–1465.

182. Becke, A. D.; Johnson, E. R. *J. Chem. Phys.* **2007**, *127* (15), 154108.
183. Becke, A. D. *J. Chem. Phys.* **2014**, *140* (18), 18–301.
184. Piela, L. *Ideas of Quantum Chemistry*; Elsevier, 2007.
185. Szabo, A.; Ostlund, N. *Modern quantum chemistry : introduction to advanced electronic structure theory / Attila Szabo, Neil S. Ostlund*; 2018.
186. Jensen, F. *Introduction to Computational Chemistry*; John Wiley & Sons, 2013.
187. Levine, I. N. *Quantum Chemistry*; Pearson, Ed.; 2014.
188. Dennington, R.; Keith, T.; Millam, J. *Semichem Inc. , Shawnee Mission, KS*. 2019.
189. Cousins, K. R. *J. Am. Chem. Soc.* **2011**, *133* (21), 8388.
190. Hanwell, M. D.; Curtis, D. E.; Lonie, D. C.; Vandermeerschd, T.; Zurek, E.; Hutchison, G. R. *J. Cheminform.* **2012**, *4* (8), 17.
191. Protein Data Bank. RCSB PDB: Homepage https://www.rcsb.org/ (accessed Jun 15, 2020).
192. Berman, H.; Henrick, K.; Nakamura, H. *Nat. Struct. Biol.* **2003**, *10* (12), 980.
193. Use of constraints in molecular dynamics - Robin Corey's Posts - Quora https://www.quora.com/q/gnvbdldrivyzzipw/Use-of-constraints-in-molecular-dynamics (accessed May 22, 2020).
194. Hess, B.; Bekker, H.; Berendsen, H. J. C. C.; Fraaije, J. G. E. M. E. M. *J. Comput. Chem.* **1997**, *18* (12), 1463–1472.
195. Ryckaert, J. P.; Ciccotti, G.; Berendsen, H. J. C. *J. Comput. Phys.* **1977**, *23* (3), 327–341.
196. Feenstra, K. A.; Hess, B.; Berendsen, H. J. C. *J. Comput. Chem.* **1999**, *20* (8), 786–798.
197. Martín-García, F.; Papaleo, E.; Gomez-Puertas, P.; Boomsma, W.; Lindorff-Larsen, K. *PLoS One* **2015**, *10* (3), e0121114.
198. Cino, E. A.; Choy, W. Y.; Karttunen, M. *J. Chem. Theory Comput.* **2012**, *8* (8), 2725–2740.
199. Shirts, M. R.; Pitera, J. W.; Swope, W. C.; Pande, V. S. *J. Chem. Phys.* **2003**, *119* (11), 5740–5761.
200. Beauchamp, K. A.; Lin, Y. S.; Das, R.; Pande, V. S. *J. Chem. Theory Comput.* **2012**, *8* (4), 1409–1414.
201. Piggot, T. J.; Piñeiro, Á.; Khalid, S. *J. Chem. Theory Comput.* **2012**, *8* (11), 4593–4609.
202. Schmid, N.; Eichenberger, A. P.; Choutko, A.; Riniker, S.; Winger, M.; Mark, A. E.; Van Gunsteren, W. F. *Eur. Biophys. J.* **2011**, *40* (7), 843–856.
203. Chebaro, Y.; Pasquali, S.; Derreumaux, P. *J. Phys. Chem. B* **2012**, *116* (30), 8741–8752.
204. Periole, X.; Marrink, S.-J. *Methods Mol. Biol.* **2013**, *924*, 533–565.
205. Singh, N.; Li, W. *Int. J. Mol. Sci.* **2019**, *20* (15), 3774.
206. Bond, P. J.; Sansom, M. S. P. *J. Am. Chem. Soc.* **2006**, *128* (8), 2697–2704.
207. Bond, P. J.; Holyoake, J.; Ivetac, A.; Khalid, S.; Sansom, M. S. P. *J. Struct.*

Biol. **2007**, *157* (3), 593–605.
208. Scott, K. A.; Bond, P. J.; Ivetac, A.; Chetwynd, A. P.; Khalid, S.; Sansom, M. S. P. *Structure* **2008**, *16* (4), 621–630.
209. Marrink, S. J.; Tieleman, D. P. *Chem. Soc. Rev.* **2013**, *42* (16), 6801–6822.
210. Chapman, J. B. J. Improving the Functional Control of Ferroelectrics using Insights from Atomistic Modelling, UCL (University College London), 2018.
211. Essmann, U.; Perera, L.; Berkowitz, M. L.; Darden, T.; Lee, H.; Pedersen, L. G. *J. Chem. Phys.* **1995**, *103* (19), 8577–8593.
212. Woodcock, L. V. *Chem. Phys. Lett.* **1971**, *10* (3), 257–261.
213. Berendsen, H. J. C.; Postma, J. P. M.; Van Gunsteren, W. F.; Dinola, A.; Haak, J. R. *J. Chem. Phys.* **1984**, *81* (8), 3684–3690.
214. Andersen, H. C. *J. Chem. Phys.* **1980**, *72* (4), 2384–2393.
215. Parrinello, M.; Rahman, A. *J. Appl. Phys.* **1981**, *52* (12), 7182–7190.
216. Brooks, B. R.; Brooks, C. L.; Mackerell, A. D.; Nilsson, L.; Petrella, R. J.; Roux, B.; Won, Y.; Archontis, G.; Bartels, C.; Boresch, S.; Caflisch, A.; Caves, L.; Cui, Q.; Dinner, A. R.; Feig, M.; Fischer, S.; Gao, J.; Hodoscek, M.; Im, W.; Kuczera, K.; Lazaridis, T.; Ma, J.; Ovchinnikov, V.; Paci, E.; Pastor, R. W.; Post, C. B.; Pu, J. Z.; Schaefer, M.; Tidor, B.; Venable, R. M.; Woodcock, H. L.; Wu, X.; Yang, W.; York, D. M.; Karplus, M. *J. Comput. Chem.* **2009**, *30* (10), 1545–1614.
217. Phillips, J. C.; Braun, R.; Wang, W.; Gumbart, J.; Tajkhorshid, E.; Villa, E.; Chipot, C.; Skeel, R. D.; Kalé, L.; Schulten, K. *J. Comput. Chem.* **2005**, *26* (16), 1781–1802.
218. Case, D. A.; Cheatham, T. E.; Darden, T.; Gohlke, H.; Luo, R.; Merz, K. M.; Onufriev, A.; Simmerling, C.; Wang, B.; Woods, R. J. *J. Comput. Chem.* **2005**, *26* (16), 1668–1688.
219. Van Der Spoel, D.; Lindahl, E.; Hess, B.; Groenhof, G.; Mark, A. E.; Berendsen, H. J. C. *J. Comput. Chem.* **2005**, *26* (16), 1701–1718.
220. Root-Bernstein, R.; Allen, L.; Beach, L.; Bhadula, R.; Fast, J.; Hosey, C.; Kremkow, B.; Lapp, J.; Lonc, K.; Pawelec, K.; Podufaly, A.; Russ, C.; Tennant, L.; Vrtis, E.; Weinlander, S. *J. Psychol. Sci. Technol.* **2009**, *1* (2), 51–63.
221. Root-Bernstein, R. S.; Bernstein, M.; Garnier, H. *Creat. Res. J.* **1995**, *8* (2), 115–137.
222. Bennie, S. J.; Ranaghan, K. E.; Deeks, H.; Goldsmith, H. E.; O'Connor, M. B.; Mulholland, A. J.; Glowacki, D. R. *J. Chem. Educ.* **2019**, *96* (11), 2488–2496.
223. Lohning, A. E.; Hall, S.; Dukie, S. *J. Chem. Educ.* **2019**, *96* (11), 2497–2502.
224. Li, L.; Yu, F.; Shi, D.; Shi, J.; Tian, Z.; Yang, J.; Wang, X.; Jiang, Q. *Am. J. Transl. Res.* **2017**, *9* (9), 3867–3880.
225. Gurnon, D.; Voss-Andreae, J.; Stanley, J. *PLoS Biol.* **2013**, *11* (2), e1001491.

226. Kendrew, J. C.; Bodo, G.; Dintzis, H. M.; Parrish, R. G.; Wyckoff, H.; Phillips, D. C. *Nature* **1958**, *181* (4610), 662–666.
227. Rubin, B.; Richardson, J. S. *Biopolymers* **1972**, *11* (11), 2381–2385.
228. Richardson, J. S. *Methods Enzymol.* **1985**, *115* (C), 359–380.
229. Richardson, J. S. *Nat. Struct. Biol.* **2000**, *7* (8), 624–625.
230. Lesk, A. M.; Hardman, K. D. *Science.* **1982**, *216* (4545), 539–540.
231. Humphrey, W.; Dalke, A.; Schulten, K. *J. Mol. Graph.* **1996**, *14* (1), 27-28,33-38.
232. DeLano, W. L. *CCP4 Newsletter On Protein Crystallography*. 2002.
233. Pettersen, E. F.; Goddard, T. D.; Huang, C. C.; Couch, G. S.; Greenblatt, D. M.; Meng, E. C.; Ferrin, T. E. *Journal of Computational Chemistry*. 2004.
234. Chavent, M.; Levy, B.; Krone, M.; Bidmon, K.; Nomine, J.-P.; Ertl, T.; Baaden, M. *Brief. Bioinform.* **2011**, *12* (6), 689–701.
235. Chavent, M.; Vanel, A.; Tek, A.; Levy, B.; Robert, S.; Raffin, B.; Baaden, M. *J. Comput. Chem.* **2011**, *32* (13), 2924–2935.
236. Kozlíková, B.; Krone, M.; Falk, M.; Lindow, N.; Baaden, M.; Baum, D.; Viola, I.; Parulek, J.; Hege, H.-C. *Comput. Graph. Forum* **2017**, *36* (8), 178–204.
237. Liu, X. H.; Wang, T.; Lin, J. P.; Wu, M. Bin. *Expert Opin. Drug Discov.* **2018**, *13* (12), 1103–1114.
238. Kenngott, H. G.; Preukschas, A. A.; Wagner, M.; Nickel, F.; Müller, M.; Bellemann, N.; Stock, C.; Fangerau, M.; Radeleff, B.; Kauczor, H. U.; Meinzer, H. P.; Maier-Hein, L.; Müller-Stich, B. P. *Surg. Endosc.* **2018**, *32* (6), 2958–2967.
239. Cipresso, P.; Giglioli, I. A. C.; Raya, M. A.; Riva, G. *Front. Psychol.* **2018**, *9*, 2086.
240. Lv, Z.; Tek, A.; Da Silva, F.; Empereur-mot, C.; Chavent, M.; Baaden, M. *PLoS One* **2013**, *8* (3), e57990.
241. Yu, C. H.; Qin, Z.; Martin-Martinez, F. J.; Buehler, M. J. *ACS Nano* **2019**, *7*, 7471–7482.
242. Zheng, M.; Waller, M. P. *J. Mol. Graph. Model.* **2017**, *73*, 18–23.
243. Borrel, A.; Fourches, D. *Bioinformatics* **2017**, *33* (23), 3816–3818.
244. Kingsley, L. J.; Brunet, V.; Lelais, G.; McCloskey, S.; Milliken, K.; Leija, E.; Fuhs, S. R.; Wang, K.; Zhou, E.; Spraggon, G. *J. Mol. Graph. Model.* **2019**, *89*, 234–241.
245. Pérez, S.; Tubiana, T.; Imberty, A.; Baaden, M. *Glycobiology* **2015**, *25* (5), 483–491.
246. Doutreligne, S.; Cragnolini, T.; Pasquali, S.; Derreumaux, P.; Baaden, M. In *IEEE Symposium on Large Data Analysis and Visualization 2014, LDAV 2014 - Proceedings*; Institute of Electrical and Electronics Engineers Inc., 2014; pp 109–110.
247. Doutreligne, S.; Gageat, C.; Cragnolini, T.; Taly, A.; Pasquali, S.; Derreumaux, P.; Baaden, M. In *2015 IEEE 1st International Workshop on Virtual and Augmented Reality for Molecular Science, VARMS@IEEEVR*

2015; Institute of Electrical and Electronics Engineers Inc., 2015; pp 1–6.
248. O'Connor, M.; Deeks, H. M.; Dawn, E.; Metatla, O.; Roudaut, A.; Sutton, M.; Thomas, L. M.; Glowacki, B. R.; Sage, R.; Tew, P.; Wonnacott, M.; Bates, P.; Mulholland, A. J.; Glowacki, D. R. *Sci. Adv.* **2018**, *4* (6), eaat2731.
249. O'Connor, M.; Bennie, S. J.; Deeks, H. M.; Jamieson-Binnie, A.; Jones, A. J.; Shannon, R. J.; Walters, R.; Mitchell, T. J.; Mulholland, A. J.; Glowacki, D. R. *J. Chem. Phys.* **2019**, *150* (22), 220901.
250. Amabilino, S.; Bratholm, L. A.; Bennie, S. J.; Vaucher, A. C.; Reiher, M.; Glowacki, D. R. *J. Phys. Chem. A* **2019**, *123* (20), 4486–4499.
251. Calvelo, M.; Piñeiro, Á.; Garcia-Fandino, R. *Comput. Struct. Biotechnol. J.* **2020**, *18*, 2621–2628.
252. Bong, D. T.; Clark, T. D.; Granja, J. R.; Ghadiri, M. R. *Angew. Chem. Int. Ed. Engl.* **2001**, *40* (6), 988–1011.
253. Richardson, J. S.; Richardson, D. C. *Proc. Natl. Acad. Sci. U. S. A.* **2002**, *99* (5), 2754–2759.
254. Fraser, R. D. B.; Parry, D. A. D. *Biophys. Rev.* **2009**, *1* (1), 27–35.
255. Chothia, C.; Janin, J. *Proc. Natl. Acad. Sci.* **1981**, *78* (7), 4146–4150.
256. Silk, M. R.; Newman, J.; Ratcliffe, J. C.; White, J. F.; Caradoc-Davies, T.; Price, J. R.; Perrier, S.; Thompson, P. E.; Chalmers, D. K. *Chem. Commun.* **2017**, *53* (49), 6613–6616.
257. Gailer, C.; Feigel, M. *J. Comput. Aided. Mol. Des.* **1997**, *11* (3), 273–277.
258. Kobayashi, K.; Granja, J. R.; Ghadiri, M. R. *Angew. Chemie Int. Ed. English* **1995**, *34* (1), 95–98.
259. Scheiner, S. *J. Phys. Chem. B* **2006**, *110* (37), 18670–18679.
260. Kuzuya, A.; Wang, R.; Sha, R.; Seeman, N. C. *Nano Lett.* **2007**, *7* (6), 1757–1763.
261. Qu, W.; Tan, H.; Chen, G.; Liu, R. *Int. J. Quantum Chem.* **2010**, *110* (9), 1648–1659.
262. Rosenthal-Aizman, K.; Svensson, G.; Undén, A. *J. Am. Chem. Soc.* **2004**, *126* (11), 3372–3373.
263. Brea, R. J.; Amorín, M.; Castedo, L.; Granja, J. R. *Angew. Chemie - Int. Ed.* **2005**, *44* (35), 5710–5713.
264. Amorín, M.; Castedo, L.; Granja, J. R. *Chem. - A Eur. J.* **2008**, *14* (7), 2100–2111.
265. Li, L.; Zhan, H.; Duan, P.; Liao, J.; Quan, J.; Hu, Y.; Chen, Z.; Zhu, J.; Liu, M.; Wu, Y.-D.; Deng, J. *Adv. Funct. Mater.* **2012**, *22* (14), 3051–3056.
266. Gauthier, D.; Baillargeon, P.; Drouin, M.; Dory, Y. L. *Angew. Chemie Int. Ed.* **2001**, *40* (24), 4635–4638.
267. Baillargeon, P.; Bernard, S.; Gauthier, D.; Skouta, R.; Dory, Y. L. *Chem. - A Eur. J.* **2007**, *13* (33), 9223–9235.
268. Marmin, T.; Dory, Y. L. *Chem. - A Eur. J.* **2019**, *25* (27), 6707–6711.
269. Seebach, D.; Matthews, J. L.; Meden, A.; Wessels, T.; Baerlocher, C.; McCusker, L. B. *Helv. Chim. Acta* **1997**, *80* (1), 173–182.

270. Clark, T. D.; Buehler, L. K.; Ghadiri, M. R. *J. Am. Chem. Soc.* **1998**, *120* (4), 651–656.
271. Jagannadh, B.; Reddy, M. S.; Rao, C. L.; Prabhakar, A.; Jagadeesh, B.; Chandrasekhar, S. *Chem. Commun.* **2006**, No. 46, 4847–4849.
272. Ishihara, Y.; Kimura, S. *J. Pept. Sci.* **2010**, *16* (2), 110–114.
273. Fujimura, F.; Hirata, T.; Morita, T.; Kimura, S.; Horikawa, Y.; Sugiyama, J. *Biomacromolecules* **2006**, *7* (8), 2394–2400.
274. Becke, A. D. *J. Chem. Phys.* **1993**, *98* (7), 5648–5652.
275. Rassolov, V. A.; Pople, J. A.; Ratner, M. A.; Windus, T. L. *J. Chem. Phys.* **1998**, *109* (4), 1223–1229.
276. Rassolov, V. A.; Ratner, M. A.; Pople, J. A.; Redfern, P. C.; Curtiss, L. A. *J. Comput. Chem.* **2001**, *22* (9), 976–984.
277. Simon, S.; Duran, M.; Dannenberg, J. J. *J. Chem. Phys.* **1996**, *105* (24), 11024–11031.
278. Kesharwani, M. K.; Karton, A.; Martin, J. M. L. *J. Chem. Theory Comput.* **2016**, *12* (1), 444–454.
279. Boys, S. F.; Bernardi, F. *Mol. Phys.* **1970**, *19* (4), 553–566.
280. Lu, T.; Chen, F. *J. Comput. Chem.* **2012**, *33* (5), 580–592.
281. Dimer dice - Apps on Google Play https://play.google.com/store/apps/details?id=com.mduse.DimerDice&hl=en (accessed Jun 18, 2020).
282. Calvelo, M.; Lamas, A.; Guerra, A.; Amorin, M.; Garcia-Fandino, R.; Granja, J. R. *Chem. – A Eur. J.* **2020**, *26* (26), 5846–5858.
283. Taylor, R.; Kennard, O. *Acc. Chem. Res.* **1984**, *17* (9), 320–326.
284. Desiraju, G. R. *Acc. Chem. Res.* **1996**, *29* (9), 441–449.
285. Brea Fernández, R. J. Diseño, síntesis y aplicaciones de sistemas supramoleculares homo- y heterodiméricos selectivos y eficientes basados en α, γ ciclopéptidos, Universidade de Santiago de Compostela, 2013.
286. Koch, U.; Popelier, P. L. A. *J. Phys. Chem.* **1995**, *99* (24), 9747–9754.
287. Alkorta, I.; Rozas, I.; Elguero, J. *Struct. Chem.* **1998**, *9* (4), 243–247.
288. Parthasarathi, R.; Subramanian, V.; Sathyamurthy, N. *J. Phys. Chem. A* **2006**, *110* (10), 3349–3351.
289. Grabowski, S. J. *J. Phys. Chem. A* **2001**, *105* (47), 10739–10746.
290. Grabowski, S. J. *J. Phys. Chem. A* **2000**, *104* (23), 5551–5557.
291. Boyd, R. J.; Choi, S. C. *Chem. Phys. Lett.* **1986**, *129* (1), 62–65.
292. Grabowski, S. J. *J. Mol. Struct.* **2001**, *562* (1–3), 137–143.
293. Espinosa, E.; Molins, E.; Lecomte, C. *Chem. Phys. Lett.* **1998**, *285* (3–4), 170–173.
294. Zarra, S.; Wood, D. M.; Roberts, D. A.; Nitschke, J. R. *Chem. Soc. Rev.* **2015**, *44* (2), 419–432.
295. Ballester, P.; Fujita, M.; Rebek, J. *Chem. Soc. Rev.* **2015**, *44* (2), 392–393.
296. Smulders, M. M. J.; Riddell, I. A.; Browne, C.; Nitschke, J. R. *Chem. Soc. Rev.* **2013**, *42* (4), 1728–1754.
297. Chakrabarty, R.; Mukherjee, P. S.; Stang, P. J. *Chem. Rev.* **2011**, *111* (11),

6810–6918.
298. Kim, H. J.; Lee, M. H.; Mutihac, L.; Vicens, J.; Kim, J. S. *Chem. Soc. Rev.* **2012**, *41* (3), 1173–1190.
299. Hasell, T.; Cooper, A. I. *Nature Reviews Materials*. Nature Publishing Group July 26, 2016, pp 1–14.
300. Rizzuto, F. J.; von Krbek, L. K. S.; Nitschke, J. R. *Nature Reviews Chemistry*. Nature Publishing Group April 1, 2019, pp 204–222.
301. Dietrich, B.; Lehn, J. M.; Sauvage, J. P. *Tetrahedron Lett.* **1969**, *10* (34), 2889–2892.
302. Lehn, J. M. *Acc. Chem. Res.* **1978**, *11* (2), 49–57.
303. Cram, D. J.; Karbach, S.; Kim, Y. H.; Baczynskyj, L.; Marti, K.; Sampson, R. M.; Kalleymeyn, G. W. *J. Am. Chem. Soc.* **1988**, *110* (8), 2554–2560.
304. Cram, D. J.; Takahiro, K.; Helgeson, R. C.; Lein, G. M. *J. Am. Chem. Soc.* **1979**, *101* (22), 6752–6754.
305. Cram, D. J.; Kaneda, T.; Helgeson, R. C.; Brown, S. B.; Knobler, C. B.; Maverick, E.; Trueblood, K. N. *J. Am. Chem. Soc.* **1985**, *107* (12), 3645–3657.
306. The Nobel Prize in Chemistry 1987 - NobelPrize.org https://www.nobelprize.org/prizes/chemistry/1987/summary/ (accessed May 18, 2020).
307. Wyler, R.; de Mendoza, J.; Rebek, J. *Angew. Chemie Int. Ed. English* **1993**, *32* (12), 1699–1701.
308. Branda, N.; Wyler, R.; Rebek, J. *Science.* **1994**, *263* (5151), 1267–1268.
309. Ajami, D.; Rebek, J. *Acc. Chem. Res.* **2013**, *46* (4), 990–999.
310. Cook, T. R.; Zheng, Y. R.; Stang, P. J. *Chem. Rev.* **2013**, *113* (1), 734–777.
311. Harris, K.; Fujita, D.; Fujita, M. *Chem. Commun.* **2013**, *49* (60), 6703–6712.
312. Fujita, D.; Ueda, Y.; Sato, S.; Yokoyama, H.; Mizuno, N.; Kumasaka, T.; Fujita, M. *Chem* **2016**, *1* (1), 91–101.
313. Ronson, T. K.; Zarra, S.; Black, S. P.; Nitschke, J. R. *Chem. Commun.* **2013**, *49* (25), 2476–2490.
314. Parac, T. N.; Caulder, D. L.; Raymond, K. N. *Journal of the American Chemical Society*. American Chemical Society August 12, 1998, pp 8003–8004.
315. Saenger, W. *Angew. Chemie Int. Ed. English* **1980**, *19* (5), 344–362.
316. Bender, M. L.; Komiyama, M. *Cyclodextrin Chemistry*; Reactivity and Structure Concepts in Organic Chemistry; Springer Berlin Heidelberg: Berlin, Heidelberg, 1978; Vol. 6.
317. Del Valle, E. M. M. *Process Biochemistry*. Elsevier May 31, 2004, pp 1033–1046.
318. dos Santos, C.; Buera, P.; Mazzobre, F. *Curr. Opin. Food Sci.* **2017**, *16*, 106–113.
319. Marques, H. M. C. *Flavour Fragr. J.* **2010**, *25* (5), 313–326.
320. Saha, S.; Roy, A.; Roy, K.; Roy, M. N. *Sci. Rep.* **2016**, *6* (1), 1–12.
321. Rekharsky, M. V.; Inoue, Y. *Chem. Rev.* **1998**, *98* (5), 1875–1917.

322. F. Garrido, P.; Calvelo, M.; Garcia-Fandiño, R.; Piñeiro, Á. *Biomolecules* **2020**, *10* (3), 431.
323. Davis, M. E.; Brewster, M. E. *Nat. Rev. Drug Discov.* **2004**, *3* (12), 1023–1035.
324. Patro, N. M.; Sultana, A.; Terao, K.; Nakata, D.; Jo, A.; Urano, A.; Ishida, Y.; Gorantla, R. N.; Pandit, V.; Devi, K.; Rohit, S.; Grewal, B. K.; Sophia, E. M.; Suresh, A.; Ekbote, V. K.; Suresh, S. *J. Incl. Phenom. Macrocycl. Chem.* **2014**, *78* (1–4), 471–483.
325. Braga, S. S. *Biomolecules* **2019**, *9* (12).
326. Ohvo, H.; Slotte, J. P. *Biochemistry* **1996**, *35* (24), 8018–8024.
327. Uekama, K. *Chem. Pharm. Bull.* **2004**, *52* (8), 900–915.
328. Garrido, P. F.; Calvelo, M.; Blanco-González, A.; Veleiro, U.; Suárez, F.; Conde, D.; Cabezón, A.; Piñeiro, Á.; Garcia-Fandino, R. *Int. J. Pharm.* **2020**, *588*, 119689.
329. Zhang, H.; Tan, T.; Hetényi, C.; Lv, Y.; Van Der Spoel, D. *J. Phys. Chem. C* **2014**, *118* (13), 7163–7173.
330. Liu, Y.; Li, L.; Chen, Y.; Yu, L.; Fan, Z.; Ding, F. *J. Phys. Chem. B* **2005**, *109* (9), 4129–4134.
331. Cheng, X.; Lu, Z.; Li, Y.; Wang, Q.; Lu, C.; Meng, Q. *Dalt. Trans.* **2011**, *40* (44), 11788–11794.
332. Ji, J.; Wu, W.; Liang, W.; Cheng, G.; Matsushita, R.; Yan, Z.; Wei, X.; Rao, M.; Yuan, D. Q.; Fukuhara, G.; Mori, T.; Inoue, Y.; Yang, C. *J. Am. Chem. Soc.* **2019**, *141* (23), 9225–9238.
333. Messner, M.; Kurkov, S. V.; Brewster, M. E.; Jansook, P.; Loftsson, T. *Int. J. Pharm.* **2011**, *407* (1–2), 174–183.
334. Márquez, C.; Hudgins, R. R.; Nau, W. M. *J. Am. Chem. Soc.* **2004**, *126* (18), 5806–5816.
335. Barrow, S. J.; Kasera, S.; Rowland, M. J.; Del Barrio, J.; Scherman, O. A. *Chem. Rev.* **2015**, *115* (22), 12320–12406.
336. Pichierri, F. *Dalt. Trans.* **2013**, *42* (17), 6083–6091.
337. Rodríguez-Vázquez, N.; Fuertes, A.; Amorín, M.; Granja, J. R. *Met. Ions Life Sci.* **2016**, *16*, 485–556.
338. Rodríguez-Vázquez, N.; García-Fandiño, R.; Aldegunde, M. J.; Brea, J.; Loza, M. I.; Amorín, M.; Granja, J. R. *Org. Lett.* **2017**, *19* (10), 2560–2563.
339. Pérez-Alvite, M. J.; Mosquera, M.; Castedo, L.; Granja, J. R. *Amino Acids* **2011**, *41* (3), 621–628.
340. Panciera, M.; Amorín, M.; Castedo, L.; Granja, J. R. *Chem. - A Eur. J.* **2013**, *19* (15), 4826–4834.
341. Ozores, H. L.; Amorín, M.; Granja, J. R. *J. Am. Chem. Soc.* **2017**, *139* (2), 776–784.
342. Miklitz, M.; Jiang, S.; Clowes, R.; Briggs, M. E.; Cooper, A. I.; Jelfs, K. E. *J. Phys. Chem. C* **2017**, *121* (28), 15211–15222.
343. Peterson, K. A.; Figgen, D.; Goll, E.; Stoll, H.; Dolg, M. *J. Chem. Phys.* **2003**, *119* (21), 11113–11123.

344. Peterson, K. A.; Shepler, B. C.; Figgen, D.; Stoll, H. *J. Phys. Chem. A* **2006**, *110* (51), 13877–13883.
345. Huang, Z.; Li, Y.; Wang, X. *Sci. Rep.* **2017**, *7* (1), 10278.
346. Voss, N. R.; Gerstein, M. *Nucleic Acids Res.* **2010**, *38* (Web Server issue), W555-62.
347. Schröder, L.; Lowery, T. J.; Hilty, C.; Wemmer, D. E.; Pines, A. *Science.* **2006**, *314* (5798), 446–449.
348. Schröder, L. *Phys. Medica* **2013**, *29* (1), 3–16.
349. Rogers, N. J.; Hill-Casey, F.; Stupic, K. F.; Six, J. S.; Lesbats, C.; Rigby, S. P.; Fraissard, J.; Pavlovskaya, G. E.; Meersmann, T. *Proc. Natl. Acad. Sci. U. S. A.* **2016**, *113* (12), 3164–3168.
350. Yang, R. T. *Gas Separation by Adsorption Processes*; Elsevier, 1987.
351. Kerry, F. G. *Industrial gas handbook: gas separation and purification. 1st ed. Boca Raton, FL: CRC Press; 2007*; CRC Press, 2007.
352. Banerjee, D.; Cairns, A. J.; Liu, J.; Motkuri, R. K.; Nune, S. K.; Fernandez, C. A.; Krishna, R.; Strachan, D. M.; Thallapally, P. K. *Acc. Chem. Res.* **2015**, *48* (2), 211–219.
353. Bazan, R. E.; Bastos-Neto, M.; Moeller, A.; Dreisbach, F.; Staudt, R. *Adsorption* **2011**, *17* (2), 371–383.
354. Chen, L.; Reiss, P. S.; Chong, S. Y.; Holden, D.; Jelfs, K. E.; Hasell, T.; Little, M. A.; Kewley, A.; Briggs, M. E.; Stephenson, A.; Thomas, K. M.; Armstrong, J. A.; Bell, J.; Busto, J.; Noel, R.; Liu, J.; Strachan, D. M.; Thallapally, P. K.; Cooper, A. I. *Nat. Mater.* **2014**, *13* (10), 954–960.
355. Liu, Y.; Liu, J.; Hu, J. *BMC Chem. Eng.* **2019**, *1* (1), 3.
356. Banerjee, D.; Simon, C. M.; Elsaidi, S. K.; Haranczyk, M.; Thallapally, P. K. *Chem* **2018**, *4* (3), 466–494.
357. Wang, C. H.; Wu, Q.; Fan, W. J.; Zhang, R. Q.; Lin, Z. *Org. Biomol. Chem.* **2012**, *10* (26), 5049–5054.
358. Zhao, X.; Fan, J. F.; Si, X. L.; Zhang, L. L.; Qu, M. N. *J. Mol. Graph. Model.* **2018**, *83*, 74–83.
359. Li, R.; Fan, J.; Li, H.; Yan, X.; Yu, Y. *J. Chem. Phys.* **2015**, *143* (1), 015101.
360. Mecozzi, S.; Julius Rebek, J. *Chem. – A Eur. J.* **1998**, *4* (6), 1016–1022.
361. Brotin, T.; Lesage, A.; Emsley, L.; Collet, A. *J. Am. Chem. Soc.* **2000**, *122* (6), 1171–1174.
362. Bartik, K.; Luhmer, M.; Heyes, S. J.; Ottinger, R.; Reisse, J. *J. Magn. Reson. Ser. B* **1995**, *109* (2), 164–168.
363. Pizzi, A.; Ozores, H. L.; Calvelo, M.; García-Fandiño, R.; Amorín, M.; Demitri, N.; Terraneo, G.; Bracco, S.; Comotti, A.; Sozzani, P.; Bezuidenhout, C. X.; Metrangolo, P.; Granja, J. R. *Angew. Chemie - Int. Ed.* **2019**, *58* (41), 14472–14476.
364. Heister, E.; Brunner, E. W.; Dieckmann, G. R.; Jurewicz, I.; Dalton, A. B. *ACS Appl. Mater. Interfaces* **2013**, *5* (6), 1870–1891.
365. Yan, Y.; Miao, J.; Yang, Z.; Xiao, F. X.; Yang, H. Bin; Liu, B.; Yang, Y.

Chem. Soc. Rev. **2015**, *44* (10), 3295–3346.
366. Baughman, R. H.; Zakhidov, A. A.; De Heer, W. A. *Science.* **2002**, *297* (5582), 787–792.
367. Bottini, M.; Bruckner, S.; Nika, K.; Bottini, N.; Bellucci, S.; Magrini, A.; Bergamaschi, A.; Mustelin, T. *Toxicol. Lett.* **2006**, *160* (2), 121–126.
368. Kobayashi, N.; Izumi, H.; Morimoto, Y. *J. Occup. Health* **2017**, *59* (5), 394–407.
369. Bianco, A.; Kostarelos, K.; Partidos, C. D.; Prato, M. *Chem. Commun.* **2005**, No. 5, 571–577.
370. Singh, P.; Campidelli, S.; Giordani, S.; Bonifazi, D.; Bianco, A.; Prato, M. *Chem. Soc. Rev.* **2009**, *38* (8), 2214–2230.
371. Britz, D. A.; Khlobystov, A. N. *Chem. Soc. Rev.* **2006**, *35* (7), 637–659.
372. Bakota, E. L.; Aulisa, L.; Tsyboulski, D. A.; Weisman, R. B.; Hartgerink, J. D. *Biomacromolecules* **2009**, *10* (8), 2201–2206.
373. Antonucci, A.; Kupis-Rozmysłowicz, J.; Boghossian, A. A. *ACS Appl. Mater. Interfaces* **2017**, *9* (13), 11321–11331.
374. Cogan, N. M. B.; Bowerman, C. J.; Nogaj, L. J.; Nilsson, B. L.; Krauss, T. D. *J. Phys. Chem. C* **2014**, *118* (11), 5935–5944.
375. Pérez, E. M. *Chem. - A Eur. J.* **2017**, *23* (52), 12681–12689.
376. Blanco, M.; Nieto-Ortega, B.; De Juan, A.; Vera-Hidalgo, M.; López-Moreno, A.; Casado, S.; González, L. R.; Sawada, H.; González-Calbet, J. M.; Pérez, E. M. *Nat. Commun.* **2018**, *9* (1), 1–7.
377. López-Moreno, A.; Nieto-Ortega, B.; Moffa, M.; De Juan, A.; Bernal, M. M.; Fernández-Blázquez, J. P.; Vilatela, J. J.; Pisignano, D.; Pérez, E. M. *ACS Nano* **2016**, *10* (8), 8012–8018.
378. Mena-Hernando, S.; Pérez, E. M. *Chem. Soc. Rev.* **2019**, *48* (19), 5016–5032.
379. Villalva, J.; Nieto-Ortega, B.; Melle-Franco, M.; Pérez, E. M. *J. Phys. Chem. C* **2020**, *124* (28), 15541–15546.
380. López-Moreno, A.; Pérez, E. M. *Chem. Commun.* **2015**, *51* (25), 5421–5424.
381. de Juan, A.; Pouillon, Y.; Ruiz-González, L.; Torres-Pardo, A.; Casado, S.; Martín, N.; Rubio, Á.; Pérez, E. M. *Angew. Chemie* **2014**, *126* (21), 5498–5504.
382. Chamorro, R.; De Juan-Fernández, L.; Nieto-Ortega, B.; Mayoral, M. J.; Casado, S.; Ruiz-González, L.; Pérez, E. M.; González-Rodríguez, D. *Chem. Sci.* **2018**, *9* (17), 4176–4184.
383. Ortiz-Acevedo, A.; Xie, H.; Zorbas, V.; Sampson, W. M.; Dalton, A. B.; Baughman, R. H.; Draper, R. K.; Musselman, I. H.; Dieckmann, G. R. *J. Am. Chem. Soc.* **2005**, *127* (26), 9512–9517.
384. Friling, S. R.; Notman, R.; Walsh, T. R. *Nanoscale* **2010**, *2* (1), 98–106.
385. Chiu, C. C.; Maher, M. C.; Dieckmann, G. R.; Nielsen, S. O. *ACS Nano* **2010**, *4* (5), 2539–2546.
386. Vidhyasankar, S.; Dharmaraj, N.; Kolandaivel, P. *J. Biomol. Struct. Dyn.*

2018, *36* (5), 1108–1117.
387. Almeida, J. G.; Preto, A. J.; Koukos, P. I.; Bonvin, A. M. J. J.; Moreira, I. S. *Biochim. Biophys. Acta - Biomembr.* **2017**, *1859* (10), 2021–2039.
388. Sisson, A. L.; Shah, M. R.; Bhosale, S.; Matile, S. *Chem. Soc. Rev.* **2006**, *35* (12), 1269–1286.
389. Chen, L.; Si, W.; Zhang, L.; Tang, G.; Li, Z. T.; Hou, J. L. *J. Am. Chem. Soc.* **2013**, *135* (6), 2152–2155.
390. Khazanovich, N.; Granja, J. R.; McRee, D. E.; Milligan, R. A.; Ghadiri, M. R. *J. Am. Chem. Soc.* **1994**, *116* (13), 6011–6012.
391. García-Fandiño, R.; Amorín, M.; Castedo, L.; Granja, J. R. *Chem. Sci.* **2012**, *3* (11), 3280–3285.
392. Vijayaraj, R.; Van Damme, S.; Bultinck, P.; Subramanian, V. *Phys. Chem. Chem. Phys.* **2012**, *14* (43), 15135–15144.
393. Song, Y.; Lee, J. H.; Hwang, H.; Schatz, G. C.; Hwang, H. *J. Phys. Chem. B* **2016**, *120* (46), 11912–11922.
394. Dehez, F.; Tarek, M.; Chipot, C. *J. Phys. Chem. B* **2007**, *111* (36), 10633–10635.
395. Zhang, M.; Fan, J.; Xu, J.; Weng, P.; Lin, H. *J. Mol. Model.* **2016**, *22* (10), 233.
396. Xu, J.; Fan, J. F.; Zhang, M. M.; Weng, P. P.; Lin, H. F. *J. Mol. Model.* **2016**, *22* (5), 1–12.
397. Farrokhpour, H.; Mansouri, A.; Najafi Chermahini, A. *J. Phys. Chem. C* **2017**, *121* (14), 8165–8176.
398. Vijayaraj, R.; Van Damme, S.; Bultinck, P.; Subramanian, V. *Phys. Chem. Chem. Phys.* **2013**, *15* (4), 1260–1270.
399. Alsina, M. A.; Gaillard, J. F.; Keten, S. *Phys. Chem. Chem. Phys.* **2016**, *18* (46), 31698–31710.
400. Ruiz, L.; Benjamin, A.; Sullivan, M.; Keten, S. *J. Phys. Chem. Lett.* **2015**, *6* (9), 1514–1520.
401. García-Fandiño, R.; Granja, J. R. *J. Phys. Chem. C* **2013**, *117* (19), 10143–10162.
402. Hou, X.; Guo, W.; Xia, F.; Nie, F. Q.; Dong, H.; Tian, Y.; Wen, L.; Wang, L.; Cao, L.; Yang, Y.; Xue, J.; Song, Y.; Wang, Y.; Liu, D.; Jiang, L. *J. Am. Chem. Soc.* **2009**, *131* (22), 7800–7805.
403. Hou, X.; Yang, F.; Li, L.; Song, Y.; Jiang, L.; Zhu, D. *J. Am. Chem. Soc.* **2010**, *132* (33), 11736–11742.
404. Calvelo, M.; Vázquez, S.; García-Fandiño, R. *Phys. Chem. Chem. Phys.* **2015**, *17* (43), 28586–28601.
405. Green, W. N.; Andersen, O. S. *Annu. Rev. Physiol.* **1991**, *53*, 341–359.
406. DeCaen, P. G.; Yarov-Yarovoy, V.; Sharp, E. M.; Scheuer, T.; Catterall, W. A. *Proc. Natl. Acad. Sci. U. S. A.* **2009**, *106* (52), 22498–22503.
407. Subramanyam, P.; Colecraft, H. M. *J. Mol. Biol.* **2015**, *427* (1), 190–204.
408. Urban, M. W. *Handbook of stimuli-responsive materials*; John Wiley & Sons, 2011.

409. Li, Q.; Schenning, A. P. H. J.; Bunning, T. J. *Adv. Opt. Mater.* **2019**, *7* (16), 1901160.
410. Li, Y.; Liu, H.; Xia, M.; Gong, H. *PLoS One* **2016**, *11* (9).
411. Flood, E.; Boiteux, C.; Allen, T. W. *PLoS Comput. Biol.* **2018**, *14* (9).
412. Csányi, É.; Boda, D.; Gillespie, D.; Kristóf, T. *Biochim. Biophys. Acta - Biomembr.* **2012**, *1818* (3), 592–600.
413. Fyles, T. M.; Tong, C. C. *New J. Chem.* **2007**, *31* (5), 655–661.
414. Tarek, M.; Delemotte, L. *Acc. Chem. Res.* **2013**, *46* (12), 2755–2762.
415. Reyes, R.; Duprat, F.; Lesage, F.; Fink, M.; Salinas, M.; Farman, N.; Lazdunski, M. *J. Biol. Chem.* **1998**, *273* (47), 30863–30869.
416. Schneider, F.; Gradmann, D.; Hegemann, P. *Biophys. J.* **2013**, *105* (1), 91–100.
417. Wang, J.; Wolf, R. M.; Caldwell, J. W.; Kollman, P. A.; Case, D. A. *J. Comput. Chem.* **2004**, *25* (9), 1157–1174.
418. Wang, J.; Wang, W.; Kollman, P. A.; Case, D. A. *J. Mol. Graph. Model.* **2006**, *25* (2), 247–260.
419. Wang, J.; Wolf, R. M.; Caldwell, J. W.; Kollman, P. A.; Case, D. A. *J. Comput. Chem.* **2004**, *25* (9), 1157–1174.
420. Wang, J.; Wang, W.; Kollman, P. A.; Case, D. A. *J. Am. Chem. Soc* **2001**, *222*, U403.
421. Berendsen, H. J. C.; Grigera, J. R.; Straatsma, T. P. *J. Phys. Chem.* **1987**, *91* (24), 6269–6271.
422. Joung, I. S.; Cheatham, T. E. *J. Phys. Chem. B* **2008**, *112* (30), 9020–9041.
423. Bussi, G.; Donadio, D.; Parrinello, M. *J. Chem. Phys.* **2007**, *126* (1), 014101.
424. Abraham, M. J.; Murtola, T.; Schulz, R.; Páll, S.; Smith, J. C.; Hess, B.; Lindahl, E. *SoftwareX* **2015**, *1–2*, 19–25.
425. Klesse, G.; Rao, S.; Sansom, M. S. P.; Tucker, S. J. *J. Mol. Biol.* **2019**, *431* (17), 3353–3365.
426. Michaud-Agrawal, N.; Denning, E. J.; Woolf, T. B.; Beckstein, O. *J. Comput. Chem.* **2011**, *32* (10), 2319–2327.
427. Hunter, J. D. *Comput. Sci. Eng.* **2007**, *9* (3), 99–104.
428. J. Bond, P.; Khalid, S. *Protein Pept. Lett.* **2012**, *17* (11), 1313–1327.
429. Shai, Y. *Biopolym. - Pept. Sci. Sect.* **2002**, *66* (4), 236–248.
430. Kumar, P.; Kizhakkedathu, J. N.; Straus, S. K. *Biomolecules* **2018**, *8* (1), 4.
431. Calvelo, M.; Granja, J. R.; Garcia-Fandino, R. *Phys. Chem. Chem. Phys.* **2019**, *21* (37), 20750–20756.
432. Franks, F.; Kern, C. W.; Karplus, M.; Rao, C. N. R.; Walrafen, G. E.; Glasel, J. A.; Hasted, J. B.; Narten, A. .; Levy, H. .; Page, D. I. *Water a Comprehensive Treatise. Volume 1.The Physics and Physical Chemistry of Water.*; Springer New York, 1972; Vol. 1.
433. Lynch, C.; Rao, S.; Sansom, M. S. *Chem. Rev.* **2020**, *120*, 10298–10335.
434. Bernal, J. D.; Fowler, R. H. *J. Chem. Phys.* **1933**, *1* (8), 515–548.
435. Barker, J. A.; Watts, R. O. *Chem. Phys. Lett.* **1969**, *3* (3), 144–145.

436. Guillot, B. *J. Mol. Liq.* **2002**, *101* (1), 219–260.
437. Jorgensen, W. L.; Tirado-Rives, J. *Proc. Natl. Acad. Sci. U. S. A.* **2005**, *102* (19), 6665 LP – 6670.
438. Cisneros, G. A.; Wikfeldt, K. T.; Ojamäe, L.; Lu, J.; Xu, Y.; Torabifard, H.; Bartók, A. P.; Csányi, G.; Molinero, V.; Paesani, F. *Chem. Rev.* **2016**, *116* (13), 7501–7528.
439. Water models http://www1.lsbu.ac.uk/water/water_models.html (accessed Apr 30, 2020).
440. Baaden, M.; Barboiu, M.; Bill, R. M.; Chen, C. L.; Davis, J.; Di Vincenzo, M.; Freger, V.; Fröba, M.; Gale, P. A.; Gong, B.; Hélix-Nielsen, C.; Hickey, R.; Hinds, B.; Hou, J. L.; Hummer, G.; Kumar, M.; Legrand, Y. M.; Lokesh, M.; Mi, B.; Murail, S.; Pohl, P.; Sansom, M.; Song, Q.; Song, W.; Törnroth-Horsefield, S.; Vashisth, H.; Vögele, M. *Faraday Discuss.* **2018**, *209* (0), 205–229.
441. Wu, K.; Chen, Z.; Li, J.; Xu, J.; Wang, K.; Li, R.; Wang, S.; Dong, X. *Langmuir* **2019**, *35* (26), 8867–8873.
442. Detcheverry, F.; Bocquet, L. *Phys. Rev. E - Stat. Nonlinear, Soft Matter Phys.* **2013**, *88* (1), 012106.
443. Fayer, M. D.; Levinger, N. E. *Annu. Rev. Anal. Chem.* **2010**, *3* (1), 89–107.
444. Collins, M. D.; Hummer, G.; Quillin, M. L.; Matthews, B. W.; Gruner, S. M. *Proc. Natl. Acad. Sci. U. S. A.* **2005**, *102* (46), 16668–16671.
445. Rasaiah, J. C.; Garde, S.; Hummer, G. *Annu. Rev. Phys. Chem.* **2008**, *59*, 713–740.
446. Beckstein, O.; Sansom, M. S. P. *Proc. Natl. Acad. Sci. U. S. A.* **2003**, *100* (12), 7063–7068.
447. Sisan, T. B.; Lichter, S. *Microfluid. Nanofluidics* **2011**, *11* (6), 787–791.
448. Walther, J. H.; Ritos, K.; Cruz-Chu, E. R.; Megaridis, C. M.; Koumoutsakos, P. *Nano Lett.* **2013**, *13* (5), 1910–1914.
449. Kashiwagi, K.; Suh, D.; Hwang, J.; Hsu, W. L.; Daiguji, H. *Nanoscale* **2018**, *10* (24), 11657–11669.
450. Lu, P.; Liu, X.; Zhang, C. *Micromachines* **2017**, *8* (6).
451. Liu, J.; Wang, M.; Chen, S.; Robbins, M. O. *J. Comput. Phys.* **2010**, *229* (20), 7834–7847.
452. Gravelle, S.; Joly, L.; Detcheverry, F.; Ybert, C.; Cottin-Bizonne, C.; Bocquet, L. *Proc. Natl. Acad. Sci. U. S. A.* **2013**, *110* (41), 16367–16372.
453. Gravelle, S.; Joly, L.; Ybert, C.; Bocquet, L. *J. Chem. Phys.* **2014**, *141* (18), 18C526.
454. Schaschke, C. *A Dictionary of Chemical Engineering*; Oxford University Press, 2014.
455. Anandakrishnan, R.; Izadi, S.; Onufriev, A. V. *J. Chem. Theory Comput.* **2019**, *15* (1), 625–636.
456. Bergonzo, C.; Cheatham, T. E. *J. Chem. Theory Comput.* **2015**, *11* (9), 3969–3972.
457. Henriksen, N. M.; Gilson, M. K. *J. Chem. Theory Comput.* **2017**, *13* (9),

4253–4269.
458. Kassinos, S. *Mol. Simul.* **2008**, *34* (7), 671–678.
459. Alexiadis, A.; Kassinos, S. *Chem. Eng. Sci.* **2008**, *63* (10), 2793–2797.
460. Alexiadis, A.; Kassinos, S. *Chem. Rev.* **2008**, *108* (12), 5014–5034.
461. Klesse, G.; Rao, S.; Tucker, S. J.; Sansom, M. S. P. *J. Am. Chem. Soc.* **2020**, *142* (20), 9415–9427.
462. Liu, L.; Patey, G. N. *J. Chem. Phys.* **2016**, *144* (18), 184502.
463. Liu, L.; Patey, G. N. *J. Chem. Phys.* **2014**, *141* (18), 18C518.
464. Jiang, Y.; Lee, A.; Chen, J.; Ruta, V.; Cadene, M.; Chait, B. T.; MacKinnon, R. *Nature* **2003**, *423* (6935), 33–41.
465. Haynes, T.; Smith, I. P. S.; Wallace, E. J.; Trick, J. L.; Sansom, M. S. P.; Khalid, S. *ACS Nano* **2018**, *12* (8), 8208–8213.
466. Song, C.; Corry, B. *J. Phys. Chem. B* **2009**, *113* (21), 7642–7649.
467. Dixit, M.; Lazaridis, T. *J. Chem. Phys.* **2020**, *153* (5), 054101.
468. Shen, J.; Ye, R.; Romanies, A.; Roy, A.; Chen, F.; Ren, C.; Liu, Z.; Zeng, H. *J. Am. Chem. Soc.* **2020**, *142* (22), 10050–10058.
469. Hourani, R.; Zhang, C.; van der Weegen, R.; Ruiz, L.; Li, C.; Keten, S.; Helms, B. A.; Xu, T. *J. Am. Chem. Soc.* **2011**, *133* (39), 15296–15299.
470. Clark, T. D.; Buriak, J. M.; Kobayashi, K.; Isler, M. P.; McRee, D. E.; Ghadiri, M. R. *J. Am. Chem. Soc.* **1998**, *120* (35), 8949–8962.
471. Kobayashi, K.; Granja, J. R.; Ghadiri, M. R. *Angew. Chemie Int. Ed. English* **1995**, *34* (1), 93–95.
472. Horne, W. S.; Stout, C. D.; Ghadiri, M. R. *J. Am. Chem. Soc.* **2003**, *125* (31), 9372–9376.
473. Leclair, S.; Baillargeon, P.; Skouta, R.; Gauthier, D.; Zhao, Y.; Dory, Y. L. *Angew. Chemie Int. Ed.* **2004**, *43* (3), 349–353.
474. Liu, J.; Fan, J.; Tang, M.; Cen, M.; Yan, J.; Liu, Z.; Zhou, W. *J. Phys. Chem. B* **2010**, *114* (38), 12183–12192.
475. Liu, J.; Fan, J.; Tang, M.; Zhou, W. *J. Phys. Chem. A* **2010**, *114* (6), 2376–2383.
476. Comer, J.; Dehez, F.; Cai, W.; Chipot, C. *J. Phys. Chem. C* **2013**, *117* (50), 26797–26803.
477. Tiangtrong, P.; Thamwattana, N.; Baowan, D. *Appl. Nanosci.* **2016**, *6* (3), 345–357.
478. Jorgensen, W. L.; Chandrasekhar, J.; Madura, J. D.; Impey, R. W.; Klein, M. L. *J. Chem. Phys.* **1983**, *79* (2), 926–935.
479. Abascal, J. L. F.; Vega, C. *J. Chem. Phys.* **2005**, *123* (23), 234505.
480. Izadi, S.; Anandakrishnan, R.; Onufriev, A. V. *J. Phys. Chem. Lett.* **2014**, *5* (21), 3863–3871.
481. Madura, J. D. *Mol. Phys.* **1985**, *56* (6), 1381–1392.
482. Lindorff-Larsen, K.; Piana, S.; Palmo, K.; Maragakis, P.; Klepeis, J. L.; Dror, R. O.; Shaw, D. E. *Proteins Struct. Funct. Bioinforma.* **2010**, *78* (8), 1950–1958.
483. Jämbeck, J. P. M.; Lyubartsev, A. P. *J. Phys. Chem. B* **2012**, *116* (10),

3164–3179.
484. Jämbeck, J. P. M.; Lyubartsev, A. P. *J. Chem. Theory Comput.* **2012**, *8* (8), 2938–2948.
485. Klauda, J. B.; Venable, R. M.; Freites, J. A.; O'Connor, J. W.; Tobias, D. J.; Mondragon-Ramirez, C.; Vorobyov, I.; MacKerell, A. D.; Pastor, R. W. *J. Phys. Chem. B* **2010**, *114* (23), 7830–7843.
486. Gowers, R. J.; Linke, M.; Barnoud, J.; Reddy, T. J. E.; Melo, M. N.; Seyler, S. L.; Domański, J.; Dotson, D. L.; Buchoux, S.; Kenney, I. M.; Beckstein, O. In *Proceedings of the 15th Python in Science Conference*; Benthall, S., Rostrup, S., Eds.; 2016; pp 98–105.
487. Harris, C. R.; Millman, K. J.; van der Walt, S. J.; Gommers, R.; Virtanen, P.; Cournapeau, D.; Wieser, E.; Taylor, J.; Berg, S.; Smith, N. J.; Kern, R.; Picus, M.; Hoyer, S.; van Kerkwijk, M. H.; Brett, M.; Haldane, A.; del Río, J. F.; Wiebe, M.; Peterson, P.; Gérard-Marchant, P.; Sheppard, K.; Reddy, T.; Weckesser, W.; Abbasi, H.; Gohlke, C.; Oliphant, T. E. *Nature* **2020**, *585* (7825), 357–362.
488. Liu, P.; Harder, E.; Berne, B. J. *J. Phys. Chem. B* **2004**, *108* (21), 6595–6602.
489. Rapaport, D. C. *Mol. Phys.* **1983**, *50* (5), 1151–1162.
490. 4.8.3. Water dynamics analysis — MDAnalysis.analysis.waterdynamics — MDAnalysis 0.20.2-dev0 documentation https://www.mdanalysis.org/mdanalysis/documentation_pages/analysis/waterdynamics.html (accessed Apr 28, 2020).
491. Onufriev, A. V.; Izadi, S. *Wiley Interdiscip. Rev. Comput. Mol. Sci.* **2018**, *8* (2), e1347.
492. Garcia-Fandiño, R.; Piñeiro, Á.; Trick, J. L.; Sansom, M. S. P. *ACS Nano* **2016**, *10* (3), 3693–3701.
493. Mills, R. *J. Phys. Chem.* **1973**, *77* (5), 685–688.
494. Krynicki, K.; Green, C. D.; Sawyer, D. W. *Faraday Discuss. Chem. Soc.* **1978**, *66* (0), 199–208.
495. Liu, L.; Patey, G. N. *J. Chem. Phys.* **2017**, *146* (7), 074502.
496. Li, J.; Gong, X.; Lu, H.; Li, D.; Fang, H.; Zhou, R. *Proc. Natl. Acad. Sci. U. S. A.* **2007**, *104* (10), 3687–3692.
497. Lisbjerg, M.; Valkenier, H.; Jessen, B. M.; Al-Kerdi, H.; Davis, A. P.; Pittelkow, M. *J. Am. Chem. Soc.* **2015**, *137* (15), 4948–4951.
498. Fu, Y.; Yan, T.; Xu, X. *J. Phys. Chem. B* **2017**, *121* (38), 9006–9012.
499. Antimicrobial resistance https://www.who.int/en/news-room/fact-sheets/detail/antimicrobial-resistance.
500. Lack of new antibiotics threatens global efforts to contain drug-resistant infections https://www.who.int/news-room/detail/17-01-2020-lack-of-new-antibiotics-threatens-global-efforts-to-contain-drug-resistant-infections.
501. Matyus, E.; Kandt, C.; Tieleman, D. *Curr. Med. Chem.* **2007**, *14* (26), 2789–2798.
502. Arasteh, S.; Bagheri, M. *Methods Mol. Biol.* **2017**, *1548*, 103–118.

503. Cirac, A. D.; Moiset, G.; Mika, J. T.; Koçer, A.; Salvador, P.; Poolman, B.; Marrink, S. J.; Sengupta, D. *Biophys. J.* **2011**, *100* (10), 2422–2431.
504. Balatti, G. E.; Martini, M. F.; Pickholz, M. *J. Mol. Model.* **2018**, *24* (8), 208.
505. Balatti, G. E.; Ambroggio, E. E.; Fidelio, G. D.; Martini, M. F.; Pickholz, M. *Molecules* **2017**, *22* (10).
506. Payne, D. J. *Science.* **2008**, *321* (5896), 1644–1645.
507. Bassetti, M.; Merelli, M.; Temperoni, C.; Astilean, A. *Ann. Clin. Microbiol. Antimicrob.* **2013**, *12* (1), 1–15.
508. da Cunha, N. B.; Cobacho, N. B.; Viana, J. F. C.; Lima, L. A.; Sampaio, K. B. O.; Dohms, S. S. M.; Ferreira, A. C. R.; de la Fuente-Núñez, C.; Costa, F. F.; Franco, O. L.; Dias, S. C. *Drug Discov. Today* **2017**, *22* (2), 234–248.
509. Fjell, C. D.; Hiss, J. A.; Hancock, R. E. W.; Schneider, G. *Nat. Rev. Drug Discov.* **2012**, *11* (1), 37–51.
510. Mahlapuu, M.; Håkansson, J.; Ringstad, L.; Björn, C. *Front. Cell. Infect. Microbiol.* **2016**, *6* (12), 194.
511. Silva, T.; Adão, R.; Nazmi, K.; Bolscher, J. G. M.; Funari, S. S.; Uhríková, D.; Bastos, M. *Biochim. Biophys. Acta - Biomembr.* **2013**, *1828* (5), 1329–1339.
512. Pasupuleti, M.; Schmidtchen, A.; Malmsten, M. *Crit. Rev. Biotechnol.* **2012**, *32* (2), 143–171.
513. Wiesner, J.; Vilcinskas, A. *Virulence* **2010**, *1* (5), 440–464.
514. Yeung, A. T. Y.; Gellatly, S. L.; Hancock, R. E. W. *Cell. Mol. Life Sci.* **2011**, *68* (13), 2161–2176.
515. Zasloff, M. *Nature* **2002**, *415* (6870), 389–395.
516. Wimley, W. C.; Hristova, K. *J. Membr. Biol.* **2011**, *239* (1–2), 27–34.
517. Leontiadou, H.; Mark, A. E.; Marrink, S. J. *J. Am. Chem. Soc.* **2006**, *128* (37), 12156–12161.
518. Jean-François, F.; Elezgaray, J.; Berson, P.; Vacher, P.; Dufourc, E. J. *Biophys. J.* **2008**, *95* (12), 5748–5756.
519. Regen, S. L. *JACS Au* **2020**, jacsau.0c00037.
520. Wu, M.; Hancock, R. E. W. *Antimicrob. Agents Chemother.* **1999**, *43* (5), 1274–1276.
521. Jelokhani-Niaraki, M.; Prenner, E. J.; Kay, C. M.; McElhaney, R. N.; Hodges, R. S. *J. Pept. Res.* **2002**, *60* (1), 23–36.
522. Qian, Z.; Martyna, A.; Hard, R. L.; Wang, J.; Appiah-Kubi, G.; Coss, C.; Phelps, M. A.; Rossman, J. S.; Pei, D. *Biochemistry* **2016**, *55* (18), 2601–2612.
523. Mika, J. T.; Moiset, G.; Cirac, A. D.; Feliu, L.; Bardají, E.; Planas, M.; Sengupta, D.; Marrink, S. J.; Poolman, B. *Biochim. Biophys. Acta - Biomembr.* **2011**, *1808* (9), 2197–2205.
524. Ongwae, G. M.; Morrison, K. R.; Allen, R. A.; Kim, S.; Im, W.; Wuest, W. M.; Wuest, W. M.; Pires, M. M. *ACS Infect. Dis.* **2020**, *6* (6), 1427–1435.
525. Mihailescu, D.; Smith, J. C. *J. Phys. Chem. B* **1999**, *103* (9), 1586–1594.
526. Mihailescu, D.; Smith, J. C. *Biophys. J.* **2000**, *79* (4), 1718–1730.

527. Chen, P. B.; Black, A. S.; Sobel, A. L.; Zhao, Y.; Mukherjee, P.; Molparia, B.; Moore, N. E.; Aleman Muench, G. R.; Wu, J.; Chen, W.; Pinto, A. F. M.; Maryanoff, B. E.; Saghatelian, A.; Soroosh, P.; Torkamani, A.; Leman, L. J.; Ghadiri, M. R. *Nat. Biotechnol.* **2020**, *38*, 1288–1297.
528. Cheng, J. T. J.; Hale, J. D.; Elliott, M.; Hancock, R. E. W.; Straus, S. K. *Biochim. Biophys. Acta - Biomembr.* **2011**, *1808* (3), 622–633.
529. Hancock, R. E. W.; Rozek, A. *FEMS Microbiol. Lett.* **2002**, *206* (2), 143–149.
530. Li, X.; Smith, A. W. *J. Phys. Chem. B* **2019**, *123* (49), 10433–10440.
531. Schmitt, P.; Rosa, R. D.; Destoumieux-Garzón, D. *Biochim. Biophys. Acta - Biomembr.* **2016**, *1858* (5), 958–970.
532. Malanovic, N.; Lohner, K. *Biochim. Biophys. Acta - Biomembr.* **2016**, *1858* (5), 936–946.
533. Yeagle, P. L.; Yeagle, P. L. *Membr. Cells* **2016**, 189–218.
534. De Jong, D. H.; Singh, G.; Bennett, W. F. D.; Arnarez, C.; Wassenaar, T. A.; Schäfer, L. V.; Periole, X.; Tieleman, D. P.; Marrink, S. J. *J. Chem. Theory Comput.* **2013**, *9* (1), 687–697.
535. Yesylevskyy, S. O.; Schäfer, L. V.; Sengupta, D.; Marrink, S. J. *PLoS Comput. Biol.* **2010**, *6* (6), e1000810.
536. Vijayakumar, V.; Vijayaraj, R.; Peters, G. H. *J. Mol. Model.* **2016**, *22* (11), 1–12.
537. Jo, S.; Kim, T.; Iyer, V. G.; Im, W. *J. Comput. Chem.* **2008**, *29* (11), 1859–1865.
538. Hsu, P.-C. C.; Bruininks, B. M. H. H.; Jefferies, D.; Cesar Telles de Souza, P.; Lee, J.; Patel, D. S.; Marrink, S. J.; Qi, Y.; Khalid, S.; Im, W. *J. Comput. Chem.* **2017**, *38* (27), 2354–2363.
539. Wu, E. L.; Cheng, X.; Jo, S.; Rui, H.; Song, K. C.; Dávila-Contreras, E. M.; Qi, Y.; Lee, J.; Monje-Galvan, V.; Venable, R. M.; Klauda, J. B.; Im, W. *J. Comput. Chem.* **2014**, *35* (27), 1997–2004.
540. Marrink, S. J.; De Vries, A. H.; Mark, A. E. *J. Phys. Chem. B* **2004**, *108* (2), 750–760.
541. Monticelli, L.; Kandasamy, S. K.; Periole, X.; Larson, R. G.; Tieleman, D. P.; Marrink, S. J. *J. Chem. Theory Comput.* **2008**, *4* (5), 819–834.
542. Siu, S. W. I.; Pluhackova, K.; Böckmann, R. A. *J. Chem. Theory Comput.* **2012**, *8* (4), 1459–1470.
543. Robertson, M. J.; Tirado-Rives, J.; Jorgensen, W. L. *J. Chem. Theory Comput.* **2015**, *11* (7), 3499–3509.
544. Gallivan, J. P.; Dougherty, D. A. *Proc. Natl. Acad. Sci. U. S. A.* **1999**, *96* (17), 9459–9464.
545. Claro, B.; González-Freire, E.; Calvelo, M.; Bessa, L. J.; Goormaghtigh, E.; Amorín, M.; Granja, J. R.; Garcia-Fandiño, R.; Bastos, M. *Colloids Surfaces B Biointerfaces* **2020**, *196*, 111349.
546. Bochicchio, D.; Pavan, G. M. *ACS Nano* **2017**, *11* (1), 1000–1011.
547. Rzepiela, A. J.; Louhivuori, M.; Peter, C.; Marrink, S. J. *Phys. Chem. Chem.*

Phys. **2011**, *13* (22), 10437–10448.
548. Wassenaar, T. A.; Ingólfsson, H. I.; Prieß, M.; Marrink, S. J.; Schäfer, L. V. *J. Phys. Chem. B* **2013**, *117* (13), 3516–3530.
549. Sharp, M. E.; Vázquez, F. X.; Wagner, J. W.; Dannenhoffer-Lafage, T.; Voth, G. A. *J. Chem. Theory Comput.* **2019**, *15* (5), 3306–3315.
550. Goga, N.; Melo, M. N.; Rzepiela, A. J.; De Vries, A. H.; Hadar, A.; Marrink, S. J.; Berendsen, H. J. C. *J. Chem. Theory Comput.* **2015**, *11* (4), 1389–1398.
551. Wassenaar, T. A.; Pluhackova, K.; Böckmann, R. A.; Marrink, S. J.; Tieleman, D. P. *J. Chem. Theory Comput.* **2014**, *10* (2), 676–690.
552. Rzepiela, A. J.; Schäfer, L. V.; Goga, N.; Jelger Risselada, H.; De Vries, A. H.; Marrink, S. J. *J. Comput. Chem.* **2010**, *31* (6), 1333–1343.
553. Brocos, P.; Mendoza-Espinosa, P.; Castillo, R.; Mas-Oliva, J.; Piñeiro, Á. *Soft Matter* **2012**, *8* (34), 9005–9014.
554. Wassenaar, T. A.; Pluhackova, K.; Böckmann, R. A.; Marrink, S. J.; Tieleman, D. P. *J. Chem. Theory Comput.* **2014**, *10* (2), 676–690.
555. Stansfeld, P. J.; Sansom, M. S. P. *J. Chem. Theory Comput.* **2011**, *7* (4), 1157–1166.
556. Otero-Mato, J. M.; Montes-Campos, H.; Calvelo, M.; García-Fandino, R.; Gallego, L. J.; Pineiro, Á.; Varela, L. M. *J. Chem. Theory Comput.* **2018**, *14* (2), 466–478.
557. GADDLE MAPS AR - Apps on Google Play https://play.google.com/store/apps/details?id=com.mduse.GADDLEMAPS&hl=en.
558. Gaddle maps AR on the App Store https://apps.apple.com/ca/app/gaddle-maps-ar/id1311726695.

USC
UNIVERSIDADE
DE SANTIAGO
DE COMPOSTELA

List of abbreviatures and acronyms

AA	All-Atom
AA-MD	All-Atom Molecular Dynamics
Acas	Aminocycloalkanecarboxylic Acid
Ach	Aminocyclohexanecarboxylic Acid
Ala	Alanine
AFM	Atomic Force Microscopy
AMP	Antimicrobial Peptide
AR	Augmented Reality
Arg	Arginine
BCP	Bond Critical Points
BSSE	Basis Set Superposition Error
CD	Cyclodextrin
CG	Coarse-Grained
CG-MD	Coarse-Grained Molecular Dynamics
CFD	Continuum Fluid Dynamic
CNT	Carbon Nanotube
CP	Cyclic Peptide
DFT	Density Functional Theory
DMPC	1,2-dimyristoyl-sn-glycero-3-phosphocholine
DMPE	1,2-dimyristoyl-sn-glycero-3-phosphoethanolamine
DMPG	1,2-dimyristoyl-sn-glycero-3-phospho-(1'-rac-glycerol)
DNA	Deoxyribonucleic Acid
DOPC	1,2-dioleoyl-sn-glycero-3-phosphocholine
DSC	Differential Scanning Calorimetry
FTIR	Fourier-Transform Infrared Spectroscopy
Gln	Glutamine
Glu	Glutamic acid
GPU	Graphics Processing Unit
H-Bond	Hydrogen bond

Leu	Leucine
Lys	Lysine
MD	Molecular Dynamics
MR	Mixed Reality
NMR	Nuclear Magnetic Resonance
PBC	Periodic Boundary Conditions
Phe	Phenylalanine
PME	Particle Mesh Ewald
PMF	Potential Mean Force
POPC	2-oleoyl-1-palmitoyl-sn-glycero-3-phosphocholine
Prg	Propargylglycine
QM/MM	Quantum Mechanic / Molecular Mechanic
QTAIM	Quantum Theory of Atoms in Molecules
RNA	Ribonucleic Acid
RECP	Relativistic Effective Small-Core Potential
RMSD	Root-Mean-Square-Deviation
SCPN	Self-assembled Cyclic Peptide Nanotube
Ser	Serine
STM	Scanning Tunnelling Microscopy
Trp	Tryptophan
Tyr	Tyrosine
UA	United-atom
VR	Virtual Reality
WHO	World Health Organization

USC
UNIVERSIDADE
DE SANTIAGO
DE COMPOSTELA